Transcriptomic analysis of the tumour vasculature and its clinical relevance

---

by

Joseph Wragg

A thesis submitted to

The University of Birmingham

for the degree of

DOCTOR OF PHILOSOPHY

Angiogenesis Group

Department of Immunity and Infection

College of Medical and Dental Sciences

The University of Birmingham

February 2016

Abstract

The vasculature of many solid tumours is highly distinct from that of its host tissue, both structurally and in terms of functional protein expression. These differences offer an opportunity for specific targeting of therapeutics against the tumour vasculature. This thesis describes the investigation of this tumour vascular profile, in clinical samples from renal cell carcinoma, colorectal cancer and colorectal liver metastases, as well as murine breast tumours resistant to the anti-angiogenic drug, sunitinib. This analysis allowed the identification of three tumour endothelial markers in renal and colorectal malignancies, MCAM, LAMA4 and GRIN2D. The expression of each of these markers was linked with patient survival with these malignancies, suggesting their utility for prognostication. MCAM and GRIN2D showed highly tumour specific expression profiles in multi-organ tissue array analysis, highlighting them as promising candidates for the targeting of therapies to the tumour vasculature. The specific localisation of monoclonal anti-MCAM antibodies to renal tumour vasculature was demonstrated, further supporting this suggestion. Putative vascular markers of tumour resistance to anti-angiogenic therapy were also identified. Aquaporin-1 (AQP1) was found to be up-regulated in cases of acquired resistance, mammalian target of rapamycin (mTOR) in innate resistance and pleiotrophin (PTN) in both, highlighting their potential as diagnostic candidates for predicting therapy response, or as targets to circumvent resistance. The need for effective diagnostic tests in this indication, was demonstrated by the finding that metastasis is enhanced by sunitinib therapy, in innately resistant tumours.

Acknowledgements

My deepest thanks to Professor Roy Bicknell for his guidance and supervision, over the last four years. I also thank him for the many opportunities he has provided me to express myself both scientifically and intellectually.

I would also like to thank my co-supervisor Dr Victoria Heath for her support, advice and encouragement over the course of my PhD studies.

I offer thanks to Dr Zsuzsanna Nagi for allowing me to use the Ingenuity pathway prediction software and the Acumen cell cytometer.

I thank Dr Peter Noy and Dr Samantha Tull for their practical support in developing my lab skills.

I express my gratitude to Henry Ferguson, Klarke Sample, Kabir Khan, Puja Lodhia and Jonathan Finnity for their peer support and friendship, in the identification and validation of tumour endothelial markers. I particularly thank Henry Ferguson for generating the GRIN2D antibody used in chapter 4.

My thanks to Cancer Research UK for their funding and active student support.

My heartfelt thanks go to my wonderful wife Sarah for her endless support, love, encouragement and friendship.

I am also deeply indebted to my family for their constant support over the years.

Table of Contents

General Introduction **1**

1.1 Targeting the tumour vasculature **2**

1.2 Vascular disrupting agents **5**

1.2.1 Small molecule VDAs 6

1.2.2 Ligand-Directed VDAs 11

1.2.3 The search for new tumour endothelial markers 13

1.2.4. Ligand directed drugs under investigation and in the clinic 16

1.3 Project aims 1: Tumour vascular targets **19**

1.4 Tumour angiogenesis **19**

1.5 Angiogenesis inhibitors **21**

1.5.1 Blocking antibodies 22

1.5.2 Soluble decoy receptors 25

1.5.3 Small molecule inhibitors 26

1.6 Antiangiogenic therapy resistance **30**

1.6.1 Evasive resistance by up regulation of alternative pro-angiogenic signalling pathways within the tumour 32

1.6.2 Recruitment of pro-angiogenic cells 33

1.6.3 Rapid vascular remodelling by recruitment of pericytes 33

1.6.4 Increased local invasion and vessel co-option, mitigating the need for neovascularisation 34

1.6.5 Increased distant metastasis 35

1.6.6 Selection of resistant endothelium 35

1.6.7 Tumour cell metabolic change 36

1.6.8 Innate insensitivity to antiangiogenic therapy 37

1.7 Project aims 2: Antiangiogenic therapy resistance **38**

Materials and Methods **40**

2.1 Materials **41**

2.1.1 RTqPCR primers 47

2.1.2 Tissue provision / processing 49

2.2 Endothelial isolation methods **50**

2.2.1 Endothelial cell extraction from human tissue 50

2.2.2 Endothelial cell isolation from mouse tissue 51

2.3 Molecular biology methods 52
2.3.1 RNA extraction 52
2.3.2 RNA integrity validation 52
2.3.3 RNA labelling 52
2.3.4 Microarray analysis 53
2.3.5 cDNA production 53
2.3.6 Quantitative Reverse Transcription Polymerase Chain Reaction (RT-qPCR) 53
2.3.7 Western blot 54
2.4 Tissue staining methods 56
2.4.1 Immunohistochemistry 56
2.4.2 Immunofluorescent staining on frozen sections 57
2.4.3 Immunofluorescent staining on paraffin embedded sections 57
2.4.4 Haematoxylin and Eosin (H&E) stain on paraffin embedded sections 58
2.5 Cell culture (*in vitro*) methods 59
2.5.1 Primary cell and cell line culture 59
2.5.2 Cell resuscitation, splitting and counting 59
2.5.3 Human umbilical cord vein endothelial cell (HUVEC) isolation 60
2.5.4 siRNA knockdown and HUVEC functional assays 61
2.5.5 HUVEC and HDMEC treatment with VEGF 63
2.5.6 Transfection of Phoenix-Ampho cells 63
2.5.7 Retroviral Harvesting 63
2.5.8 Transduction of 4T1 cells 63
2.5.9 MTS viability assay 64
2.5.10 Puromycin selection of 4T1 cells 64
2.5.11 IVIS analysis of 4T1 cells 65
2.6 *In vivo* methods 65
2.6.1 Sourcing and caring for mice 65
2.6.2 RENCA tumour and antibody localisation 65
2.6.3 Initiation of 4T1-LUC tumours in the murine mammary fat pad 66
2.6.4 *Ex vivo* imaging 66
2.6.5 Sunitinib drug trial 66
2.7 Imaging quantitation 67
2.7.1 Command line for localisation quantitation 67
2.7.2 Command lines for vascular density and target staining quantitation 68
2.7.3 Quantification of metastasis by H&E staining 69

2.7.4 IVIS *ex vivo* imaging settings 69
2.7.5 Directions for the quantification of *ex vivo* bioluminescence 69
2.8 Bioinformatic methods 70
2.8.1 Microarray bioinformatic analysis 70
2.8.2 Ingenuity bioinformatics analysis 73
2.8.3 Bioinformatic websites 74
Endothelial Isolation and Microarray Analysis 75
3.1 Introduction 76
3.2 Results 77
3.2.1 Sample collection and endothelial isolation 77
3.2.2 RNA integrity validation 79
3.2.3 RTqPCR and validation of endothelial isolation 82
3.2.4 RNA labelling and hybridisation for microarray 85
3.2.5 Microarray data normalisation and generation of comparison matrices 88
3.3 Discussion 89
3.3.1 *Ulex* lectin vs. PECAM-1 89
3.3.2 Magnetic bead isolation vs. fluorescence-activated cell sorting (FACS) 90
3.3.3 Microarray analysis vs. next-generation sequencing 90
Colorectal Tumour Endothelial Markers 92
4.1 Introduction 93
4.2 Results 95
4.2.1 Comparative microarray analysis of CRC versus healthy colon 95
4.2.2 Known tumour associated genes, matrix metallopeptidases and collagens 95
4.2.3 Selection of genes of interest 97
4.2.4 Validation of genes of interest 99
4.2.5 Analysis of the functional role in endothelium of GRIN2D 106
4.3 Discussion 117
MCAM, LAMA4 and Other Pan-Tumour Endothelial Markers 121
5.1 Introduction 122
5.2 Results 124
5.2.1 Identification of a pan-tumour endothelial expression profile 124
5.2.2 Validation of MCAM and LAMA4 as tumour endothelial markers 130
5.2.3 MCAM expression is induced by vascular endothelial growth factor (VEGF) 134

5.2.4 Identification of strong MCAM and LAMA4 expression as potent adverse prognostic indicators in RCC 137
5.2.5 MCAM and LAMA4 expression is enhanced in locally invasive and metastatic disease 145
5.2.6 Monoclonal anti-MCAM antibodies specifically localise to murine RCC tumour vessels 147
5.3 Discussion 150

An *In Vivo* Breast Cancer Model of Sunitinib Resistance 157
6.1 Introduction 158
6.2 Results 161
6.2.1 Production of 4T1-luc cells 161
6.2.2 4T1 tumour growth under sunitinib treatment 165
6.2.3 Differential sunitinib mediated effects on tumour vascular patterning 170
6.2.4 Sunitinib enhances metastasis in innately resistant tumours 173
6.3 Discussion 177

The Molecular Profile of Breast Cancer Sunitinib Drug Resistance 182
7.1 Introduction 183
7.2 Results 184
7.2.1 Murine tumour endothelial isolation and microarray analysis 184
7.2.2 The impact of sunitinib treatment on tumour and endothelial gene expression 187
7.2.3 The selection and validation of acquired resistance markers 199
7.2.4 Expression changes of candidate markers of acquired resistance over time 201
7.2.5 Validation of aquaporin on the protein level 203
7.3 Discussion 205
7.3.1 Innate resistance 206
7.3.2 Acquired resistance 208
7.3.3 AQP1 in acquired resistance to sunitinib 209

Concluding Remarks 210

Appendix 216
Supplementary section to 7.2.2 "The impact of sunitinib treatment on tumour and endothelial gene expression." 218

References 248

List of Illustrations

Chapter One

Figure 1.1. Abnormal tumour vasculature from colorectal carcinoma 4
Figure 1.2. Ligand directed VDA induced tumour necrosis 12
Figure 1.3. Tumour angiogenesis 21
Figure 1.4. Anti-angiogenic therapy resistance 31

Chapter Three

Figure 3.1 Isolation of endothelial cells using *Ulex* lectin coated magnetic beads 79
Figure 3.2 Agilent bioanalyser electrophoresis 81
Figure 3.3 Agilent bioanalyser electropherograms of good to perfect quality RNA 82
Figure 3.4 Confirmation of endothelial isolation efficiency by RTqPCR 85
Figure 3.5 RNA labelling for microarray analysis 86
Figure 3.6 Labelled cRNA hybridisation for microarray analysis 87

Chapter Four

Figure 4.1. Validation of putative colorectal cancer vascular markers by RTqPCR 100
Figure 4.2. Confirmation of colon cancer specific enrichment of GRIN2D by immunohistochemistry 103
Figure 4.3. GRIN2D vascular expression is positively correlated with survival in colorectal cancer 104
Figure 4.4. siRNA duplexes successfully knockdown GRIN2D expression 108
Figure 4.5. Loss of GRIN2D impairs endothelial matrigel tube formation 110
Figure 4.6. Loss of GRIN2D impairs scratch wound closure 112
Figure 4.7. Loss of GRIN2D impairs endothelial cell transmigration and chemotaxis 114
Figure 4.8. siRNA knockdown of GRIN2D in HUVEC does not affect cell viability, proliferation or progression through the cell cycle 116

Chapter Five

Figure 5.1. Venn diagram showing the commonality of genes at least 2 fold upregulated in four tumour vs. healthy tissue 127

Figure 5.2: Confirmation of cancer specific enrichment of MCAM and LAMA4 by RTqPCR 130

Figure 5.3. Confirmation of cancer specific enrichment of MCAM and LAMA4 by immunohistochemistry 131

Figure 5.4. A, MCAM expression is specifically enriched on the vasculature of renal cancer 132

Figure 5.4. B, multi-organ tissue and cancer array analysis of MCAM and LAMA4 expression by IHC 133

Figure 5.5. VEGF significantly induces MCAM expression in endothelial cells 135

Figure 5.6. High MCAM and LAMA4 tumour vessel expression has a significant detrimental effect on the survival of RCC patients but not CRC patients 139

Figure 5.7. MCAM and LAMA4 expression is enhanced in metastatic and locally advanced clear cell RCC 146

Figure 5.8. A monoclonal anti-MCAM antibody specifically localises to murine RCC tumour vessels 149

Chapter Six

Figure 6.1. Map of the of the MSCVpuro plasmid used for retroviral transduction of the luciferase gene into 4T1 cells 161

Figure 6.2. Retroviral transduction of the MSCV-puro-luc plasmid into 4T1 cells and puromycin selection 164

Figure 6.3. Experimental set up for sunitinib drug trial 165

Figure 6.4. Sunitinib therapy bisects the treated group into responsive and non-responsive cohorts 167

Figure 6.5. Sunitinib treatment significantly retards growth of responsive tumours 169

Figure 6.6. Sunitinib treatment reduces vascularity and impacts the vascular patterning of 4T1 tumours 172

Figure 6.7. *Ex vivo* bioluminescent imaging and H&E staining correlate as methods to determine metastatic tumour burden 174
Figure 6.8. Sunitinib treatment enhances 4T1 tumour metastasis 176

Chapter Seven

Figure 7.1. Endothelial isolation from murine breast tumours 185
Figure 7.2. Representative tumours from each response group and time period were subjected to microarray transcriptomic analysis 186
Figure 7.3. Aquaporin is significantly enriched in the vessels of responsive tumours on the RNA level 202
Figure 7.4. Aquaporin is significantly enriched in the vessels of responsive tumours on the protein level 204

Appendix

Appendix figure A 221-229
Appendix figure B 230-238
Appendix figure C 239-247

List of Tables

Chapter One

Table 1.1. Small molecule VDAs in the clinic 9

Table 1.2. Tumour vascular specific targets 17

Table 1.3. Effector molecules used in vascular targeting 18

Table 1.4. Ligand directed VDAs in the clinic 18

Table 1.5. Antiangiogenic blocking antibodies in the clinic 25

Table 1.6. Antiangiogenic small molecule inhibitors in the clinic 29

Chapter Two

Table 2.1. Equipment used for the research detailed in this thesis 41

Table 2.2. Chemicals and drugs used for the research detailed in this thesis 42

Table 2.3. Organic products and culture media used for the research detailed in this thesis 43

Table 2.4. Kits used for the research detailed in this thesis 43

Table 2.5. Human tissue arrays used for the research detailed in this thesis 44

Table 2.6. Other materials used for the research detailed in this thesis 44

Table 2.7. Solution formulations used for the research detailed in this thesis 45

Table 2.8. Plasmids used for the research detailed in this thesis 45

Table 2.9. Cultured cells used for the research detailed in this thesis 45

Table 2.10. Antibodies used for the research detailed in this thesis 46

Table 2.11. SiRNA dupexes used for the research detailed in this thesis 46

Table 2.12. Human RTqPCR primers used for the research detailed in this thesis 47

Table 2.13. Mouse RTqPCR primers used for the research detailed in this thesis 48

Chapter Three

Table 3.1. Clinical-pathological data for colorectal cancer patients used for genomic analysis and validation 78

Table 3.2. Clinical-pathological data for colorectal liver metastasis patients used for genomic analysis and validation 78

Table 3.3. Clinical-pathological data for renal cancer patients used for genomic analysis and validation 78

Chapter Four

Table 4.1. Known tumour associated or angiogenic genes enriched in colorectal cancer vessels 96

Table 4.2. Collagens enriched in colorectal cancer vessels 96

Table 4.3. Matrix metallopeptidases enriched in colorectal cancer vessels 97

Table 4.4. Transmembrane genes greater than 5 fold enriched in colorectal cancer vessels 98

Table 4.5. Selection of genes of interest for further investigation and validation 101

Table 4.6. Key clinical data for CRC cohort showing overall survival (OS) 105

Chapter Five

Table 5.1. Collagen regulation across tissue types 125

Table 5.2. Matrix metallopeptidase regulation across tissue types 126

Table 5.3. Consistently upregulated vascular genes across cancer types (gene expression comparison shown as Log2 fold change) 128

Table 5.4. Consistently downregulated vascular genes across cancer types (gene expression comparison shown as Log2 fold change) 129

Table 5.5. Key clinical data for different types of kidney cancer and metastasis 136

Table 5.6. Key clinical data for clear cell RCC cohort 1, showing overall survival (OS) 140

Table 5.7. Key clinical data for clear cell RCC cohort 2, showing overall survival (OS) 141

Table 5.8. Key clinical data for clear cell RCC cohort 3, showing overall survival (OS) 142

Table 5.9. Key clinical data for the CRC cohort, showing overall survival (OS). 143

Table 5.10. Multivariate analysis (Cox regression) of prognostic markers in RCC cohort 1 144

Chapter Six

Table 6.1. IC_{50} values for sunitinib inhibition of receptor tyrosine kinases 159

Chapter Seven

Table 7.1. & 7.2. Expression change of genes on which sunitinib has a predicted effect 189

Table 7.3. & 7.4. Expression change of genes that enhance metastasis 193-194

Table 7.5 & 7.6. Expression change of genes that enhance endothelial migration 197-198

Table 7.7. Genes significantly enriched in the endothelial isolates from responsive vs. untreated tumours harvested at 1300 mm^3 199

Table 7.8. Selection of genes of interest for further analysis by RTqPCR 200

List of abbreviations

Ab Antibody
BBB Blood brain barrier
BSA Bovine serum albumin
CA4P Combretastatin A-4 Disodiumphosphate
ccRCC clear cell RCC
cDNA complementary DNA
CRC colorectal cancer
CRM colorectal liver metastasis
cRNA complementary RNA
DAPI 4,6-diamino-2-phenylindole
DMSO Dimethyl sulfoxide
DNA Deoxyribonucleic acid
EC Endothelial cell
ECL Enhanced chemoluminescence
EDTA Ethylenediaminetetraacetic acid
FACS Fluorescent activated cell sorting
FCS Fetal calf serum
FDA Food and Drug Administration
FGF Fibroblast growth factor
FITC Fluorescein isothiocyanate
H&E Hematoxylin and eosin stain
HBRC Human Biomaterials Resource Centre
HDMEC Human dermal microvascular endothelial cells
HUVEC Human umbilical cord endothelial cells
IF Immunofluorescence
IFN Interferon
IHC Immunohistochemistry
IP Intraperitoneal
IVIS *In Vivo* Imaging System

KD Knockdown

Kd Dissociation constant

LPA lysophosphatidic acid

mAb monoclonal antibody

miRNAs micro RNAs

MMPs Matrix metallopeptidases

mRCC Metastatic RCC

mRNA messenger RNA

MTD Maximum tolerated dose

NSCLC non-small cell lung cancer

OD Optical density

PAGE Polyacrylamide gel electrophoresis

PCR Polymerase chain reaction

PDGF(R) Platelet derived growth factor (receptor)

PECAM-1 Platelet endothelial cell adhesion molecule

PFS Progression free survival

RCC renal cell carcinoma

RIN RNA integrity number

RNA Ribonucleic acid

ROI Region of interest

RTK Receptor tyrosine kinase

RTqPCR Quantitative reverse transcription PCR

S1P sphingosine-1-phosphate

SAGE Serial analysis of gene expression

SDS Sodium dodecylsulfate

SEM Standard error of the mean

siRNA Small interfering RNA

TEM Tumour endothelial marker

TNBC Triple negative breast cancer

TNF Tumour necrosis factor

VEGF(R) Vascular endothelial growth factor (receptor)

Chapter One

General Introduction

NB, sections of this introduction have been adapted from excepts of Vascular Targeting Approaches to Treat Cancer, Wragg and Bicknell, 2013 (1)*, reproduced with permission.*

Specific targeting of therapeutics to the tumour has long been a quest in cancer research. Systematic cytotoxics do not target cancer cells or the pro-tumourigenic environment selectively and so lead to adverse side effects and provide a limited anti-tumour effect, particularly in advanced cancer. Most chemotherapeutics do not accumulate preferentially in the tumour site; indeed the drug dose is often 10-20 times higher in healthy tissue than in the tumour (2,3). This poor drug infiltration is thought to be due to irregular tumour vasculature and high interstitial pressure (4,5). Therefore an improved approach to targeting the tumour is warranted.

1.1 Targeting the tumour vasculature

The vasculature is postulated to be an ideal candidate for targeted anti-cancer therapies. It is a key part of the tumour microenvironment required for the delivery of nutrients and removal of toxic waste products and so is essential for tumour growth and metastasis (6). The tumour vasculature is directly accessible to drugs via the circulation and composed of endothelial cells thought to be genetically stable and less adaptive than tumour cells, therefore they are less likely to acquire drug resistance (7,8). In addition it is estimated that up to 100 tumour cells are fed from a single

endothelial cell (3), and so a therapeutic targeting the vasculature should achieve a more potent anti-cancer effect than targeting the tumour cells directly.

The tumour acquires a vascular network by the formation of neovessels (angiogenesis), the incorporation of existing blood vessels (vessel co-option), the splitting of existing vessels into daughter vessels (intussusception) and even by mimicking the vasculature by forming blood vessel like tubes lined with tumour cells (vascular mimicry) (9). Tumour angiogenesis is essential for the survival and development of a tumour greater than 2 mm^3 in size (6,10,11). However, tumour vascularisation invariably lags behind the expanding tumour mass (12) resulting in highly abnormal tumour vasculature that morphologically and functionally differs from the vasculature of healthy tissues (13). It is highly chaotic in nature composed of tortuous, dilated and elongated vessels with blind ends, bulges, leaky sprouts and considerable variability in diameter (14) (Figure 1.1). The tumour vascular endothelial cells themselves are highly abnormal, expressing several cell surface markers barely detectable on healthy tissue or quiescent vascular endothelial cells (15). The abnormality of the tumour vasculature is often associated with treatment failure due to poor drug penetrance (4,5), however, it could offer an opportunity for targeted anti-cancer therapy if these differences can be used to specifically target therapies against the tumour vasculature.

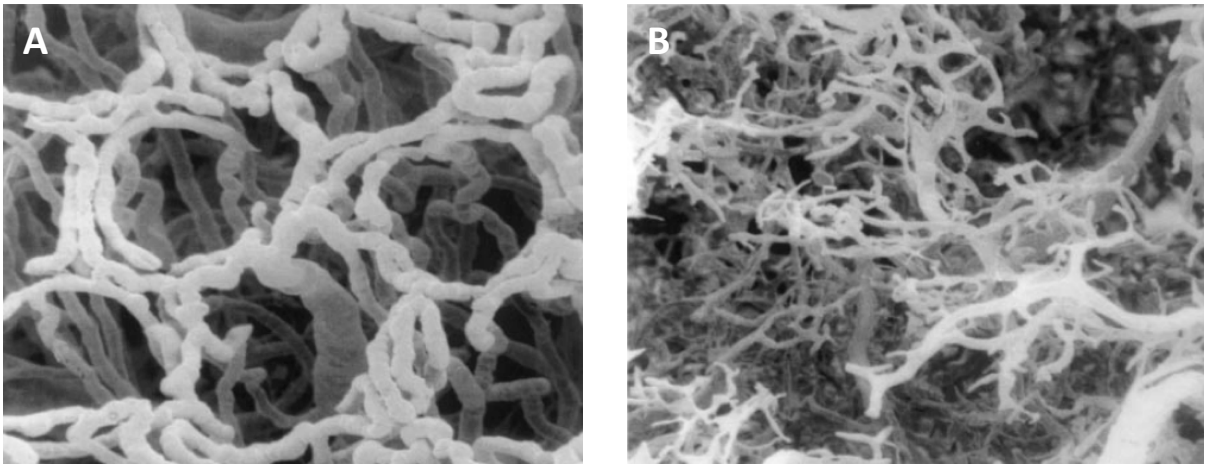

Figure 1.1. Abnormal tumour vasculature in colorectal carcinoma.
Micro-vascular corrosion casts of human A, healthy ascending colon and B, colorectal carcinoma (13). Image reproduced with permission.

To this end, many anti-tumour-vasculature therapeutics have been developed over the last 20 years with a number reaching the clinic. There are a wide variety of different therapeutics, but they can be very broadly divided into vascular disrupting agents (VDAs), which target and occlude the existing tumour vasculature, and angiogenesis inhibitors (or antiangiogenics, AIs), which inhibit neovascularisation of the tumour. Collectively they aim to devascularise and starve the tumour, thus achieving tumour regression (6).

1.2 Vascular disrupting agents

It has long been known that the disruption of the blood supply to a tissue causes rapid and extensive cell death by ischemia and hemorrhagic necrosis. This phenomenon was first described in 1852 in relation to testicular torsion (16). The testicular torsion condition is caused when the spermatic cord, which carries blood to the testicles, becomes twisted, reducing blood flow and causing necrosis in the affected testicle. It was not until 1923 however, that the potential of vascular disruption to starve a tumour was realised. In a seminal paper, William Woglam described how the disruption of the blood supply to a tumour could cause regression and suggested the potential for novel therapies to achieve this. He did however, observe that the difficulty posed by this treatment would be effective targeting, so that the vessels of the tumour are disrupted but no others (17). It took another 60 years for the idea to be seriously appreciated and investigated. Juliana Denekamp and her group demonstrated that the physical obstruction of the blood supply to transplanted tumours in mice, using D-shaped metal clamps, caused tumour cell death directly proportional to the length of the clamping (18). Denekamp over the subsequent years championed the idea of tumour vascular disruption as an anti-cancer treatment.

As William Woglam explained many years ago, the key to the use of vascular targeting therapies is to achieve maximum tumour endothelium disruption while leaving healthy tissue endothelium unaffected. To this end, therapeutics have been developed that take

advantage of the many differences between healthy tissue and tumour endothelium. Such tumour specific disrupting agents can be broadly divided into two types:

1. Small molecule disrupting agents exploit physiological differences between tumour and healthy tissue vasculature to destroy the vessels. This class is primarily made up of microtubule destabilizing agents.
2. Ligand-based VDAs use antibodies, peptides or growth factors that specifically bind to the tumour vasculature and deliver agents that destroy the vessels.

1.2.1 Small molecule VDAs

1.2.1.1 Microtubule destabilizing agents

Tumour endothelium is immature in nature and highly proliferative and thus is dependent on a tubulin cytoskeleton to maintain cell shape (19,20). Tubulin is also essential for cell motility, invasion, attachment and proliferation**.** Mature quiescent vasculature, which supplies most healthy tissues has a far more developed actin cytoskeleton and so is far less dependent on the tubulin cytoskeleton for cellular functions (19). Microtubule destabilizing agents act by disrupting the tubulin cytoskeleton. This has the duel effect of inhibiting spindle formation, leading to mitotic arrest in tumour cells and causing tumour vascular collapse, reducing blood flow. Drugs that block tubulin function therefore, can have both anti-mitotic and anti-vascular effects (21). In practice the dominant mechanism of action for these drugs is to cause mitotic arrest with anti-vascular activity only seen at close to the maximum tolerated dose (MTD) (22).

1.2.1.2 Combretastatin A-4 Disodium Phosphate

Combretastatin A-4 Disodium Phosphate (also known as CA4P, fosbretabulin, Zybrestat) and formulated by Oxigene, was the first microtubule-destabilizing agent observed to have anti-vascular effects below the MTD (23). It is delivered as a pro-drug, which is cleaved to its natural form by endogenous phosphatases. CA4P binds to tubulin disrupting microtubule polymerisation, resulting in mitotic arrest and apoptosis of endothelial cells. In addition it destabilises vascular endothelial cadherin (VE-cadherin) mediated vascular junctions inhibiting the VE-cadherin/ β-catenin/Akt signalling pathway, reducing endothelial cell migration and capillary formation (23).

In experimental tumour models, CA4P causes extensive vascular damage with haemorrhagic necrosis within one hour of treatment, coupled with subsequent tumour growth delay (23-26). The effect of CA4P on the tumour is considerable greater than its effect on the healthy tissue (27). CA4P is the subject of a number of clinical trials for advanced anaplastic thyroid cancer, non-small cell lung cancer, gynaecological cancers and high-grade glioma (Table 1.1). A recent phase II/III clinical trial for advanced anaplastic thyroid cancer showed considerable survival benefit in patients treated with CA4P in combination with chemotherapeutics; 26% of patients treated with CA4P survived one year compared to 9% treated with chemotherapy alone. The clinical trial was, however, halted early due to lack of funding (28). The success of CA4P has led to the development of a number of derivative drugs including Oxi 4503 (Oxigene), Ombrabulin (AVE8062) (Aventis Pharma), which are under investigation in clinical trials (Table 1.1).

1.2.1.3 N-Cadherin antagonist

The adhesive interactions between endothelial cells are essential for the maintenance of functional integrity of the vasculature (29,30). N-Cadherin is a cell surface protein involved in mediating these interactions. A cyclic peptide named ADH-1 competitively inhibits N-Cadherin homotypic binding and has been shown to reduce blood flow and cause haemorrhage necrosis in animal tumour models (31-33). ADH-1 has been investigated in phase I/II trials as a monotherapy and phase I in combination with chemotherapeutics in a range of tumours (Table 1.1). It was well tolerated and showed a modest anti-tumour effect (34,35).

Table 1.1. Small molecule VDAs in the clinic.
Information retrieved from: http://clinicaltrials.gov and http://www.cancer.gov (accessed: 19.1.2016)

Agent	Company	Type	Clinical trials
CA4P (fosbretabulin, Zybrestat)	Oxigene	Microtubule destabilizing agent	Phase III: advanced anaplastic thyroid cancer **(failed to achieve primary endpoints)**, ovarian cancer **(ongoing)** Phase II: fallopian tube cancer, peritoneal cavity cancer, pancreatic cancer, neuroendocrine tumours **(all ongoing)**
Oxi4503	Oxigene	Microtubule destabilizing agent	Phase II: acute myeloid leukaemia **(ongoing)** Phase I: liver and other solid tumours **(Completed with positive data)**
AVE8062 (Ombrabulin)	Sanofi-Aventis	Microtubule destabilizing agent	Phase III: soft tissue sarcoma Phase II: metastatic non-small cell lung cancer, recurrent ovarian cancer **(all failed to achieve primary endpoints) Discontinued**
Dolastatin-10	National Cancer Institute	Microtubule destabilizing agent	Phase II: lymphoma, macroglobulinema, lymphocytic leukaemia, colorectal adenocarcinoma, melanoma, soft tissue sarcoma, breast, liver, prostate, pancreatic, ovarian, renal and non-small cell lung cancer **(outcome data unavailable) Not presently in clinical trials**
ZD6126	AstraZeneca/ Angiogene pharmaceuticals	Microtubule destabilizing agent	Phase II: metastatic renal cell carcinoma and colorectal carcinoma **(failed to achieve primary endpoints) Not presently in clinical trials**
CYT997	Cytopia	Microtubule destabilizing agent	Phase II: glioblastoma and myeloma **(failed to achieve primary endpoints) Not presently in clinical trials**
NPI 2358 (Plinabulin)	Nereus	Microtubule destabilizing agent	Phase III: non-small cell lung cancer **(ongoing)**
BNC-105	Bionomics	Microtubule destabilizing agent	Phase II: renal cell carcinoma **(ongoing)** and ovarian cancer **(terminated)**
DMXAA (Vadimezan, ASA404)	Novartis	Cytokine inducing agent	Phase II: metastatic prostate cancer, non-small cell lung cancer and urothelial carcinoma **(outcome data unavailable) Not presently in clinical trials**
ADH-1 (Exherin)	Adherex Technologies	N-Cadherin antagonist	Phase II: melanoma **(ongoing)** Phase I/II: incurable solid tumours **(Completed with positive data)**

1.2.1.4 Toxicity

Toxicity is an important issue limiting the clinical development of small molecule VDAs. ZD6126 is a phosphate pro-drug of the tubulin-binding agent *N*-acetylcolchinol. The drug disrupts the tubulin cytoskeleton of endothelial cells causing endothelial cell detachment. *In vivo*, ZD6126 was shown to cause endothelial cell retraction, extensive endothelial cell loss (36), a reduction on tumour blood flow (37), and reduced vascularisation (38). ZD6126 was also shown to cause extensive tumour necrosis in a range of animal xenograft models (36,39,40) and inhibit metastasis from lung adenocarcinomas (41). When ZD6126 progressed to clinical trials, however, its was observed to have severe side effects at the clinically required dose. Phase II clinical trials involving ZD6126 for the treatment of metastatic renal cell carcinoma and metastatic colorectal cancer had to be halted in 2006 due to excessive cardio-toxicity (42) and no subsequent clinical trials have been arranged (Table 1.1).

Likewise, almost half of the small molecule VDAs that have reached clinical trials have subsequently had their development halted, often due to insufficient efficacy at dosages with an acceptable level of side effects (42). Clinical trials involving these drugs show side effects that are consistent with anti-vascular activity and include transient hypertension, myocardial infarction, and cardiac ischemia (43). This type of toxicity suggests that small molecule VDAs are having an effect on healthy vasculature as well as other non-cancerous cell types, and therefore the drugs are insufficiently selective for the tumour endothelium. Experimental models have shown that antihypertensive therapy can prevent some of the side effects of tubulin-targeting drugs in particular, without reducing the clinical efficacy of the therapy (43). Another idea that has been suggested to improve the selectivity of this therapy involves incorporating ligands

specific for tumour endothelium in order to better target these small molecule vascular disrupting therapies (44).

1.2.2 Ligand-Directed VDAs

Ligand directed VDAs act directly on the vasculature. Therapeutics of this class are made up of two components joined by chemical cross-linkers or peptide bonds; a ligand, such as an antibody, peptide or growth factor, which binds specifically to the tumour vasculature and an effector, which once delivered to the tumour vasculature, destroys it. These effectors are bioactive molecules, which include, coagulation inducing proteins, toxins, cytokines, apoptosis inducing agents, cytotoxic agents, and radioisotopes.

Burrows and Thorpe (45) were the first to demonstrate that ligand-directed approaches for disrupting the vasculature of tumours could be effective. They set up subcutaneous neuroblastoma tumours in nude mice. The tumours were engineered to express interferon gamma, which induced the vasculature of the tumour to express MHC class II. They targeted the tumour vasculature with a high affinity antibody to mouse MHC class II, coupled with the toxin, ricin. This approach destroyed the tumour vasculature, causing rapid tumour shrinkage, whilst leaving the vasculature of the healthy tissue unaffected (45) (Figure 1.2).

A key requirement for success using this treatment strategy is the discovery of appropriate targets on the tumour vasculature for ligands to bind to and deliver their effector component. Vessels infiltrating and supplying a tumour are exposed to unusual physiological conditions including; hypoglycaemia, severe hypoxia, oxidative stress,

excessive growth factor receptor activation, infiltration of inflammatory cells and cytokine activation, as well as reduced blood perfusion and shear stress (46). These factors lead to distinct cancer vessel gene expression profiles that can be exploited by ligand-targeted therapies. A number of cell surface molecules have been found to be up-regulated on the tumour vasculature when compared to healthy tissue vasculature and the discovery of additional cell surface targets is a continuing quest in this field.

Figure 1.2. Ligand directed VDA induced tumour necrosis. Gross appearance of subcutaneous neuroblastoma tumours treated with an anti-MHC class II immunotoxin. At day 0 the tumours are pink/purple (highly vascular). Two days after treatment the tumour is blackened (indicating massive intra-tumoural haemorrhage). At day 7 the tumour has collapsed into a scab-like plug and by day 10 there is no visible living tumour (45). Image used with permission.

1.2.3 The search for new tumour endothelial markers

The search for new, more specific or more selectively expressed tumour endothelial markers (TEMs) is on-going. The aim is to find markers that allow drugs to be efficiently targeted to the tumour endothelium with appropriate specificity so that the effector dosage at the tumour is sufficient to cause vascular destruction, while ensuring the effector dosage in the healthy tissue vascular bed is below threshold levels for a destructive response. To this end several techniques have and are being used to identify differentially expressed genes on tumour endothelium.

1.2.3.1 Immunohistochemical analysis

Historically, the first markers of tumour endothelium were discovered through extensive immunohistochemical profiling with monoclonal antibodies. The discovery of the tumour specific fibronectin extra-domain B (EDB) was achieved through the observation that antibodies specific to EDB-containing fibronectin stain blood vessels in many cancer types but not most healthy tissues (47-53).

1.2.3.2 *In silico* analysis

In silico techniques have also been used to predict tumour endothelial markers, which can then be further validated (54,55). One group developed a subtractive algorithm to screen publically available sequence tag expression data as a method to identify novel endothelial specific genes (56). The expression of these genes was then screened by *in situ* hybridisation, which identified ROBO4 and EndoPDI as markers of active angiogenesis and tumour endothelium (57,58). Herbert *et al*., 2008 (59), used publically available cDNA libraries, which were split into two pools, one containing

gene expression profile information from non-endothelial cell isolates, cell lines and bulk tissues and the other, endothelial cell isolates. Gene expression from the non-endothelial pool was subtracted from the endothelial pool, thus generating a list of genes with endothelial-restricted expression. This list is employed in chapter 5 to aid with selection of tumour endothelial markers. A second step to the analysis was then performed, subtracting healthy bulk tissue gene expression from tumour bulk tissue. Genes displaying both tumour and endothelial restricted expression profiles were then taken forward as putative tumour endothelial markers. This approach identified 27 genes as being tumour endothelial markers (TEMs) in multiple malignancies (59), including known TEMs such as Robo4 and novel targets such as ECSCR.

1.2.3.3 *In vivo* phage display analysis

In vivo phage display analysis has been used to identify endothelial targets. Vast numbers of phage, each expressing a different protein, are injected into animals (60) or terminally ill patients (61). After a period of time, tumour and healthy tissues are removed, the endothelium recovered and phage specifically localised to the tumour endothelium are isolated and analysed. This method was used to identify an amino-peptidase as a target on breast tumour vasculature (62). Similarly, phage display analysis has been used on laser micro-dissected tissue sections (63), and on tumour-associated endothelial cells in culture (64).

1.2.3.4 *In vivo* protein labelling and isolation

A number of groups have used direct vascular labelling techniques to identify differentially expressed cell surface TEMs. One group perfused tumour-bearing rodents

with silica beads, which stripped the membrane proteins from the surface of the tumour endothelium. From subsequent proteomic analysis of beads perfusing tumour and healthy tissues, a number of cell surface proteins were found to be enriched on tumour endothelium (65). Other groups chemically labelled vascular proteins with biotin (66). The biotinylated cell surface proteins on tumour vasculature, were purified on a streptavidin column and subjected to proteomic analysis, to quantify expression differences between hundreds of cell surface proteins that were identified. A similar approach has also been used *ex vivo* to analyse surgically resected cancerous human kidney and colon (67).

1.2.3.5 Expression profiling of cultured ECs

Researchers have challenged cultured endothelium with various facets of the tumour microenvironment, such as inflammatory or immune cytokines (68), matrix induced vascular tubulogenesis (69) or reduced shear stress (70), with the aim of inducing an expression profile akin to that found in the tumour. By then conducting microarray or RTqPCR based expression analysis on these samples, tumour endothelial markers can be identified.

1.2.3.6 Genetic approaches in animal models

Some groups have used genetically modified animals, where haematopoiesis and vasculogenesis is disrupted, to investigate embryonic blood vessel development. By genetically profiling these mutants, the processes by which embryonic tissue, to which tumours show considerable similarity, acquire their vasculature and how this can been disrupted, was elucidated (71-73).

1.2.3.7 Isolation of tumour associated ECs from tumour resections.

Other researchers have extracted endothelial RNA from clinical samples of various tumours together with paired healthy host tissue and conducted Serial Analysis of Gene Expression (SAGE) (74-76) or microarray analysis (15,77-80) to identify differentially expressed genes between the endothelium derived from the host healthy tissue and the tumour. These approaches have led to the discovery of several tumour endothelial markers (TEMs).

1.2.4. Ligand directed drugs under investigation and in the clinic

A number of the targets identified by these analyses have subsequently been validated for vascular targeting (Table 1.2) and when coupled to bioactive effector molecules (Table 1.3) have shown promise in tumour models and clinical trials (Table 1.4). EndoTAG-1 (Medigene) is composed of the cytostatic drug paclitaxel combined with cationic lipids. The positively charged lipids allow EndoTAG-1 to bind to newly developed, negatively charged endothelial cells that make up the tumour vasculature and selectively deliver paclitaxel to this site. EndoTAG-1 has been successful in two proof-of-concept clinical trials. In a phase II clinical trial for pancreatic cancer EndoTAG-1 in combination with gemcitabine significantly increased survival rates compared to gemcitabine therapy alone (81). A phase II clinical trial involving EndoTAG-1 for the treatment of triple negative breast cancer also showed promising results (82). A phase III clinical trial for this indication is planned (Medigene press statement: http://www.medigene.com/products-pipeline/development-projects/endotag-1) (accessed: 7.8.2015).

Another ligand-directed vascular targeting therapy to progress to clinical trials is L19-IL-2. This molecule is an immunoconjugate consisting of a human single chain Fv antibody fragment, directed against fibronectin ED-B (known to be up-regulated in proliferating tumour vasculature) and a recombinant form of the cytokine IL-2 (known to locally induce a T cell cytotoxic immune response). L19-IL-2 has shown promising results in mouse models of cancer (83,84) and has progressed to human trials, showing clinical activity against advanced solid tumours, including renal cell carcinoma and metastatic melanoma (85,86). Phase II clinical trials for the treatment of advanced pancreatic cancer and metastatic melanoma are on-going.

Table 1.2. Tumour vascular specific targets.

Class	**Examples**	**Reference**
Angiogenesis / Vascular remodelling	Fibronectin ED-A and ED-B domains	(83,87-89)
	Endoglin	(90)
	Extra domains of Tenascin-C	(91)
	Prostate-specific membrane antigen	(92)
	Robo 4	(57)
	TEM7	(75)
	TEM8 / anthrax toxin receptor	(75)
	CD44-related antigen (TES-23)	(93)
	MMP2	(94)
	MMP9	(94)
	STEAP1	(80)
Cell adhesion	Integrins ($\alpha_v\beta_3$)	(95)
	VCAM-1	(96)
	E-selectin	(97)
	CLEC14A	(98,99)
	TEM1 / Endosialin	(75,100)
Thrombosis	Phosphatidylserine phospholipids	(101)
	Tissue factor	(102)
Inflammatory modulation	Annexin A1	(65)

Table 1.3. Effector molecules used in vascular targeting.

Class	Examples	Reference
Coagulation-inducing proteins	Tissue factor	(87,92,96,103)
Toxins	Ricin	(45)
	Diphtheria toxin	(104,105)
Cytotoxic agents	Doxorubicin	(106)
	Paclitaxel	(107)
Cytokines	Interleukin-2	(83)
	Interleukin-12	(88)
	Tumour necrosis factor-α	(108)
Apoptosis-induction	RAF-1 gene	(109)
	Mitochondrial-membrane disrupting peptide	(110)
Radioisotopes	Iodine-131	(111)
	Actinium-225	(112)
	Bismuth-213	(39)

Table 1.4. Ligand directed VDAs in the clinic.
Information retrieved from: http://clinicaltrials.gov and http://www.cancer.gov (accessed: 7.8.2015).

Agent	Company	Target	Description	Clinical trials
EndoTAG-1	Medigene	Negatively charged EC membrane	Cationic lipid directed- cytotoxic	Phase II: advanced pancreatic cancer, triple negative breast cancer, liver tumours
L19-Il2	Philogen	ED-B of fibronectin	Antibody fragment directed Il-2	Phase II: Metastatic melanoma, advanced pancreatic cancer Phase I/II: Advanced renal cancer.
131I-L19	Philogen	ED-B of fibronectin	Antibody fragment directed radioisotope	Phase II: Brain metastasis Phase I: Non small cell lung cancer
111In-J591	Weill Medical College of Cornell University	Prostate-specific membrane antigen	Antibody directed radioisotope	Phase II: Prostate cancer
NGR-hTNF	MolMed	CD13, integrin	Peptide directed TNF	Phase III: pleural mesothelioma Phase II: Soft tissue sarcoma, non small cell lung cancer, ovarian cancer, colorectal cancer, hepatocellular carcinoma

1.3 Project aims 1: Tumour vascular targets

One of the primary aims of the project detailed in this thesis was to profile the tumour vasculature, with the aim of identifying and validating novel tumour specific ligands that can be incorporated into the pipeline of drug development, detailed previously in this section. Work to achieve this, involving magnetic bead isolation of tumour and healthy tissue derived endothelium, microarray transcriptomic analysis and validation of gene and protein expression in tumour and healthy tissue, is detailed in chapters 3, 4 and 5.

1.4 Tumour angiogenesis

Tumours generally arise from a single cell in which several genetic events have occurred, allowing the cell to escape the normal growth control mechanisms in operation in the tissue. Initially the cancer cell can proliferate and develop into a tumour while receiving sufficient oxygen and nutrients by diffusion from the surrounding healthy tissue vasculature. However, as the mass increases the tumour rapidly reaches a point whereby the cancer cells furthest from a blood vessel do not receive sufficient oxygen and nutrients to survive. Further expansion of the tumour is restricted and the tumour remains localised and dormant (6) (Figure 1.3A).

To develop further and metastasise the tumour must develop its own blood supply. The vascularisation of a tumour, known as angiogenesis, is a complex and multistep process, driven primarily by a combination of tumour-associated hypoxia and cellular transformation (113,114). Oncogene activation in tumour cells can result in the secretion of a number of pro-angiogenic growth factors including platelet derived growth factor (PDGF), vascular endothelial growth factor (VEGF) and basic fibroblast growth factor (bFGF) (114). These factors recruit endothelial cells and promote their proliferation and migration to the source of the angiogenic signals, where they create blood vessels (115) (Figure 1.3). It is not only cancerous cells that promote angiogenesis in the tumour. When stimulated by PDGF from the tumour cells, stromal cells and pericytes are known to produce growth factors that support angiogenesis (116). In addition tumour associated hypoxic conditions can lead to the activation of the transcription factor hypoxia inducible factor-1a (HIF-1α) (117) in multiple cell types, including tumour-associated macrophages, leading to the expression of multiple angiogenic factors such as VEGF and PDGF (118). Besides this, in the tumour environment, both pro and anti-angiogenic factors have been found to emanate from endothelial cells, blood and even the extracellular matrix (113).

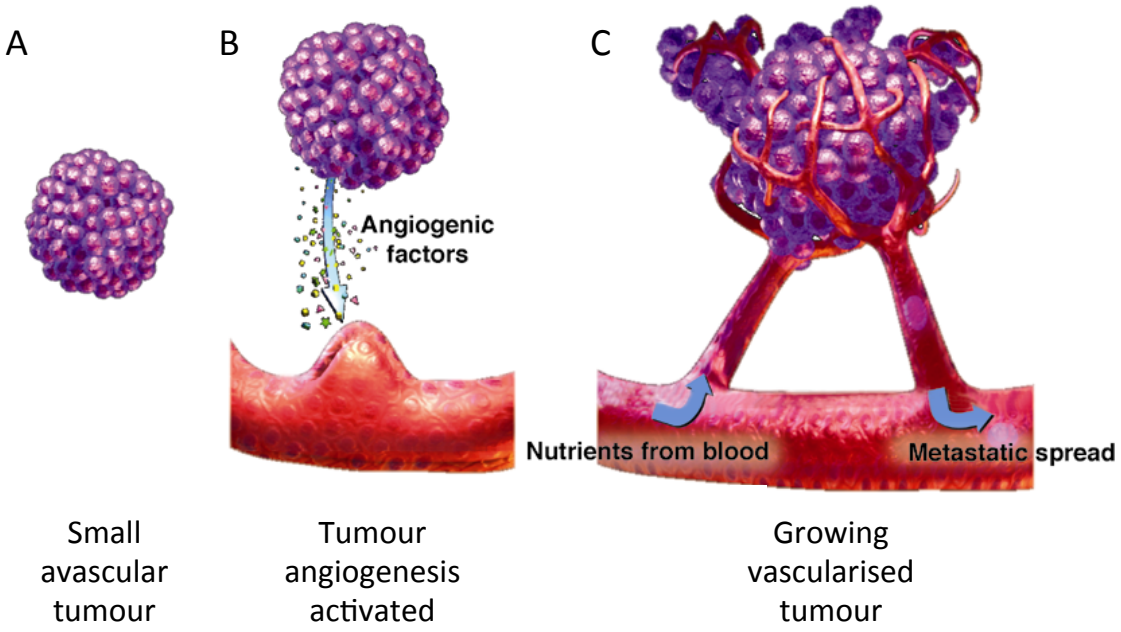

Figure 1.3. Tumour angiogenesis. A, the tumour is initially small and avascular, not exceeding 2 mm^3 in size. B, pro-angiogenic molecules emanating from the tumour initiates sprouting angiogenesis from a nearby capillary. C, The new tumour vasculature supplies nutrients and oxygen, facilitating further growth and metastasis. Tumours additionally vascularise via vessels co-option and other mechanisms. Adapted from (119). Reproduced with permission.

1.5 Angiogenesis inhibitors

Folkman was the first to champion the idea of using therapeutics to inhibit tumour angiogenesis and thus maintain the tumour in a dormant, avascular state (6,120). The majority of successful antiangiogenic therapies have been those developed to target and block VEGF pro-angiogenic signalling pathways in the tumour. These therapeutics are broadly split into three types, blocking antibodies, soluble decoy receptors and small molecule inhibitors.

1.5.1 Blocking antibodies

1.5.1.1 Anti-VEGF antibodies: Bevacizumab

Bevacizumab (Genentech), marketed as Avastin, is a humanised monoclonal antibody that is designed to bind to VEGF, blocking its association with VEGF receptors on endothelial cells and thus blocking angiogenesis (121,122).

In the clinic, with the exception of metastatic renal cell carcinoma (123), no single agent efficacy has been shown with the use of bevacizumab in cancer. It has however been found to improve therapeutic efficacy of chemotherapeutics when used in combination, in colorectal (124), breast (125), and non-small cell lung cancer (NSCLC; (126)). This finding at first glance could appear counterintuitive, as a therapeutic that devascularises the tumour would presumably inhibit the delivery of chemotherapeutics, reducing their efficacy. In 2001, however, Rakesh Jain proposed the now popular "vascular normalisation theory" as explanation for this phenonomon. He proposed that bevacizumab (and perhaps other antiangiogenic therapies), by reducing aberrant and excessive VEGF signalling in the tumour, causes the structural and functional normalisation of the tumour vasculature, reducing interstitial fluid pressure and improving drug penetration, thereby enhancing the efficacy of chemotherapeutic agents (127). This theory has gained widespread acceptance, largely based on preclinical data (reviewed in (128,129)), however despite some examples of structural normalisation and vascular maturation in the clinic (130), to date there is little evidence of improved drug infiltration upon treatment with bevacizumab. Demonstration of reduced perfusion of the chemotherapy, docetaxel, in NSCLC after treatment with bevacizumab (131), has thrown this theory further into controversy. It

is likely therefore that there are other mechanisms, additional to vascular normalisation, mediating bevacizumab-chemotherapy drug synergy.

In 2004 bevacizumab, in combination with irinotecan, fluorouracil and leucovorin, showed efficacy against metastatic colorectal carcinoma in a phase III trial (124). Patients treated with bevacizumab benefited from a 4.7-month increase in overall survival and the result caused the U.S Food and Drug Administration (FDA) to approve the use of bevacizumab for the treatment of colorectal cancer. Similar results against other cancers meant that bevacizumab was approved for the treatment of non-small cell lung cancer in 2006, renal cancer in 2007, breast cancer in 2008 and glioblastoma multiforme in 2009 (Table 1.5). However, its indication in breast cancer was subsequently revoked by the FDA in 2011 because of clinical trial data showing that bevacizumab nether prolonged overall survival nor slowed disease progression sufficiently to outweigh its risk of side effects, which include hypertension, proteinuria, bleeding, thrombotic events and in very rare cases pulmonary embolisms (132).

1.5.1.2 Anti-VEGFR-2 Antibodies: DC101, Ramucirumab and CDP-791

A number of monoclonal antibodies raised against the extracellular domain of VEGFR-2 have been designed to block the binding of VEGF to its receptor and thus inhibit angiogenesis. DC101 was the first drug of this type to show antiangiogenic effectiveness (133). The rat anti-mouse monoclonal antibody (ImClone) has been shown to be a potent antagonist to VEGF binding, VEGFR-2 signalling and endothelial cell proliferation in *in vitro* models (133). In animal models DC101 has been shown to have potent antiangiogenic, antitumour and anti-metastatic activity (133-135).

Studies using DC101 led to the development of ramucirumab (IMC-1121b) (ImClone), a fully human anti-VEGFR2 monoclonal antibody and CDP-791 (Celltech, UCB), a PEGylated, humanised anti-VEGFR-2 F(ab')2 fragment. Ramucirumab has recently been FDA approved for use in gastric or gastro-esophageal junction adenocarcinoma and metastatic non-small cell lung cancer, in combination with paclitaxel and docetaxel respectively, following successful phase III clinical trials (136-138). Ramucirumab is additionally currently in phase II and II clinical trials for the treatment of a range cancers including breast cancer, hepatocellular carcinoma, and metastatic colorectal carcinoma (Table 1.5).

CDP-791 has reached phase II clinical trials against non-small cell lung cancer in combination with carboplatin and paclitaxel, however, its development is currently on hold, as progression-free survival was not improved by CDP-791 treatment in this study (UCB press statement: 01.04.2008: http://www.bionity.com/en/news/80262/ucb-phase-ii-results-for-cdp791-in-non-small-cell-lung-cancer-support-further-clinical-development.html. Accessed: 07.08.2015).

Table 1.5. Antiangiogenic blocking antibodies in the clinic.
Information retrieved from: http://clinicaltrials.gov and http://www.cancer.gov (accessed: 07.08.2015).

Antibody	Company	Antibody type	Target	Indications/ clinical trials
Bevacizumab (Avastin)	Genentech	Humanised IgG1	VEGF-A	**FDA approved for**: first and second line metastatic colorectal carcinoma, first-line advanced non-squamous non-small cell lung cancer, metastatic renal cell cancer, recurrent glioblastoma multiforme. Phase III: ovarian cancer **(ongoing)** **FDA approval revoked for metastatic breast cancer**
Ramucirumab (IMC-1121b)	ImClone Systems	Fully human IgG1	VEGFR-2	**FDA approved for**: second-line advanced gastric or gastro-esophageal junction adenocarcinoma and metastatic non-small cell lung cancer. Phase III: breast cancer, hepatocellular carcinoma, metastatic colorectal carcinoma. Phase II: stomach, renal, bladder, prostate, ovarian cancers and melanoma **(all ongoing)**
CDP-791	Celltech	Pegylated humanised DiFab	VEGFR-2	Phase II: non-squamous non-small-cell lung cancer **(failed to achieve primary endpoints)**
IMC-18F1	ImClone Systems	Fully human IgG1	VEGFR-1	Phase II: breast **(ongoing)**, colorectal and renal cancers **(outcome data unavailable)**

1.5.2 Soluble decoy receptors

Aflibercept, also known as ziv-aflibercept or ZALTRAP (Sanofi-aventis and Regeneron) is a fusion protein incorporating the second binding domain of the VEGFR-1 receptor and the third domain of the VEGFR-2 receptor (139). It binds VEGF with high affinity (Kd~1pM) (140) and so acts as a potent competitive inhibitor of VEGF-R binding. Aflibercept has been shown to be a potent angiogenesis inhibitor (140), and is highly effective against neovascularisation related macular degeneration (141). Aflibercept is the subject of clinical trials against a number of cancers. A phase III clinical trial involving aflibercept in combination with docetaxel and dexamethasone for the treatment of non-small-cell lung cancer reported that aflibercept improved progression

free survival but not overall survival relative to placebo (142). However, a phase III trial involving aflibercept in combination with Irinotecan, 5-Fluorouracil, and Leucovorin for the treatment of metastatic colorectal cancer reported that aflibercept improved overall survival relative to placebo (143). Because of this trial, in 2012 FDA approval was given for this drug to be used against metastatic colorectal cancer.
A subsequent phase III clinical trial, involving aflibercept for the treatment of metastatic colorectal cancer, also showed statistically significant improvements in overall survival, progression free survival and overall tumour response rate, relative to placebo (144). This trial provides further support for the use of aflibercept against metastatic colorectal cancer.

1.5.3 Small molecule inhibitors

The small molecule inhibitors are an alternative form of antiangiogenic therapy. Rather than blocking the binding of VEGF to its receptor, they block angiogenesis by inhibiting downstream signalling from the activated proangiogenic receptors in the endothelial cells. Drugs of this class are receptor tyrosine kinase inhibitors. They bind to and inhibit the kinase activity of certain receptor tyrosine kinases (RTKs) such as the VEGFRs. VEGFRs are not the only receptor tyrosine kinases involved in cancer, or normal cellular functions however. Unlike targeted anti-VEGF signalling therapies discussed previously, this therapeutic class additionally blocks other pathways involved in angiogenesis and tumourgenesis and thus has antitumour, as well as anti-angiogenic activity (145) (Table 1.6). Additionally small molecule inhibitors are orally available

and therefore cheaper to manufacture and administer to patients than many anti-VEGF signalling therapies.

Five antiangiogenic small molecule inhibitors have received FDA approval for use against various malignancies. Sorafenib (Bayer and Onyx pharmaceuticals), sunitinib, axitinib (both Pfizer) pazopanib (GlaxoSmithKline) and vandetanib (Astrazeneca) are collectively approved for the treatment of renal cell carcinoma, gastrointestinal stromal tumours, pancreatic tumours, hepatocellular carcinoma, soft tissue sarcoma and medullary thyroid cancer. These drugs and those of their class are also undergoing many clinical trials in other tumour types (Table 1.6).

Unlike bevacizumab, RTKIs predominantly display a direct antiangiogenic effect, with a number of the drugs of this class showing significant single agent activity in the form of tumour growth inhibition and devascularisation, in both clinical and preclinical settings (145). Indeed sorafenib, sunitinib, pazopanib and axitinib are licensed as monotherapies, suggesting that these drugs may mediate their anti-cancer effect in quite a distinct manner to bevacizumab. Some newer antiangiogenic RTKIs (cediranib and tivozanib) have shown aspects of vascular normalisation (the widely accepted method of action of bevacizumab) (146,147). However like bevacizumanb, no compelling evidence of improved perfusion of the tumour has been demonstrated for this type of therapy in the clinic. This could be due to dosing, however. Low dose (20mg/ml) sunitinib was shown to improve the tumour distribution of temozolomide in a preclinical model of glioma, when compared to controls. High dose sunitinib (60mg/ml) on the other hand, reduced perfusion of the drug (148). Despite the lack of

obvious mechanistic synergy in humans, several clinical trials are underway to investigate the effectiveness of antiangiogenic RTKis in combination with tumour cell directed therapy (e.g. chemotherapy and radiotherapy).

Table 1.6. Antiangiogenic small molecule inhibitors in the clinic. Information retrieved from: http://clinicaltrials.gov and http://www.cancer.gov (accessed: 07.08.2015).

Inhibitor	Alternative names	Company	Activity	Indications/clinical trials
Sunitinib	Sutent, SU11248	Pfizer	VEGFR-2, PDGFRα & β, c-kit, Flt3, RET	**FDA approved for**: first and second line treatment for metastatic renal cell carcinoma, gastrointestinal stromal tumours. progressive, unresectable, neuroendocrine pancreatic tumours Phase III: breast **(failed to achieve primary endpoints repeatedly, but trials ongoing)**, colorectal and lung cancer **(ongoing)**
Sorafenib	Nexavar, BAY 43-9006	Bayer HealthCare Pharmaceuticals and Onyx Pharmaceuticals	VEGFR2 & 3, Raf, PDGFRβ, Flt3 and c-kit	**FDA approved for**: unresectable hepatocellular carcinoma, advanced renal cell carcinoma Phase III: non-small cell lung carcinoma and melanoma **(failed to achieve primary endpoints in both)**
Pazopanib	Armala, GW786034	GlaxoSmithKline plc	VEGFR1-3, PDGFRα & β, c-kit	**FDA approved for**: renal cell carcinoma, soft tissue sarcoma Phase II: non-small cell lung carcinoma **(failed to achieve primary endpoints)**, ovarian cancer **(ongoing)** Phase I: colorectal cancer
Axitinib	AG-013736 Inlyta	Pfizer	VEGFR1-3, PDGFRβ, c-kit	**FDA approved for**: second line treatment for renal cell carcinoma Phase III: pancreatic cancer **(failed to achieve primary endpoints)** Phase II: lung, gastrointestinal, thyroid and breast cancer **(ongoing)**
Vandetanib	Zactima, ZD6474	Astrazeneca	VEGFR1-3, PDGFRβ, EGFR, RET	**FDA approved for**: medullary thyroid cancer Phase III: non small cell lung carcinoma **(ongoing)**
Cediranib	Recentin, AZD2171	Astrazeneca	VEGFR1-3, PDGFRα & b, c-kit	Phase III: recurrent ovarian, fallopian tube, primary peritoneal cancer, glioblastoma, colorectal cancer **(all ongoing)**, non small cell lung carcinoma **(failed to achieve primary endpoints)**
Vatalanib	PTK787, ZK222584 Caprelsa	Novartis	VEGFR1-3, PDGFRα & b, c-kit	Phase III: Colorectal carcinoma **(failed to achieve primary endpoints)** Phase II: Metastatic neuroendocrine tumours, Brain and central nervous system tumours, sarcoma **(outcome data unavailable)**
Brivanib alaninate	BMs-582664	Bristol-Myers Squibb	VEGFR1–3, FGFR1-3	Phase III: colorectal cancer, hepatocellular carcinoma **(ongoing)** Phase II: multiple tumour types **(ongoing)**
Nintedanib	Vargatef BIBF 1120	Boehringer ingelheim	VEGFR1–3, PDGFRα & β, FGFR1–3, Flt3, Src, Fyn, Lck	Phase III: Non small cell lung cancer (NSCLC), Ovarian cancer **(ongoing)** Phase II: Breast cancer, prostate cancer, acute myeloid leukaemia, glioblastoma, hepatocellular carcinoma, colorectal cancer, high grade glioma **(all ongoing)**
Tivozanib	KRN951, AV-951	AVEO Pharmaceuticals, Inc.	VEGFR-2, PDGFR-β, c-Kit	Phase III: renal cell carcinoma **(completed with positive results but insufficient for FDA approval)**

1.6 Antiangiogenic therapy resistance

Antiangiogenic therapies have had great success in treating a number of solid tumours as demonstrated by FDA approval for their use against nine different malignancies. They are primarily used in advanced or metastatic settings and rarely provide long-term survival benefits. Long-term PFS on antiangiogenic drugs is prevented by the almost inevitable acquisition of resistance to the treatment. Additionally tumours often return with a more aggressive, invasive and metastatic phenotype. Because of this, the survival benefits provided by antiangiogenic treatments in the clinic are often measured in months, rather than years (149-151).

There is a considerable need for research into why certain tumours are unresponsive to antiangiogenic treatments and why initially sensitive tumours frequently then progress after a short period of stasis or shrinkage (152-154) (Figure 1.4). The current hypothesis is that tumours adapt to therapeutic blockade of angiogenesis by acquiring new mechanisms to functionally evade it (149,152,155). Current experimental evidence suggests five distinct adaptive mechanisms employed by the tumour and surrounding tissue, to evade inhibition.

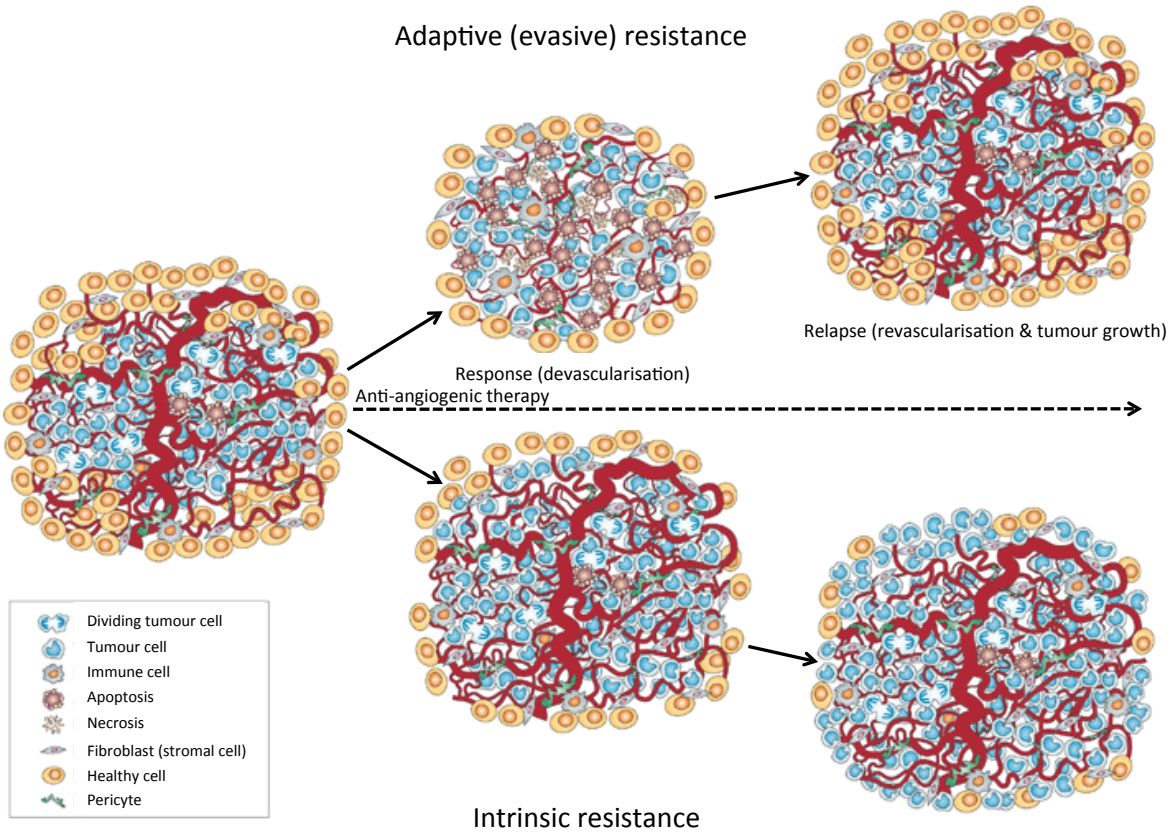

Figure 1.4. Modes of anti-angiogenic therapy resistance. Tumours respond to antiangiogenic therapy in two distinct ways. Either the tumour initially responds, via devascularisation and tumour shrinkage, with increased apoptosis and necrosis. After a time however, the tumour reestablishes its vascular network and ceases to respond to anti-angiogenic blockade, becoming adaptively resistant. Alternatively the tumour never responds to anti-angiogenic at all and is considered intrinsically resistant. Adapted from (149), reproduced with permission.

1.6.1 Evasive resistance by up regulation of alternative pro-angiogenic signalling pathways within the tumour

An elegant example of adaptation to evade the actions of anti-angiogenic agents was observed in a preclinical trial of the monoclonal VEGFR blocking antibody (DC101) in murine pancreatic neuroendocrine cancer (*Rip1-Tag2*) (156). The antibody initially elicited a response in the form of tumour stasis and reduced vascularity. However, this responsiveness was short lived, after 10-14 days the tumour regrew and dense vasculature was restored. This response suggested a reinitiation of tumour angiogenesis bypassing the monoclonal VEGFR blockade. The investigators found that the relapsing tumours had heightened expression levels of a number of angiogenic factors, including several members of the fibroblast growth factor family, ephrin A1 and A2 as well as angiopoietin-1 (156). To confirm that these expression changes were responsible for cancer relapse, tumours were first treated with the monoclonal antibody, but after the 10-14 day responsive phase had elapsed, a second line treatment consisting of an FGFR-FC fusion protein, shown to suppress signalling through the FGF ligands, was used to treat the tumour. The investigators found that tumour growth was slowed and revascularisation attenuated relative to untreated controls. This result indicated that FGF signalling played a part in the tumour relapse (156) and that dual targeting of the VEGF/FGF pathways could slow the onset of resistance. Preclinical evaluation of brivanib alaninate, a dual inhibitor of VEGFR and FGFR, showed it to be effective both as a first line therapy and as a second line therapy against tumours that had relapsed on sorafenib or DC101 treatment (157). In the BRISK-PS phase III clinical trial however, brivanib alaninate treatment failed to

improve survival over placebo, in patients with hepatocellular carcinoma that had relapsed under sorafenib treatment (158).

Another study showed that the angiogenic capability of tumours deficient in a key inducer of VEGF expression, hypoxia-inducible factor 1a (HIF1a), could be saved by inducing the expression of the pro-angiogenic cytokine interleukin-8 (IL-8) (159). This suggests that over-expression of IL-8 could be one of the mechanisms used by tumours to evade VEGF signalling blockade.

In agreement with this, a study showed that tumours in which growth was initially halted by ectopic expression of the angiogenesis inhibitors; thrombospondin, tumstatin and endostatin, quickly bypassed growth inhibition by up-regulating a number of pro-angiogenic factors such as, PDGF, FGF and VEGF (160).

1.6.2 Recruitment of pro-angiogenic cells

Cells under hypoxic stress caused by anti-angiogenic therapy induced vessel regression have been shown to recruit various bone marrow derived cells (BMDCs) that elicit a pro-angiogenic response, fuelling the tumour (161,162). These pro-angiogenic BMDCs consist of vascular progenitors and vascular modulatory cells, either differentiating into new endothelial cells and pericytes, or expressing various cytokines and growth factors that promote vascular development (161,162).

1.6.3 Rapid vascular remodelling by recruitment of pericytes

Several groups have observed that although there is a substantial reduction in vascularity in tumours treated with VEGF signalling inhibitors, a small population of functional vessels remain, which are morphologically distinctive from untreated

tumour vasculature. These vessels are far thinner, less dilated and far more densely covered in pericytes (163,164). These observations suggest that endothelial cells recruit pericytes to protect against VEGF signalling blockade-induced death. In support of this suggestion, it has been observed that vessels with low pericyte coverage are more sensitive to VEGF inhibition (163,165).

1.6.4 Increased local invasion and vessel co-option, mitigating the need for neovascularisation

It has been widely observed that some angiogenically inhibited tumours become more invasive than they were before treatment (150,151). This increased invasive phenotype was first observed in orthotropic mouse models of glioblastoma multiforme (GBM), in which angiogenesis was thwarted either by deletion of a number of angiogenic factors, VEGF, HIF1α, matrix metalloproteinase 9 (MMP9) or by treatment with the VEGF inhibitor semaxanib. In these models the tumours were found to adapt to angiogenic inhibition by becoming more invasive, extensively infiltrating into the brain (166-168). It was suggested that the glioblastoma cells managed to maintain vascular sufficiency, and so continue to grow, by co-opting healthy tissue vessels, migrating along these vessels and thus dispersing throughout the brain. This response was also observed in clinical trials of bevacizumab therapy in GBM (169,170).

Vessel co-option has been observed in a range of tumours as an alternative method of tumour vascularisation, independent of angiogenesis (171). It is most reported in tumours of highly vascular tissues, such as the brain, liver and lungs, with 10-30% of lung tumours using this method to maintain vascular sufficiency (172). Vessel co-option is therefore of great interest as a potential method by which tumours can

become resistant to antiangiogenic therapy (172). Certainly the tumour stromal architecture, including the utilisation of co-opted vessels, has been reported to be predictive of intrinsic resistance to antiangiogenic therapy (173).

1.6.5 Increased distant metastasis

Besides increased local invasion, potentially mediated by a switch towards vessel co-option, there is extensive preclinical data suggesting that metastatic seeding of tumour cells is enhanced by antiangiogenic therapy usage (150,151). This effect is not universal however, being dependent on tumour type and cell line (174), the class of therapy used (TKI vs. monoclonal anti-VEGF antibody) (175) and drug dosage (174,176). Additionally there is little substantive evidence suggesting this effect is recapitulated in the clinical setting (177). Nevertheless the potential for antiangiogenic therapies to enhance metastasis is still an area of great concern and research, due to the potential for a patient's condition to be worsened by this type of therapy in certain settings.

1.6.6 Selection of resistant endothelium

There is increasing interest in the role endothelial cells play in mediating antiangiogenic resistance. Isolated endothelium from hepatocellular carcinoma were found to behave quite differently from healthy liver endothelium in culture. They exhibited an increased rate of migration and proliferation, were far less dependent on growth factors for their survival as well as being more resistant to antiangiogenic and other chemotherapeutic treatments (178). This result suggests that the tumour endothelium is quite adaptive and that the environment within the tumour could

induce permanent epigenetic changes, which reduce endothelial responsiveness to anti-angiogenic therapies.

1.6.7 Tumour cell metabolic change

Over the last decade increasing evidence points to the role of hypoxia induced metabolic changes in the acquisition of resistance. Many studies report an increase in tumour hypoxia induced by antiangiogenic therapy (reviewed in (179)), in line with the expected mode of operation of most anti-angiogenic therapies (namely devascularisation). This increased hypoxia has been reported to result in the activation of a number of gene transcription programs, including HIF1 and HIF2, the unfolded protein response (UPR) (180) and ATF4 (181), making fundamental changes to energy metabolism in the tumour. HIF induced changes to genes regulating glycolysis and oxidative phosphorylation were found to be responsible for bevacizumab resistance in glioblastoma (182). Increase tumour cell autophagy has also been reported as a response to antiangiogenic blockade (183). A recent study charting metabolic changes in a range of tumour xenographs, occurring after removal of sorafenib and sunitinib treatment, revealed a rapid shift from glycolysis to lipid metabolism, concurrent with a drastic increase in metastatic tumour spread (184). In summary, antiagiogenic blockade appears to induce drastic changes in tumour cell metabolism, potentially via a normal physiological response to hypoxia, which at least in part leads to a loss of tumour cell sensitivity to antiangiogenic therapy.

1.6.8 Innate insensitivity to antiangiogenic therapy

A significant minority of patients enrolled in clinical trials, where the efficacy of antiangiogenic drugs was tested, are documented to fail to respond at all to treatment (Figure 1.4). There is no discernable beneficial effects from treatment, no tumour shrinkage or stasis and no improvement in quality of life or survival (154). It is possible that the tumours of these patients adapted to anti-angiogenic treatment before any benefit could be observed, but a more plausible explanation is that these tumours have intrinsic resistance to anti-angiogenic therapy (149). The mechanism of resistance could be quite similar to that of tumours that gain resistance, however, the necessary changes have been driven by pressures from the intrinsic tumour microenvironment rather than by pressures from anti-angiogenic treatment (149). VEGF is not the only growth factor capable of mediating angiogenesis in the tumour. Some tumours may be intrinsically resistant to VEGF targeted antiangiogenic therapies because their vasculature has developed to be dependent on a different angiogenic growth factor, such as FGF or IL-8.

Given the considerable proportion of people who don't respond or respond very poorly to antiangiogenic therapies, there appears to be a need for predictive biomarkers of response, so that those for whom antiangiogenic therapy would be effective can be identified. A few potential biomarkers have been identified from clinical trials, such as VEGF polymorphisms or pharmacodynamics changes induced by antiangiogenic treatment (185), but further analysis is warranted.

1.7 Project aims 2: Antiangiogenic therapy resistance

The other primary aim of this project was to investigate the development of antiangiogenic small molecular inhibitor therapy resistance *in vivo*, with particular focus on the molecular mechanisms behind enhanced metastatic growth after treatment relapse. This being an area of paticular concern, due to the potential for treatment to worsen the status of the patient if metastasis is enhanced. As discussed however, there are many other potential factors limiting the efficacy of antiangiogenic therapy use, including vessel co-option, the use of alternative pro-angiogenic growth factors and the metabolic adaption of cancer cells to hypoxia and attention will be paid to some of these factors as well.

For this purpose the 4T1 syngeneic model of metastatic breast cancer was selected. This is one of the very few genuine *in vivo* metastatic models. It is a faithful model of spontaneous lymphatic metastasis from a primary mammary tumour (186). Chapter 6 of this thesis reports the development of a reliable model of breast cancer growth and metastasis in which both primary tumour growth and metastasis can be readily traced *in vivo* and *ex vivo*.

Sunitinib was selected as the drug of choice for the investigation of post-treatment relapse, as it has repeatedly failed to achieve primary endpoint goals of prolonged progression free survival and overall survival in phase III trials of metastatic breast cancer, as a monotherapy (187) or in combination with chemotherapy (188-190), compared with standard-of-care, with only overall response rate being improved in combination with docetaxel, compared with docetaxel alone (189). Consequently

sunitinib has been broadly dismissed as a therapeutic agent in breast cancer. Despite this, the molecular mechanisms behind this treatment failure warrant investigation, as it can inform about the nature of antiagiogenic resistance applicable to other malignancies.

Chapter Two

Materials and Methods

2.1 Materials

Table 2.1. Equipment used for the research detailed in this thesis.

Equipment	Product code	Manufacturer
Barnstead Nanopure diamond water purifier (for deionised water)	D11901	Thermo Scientific, Walmington, UK
Magnetic particle concentrator	123-21D	Invitrogen, Paisley, UK
Nanodrop	1000	Thermo Scientific, Walmington, UK
Agilent Bioannalyser	2100	Agilent, Stockport, UK
High Resolution Microarray Scanner	G2565CA	Agilent, Stockport, UK
Rotor-gene	RG-3000	Qiagen, Manchester, UK
Light and fluorescent microscope	DM6000	Leica, Milton Keynes, UK
60°C Baking oven	HIS25	Grant Boekel Scientific, Feasterville, USA
Gyro-Rocker	SSL3	Stuart, Stone, UK
Roller-mixer	SRT6D	Stuart, Stone, UK
Block heater	SBH200D	Stuart, Stone, UK
AccuSPIN 17R Micro centrifuge	13-100-676	Fisher Scientific, Loughborough, UK
Mikro 22R Refrigerated centrifuge	C1110	DJB Labcare, Newport Pagnell, UK
Heraeus Labofuge 400R microplate centrifuge	75008371	Thermo Scientific, Walmington, UK
Category 2 tissue culture hood	Holten Lamin air	Thermo Scientific, Walmington, UK
Cell culture incubator CO_2 incubator	INCUsafe	Sanyo, Osaka. Japan
Haemocytometer	0630010	Marienfeld, Lauda-Königshofen, Germany
Acumen high content screening machine	eX3	TTP labtech, Melbourn, UK
IVIS Spectrum Preclinical In Vivo Imaging System	IVISSPE	PerkinElmer, Waltham, USA

Table 2.2. Chemicals and drugs used for the research detailed in this thesis.

Chemicals / drugs	Product code	Manufacturer
Sodium azide (NaN_3)	S8032	Sigma-Aldrich, Gillingham, UK
Glycine	G8898	Sigma-Aldrich, Gillingham, UK
Tetramethylethylenediamine (TEMED)	T9281	Sigma-Aldrich, Gillingham, UK
Ammonium persulphate (APS)	A3678	Sigma-Aldrich, Gillingham, UK
Sodium chloride (NaCl)	S9625	Sigma-Aldrich, Gillingham, UK
IGEPAL CA-630	I8896	Sigma-Aldrich, Gillingham, UK
Deoxycholic acid (DOC)	D2510	Sigma-Aldrich, Gillingham, UK
Sodium dodecyl sulfate (SDS)	A1112,0100	AppliChem, St Louis, USA
Bromophenol blue	B0126	Sigma-Aldrich, Gillingham, UK
Glycerol	G5516	Sigma-Aldrich, Gillingham, UK
Tris(hydroxymethyl)aminomethane (Tris)	T1503	Sigma-Aldrich, Gillingham, UK
Dithiothreitol (DTT)	43819	Sigma-Aldrich, Gillingham, UK
Triton X-100	T8787	Sigma-Aldrich, Gillingham, UK
Propidium iodide	P4170	Sigma-Aldrich, Gillingham, UK
Actinomycin D	A9415	Sigma-Aldrich, Gillingham, UK
Phosphate buffered saline (PBS)	P4417	Sigma-Aldrich, Gillingham, UK
Qiazol lysis reagent	79306	Qiagen, Manchester, UK
Express qPCR Supermix	A10312	Invitrogen, Paisley, UK
Histoclear	HS-200	National diagnostics, Hessle, UK
Ethanol	20821-330	VWR chemicals, East Grinstead, UK
Hydrogen peroxide	H1009	Sigma-Aldrich, Gillingham, UK
Casein solution	SP-5020	Vector labs, Orton, UK
Ethylenediaminetetraacetic (EDTA)	E5134	Sigma-Aldrich, Gillingham, UK
Tween 20	P1379	Sigma-Aldrich, Gillingham, UK
Mayers Haematoxylin solution	MHS32	Sigma-Aldrich, Gillingham, UK
Surgipath Eosin Y-alcoholic solution	01602	Leica, Milton Keynes, UK
Formaldehyde	252549	Sigma-Aldrich, Gillingham, UK
Bisbenzimide	B1155	Sigma-Aldrich, Gillingham, UK
Acetone	A/0520/17	Fisher Scientific, Loughborough, UK
Polybrene	107689	Sigma-Aldrich, Gillingham, UK
Puromycin dihydrochloride	P8833	Sigma-Aldrich, Gillingham, UK
D-luciferin	122799	PerkinElmer, Waltham, USA
Dimethyl sulfoxide (DMSO)	D2650	Sigma-Aldrich, Gillingham, UK
Sunitinib malate	S1042	Selleck Chemicals, Houston, US
Acrylamide Protogel	A2-0072	National diagnostics, Hessle, UK
Gentamicin/amphotericin	R-015-10	Gibco, Paisley, UK
Penicillin-streptomycin	15140-122	Gibco, Paisley, UK

Table 2.3. Organic products and culture media used for the research detailed in this thesis.

Organic products and culture media	Product code	Manufacturer
Bovine serum albumin (BSA)	421501L	VWR chemicals, East Grinstead, UK
Milk	92964	Marvel, St Albans, UK
RNAse free DNAse	79254	Qiagen, Manchester, UK
RNAse A	19101	Qiagen, Manchester, UK
Collagenase type V from *Clostridium histolyticum*	C9263	Sigma-Aldrich, Gillingham, UK
Biotyinylated lectin from *Ulex europaeus*	L8262	Sigma-Aldrich, Gillingham, UK
Medium 199 (M199)	M2154	Sigma-Aldrich, Gillingham, UK
High glucose Dulbecco's Modified Eagle Medium (DMEM)	51435C	Sigma-Aldrich, Gillingham, UK
Optimem	31985070	Gibco, Paisley, UK
L-Glutamine	25030	Gibco, Paisley, UK
Heparin sodium salt from porcine intestinal mucosa	H3149	Sigma-Aldrich, Gillingham, UK
Collagenase 1A from *Clostridium histolyticum*	C9891	Sigma-Aldrich, Gillingham, UK
Gelatin from porcine skin	04055	Sigma-Aldrich, Gillingham, UK
Fetal calf serum (FCS)	10270	PAA, Cambridge, UK
Trypsin-EDTA	L11-003	PAA, Cambridge, UK
Recombinant human VEGF-165	100-20	Peprotech, London, UK
Brain extract (prepared as described in (191))	N/A	N/A

Table 2.4. Kits used for the research detailed in this thesis.

Kits	Product code	Manufacturer
miRNeasy mini kit	217004	Qiagen, Manchester, UK
Low Input Quick Amp Labelling Kit, One-Color	5190-2305	Agilent, Stockport, UK
SurePrint G3 Human Gene Expression 8x60K v2 Microarray kit	G4851B	Agilent, Stockport, UK
SurePrint G3 Mouse Gene Expression v2 8x60K Microarray Kit	G4852B	Agilent, Stockport, UK
High-capacity cDNA reverse transcription kit	4368813	Invitrogen, Paisley, UK
Universal Probe Library set, Human	04683633001	Roche, Burgess Hill, UK
ImmPRESS universal secondary antibody (rabbit and mouse IgG)	MP-7500	Vector labs, Orton, UK
ImmPRESS anti-rabbit secondary antibody	MP-7401	Vector labs, Orton, UK
ImmPACT NovaRed peroxidase HRP substrate	SK-4805	Vector labs, Orton, UK
RNAiMAX lipofectamine transfection reagent kit	13778030	Invitrogen, Paisley, UK
Lipofectamine 2000 transfection reagent kit	11668027	Invitrogen, Paisley, UK
ECL prime western blotting detection reagent kit	45-002-401	GE Healthcare, Amersham, UK
CellTiter 96® AQueous One Solution Cell Proliferation Assay (MTS)	G3582	Promega, Southampton, UK

Table 2.5. Human tissue arrays used for the research detailed in this thesis.

Tissue arrays	Product code	Manufacturer
Human, common cancers (1)	MA2	Superbiochip, Seoul, Korea
Human, normal matching tissue of MA2	MAN2	Superbiochip, Seoul, Korea
Human, common cancers (2)	MB4	Superbiochip, Seoul, Korea
Human, normal matching tissue of MB4	MBN4	Superbiochip, Seoul, Korea
Human, common cancers (3)	MC4	Superbiochip, Seoul, Korea
Human, normal matching tissue of MC4	MCN4	Superbiochip, Seoul, Korea
Human, colorectal cancer	CD4	Superbiochip, Seoul, Korea
Human, normal colon and rectum (matching CD4)	CDN4	Superbiochip, Seoul, Korea
Human, colorectal cancer-metastasis-normal	CDA3	Superbiochip, Seoul, Korea
Human, Kidney cancer	CL2	Superbiochip, Seoul, Korea
Kidney clear cell carcinoma	Hkid-CRC180Sur-01	US biomax, Rockville, USA
Kidney cancer with matched normal adjacent tissue and metastatic carcinoma	KD951a	US biomax, Rockville, USA
Kidney disease spectrum (kidney cancer progression)	BC07001	US biomax, Rockville, USA
Kidney disease spectrum (renal cancer progression)	KD807	US biomax, Rockville, USA

Table 2.6. Other materials used for the research detailed in this thesis.

Other materials	Product code	Manufacturer
PVDF immobilon transfer membrane	IPFL00010	Merck-Millipore, Darmstadt, Germany
Amersham Hyperfilm™ ECL	10534205	GE Healthcare, Amersham, UK
100 µm cell strainer	352360	BD Falcon, Oxford, UK
8µm pore well inserts		
Corning® Costar® 6-well plate	CLS3516	Sigma-Aldrich, Gillingham, UK
Corning® Costar® 12 well plate	CLS3512	Sigma-Aldrich, Gillingham, UK
Corning® Costar® 24 well plate	CLS3527	Sigma-Aldrich, Gillingham, UK
Scalpel	GC686	Swann-Morton, Sheffield, UK
ProLong Gold mounting media not containing DAPI	P36930	Invitrogen, Paisley, UK
ProLong Gold mounting media containing DAPI	P-36931	Invitrogen, Paisley, UK
Streptavidin coated M-280 dynabeads	11205D	Invitrogen, Paisley, UK
Sheep anti-rat IgG coated M-280 dynabeads	11035	Invitrogen, Paisley, UK
Distyrene–plasticiser–xylene resin	06522	Sigma-Aldrich, Gillingham, UK

Table 2.7. Solution formulations used for the research detailed in this thesis.

Solutions:	**Constituents:**
Tissue digestion solution	Dulbecco's Modified Eagle Medium (DMEM), 25mg/ml Collagenase type V, 7.4 µg/ml Actinomycin D and 3.6 kunits DNAse
RTqPCR reaction mix	1µl forward primer (10µM), 1µl reverse primer (10µM), 0.25µl of the appropriate probe from the Universal Probe Library set, Human, 0.25µl deionised water, 12.5µl Express qPCR Supermix
Antigen unmasking solution	0.1mM EDTA pH 8, 0.01% Tween 20 in distilled water
Propidium iodide staining solution	0.1% Triton X-100, 100 ug/mL RNAse A and 10 ug/mL propidium iodide made up in PBS
RIPA buffer	150 mM NaCl, 1% IGEPAL CA-630, 0.5% DOC, 0.1% SDS and 50 mM Tris-HCl pH 7.5 in deionised water
SDS loading buffer	200 mM Tris HCL pH 6.8, 8% SDS, 0.4% bromophenol blue, 40% glycerol and 400 mM DTT
8% SDS-polyacrylamide gel	Resolving gel: 8% acrylamide, 0.1% SDS, 375 mM Tris-HCl pH 8.8, 0.1% APS, 0.06% TEMED in deionised water. Stacking gel: 4.5% acrylamide, 0.1% SDS, 125 mM Tris-HCl, pH 6.8, 0.1% APS, 0.1% TEMED in deionised water
Running buffer	0.1% SDS, 25 mM Tris, 192 mM Glycine in deionised water
Transfer buffer	10 mM Tris, 100 mM glycine, 0.005% SDS in deionised water
PBS-Tween	0.1% Tween in PBS
Primary endothelial cell growth media (cM199)	Medium 199, 10% fetal calf serum (FCS), 2 mM L-Glutamine, 100 U/ml penicillin-streptomycin, 90 ug/ml heparin and 0.3% brain extract
Low serum endothelial growth media (lsM199)	Medium 199, 1% fetal calf serum (FCS), 2 mM L-Glutamine, 100 U/ml penicillin-streptomycin, 90 ug/ml heparin
Cancer cell line growth media (cDMEM)	High glucose Dulbecco's Modified Eagle Medium, 10% FCS, 100 U/ml penicillin-streptomycin and 2 mM L-glutamine

Table 2.8. Plasmids used for the research detailed in this thesis.

Plasmids	**Details**
MSCV-LUC	MSCV plasmid (Clonetech) containing the luciferase gene, generated by the Hwang group (192).

Table 2.9. Cultured cells used for the research detailed in this thesis.

Cultured cells	**Details**
4T1	Murine breast cancer cell line of BALB/c origin, distributed by ATCC, Teddington, UK (product code: CRL-2539).
4T1-LUC	4T1 cell line containing the MSCV-LUC plasmid.
RENCA	Murine renal adenocarcinoma cell line of BALB/c origin, gift of the Reynolds group.
HUVEC	Human umbilical vein endothelial cells, extracted from a human umbilical cord by the Bicknell group.
HDMEC	Human dermal micro-vascular endothelial cells of multiple origins distributed by PromoCell, Heidelberg, Germany (product code: C-12210).
Phoenix-Ampho	293T derived cell line containing retroviral packaging constructs, generated by the Nolan lab (193).

Table 2.10. Antibodies used for the research detailed in this thesis.

Target	Antibody type	Product code	Manufacturer	Region of recognition	Application and Concentration
Human MCAM	Rabbit polyclonal	HPA008848	Sigma-Aldrich, Gillingham, UK	225-374aa (Extracellular region)	1.500-1.1000 (IHC) 1.1000 (WB) [0.3-0.6 µg/ml]
Human LAMA4	Rabbit polyclonal	HPA015693	Sigma-Aldrich, Gillingham, UK	638-777aa	1.200 (IHC) [0.5 µg/ml]
Human PECAM	Mouse monoclonal	JC70A	Dako, Cambridge, UK	Cell membrane preparation from the spleen of a patient with hairy cell leukaemia	1.100 (IHC) [2 µg/ml]
Human GRIN2D	Vaccinated rabbit serum	Custom-7GB14072-686	Eurogenetec, Southampton, UK	1-78aa (Extracellular region)	1.500 (IHC)
Mouse PECAM (1)	Rabbit polyclonal	ab28364	Abcam, Cambridge, UK	C-terminus	1.200 (IF)
Mouse PECAM (2)	Rat monoclonal	553369 (clone: MEC13.3)	BD Falcon, Oxford, UK	129/Sv mouse-derived endothelioma cell line tEnd.1	1.200 (IF) [75 ng/ml] 2.5 µg per 10^7 beads
Mouse MCAM	Rat monoclonal	MAB7718 (clone: 733216)	R&D, Minneapolis, US	1-563aa (Extracellular region)	1.200 (IF) [5 µg/ml] 20 µg (AL)
Mouse AQP1	Rabbit polyclonal	PA1010	Boster Immunoleader, Pleasanton, USA	251-269aa	1.500 (IF) [2 µg/ml]
Mouse IgGs	Sheep polyclonal conjugated to ECL peroxidase	NA931	GE Healthcare, Amersham, UK	Mouse gamma immunoglobins heavy and light chains	1.2500 (WB) [0.4 µg/ml]
Rabbit IgGs (1)	Donkey polyclonal conjugated to alexafluor 488	A21206	Invitrogen, Paisley, UK	Rabbit gamma immunoglobins heavy and light chains	1.500 (IF) [4 µg/ml]
Rabbit IgGs (2)	Donkey polyclonal conjugated to ECL peroxidase	NA934	GE Healthcare, Amersham, UK	Rabbit gamma immunoglobins heavy and light chains	1.2500 (WB) [0.4 µg/ml]
Rat IgGs	Goat polyclonal conjugated to alexafluor 546	A11081	Invitrogen, Paisley, UK	Rat gamma immunoglobins heavy and light chains	1.500 (IF) [4 µg/ml]
IHC: Immunohistochemistry; IF: Immunofluorescence; WB: Western blot AL: Antibody localisation					

Table 2.11. siRNA duplexes used for the research detailed in this thesis.

Duplex name	Duplex sequence
Scrambled duplex	rCrGrUrUrArArUrCrGrCrGrUrArUrArArUrArCrGrCrGrUAT
GRIN2D duplex 1	rGrCrArArGrCrArCrGrGrArArArGrArArGrArUrCrGrArUGG
GRIN2D duplex 2	rGrGrArUrUrArCrUrCrCrUrUrCrArArUrGrArGrGrArCrGGC

2.1.1 RTqPCR primers

A web-based tool, "Universal Probe Library Assay Design Centre" (Roche, Burgess Hill, UK) was used to design the forward and reverse primers. These primers amplify a region containing a sequence where a probe could bind and amplify a product crossing an exon boundary. Primers were generated by Eurogentec, Southampton, UK.

Table 2.12. Human RTqPCR primers used for the research detailed in this thesis.

Target name	Primer sequences	Probe number
CD11b	Fwd: ggcatccgcaaagtggta	9
	Rev: ggatcttaaaggcattctttcg	
CD68	Fwd: gtccacctcgacctgctct	1
	Rev: cactggggcaggagaaact	
EPCAM	Fwd: ccatgtgctggtgtgtgaa	3
	Rev: tgtgttttagttcaatgatgatcca	
PDGFRA	Fwd: ccacctgagtgagattgtgg	27
	Rev: tcttcaggaagtccaggtgaa	
PECAM	Fwd: gcaacacagtccagatagctgt	14
	Rev: gacctcaaactgggcatcat	
FLOT2	Fwd: gatcctcagcttcaccatcaa	61
	Rev: tcagcatctctctgcaccac	
MCAM	Fwd: gggtaccccattcctcaagt	63
	Rev: cagtctgggacgactgaatg	
LAMA4	Fwd: gaccctgaggacacagtgtttta	22
	Rev: aggcaggtttaagctggtagg	
STRA6	Fwd: ctctggcctgactgtgtgc	23
	Rev: tgtccccagccaagaaatc	
GRIN2D	Fwd: ggctcagtgaccgcaagt	57
	Rev: gcacggtcccaaacttca	
FNDC1	Fwd: agactgaggggaaagtgaaaga	80
	Rev: atccaccagggcagaagtag	
GPR4	Fwd: ttccgccatccctctacat	44
	Rev: ccacagagccaggcagtt	
RGS5	Fwd: cccactcatgcctggaaa	65
	Rev: tgacaaggtcaccaactgagtc	
TGM2	Fwd: agggtgacaagagcgagatg	86
	Rev: tggtcatccacgactccac	
KCNJ8	Fwd: cgctacccggagtctgag	34
	Rev: cagcttagccacctccctct	
OR51E1	Fwd: cagcctgccagacctctt	69
	Rev: cagcaccaggcaggtagag	

Table 2.13. Mouse RTqPCR primers used for the research detailed in this thesis.

Target name	Primer sequences	Probe number
CD11b	Fwd: gcacctcggtatcagcatatt	9
	Rev: cccaggtaccgaaattctcc	
CD68	Fwd: ttctcttgcaaccgtgacc	34
	Rev: gaggaggaccaggccaat	
EPCAM	Fwd: ggttagcgcttccgaggta	53
	Rev: tgttggatagtcaaggccagt	
PDGFRA	Fwd: aacggggctagaagtcaacc	4
	Rev: tgacatgaagccaagaacttaaac	
PECAM	Fwd: gctggtgctctatgcaagc	30
	Rev: atggatgctgttgatggtga	
β-ACTIN	Fwd: ggagggggttgaggtgtt	71
	Rev: gtgtgcacttttattggtctcaa	
LEPR	Fwd: cctccatctaacgtaaaagcaga	47
	Rev: tggcttttcccaagatactttc	
PRLR	Fwd: gccttcctgctctgtctcac	55
	Rev: cctgagccccgtgtaaaat	
ESAM	Fwd: tgattcttcaggctggaacc	54
	Rev: tcagtcccaggaacaaaacc	
PTN	Fwd: tgtcactttgctctccttgg	55
	Rev: agtgggcttcctggcttc	
AQP1	Fwd: atcaactcagcaccccactc	25
	Rev: caggtgggtccctcacttt	
ANGPT2	Fwd: aagagcgtggacagcacag	8
	Rev: gtagctgcagggtccgttc	
DARC	Fwd: cttcaccttgggactcagtgt	32
	Rev: gactggcagccctaagagg	
ECSCR	Fwd: gctagacacttggcctgctc	18
	Rev: ttgactcctcgttcctgagttt	
TSPAN7	Fwd: ttggatgctttgctacatgc	89
	Rev: gggacaggaacatggcatac	
STC2	Fwd: catgccctgcgtcataaat	18
	Rev: catttccctaattgctggaca	
RET	Fwd: cacagcccagcaacttacg	2
	Rev: ggccctgagaattctgctct	
MMRN2	Fwd: agcccctcaccatgatcc	3
	Rev: agtccccagctcaggtacac	
VEGFR2	Fwd: accagagaccctcgttttca	22
	Rev: catttgcttgcaggaggttt	
EDN1	Fwd: cagcatccttgatccaaaca	30
	Rev: gacgcagacaggctaggg	

2.1.2 Tissue provision / processing

Queen Elizabeth Hospital, Mindelsohn Way, Edgbaston, Birmingham, West Midlands, B15 2GW

Queen Elizabeth Women's Hospital, Mindelsohn Way, Birmingham, West Midlands, B15 2TG

University of Birmingham Tissue Bank Service, Human Biomaterials Resource Centre, University of Birmingham, Edgbaston, Birmingham, West Midlands, B15 2TT

2.1.3 Facilities

Animal care and housing, Biomedical Services Unit (BMSU), University of Birmingham, Edgbaston, Birmingham, West Midlands, B15 2TT

Agilent bioanalysis and microarray slide scanning, Technology Hub, University of Birmingham, Edgbaston, Birmingham, West Midlands, B15 2TT

2.2 Endothelial isolation methods

2.2.1 Endothelial cell extraction from human tissue

2.2.1.1 Tissue collection and ethics.

Tumour and distant healthy tissue were obtained immediately post-surgery. Full patient consent and ethical approval was granted (Queen Elizabeth Hospital Birmingham: Colorectal cancer (CRC) and Colorectal liver metastasis (CRM), South Birmingham REC, No. 2003/242. Renal Cell Carcinoma (RCC), No. 12-090.

2.2.1.2 Digestion of tissue

The tissue was weighed, soaked in tissue digestion solution and then finely sliced with a scalpel to roughly 1-3 mm^3 pieces. The tissue was digested for 1.5 hours in a shaking 37°C incubator.

The digested tissue was filtered through a 100 μm cell strainer. The resulting cell suspension was washed twice by centrifugation for 5 minutes at 300 × g and resuspended in phosphate buffered saline (PBS).

2.2.1.3 Preparation of Ulex lectin coated dynabeads

Streptavidin coated M-280 dynabeads were washed twice: the beads were pelleted on a magnetic particle concentrator and resuspended in PBS. 50 μg biotyinylated lectin from *Ulex europaeus* was added to the bead suspension and incubated for 30 minutes in a shaking 37°C incubator.

2.2.1.4 Endothelial cell isolation

$1.4x10^7$ Ulex lectin coated dynabeads per gram of tissue were added to the cell suspension and the solution mixed on a rotator at 4°C for 30 minutes. The bead rosetted endothelial cells were then pelleted out of suspension using a magnetic particle concentrator. The pelleted cells were washed with PBS as described in section 2.2.1.3. The pelleted cells were then resuspended in Qiazol lysis reagent in preparation for RNA extraction.

2.2.2 Endothelial cell isolation from mouse tissue

2.2.2.1 Digestion of tissue

As described in section 2.2.1.2

2.2.2.2 Preparation of Rat anti-mouse PECAM-1 antibody coated dynabeads

Sheep anti-rat IgG coated M-280 dynabeads were washed twice: the beads were pelleted on a magnetic particle concentrator and resuspended in PBS. 2.5 μg rat anti-mouse PECAM-1 antibody was added per 10^7 beads and incubated for overnight at 4°C on a rotator.

2.2.2.3 Mouse tumour endothelial cell isolation

$2 x 10^7$ rat anti-mouse PECAM-1 antibody coated dynabeads per gram of tissue were added to the cell suspension and the solution mixed on a rotator at 4°C for 30 minutes. The bead rosetted endothelial cells were then pelleted out of suspension using a magnetic particle concentrator. The pelleted cells were washed with PBS as described

in section 2.2.1.3. The pelleted cells were then resuspended in Qiazol lysis reagent in preparation for RNA extraction.

2.3 Molecular biology methods

2.3.1 RNA extraction

RNA was extracted from Qiazol lysed cells using the miRNeasy mini kit following manufacturer's conditions. The protocol used was taken from the October 2007 "miRNeasy minihandbook; Purification of total RNA from animal cells;" p.19-22. RNA concentration was quantified by use of the Nanodrop spectophotometer.

2.3.2 RNA integrity validation

RNA integrity was assessed using an Agilent Bioannalyser, by Steve Kissane, a University of Birmingham technician.

2.3.3 RNA labelling

RNA was labelled using the "Low Input Quick Amp Labelling Kit, One-Color," following the manufacturer's protocol detailed in the "One-Color Microarray-Based Gene Expression Analysis, low input Quick Amp Labelling" handbook, p.19-30.

2.3.4 Microarray analysis

Labelled cRNA was hybridised onto an Agilent SurePrint G3 Human Gene Expression 8x60K v2 Microarray slide following the manufacturer's protocol detailed in the "One-Color Microarray-Based Gene Expression Analysis, low input Quick Amp Labelling" handbook, p. 31-41. The hybridised slide was scanned using a High Resolution Microarray Scanner and the features extracted with Agilent feature extraction software using the protocol detailed in the "One-Color Microarray-Based Gene Expression Analysis, low input Quick Amp Labelling" handbook, p. 42-51.

2.3.5 cDNA production

cDNA was generated using between 50-100 µg of template RNA in a master mix generated from the "High-capacity cDNA reverse transcription kit". The thermal cycling conditions were:

- 25°C for 10 minutes
- 37°C for 120 minutes
- 85°C for 5 minutes
- 4°C indefinitely

2.3.6 Quantitative Reverse Transcription Polymerase Chain Reaction (RT-qPCR)

The "Roche Exiqon universal probe system" was used to perform RT-qPCR (see Table 2.1.1 for primer sequences and probe numbers). The RTqPCR reaction mix was combined with 10µl of cDNA, diluted 1 in 10 from that produced in section 2.3.5.
The RT-qPCR was conducted on a Rotor-gene RG-3000 using a 36 well rotor and the following program.

- 92°C for 10 minutes
- 92°C for 15 seconds
- 60°C for 45 seconds — 45 Cycles
- 55°C for 30 seconds
- Ramp up from 55-95°C by 1°C per 5 seconds

RNA samples were assessed in triplicate and the expression levels of the genes of interest were determined using the delta-delta CT method normalised to flotillin-2.

2.3.7 Western blot

2.3.7.1 Preparation of protein extract

Cells were harvested by scraping, lysed with RIPA buffer and disrupted by being drawn through a 19 gauge needle several times. The cell lysate was agitated for 15 minutes on a tube rotator at 4°C, then centrifuged at 21910×g for 15 minutes and supernatant collected.

2.3.7.2 SDS-polyacrylamide gel production and running

Protein samples were mixed with one part SDS loading buffer to three parts sample and loaded onto an 8% SDS-polyacrylamide gel. The gel was immersed in running buffer and run at 140 V for 90 minutes.

2.3.7.3 Protein transfer

A PVDF immobilon transfer membrane was hydrated by emersion in methanol for 30 seconds, deionised water for 5 minutes and then transfer buffer. Once the SDS-polyacrylamide gel had run it was clamped into a cassette with the membrane, immersed in transfer buffer and proteins transferred from the gel to the membrane for 2 hours at 4°C, using a maximum current of 400 mA with voltage capped at 30 V.

2.3.7.4 Development of the membrane

Once the proteins were transferred, the membrane was washed twice with PBS-Tween for 5 minutes. The membrane was blocked using 10% milk in PBS-Tween for 1 hour, then washed three times with PBS-Tween for 5 minutes then incubated with the primary antibody, at the appropriate concentration, in a 3% bovine serum albumin (BSA), NaN^{-}_{3}, PBS-tween solution overnight at 4°C. The membrane was washed four times with PBS-Tween for 5 minutes then incubated with a secondary antibody conjugated to ECL peroxidase in 10% milk in PBS-Tween for 1 hour. The membrane was washed four times with PBS-Tween for 5 minutes, then incubated with ECL detection reagent for 1 minute. The membrane was then used to develop Amersham Hyperfilm™ ECL.

2.4 Tissue staining methods

2.4.1 Immunohistochemistry

Immunohistochemistry was performed on formalin fixed, paraffin embedded sections by first deparaffinising by emersion in two tanks of Histoclear for 5 minutes each. Sections were then placed in 100%, 90% and 70% ethanol sequentially for 5 minutes each. Sections were then rehydrated with tap water for 5 minutes. A blocking step for endogenous tissue peroxidases was performed, using 0.3% hydrogen peroxide, for 15 minutes. The sections were then washed with water and placed in the antigen unmasking solution and left at 60°C overnight under constant stirring.

The following morning the sections in the unmasking solution were slowly cooled in a bath of ice and water until at room temperature. The slides were then washed with PBS for 5 minutes. A second blocking step, for non-specific protein binding, was performed using 20% Casein solution for 10 minutes. The sections were incubated with the primary antibody at the appropriate concentration in PBS, for 1 hour at room temperature. The sections were washed three times with PBS-Tween (0.1%) for 5 minutes each and then incubated with the "ImmPRESS universal secondary antibody" for 30 minutes. The sections were again washed 3 times with PBS-Tween for 5 minutes and then stained using the "ImmPACT NovaRed chromogen" for 2 minutes. The sections were washed with water for 5 minutes, counterstained with haematoxylin solution for 1 minute, washed in warm tap water for 5 minutes then dehydrated by immersion in 100% ethanol and Histoclear for 5 minutes each. The sections were finally mounted in distyrene–plasticiser–xylene resin. All IHC staining images were acquired using a Leica DM6000 light microscope.

Note: For immunohistochemistry involving commercial tissue arrays an additional 1 hour bake in a 60°C oven was performed to remove an additional layer of paraffin wax added for shipping and storage purposes.

2.4.2 Immunofluorescent staining on frozen sections

Frozen sections were defrosted for 10 minutes at room temperature and then fixed with acetone for 5 minutes. Sections were rinsed with deionised water 4 times and blocked with 20% Casein for 10 minutes. The sections were incubated with the primary antibody at the appropriate concentration for 2 hours. The sections were then washed three times with PBS-Tween for 5 minutes and incubated with the appropriate fluorescently labelled secondary antibody, at 1 in 500 dilution in PBS, for 1 hour. The sections were washed three times with PBS-Tween and then once with deionised water for 5 minutes and mounted in ProLong Gold mounting media containing DAPI. Quantification of fluorescence was conducted using the ImageJ software package (194).

2.4.3 Immunofluorescent staining on paraffin embedded sections

Sections were deparaffinised by emersion in two tanks of Histoclear for 5 minutes each. Sections were then placed in 100%, 90% and 70% ethanol sequentially for 5 minutes each. Sections were then rehydrated with tap water for 5 minutes. The sections were placed in an antigen unmasking solution and left at 60°C overnight in the continuously stirred solution.

The following morning the sections in the unmasking solution were slowly cooled in a bath of ice and water until at room temperature. The slides were then washed with PBS for 5 minutes. A second blocking step, for non-specific protein binding, was performed

using 20% Casein for 10 minutes. The sections were incubated with the primary antibody at the appropriate concentration for 2 hours. The sections were then washed three times with PBS-Tween for 5 minutes and incubated with the appropriate fluorescently labelled secondary antibody, at 1 in 500 dilution in PBS, for 1 hour. The sections were washed three times with PBS-Tween and then once with deionised water for 5 minutes and mounted in ProLong Gold mounting media containing DAPI.

2.4.4 Haematoxylin and Eosin (H&E) stain on paraffin embedded sections

Sections were deparaffinised by emersion in two tanks of Histoclear for 5 minutes each. Sections were then placed in 100%, 90% and 70% ethanol sequentially for 5 minutes each. Sections were then rehydrated with tap water for 5 minutes. Sections were incubated in Mayers Haematoxylin for 10 minutes, then washed in warm tap water for 3 minutes. Sections were then incubated in Eosin for 10 minutes. Sections were then sequentially washed in tap water, 70% ethanol, 90% ethanol, 100% ethanol then Histoclear before being mounted in DPX on a coverslip.

2.5 Cell culture (*in vitro*) methods

2.5.1 Primary cell and cell line culture

All cell work was performed in a category 2 tissue culture hood using aseptic techniques. Cells were incubated in their appropriate growth media at 37°C and 5% CO_2 unless stated otherwise. The use of five cell types is detailed in this report; Human umbilical cord vein endothelial cells (HUVEC), Human dermal micro-vascular cells (HDMEC), 4T1, Phoenix-Ampho and RENCA. HUVEC are freshly isolated primary cells, HDMEC are commercially produced primary cells, 4T1 and RENCA are cancer cell lines and Phoenix-Ampho is an immortalised embryonic kidney cell line. All these cell types are adherent.

2.5.2 Cell resuscitation, splitting and counting

Cells were resuscitated from liquid nitrogen storage by defrosting rapidly at 37°C, suspending the cells in 10 ml culture medium, pelleting the cells by centrifugation for 5 minutes at 300 × g, resuspending the pellet in the appropriate growth medium and plating the cells onto 10 cm plates.

Culture media was changed every 2-3 days by aspirating off the old media from the plates and replacing it with fresh media warmed to 37°C

Cell plates were split, when confluent, by aspirating off the media from the plates, washing the plate with PBS, deadhering the cells from the plate with 3 ml trypsin-EDTA (0.1%) and incubating the plate for 2 minutes at 37°C. 6 ml culture media was added to

the suspended cells to neutralise the trypsin, the cells were plated onto 10 cm plates and the volume of the suspension in each plate was made up to 10 ml with the addition of culture media.

Where necessary the cellular concentration of a cell suspension was determined by use of a haemocytometer.

2.5.3 Human umbilical cord vein endothelial cell (HUVEC) isolation

Cords were collected from the delivery suite in the Queen Elizabeth Women's Hospital, Birmingham, anonymised by the University of Birmingham HBRC and delivered to the tissue culture laboratory. The exterior of the cords were cleaned with 70% ethanol, examined for holes and dissected around these holes or into roughly 6-inch sections. Cannula were inserted into the vein at either end of the cord section and secured with cable ties. Using the cannulae as an entrance and exit, the cord vein was washed through with PBS in a pulsatile manner until the effluent ran clear. The valve on the exit cannula was closed, the cord filled with 1 mg/ml collagenase 1A in M199, the valve on the entrance cannula was then closed. The cord was incubated for 15-20 minutes at 37°C and 5% CO_2, then the collagenase digestion solution was flushed out of the cord using PBS then air and the solution continually collected. The solution was span down at 300 × g for 6 minutes. The cell pellet was then resuspended in HUVEC early growth media (complete M199 plus 0.2% gentamicin/amphotericin) and applied to gelatine-coated flasks.

2.5.4 siRNA knockdown and HUVEC functional assays

2.5.4.1 siRNA transfection

HUVEC were plated on gelatin coated plates at a density of 175000 cells per well in a 6 well plate and incubated overnight at 37°C and 5% CO_2. A duplex mix of 50 nM siRNA was generated in optimem and incubated for 10 minutes with 0.3% RNAiMAX lipofectamine.

The plated cells were washed twice with PBS and then the siRNA duplex mix was added to the cells and incubated at 37°C and 5% CO_2 for 4 hours. The duplex mix was then replaced with cM199 (except without antibiotics) and incubated in standard growth conditions overnight. These cells were then used for functional assays or harvested to confirm knockdown of target genes.

2.5.4.2 Scratch wound assay

HUVEC were plated at a density of 300,000 cells per well in a 6-well plate. The cells were then allowed to grow to confluence. 6 scratches were made in the cell monolayer, 3 from top to bottom and 3 left to right, making 9 intersections which were then incubated at 37°C and 5% CO_2 and imaged regularly for analysis of scratch wound closure.

2.5.4.3 Transfilter assay

Both sides of an 8 μm pore well inserts were gelatin coated in a 24 well plate. HUVEC were harvested and suspended in optimem for 15 minutes. The cells were then added into the top of the well inserts at a density of 30,000 cells per well. The top portion of

the well was then filled with low serum medium 199. Complete M199 was added to the bottom of the well in sufficient quantities to bath the underside of the well insert. This set up was then incubated for 16 hours at 37°C and 5% CO_2.

After this period cell growth medium was removed from the wells and inserts, the inserts were washed with PBS and cells on both sides of the insert were fixed for 15 minutes at room temperature with a solution consisting of 2% formaldehyde and 2 ug/ml bisbenzimide in PBS. Using a scalpel the bottom of the insert was cut out and mounted onto a slide using the ProLong Gold mounting media not containing DAPI. Both sides of the well were then imaged using a Leica DM6000 fluorescent microscope.

2.5.4.4 Matrigel tube formation assay

Matrigel was plated and allowed to solidify in the wells of a 12 well plate at 37°C for 30 minutes. 140,000 HUVEC per well were plated on the matrigel. The cells were then incubated for 16 hours at 37°C and 5% CO_2 after which images were taken for analysis.

2.5.4.5 Acumen cell cycle cytometry

A 96 well plate was prepared by coating the appropriate wells with 0.1% gelatin and incubated for 30 minutes at 37°C. 4000 HUVEC in complete M199 were added to each well. There were 8 repeats for each condition.

The plates were incubated overnight at 37°C, 5% CO_2. The cells were then fixed with 85% ethanol. The plates were kept at 4°C until staining.

The cells were stained by aspiration of the ethanol fixative and addition of 100 µl propidium iodide staining solution. The plates were incubated at 37°C for 20 minutes and then imaged on the Acumen eX3 high content screening machine.

2.5.5 HUVEC and HDMEC treatment with VEGF

Passage 2 HUVEC isolates / HDMEC used within 2 passages of receipt, were plated at a density of 14,000 cells cm^{-2}, grown in low serum medium 199 for 16 hours, then cultured ± 100 ng/ml recombinant human VEGF for 24 hours before being harvested for western blot and RTqPCR analysis.

2.5.6 Transfection of Phoenix-Ampho cells

$2x10^6$ Phoenix-Ampho cells were plated onto a 60 mm plate and incubated at 37°C and 5% CO_2 overnight. The cell culture media was then replaced with optimem supplemented with 10 µg MSCV-LUC plasmid DNA (192) and 4% lipofectamine 2000. The cells were incubated overnight at 37°C and 5% CO_2. The optimem was then replaced with cDMEM and the cells incubated at 32°C and 5% CO_2.

2.5.7 Retroviral Harvesting

Every day, for 5 days after the transfection, the viral media was collected, centrifuged for 10 minutes at 300 × g to pellet any cells. The supernatant was aspirated, snap frozen on dry ice and stored at -80°C. The viral media was replaced with fresh media and the cells were once again incubated at 32°C and 5% CO_2.

2.5.8 Transduction of 4T1 cells

4T1 cells were plated at a density of $1x10^5$ cells per well in a 6 well plate. The cells were incubated overnight in culture medium at 37°C and 5% CO_2. The culture media was replaced by MSCV-LUC viral media, mentioned in "2.5.7 Retroviral Harvesting", supplemented with 8 µg/ml polybrene. The cells were then centrifuged in a plate

spinner at 300 × g for 1 hour. The viral media was then replaced with fresh media and the cells were incubated for 48 hours at 37°C and 5% CO_2.

2.5.9 MTS viability assay

4T1 cells were plated at a density of $5x10^4$ cells per well in a 6 well plate. The cells were incubated overnight in cDMEM at 37°C and 5% CO_2. The culture media was replaced by cDMEM, containing puromycin dihydrochloride at various concentrations. The cells were then incubated at 37°C and 5% CO_2 for 3 days. MTS was then added to the media in each well and the plate was incubated at 37°C and 5% CO_2 for 4 hours. The MTS media was transferred to a 96 well plate and the absorbance at 490 nm, of each well, was recorded by a plate reader.

2.5.10 Puromycin selection of 4T1 cells

MSCV-LUC virally transduced 4T1 cells were plated at a density of $1x10^5$ cells per well in a 6 well plate. The cells were incubated overnight in culture medium at 37°C and 5% CO_2. The culture media was replaced by media, containing puromycin dihydrochloride at the appropriate concentration. The cells were then incubated at 37°C and 5% CO_2 for 3 days. Untransduced 4T1 cells were plated alongside and treated in the same way to act as a control. The 4T1 cells were re-plated and the cycle of puromycin treatment repeated until the point where the MSCV-LUC virally transduced 4T1 cells were completely confluent and the untransduced cells completely dead.

2.5.11 IVIS analysis of 4T1 cells

D-luciferin was added at a concentration of 150 μg/mL to a confluent plate of puromycin selected, MSCV-LUC virally transduced 4T1 cells. The bioluminescence of the cells was then determined using an In-Vivo Imaging System (IVIS) machine.

2.6 *In vivo* methods

2.6.1 Sourcing and caring for mice

Eight week old, BALB/c mice (18–25 g) were obtained from the Harlan Laboratories (UK). The mice were housed in a ventilated barrier rack in a temperature-controlled facility on a 12-hour photoperiod. The mice were given food and water *ad libitum*. Mice were handled and treated in accordance with UK Home Office requirements under Licence (PPL. 40/3339).

2.6.2 RENCA tumour and antibody localisation

The RENCA murine renal cell carcinoma cell line was used to develop subcutaneous tumours. $1.25x10^5$ RENCA cells were injected in optimem into the flank of healthy male Balb/c mice, using a 26-gauge needle. Tumours were permitted to grow to 1 cm^3. Mice were then intravenously inoculated with 20 μg monoclonal rat anti-mouse MCAM antibodies one hour prior to cull. The tumours and several other organs were then collected snap frozen in liquid nitrogen and stored at -80°C for sectioning by the University of Birmingham HBRC.

2.6.3 Initiation of 4T1-LUC tumours in the murine mammary fat pad

$2.5x10^5$ 4T1 cells suspended in Optimem and in a volume of 100 μL, were injected into the second mammary fat pad of anaesthetised 8-week-old female Balb/C mice, using a 26-gauge needle.

2.6.4 *Ex vivo* imaging

At the experimental endpoint all mice (including controls) were IP injected with 150mg D-luciferin / kg body weight, left for 5 minutes and then culled at the same time point. The liver, spleen and lungs were rapidly dissected from each mouse and imaged in parallel using the IVIS imaging system. Luminescent quantification was performed on the two opposite sides of each organ and the results averaged.

2.6.5 Sunitinib drug trial

4T1 tumours were initiated in female Balb/c mice as described in section "2.6.3 Initiation of 4T1-LUC tumours in the murine mammary fat pad". After a 1 week tumour establishment period the Sunitinib treatment group received daily IP injections of 40mg Sunitinib per kg body weight in PBS and 3.72% DMSO. The untreated control group received daily intraperitoneal (IP) injections of the drug vehicle (PBS and 3.72% DMSO). Tumour growth was measured daily using a caliper. At the experimental endpoint *ex vivo* imaging was performed as described in section 2.6.4. Tumour and key organ tissue was collected, frozen for sections, RTqPCR and microarray analysis, formalin fixed for paraffin embedded sections or subjected to endothelial isolation.

2.7 Imaging quantitation

2.7.1 Command line for localisation quantitation

Antibodies were localised to tumour vessels as described in "2.6.2 RENCA tumour and antibody localisation", the mouse tissue was sectioned and stained as described in "2.4.2 Immunofluorescent staining on frozen sections" and imaged with the DM6000 fluorescent microscope. Quantitation of antibody localisation was performed as follows.

Split image file into red, green and blue channels and input into the Image J software package (194).

- run("image file (green channel-CD31)");

- run("16-bit");

- run("Threshold...");

- setThreshold(9, 255);

- run("Convert to Mask");

Apply mask to red channel

- run("Add Selection...")

- selectWindow("image file (red channel-MCAM)");

- run("Measure");

Readout:

Measurement number	File name	Mean grey scale (pixel density)
1	M6 RENCA 1 red channel.tif	14.385

2.7.2 Command lines for vascular density and target staining quantitation

Sections were stained as described in "2.4.2 Immunofluorescent staining on frozen sections" and imaged with the DM6000 fluorescent microscope. Quantitation of marker staining was performed as follows.

Image file split into red, green and blue channels and input into the Image J software package (194).

- run("image file");
- run("16-bit");
- run("Threshold...");
- setThreshold(9, 255);
- run("Convert to Mask");
- run("Measure");

Readout:

Measurement number	**File name**	**Mean grey scale (pixel density)**	**% area occupied by mask**
1	M1 UT 9 days red channel.tif	3.6802	1.443
2	M1 UT 9 days green channel.tif	4.6056	1.806

2.7.3 Quantification of metastasis by H&E staining

Three sections were taken from liver, lung and spleen samples at ~300 μm intervals and stained by H&E as described in "2.4.4 Haematoxylin and eosin (H&E) stain on paraffin embedded sections". Five images were taken at random by light microscopy from each section. Areas of metastasis in each field were identified and quantified by Image J software. Metastatic burden was determined as the average area of metastasis from the fifteen fields of view corresponding to each organ.

2.7.4 IVIS *ex vivo* imaging settings

- Luminescent settings-

- Exposure: Auto

- Binning: medium

- F/stop: 1

- Emission filter: open

2.7.5 Directions for the quantification of *ex vivo* bioluminescence

- Tool palette- ROI tools

- Draw region of interest (ROI)

- Measure- set to radiance (photons)

- Export

Readout:

Image Number	**ROI**	**Image Layer**	**Avg Radiance [p/s/cm≤/sr]**
JWW20130208113504_001	ROI 1	Overlay	2.98E+05

2.8 Bioinformatic methods

2.8.1 Microarray bioinformatic analysis

The microarray expression analysis data was normalised, annotated and analysed using the R-software package (version 2.15.0. 2012) along with the marray (195) and limma (196) expansions. Target selection was performed on this data as follows:

A "targets.txt file" was generated detailing the categories under which the microarray raw data text files will be compared. In this example these categories are Cancer and Healthy (highlighted in red below).

Targets.txt file

Sample Number	*File Name*	*Condition*
1	cancer1.txt	cancer
2	cancer2.txt	cancer
3	cancer3.txt	cancer
4	cancer3.txt	cancer
5	healthy1.txt	healthy
6	healthy2.txt	healthy
7	healthy3.txt	healthy
8	healthy4.txt	healthy

The raw data files plus the targets file was placed in a folder on the desktop named 'files' (highlighted in green below).

The following blue commands were inserted into the R 64bit console. Descriptions of the steps are in black.

Select the analysis package: library(limma)

Select the data location: setwd("~/Desktop/files")

Select the targets file: targets <- readTargets("targets.txt")

Load the raw data files into the analysis package and set output columns:

RG <- read.maimages(targets, path="~/Desktop/files", columns = list(G =

"gMedianSignal", Gb = "gBGMedianSignal", R = "gProcessedSignal",

Rb = "gIsPosAndSignif"), annotation = c("Row", "Col","FeatureNum",

"ControlType","ProbeName"))

Correct for background: RG <- backgroundCorrect(RG, method="normexp", offset=16)

Normalise between arrays under analysis:

RG$G <- normalizeBetweenArrays(RG$G, method="quantile")

Log2 transform the data intensity values: RG$G <- log2(RG$G)

Convert the RGList into an MAList for further manipulation:

E <- new("MAList", list(targets=RG$targets, genes=RG$genes, source=RG$source,

M=RG$Gb, A=RG$G))

Use the avereps function to average replicate spots:

E.avg <- avereps(E, ID=E$genes$ProbeName)

Build the design matrix for the linear modelling function:

```
f <- factor(targets$Condition, levels = unique(targets$Condition))

design <- model.matrix(~0 + f)

colnames(design) <- levels(f)
```

Apply the intensity values to lmFit: `fit <- lmFit(E.avg$A, design)`

Create a contrast matrix. In this example, cancer – healthy (meaning that in the resultant analysis, positive values denote gene expression in cancer > healthy and negative values, cancer < healthy):

```
contrast.matrix <- makeContrasts("cancer-healthy", levels=design)
```

Apply this contrast matrix to the modelled data and compute statistics for the data (in this case the empirical Bayes statistical test):

```
fit2 <- contrasts.fit(fit, contrast.matrix)

fit2 <- eBayes(fit2)
```

Output the statistics for the dataset and write them into a data file for further analysis:

```
output <- topTable(fit2, adjust="BH", coef="cancer-healthy", genelist=E.avg$genes,
number=66,000)
```

```
write.table(output, file="cancer_vs_healthy.txt", sep="\t", quote=FALSE)
```

Following these steps resulted in the generation of a text file named, in this example, cancer_vs_healthy.txt, with comparative analysis data of condition 1 (cancer) vs. condition 2 (healthy).

This was inserted into an Microsoft Excel spreadsheet and the gene identity data was translated from microarray probe IDs to gene names, using an annotation file corresponding to the microarray slide in use, downloaded from the Agilent website.

Human: 028004_D_AA_20120130_annotation.xlsx

Mouse: 028005_D_Mouse_20121126.xlsx

2.8.2 Ingenuity bioinformatics analysis

Bioinformatic analysis was conducted on processed microarray data, using the Ingenuity pathway analysis (IPA) software (Qiagen, Manchester, UK).

The IPA Core Analysis package was used with the following settings:

- Network interactions – Include genes and endogenous chemicals
- Data sources – All
- Confidence – Proven and strongly predicted interactions only
- Species – All
- Tissue cell lines – All
- Mutations – All

The Molecule Activity Predictor (MAP) package was used to predict the impact of sunitinib therapy on selected pathways.

2.8.3 Bioinformatic websites

Universal Probe Library Assay Design Centre:
https://lifescience.roche.com

NCBI:
http://www.ncbi.nlm.nih.gov

PubMed:
http://www.ncbi.nlm.nih.gov/pubmed

TMHMM Server v. 2.0:

2.9 Statistical methods

Excel (Microsoft, Redmond, USA) was used to generate graphs. All error bars depict the standard error of the mean (SEM).

Mann-Whitney, Kaplan-Meier, Chi-squared, Log-ranks and Cox-regression statistical analyses were performed using the SPSS statistics suite (IBM, New York, USA).

P-value	Summary
< 0.001	***
0.001 to 0.01	**
0.01 to 0.05	*
> 0.05	Not significant (NS)

Chapter Three

Endothelial Isolation and Microarray Analysis

3.1 Introduction

The search for genuine tumour vessels specific markers is an on going effort. Despite considerable work and a number of promising targets, discussed in chapter one, the need for further targets is clear. Cancer is an extremely heterogeneous disease, or even a loose collection of mildly similar diseases and tumour endothelial marker expression is equally varied. This means that the current focus on the identification of pan-tumour endothelial markers, whilst still valid should be mixed with an effort to find truly specific targets in individual cancers. This principle guides the work discussed in chapters 3-5.

This chapter discusses the isolation of endothelium from colorectal cancer (CRC), colorectal liver metastasis (CRM) and renal cell carcinoma (RCC) and matched healthy tissues, sample processing for microarray transcriptomic analysis and bioinformatics processing of data to find putative tumour endothelial markers.

3.2 Results

3.2.1 Sample collection and endothelial isolation

In order to facilitate the identification of novel tumour endothelial markers, fresh matched healthy and tumour tissues were collected from resections of CRC (n=8, Table 3.1), CRM (n=7, Table 3.2) and RCC (n=8, Table 3.3), which had not received neoadjuvant therapy, and were processed within three hours of surgery. The endothelium was isolated from these tissues, according to the workflow shown in Figure 3.1. Briefly the tissue was minced, digested with a collagenase V solution to a single cell suspension. Magnetic beads conjugated to *Ulex* agglutinin I were prepared and incubated with the single cell suspension. *Ulex* agglutinin I, a lectin isolated from *Ulex europaeus* binds specifically to the L-fucose residues present within glycoproteins on the surface of human endothelial cells (197). The endothelium within the single cell suspension therefore became rossetted with beads allowing them to be magnetically isolated. RNA was extracted using the Qiagen miRNeasy mini kit, by a process of phenol and guanidine thiocyanate lysis, chlorophorm precipitation, silica-membrane based purification, selective digestion of unwanted DNA and elution into nuclease-free water. This process resulted in the isolation of total RNA, by permitting the capture of fragments of 18 nucleotides or greater. This allowed for the investigation of both macro and micro-RNA expression profiles.

Table 3.1. Clinical-pathological data for colorectal cancer patients used for genomic analysis and validation.

ID	Age	Gender	Tumour Location	Tumour Grade (differentiation)	Tumour Stage (Dukes)	Applications
1	71	Female	Sigmoid	Moderate	C1	Microarray and RTqPCR
2	85	Male	Rectum	Moderate	B	Microarray and RTqPCR
3	90	Male	Rectum	Poor	C1	Microarray and RTqPCR
4	83	Male	Caecum	Moderate	B	Microarray and RTqPCR
5	71	Male	Rectum	Moderate	C1	RTqPCR only
6	62	Male	Sigmoid	Moderate	C1	RTqPCR only
7	64	Male	Sigmoid	Moderate	C1	RTqPCR only
8	77	Female	Caecum	Moderate	B	RTqPCR only

Table 3.2. Clinical-pathological data for colorectal liver metastasis patients used for genomic analysis and validation.

ID	Age	Gender	Origin Location	Tumour Grade (differentiation)	Tumour Stage (Dukes)	Applications
1	79	Female	-	Moderate	-	Microarray and RTqPCR
4	73	Male	Caecum	Moderate	B	Microarray and RTqPCR
6	71	Female	-	Moderate	-	Microarray and RTqPCR
3	79	Male	Rectum	Moderate	C1	Microarray only
2	65	Male	Right colon	Moderate	-	RTqPCR only
5	68	Male	Right Colon	Moderate	-	RTqPCR only
7	66	Male	-	Moderate	-	RTqPCR only

Table 3.3. Clinical-pathological data for renal cancer patients used for genomic analysis and validation.

ID	Age	Gender	Tumour Type	Tumour Grade (Fuhrman)	Tumour Stage	Applications
1	59	Female	Papillary	3	pT3c N0	Microarray and RTqPCR
2	70	Male	Clear cell (cystic)	1	pT2a Nx	Microarray and RTqPCR
3	69	Female	Clear cell	2 to 3	pT3a Nx	Microarray and RTqPCR
4	66	Female	Papillary	4	PT3a/b N0	Microarray and RTqPCR
5	66	Male	Clear cell	3	-	RTqPCR only
6	69	Female	Clear cell	2	pT1a Nx	RTqPCR only
7	77	Female	Clear cell	2	pT2b Nx	RTqPCR only
8	66	Female	Clear cell	2	pT1b Nx	RTqPCR only

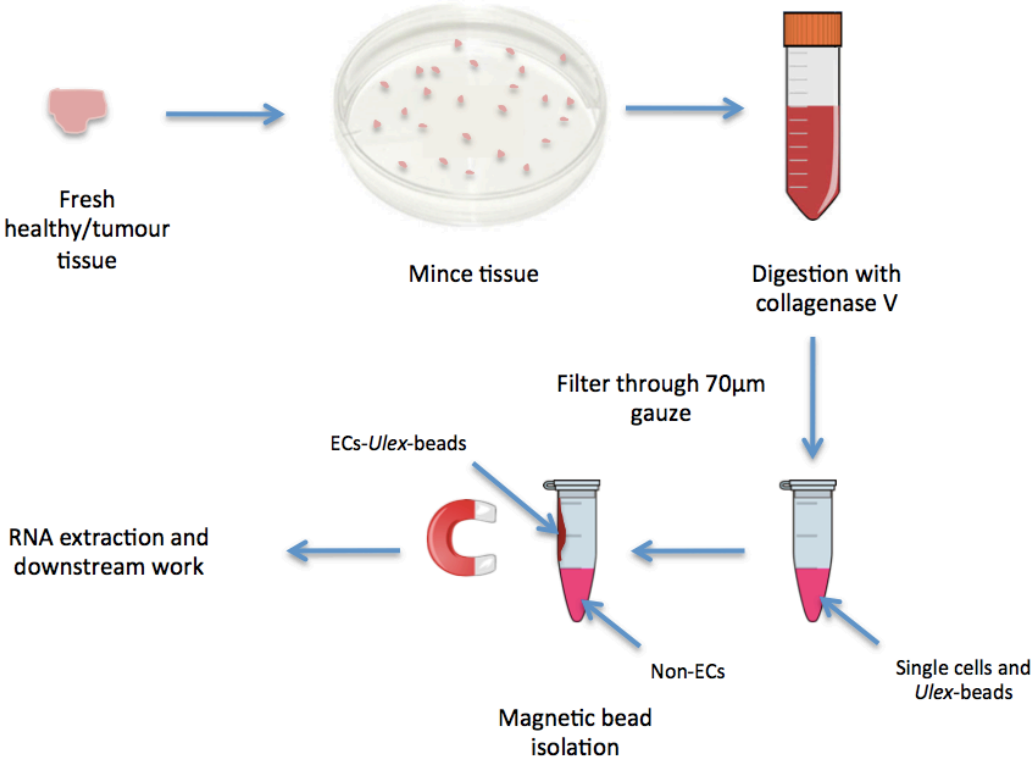

Figure 3.1 Isolation of endothelial cells using *Ulex* lectin coated magnetic beads. The workflow of the main steps involved in the endothelial isolation procedure.

3.2.2 RNA integrity validation

Successful transcriptomic analysis of gene expression by RTqPCR or microarray analysis, requires RNA of high quality and integrity (198), although meaningful data can be acquired from lower quality samples (199). The integrity of isolated RNA was assessed by Agilent Bioanalyser according to the workflow shown in Figure 3.2A. The bioanalyser operates similarly to agarose gel-slab electrophoresis, it however uses far smaller amounts of RNA and as the concentration of RNA isolated from human tissue endothelium was limited, it was selected. The bioanalyser chip contains an interconnected network of micro-channels linking the wells into which samples are added. The micro-channels are filled with a sieving polymer and fluorescent dye. When

the wells and channels are filled, the chip becomes an integrated circuit through which a charge is applied. RNA, as a charged biomolecule is driven by a voltage gradient formed within the chip. RNA has a constant mass-to-charge ratio, the samples are therefore separated by charge but also size. The fluorescent dye within the micro-channels intercalates into the RNA, permitting fluorescent laser detection. A ladder containing RNA fragments of known molecular size and concentration is run alongside the samples under analysis. By comparing when the fluorescently labelled RNA from the ladder and the unknown samples pass the detector and the relative strength of signal, the analysis software is able to identify the size and concentration of RNA fragments within these samples. This data is converted into electropherograms for interpretation (Figure 3.2B). The software automatically identifies the ribosomal RNA peaks 18s and 28s (Figure 3.2B[ii]) and by comparing their relative levels and the level of background signal, an RNA integrity number (RIN) is assigned to the sample, ranging from 10 (perfectly intact) to 1 (completely degraded) (Figure 3.3). Agilent Microarray analysis requires a RIN of 7 or greater, therefore only RNA samples achieving this level were taken forward for microarray transcriptomic analysis.

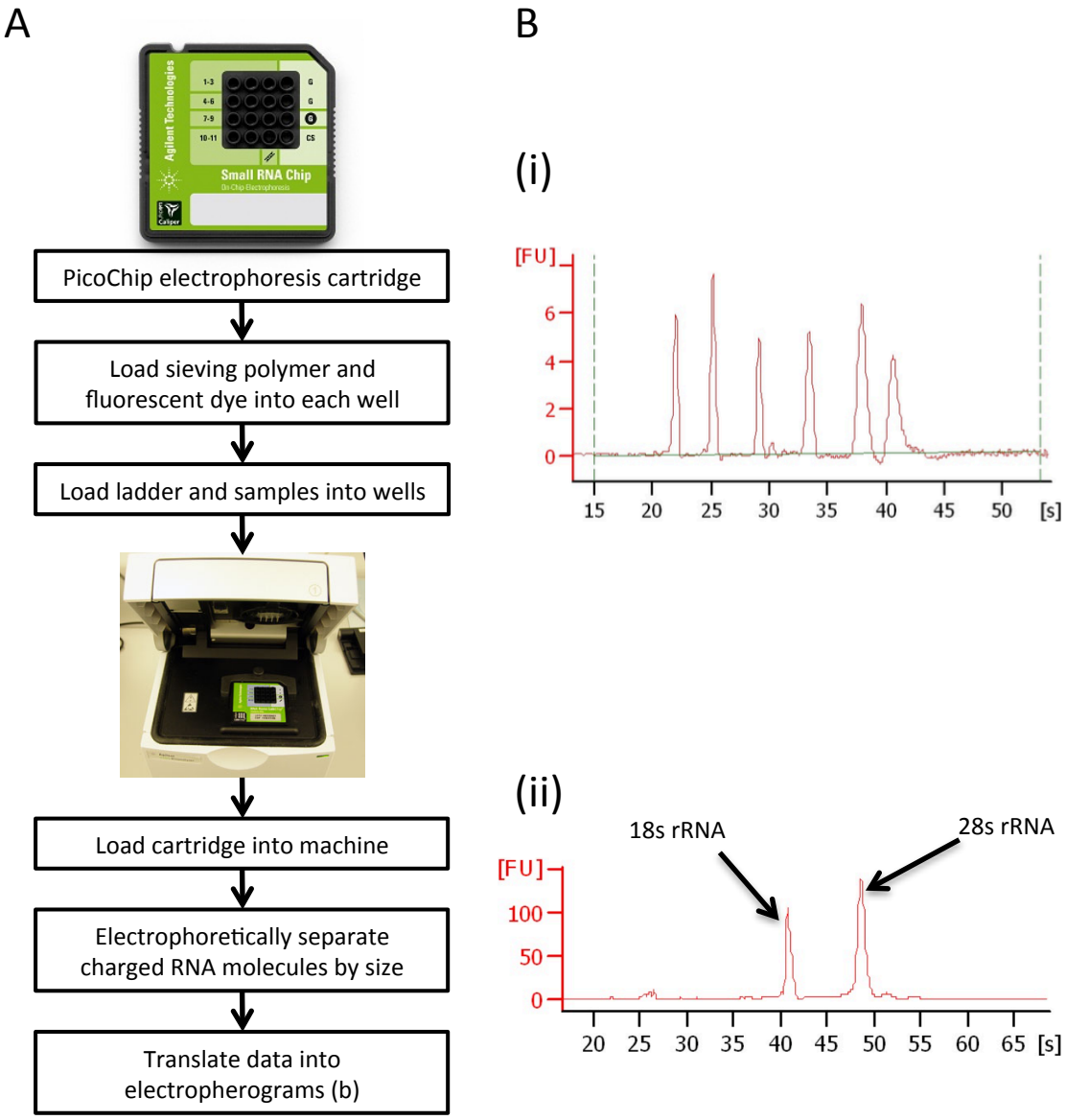

Figure 3.2 Agilent bioanalyser electrophoresis. A, flow diagram of bioanalyser RNA-integrity analysis. B, electropherograms from (i) the ladder reference sample and (ii) an RNA sample with the twin 18s and 28s ribosomal RNA peaks highlighted.

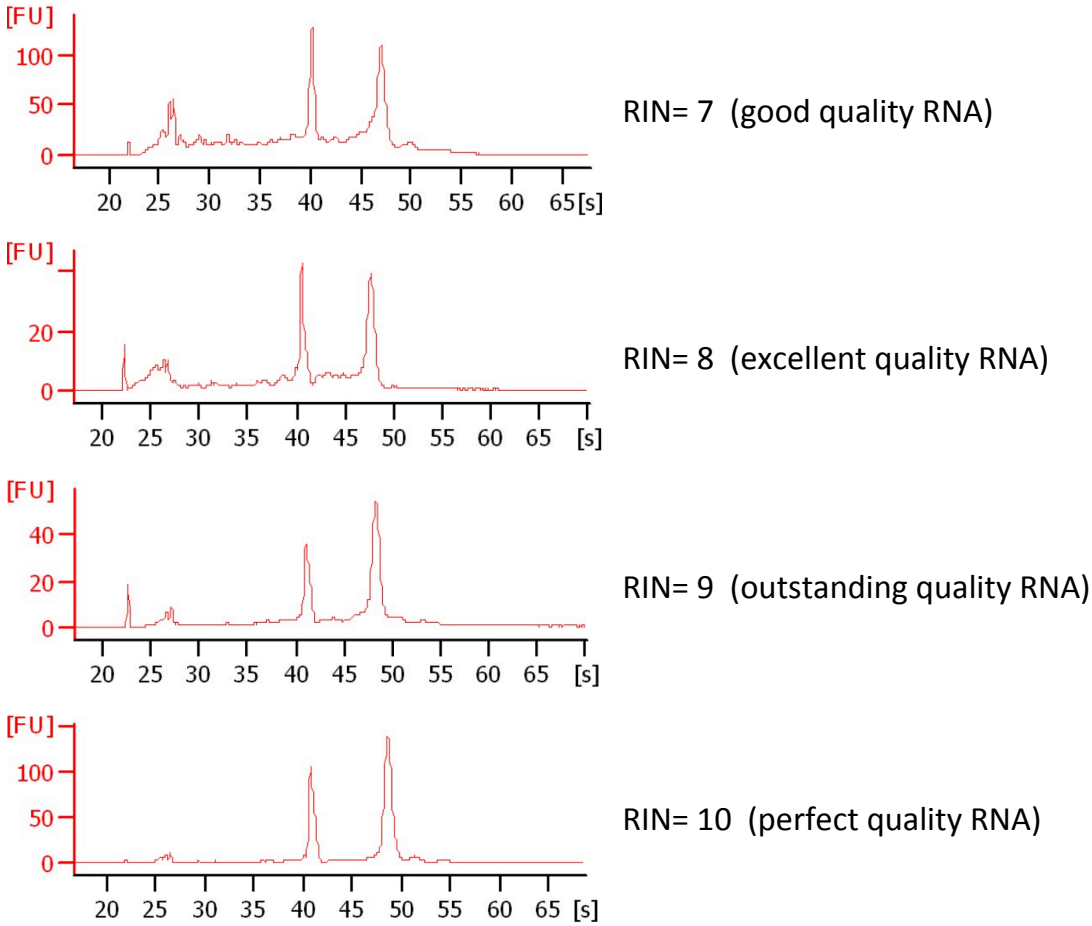

Figure 3.3 Agilent bioanalyser electropherograms of good to perfect quality RNA.

3.2.3 RTqPCR and validation of endothelial isolation

In order to ensure that endothelial specific isolation had been achieved, the isolate samples along with the matched endothelial depleted fraction, were probed for the expression of markers of common cell types by two-step quantitative reverse transcription polymerase chain reaction (RTqPCR), using the Roche Exiquon ProbeLibrary system. RTqPCR is a commonly used technique to quantify RNA expression. Total RNA is first converted to complementary DNA (cDNA) by a process of reverse transcription, using random primers and a reverse transcriptase. In the qPCR

stage, primers are used that are specifically designed to be complementary to either end of a small region of the gene of interest and to span at least one exon-exon junction, so as to avoid polymerisation of any genomic DNA contamination, which would not contain this junction. In the Roche Exiquon ProbeLibrary system this region is designed to contain an 8-9 base recognition site for one of 165 unique fluorescent probes. The cDNA is exposed to cycling conditions wherein the primers bind and a DNA polymerase synthesises the small region, during which the fluorescent probe is incorporated. When the new DNA fragment is released from the synthesis machinery the probe is cleaved, activating its fluorescence, which is then detected by a laser. Since this amplification process can only occur once per cycle it is generally accepted that the population of DNA corresponding to this region doubles each time. Therefore the fluorescent signal increases exponentially at a logarithmic factor of 2. The delta-delta cycle threshold (ΔΔCT) method for quantifying RNA expression is based upon this principle. The number of cycles it takes for the fluorescent signal to exceed a set threshold level is used as a relative marker of how much cDNA (and originally RNA) corresponding to the gene of interest, was present in the original sample. To compare the RNA expression level of a gene between two samples, the expression of a consistently expressed "housekeeping gene," in this study flotillin-2, must also be probed. This housekeeping gene is assumed to be expressed at the same level in both samples and is used to normalise for differences in the concentration of the samples as follows:

Delta-delta cycle threshold method

CT of target gene in sample 1 (CTgS1)

CT of housekeeping gene in sample 1 (CThkS1)

CT of target gene in sample 2 (CTgS2)

CT of housekeeping gene in sample 2 (CThkS2)

2^[(CThkS1 - CTgS1) – (CThkS2 - CTgS2)] = Fold expression difference for target gene in sample 1 vs. sample 2

The expression of markers of leukocytes (CD11b), macrophages (CD68), epithelium (EPCAM), smooth muscle (PDGFRA) and endothelium (PECAM) was compared between the endothelial isolate fractions and the matched endothelial depleted fractions by this method. This analysis determined that endothelium alone was enriched by between 7 and 17 fold in the endothelial isolate fractions (Figure 3.4).

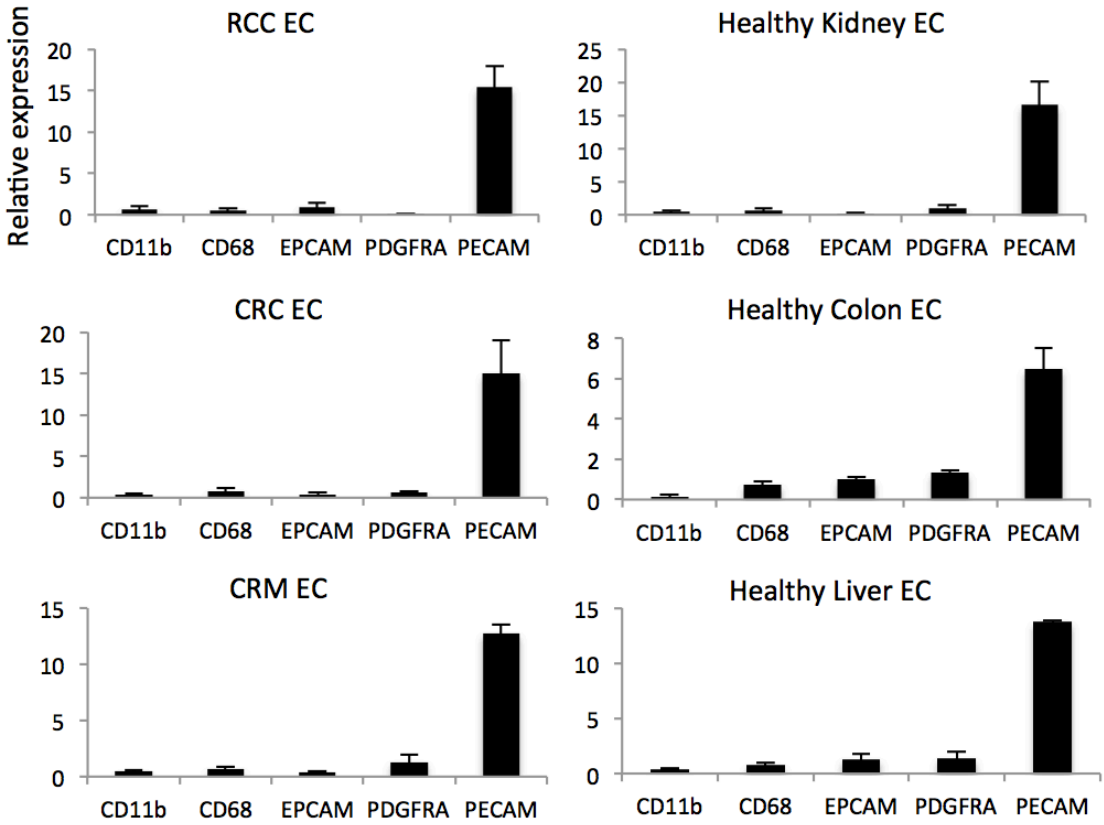

Figure 3.4 Confirmation of endothelial isolation efficiency by RTqPCR for markers of leukocytes (CD11b), macrophages (CD68), epithelium (EPCAM), smooth muscle (PDGFRA) and endothelium (PECAM) in the endothelial isolates (EC) from renal cell carcinoma (RCC, n = 8), colorectal carcinoma (CRC, n = 8), colorectal liver metastases (CRM, n = 7) and matched surrounding healthy tissues (n = 8,8,7), standardised to flotillin-2 (a house keeping gene) and normalised for marker expression to patient matched bulk tissue. The fold change of marker expression between the endothelial and bulk fraction is shown. Confidence limits are ± standard error of the mean (SEM).

3.2.4 RNA labelling and hybridisation for microarray

In order to conduct large-scale microarray transcriptomic analysis, Cyanine 3 fluorescently labelled cRNA was first generated from the RNA of selected samples, as described in Figure 3.5. Briefly cDNA was synthesised from the RNA samples using a primer containing poly dT and a T7 promoter and catalysed by Affinity Script reverse

transcriptase. This generated random cDNA fragments with a 5' T7-promoter sequence. Next, cRNA was synthesised from the cDNA using T7-RNA polymerase, which simultaneously incorporates Cy3 labelled nucleotides. Once labelled the cRNA samples were hybridised to an 8-pack Agilent microarray slide (Figure 3.6). This slide contains 8 distinct domains, for 8 samples, each spotted with 66,000 unique cDNA fragments complementary to every known gene in the genome (~20,000) and selected micro-RNAs (miRNAs), with an average of 3 forms of cDNA per gene. During hybridisation labelled cRNA binds to its complementary cDNA fragments. Each spot is then probed and quantified by a scanning laser, generating data about the relative expression levels of the genes probed for computational analysis.

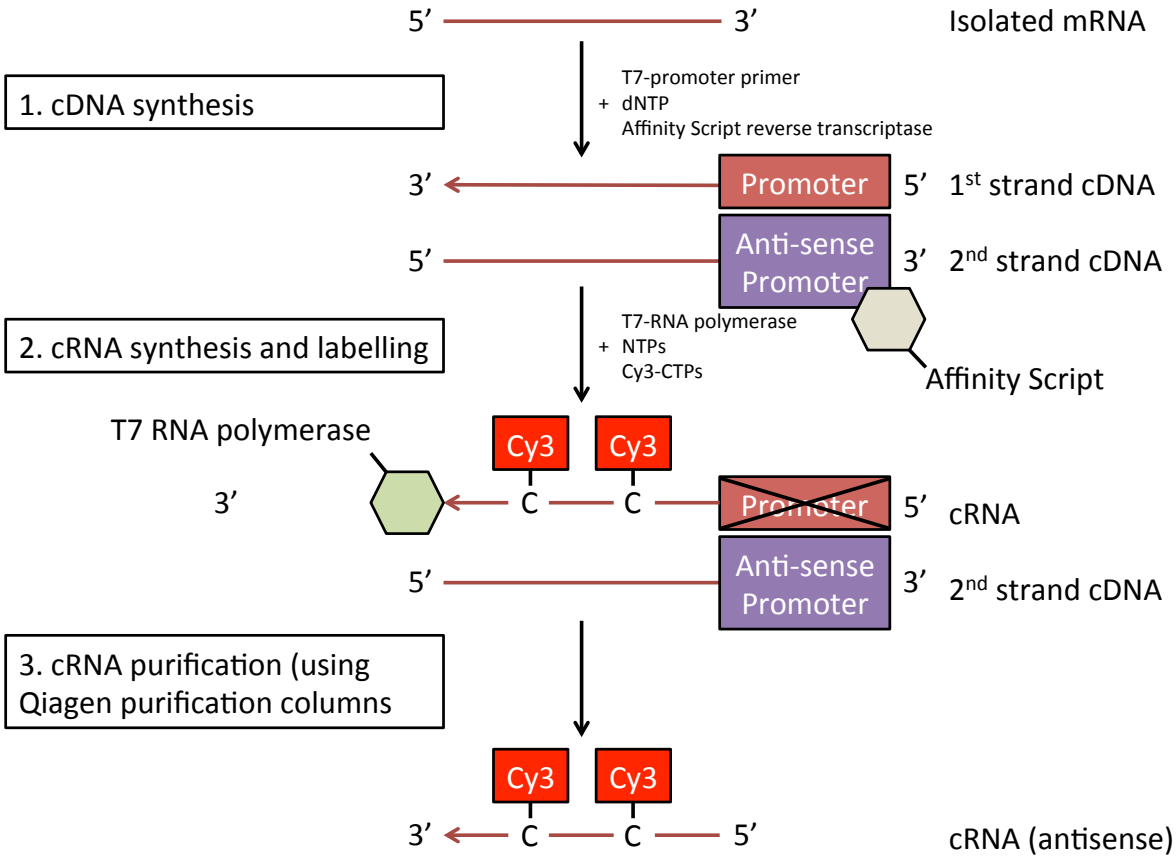

Figure 3.5 RNA labelling for microarray analysis. Flow diagram showing the multiple steps involved with the synthesis and amplification of labelled cRNA from isolated RNA.

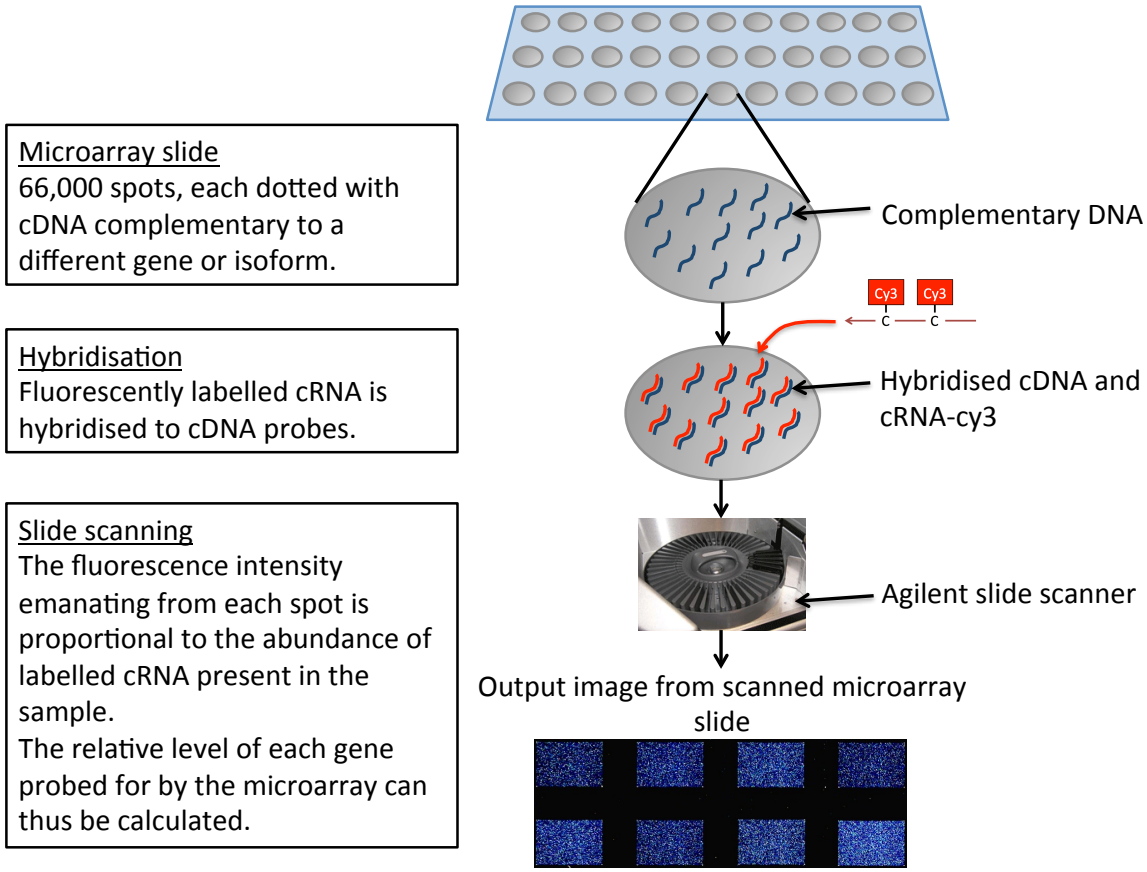

Figure 3.6 Labelled cRNA hybridisation for microarray analysis. Schematic showing the key steps in the hybridisation process of labelled cRNA, to specifically designed cDNA fragments, fused to a microarray chip.

3.2.5 Microarray data normalisation and generation of comparison matrices

Raw microarray data was background corrected and normalised between the arrays under comparison, before being formatted into comparison matrices.

The following comparison matrices were generated using this method:

Colorectal cancer – Healthy colon (Table 3.1, used in chapters 4 & 5).

Colorectal liver metastasis – Healthy liver (Table 3.2, used in chapter 5).

Colorectal liver metastasis – Healthy colon (Table 3.1 & 3.2, used in chapter 5).

Renal cell carcinoma – Healthy kidney (Table 3.3, used in chapter 5).

3.3 Discussion

This chapter discusses the isolation of endothelium from colorectal tumours, colorectal liver metastasis and renal cell carcinoma, validation of the isolation process by RTqPCR and microarray based comparative gene expression analysis, between the endothelial isolates.

Endothelium was isolated from the tumour and healthy tissue resections with the use of magnetic beads conjugated to a lectin from *Ulex europeaus*, which binds very specifically to human endothelial cells (197). It has also been reported to bind to blood group H, expressed on the red blood cells of a roughly a quarter of humans (197), resulting in red blood cells being isolated alongside the endothelium in some isolates. As red blood cells are not a source of mRNA, this was not considered an issue for molecular profiling purposes.

3.3.1 *Ulex* lectin vs. PECAM-1

Other endothelial markers are available for isolation purposes, such as Platelet endothelial cell adhesion molecule (PECAM-1), however, this marker is additionally expressed on a subset of leukocytes (200), resulting in the potential for considerable contamination from this cell type. In order to remove this contamination a second endothelial marker, such as CD34 or Von Willebrand factor (VWF) must also be selected for. Two-step isolation would be difficult with magnetic beads and result in a loss of sample and therefore single step isolation using *Ulex* lectin was favoured.

3.3.2 Magnetic bead isolation vs. fluorescence-activated cell sorting (FACS)

One approach that would permit simple two way selection, thus excluding contamination from red blood cells or leukocytes, would be by fluorescence-activated cell sorting (FACS). Additionally this would allow a direct assessment of the purity of the sample in percentage terms, something the RTqPCR analysis used in this chapter cannot replicate. Unfortunately from consultation with the wider scientific community, it became clear that very large samples or the pooling of samples would be required to generate enough RNA to conduct microarray or RTqPCR analysis. This would result in a loss of personalised patient-specific gene analysis, a far slower, more expensive process of sample collection and certainly a considerable waste of a precious and difficult to acquire resource. Additionally absolute purity is not required at this stage for the generation of a short list of candidate tumour endothelial markers. By a subsequent process of literature searching, *in silico*, *in vitro* and molecular analysis, detailed in chapters 4 and 5, genuine targets were validated from the lists generated in this chapter. Magnetic bead isolation was found to be an extremely efficient (being successful on small tissue samples) and effective (resulting in good, consistent enrichment) method of endothelial isolation and was therefore selected above FACS.

3.3.3 Microarray analysis vs. next-generation sequencing

Microarray based analysis was used to conduct transcriptomic profiling of cancer and healthy endothelial isolates. This is an effective, robust and reliable method of profiling however, others with a potentially greater scope for investigation are available. As discussed in Wragg and Bicknell 2015 (201), next generation sequencing is an exciting new method of genomic and transcriptomic analysis allowing investigation of splice

variant and non-coding RNA expression in a way that a limited probe based microarray system cannot replicate. Certainly next generation sequencing is the future, however, despite becoming more efficient and sensitive over time, it still requires over ten fold more RNA than microarray analysis. It is several times more expensive, depending on scale, to generate the raw data. Programs designed to analyse and interpret the data are in their infancy and difficult to use, often generating a considerable amount of confounding data and requiring input from specialist bioinformaticians, often unfamiliar with the area of biology under investigation. For the budget and time allotted a considerably fuller investigation could be achieved by the older microarray based analysis systems and therefore for this investigation it was favoured.

Chapter Four

Colorectal Tumour Endothelial Markers

4.1 Introduction

Colorectal cancer is the third most common cancer globally, making up about 10% of all cases (202). There are over 1.4 million new cases annually, 65% of which are found in developed countries, with 695,000 deaths from the disease. Early stage colorectal cancer, confined to the wall of the colon, is usually curable with surgery. More advanced disease, making up 25% of cases in the UK, is often treated with a combination of surgery, radio and chemotherapy and is usually incurable (202).

The five-year survival rate in developed countries is around 65%, however, this drops to below 10% with metastatic disease (203). Curative treatment heavily relies upon the achievement of a histologically clear resection margin at surgery (204,205) and although 80% of CRC resections do achieve this, 50% will relapse to metastatic disease, due to the presence of micro-metastases present at the time of resection (203,206). Improvements in treatment and prevention of metastatic disease, are of vital importance to achieve better outcomes in CRC. It is upon this premise that the idea of targeting the tumour vessels in colorectal cancer is based. As has been mentioned in chapter 1, the vasculature is of vital importance to cancer spread and development of metastasis, and indeed vascular targeted anti-angiogenic drugs such as bevacizumab are often included alongside traditional chemotherapies in first line and second line treatment for advanced CRC (207). Reports of its effectiveness have been mixed however, with two large randomised studies showing no significant benefit and even a potential to cause harm in the adjuvant setting (208). Vascular targeting approaches to treat CRC are therefore in need of improvement and the identification of novel targets

on colorectal cancer vessels, which can be used to localise therapeutics to the tumour, could benefit the treatment of colorectal cancer.

4.2 Results

4.2.1 Comparative microarray analysis of CRC versus healthy colon

In order to investigate the relative expression of genes in the endothelium of colorectal cancer and patient matched healthy colon tissue, a comparison matrix was setup from the microarray data generated in chapter 3. This was:

Colorectal cancer – Healthy colon

This analysis compared the microarray gene expression data from four colorectal cancer endothelial isolates and patient matched healthy colon endothelial samples.

4.2.2 Known tumour associated genes, matrix metallopeptidases and collagens

A number of known tumour associated angiogenic genes were identified by this analysis (Table 4.1), including interleukin 8, angiopoietin 2 and lysyl oxidase like 2, validating the approach as a method for identifying genes enriched on tumour endothelium. This analysis additionally identified a host of collagens (Table 4.2) and matrix metallopeptidases (Table 4.3), key components of active extracellular matrix remodelling, important for endothelial migration and angiogenesis within the tissue. This data collectively implies a pattern of active angiogenesis occurring within the tumour, outstripping that of the surrounding healthy colon tissue.

Table 4.1. Known tumour associated or angiogenic genes enriched in colorectal cancer vessels.

Gene ID	Gene Symbol	GeneBank accession no.	LogFC	P-value
Interleukin 8	IL8	NM_000584	3.42	0.00
Angiopoietin 2	ANGPT2	NM_001147	3.40	0.00
Plexin domain containing 1	PLXDC1	NM_020405	3.12	0.01
Lysyl oxidase-like 2	LOXL2	NM_002318	3.11	0.01
Hairy/enhancer-of-split related with YRPW motif-like	HEYL	NM_014571	3.01	0.00
Placental growth factor	PGF	NM_002632	2.92	0.01
Platelet-derived growth factor receptor, beta polypeptide	PDGFRB	NM_002609	2.82	0.00
Endothelial cell-specific molecule 1	ESM1	NM_007036	2.63	0.00
CD86 molecule	CD86	NM_006889	2.42	0.05
Apelin	APLN	NM_017413	1.98	0.00
Insulin-like growth factor binding protein 7	IGFBP7	NM_001553	1.93	0.01
Angiopoietin-like 2	ANGPTL2	NM_012098	1.65	0.09
Major histocompatibility complex, class II, DR alpha	HLA-DRA	NM_019111	1.65	0.05
Tenascin C	TNC	NM_002160	1.42	0.12
Secreted protein, acidic, cysteine-rich (osteonectin)	SPARC	NM_003118	1.39	0.13
Neuropilin 1	NRP1	NM_001024629	1.23	0.08
Lysyl oxidase	LOX	NM_002317	1.20	0.21
Anthrax toxin receptor 1	ANTXR1	NM_053034	1.01	0.20

Table 4.2. Collagens enriched in colorectal cancer vessels.

Gene ID	Gene Symbol	GeneBank accession no.	LogFC	P-value
Collagen, type I, alpha 1	COL1A1	NM_000088	4.18	0.00
Collagen, type XII, alpha 1	COL12A1	NM_004370	3.13	0.00
Collagen, type IV, alpha 1	COL4A1	NM_001845	2.86	0.00
Collagen, type I, alpha 2	COL1A2	NM_000089	2.79	0.01
Collagen, type XV, alpha 1	COL15A1	NM_001855	2.56	0.01
Collagen, type XVIII, alpha 1	COL18A1	NM_030582	2.42	0.00
Collagen, type IV, alpha 2	COL4A2	NM_001846	2.36	0.00
Collagen, type V, alpha 1	COL5A1	NM_000093	2.30	0.04
Collagen, type VIII, alpha 1	COL8A1	NM_001850	2.28	0.02
Collagen, type V, alpha 2	COL5A2	NM_000393	2.10	0.03
Collagen, type VII, alpha 1	COL7A1	NM_000094	2.00	0.17
Collagen, type V, alpha 3	COL5A3	NM_015719	1.79	0.01
Collagen, type X, alpha 1	COL10A1	NM_000493	1.69	0.06
Collagen, type III, alpha 1	COL3A1	NM_000090	1.66	0.10
Collagen, type XIV, alpha 1	COL14A1	NM_021110	1.54	0.08
Collagen, type VI, alpha 1	COL6A1	NM_001848	1.45	0.14
Collagen, type VI, alpha 3	COL6A3	NM_004369	1.44	0.08
Collagen, type IX, alpha 1	COL9A1	NM_001851	1.08	0.11

Table 4.3. Matrix metallopeptidases enriched in colorectal cancer vessels.

Gene ID	Gene Symbol	GeneBank accession no.	LogFC	P-value
Matrix metallopeptidase 3 (stromelysin 1, progelatinase)	MMP3	NM_002422	5.72	0.01
Matrix metallopeptidase 7 (matrilysin, uterine)	MMP7	NM_002423	5.54	0.00
Matrix metallopeptidase 12 (macrophage elastase)	MMP12	NM_002426	4.86	0.00
Matrix metallopeptidase 1 (interstitial collagenase)	MMP1	NM_002421	4.49	0.04
Matrix metallopeptidase 9 (gelatinase B)	MMP9	NM_004994	4.10	0.00
Matrix metallopeptidase 11 (stromelysin 3)	MMP11	NM_005940	3.25	0.01
Matrix metallopeptidase 10 (stromelysin 2)	MMP10	NM_002425	2.54	0.10
Matrix metallopeptidase 14 (membrane-inserted)	MMP14	NM_004995	1.94	0.04
Matrix metallopeptidase 2 (gelatinase A)	MMP2	NM_004530	1.51	0.16
Matrix metallopeptidase 13 (collagenase 3)	MMP13	NM_002427	1.18	0.11

4.2.3 Selection of genes of interest

In order to identify potential endothelial markers in colorectal cancer, which can then be used to target therapeutics to the tumour vascular bed, a short list of genes of interest was generated (Table 4.4). This list detailed genes at least 5 times enriched on colorectal cancer vessels and with considerable evidence of trans-plasma-membrane expression. This was done to ensure that selected genes had both considerable differential expression, but were also directly targetable from the blood. This would simplify the mode of delivery of any potential therapeutics targeted against them. A literature review was undertaken on all targets, and those with prior published evidence of investigation in the context of colorectal cancer endothelium, were excluded from further study. This left eight candidate targets; stimulated by retinoic acid gene 6 (STRA6), glutamate receptor, ionotropic, N-methyl D-aspartate 2D (GRIN2D), fibronectin type III domain containing 1 (FNDC1), G protein-coupled receptor 4 (GPR4), regulator of G-protein signalling 5 (RGS5), transglutaminase 2 (TGM2), potassium inwardly-rectifying channel, subfamily J, member 8 (KCNJ8) and olfactory receptor, family 51, subfamily E, member 1 (OR51E1).

Table 4.4. Trans-membrane genes greater than 5 fold enriched in colorectal cancer vessels.

Gene ID	Gene Symbol	GeneBank accession no.	LogFC	P-value
EGF-like-domain, multiple 6	EGFL6	NM_001167890	4.86	0.00
Thrombospondin 2	THBS2	NM_003247	4.26	0.00
Fibroblast activation protein, alpha	FAP	NM_004460	4.11	0.00
Leucine zipper, putative tumor suppressor 1	LZTS1	NM_021020	4.03	0.00
Thy-1 cell surface antigen	THY1	NM_006288	3.87	0.00
Fc fragment of IgG, low affinity IIIa, receptor (CD16a)	FCGR3A	NM_000569	3.58	0.00
Interleukin 6 (interferon, beta 2)	IL6	NM_000600	3.40	0.00
Stimulated by retinoic acid gene 6 homolog (mouse)	STRA6	NM_001199042	3.15	0.00
Plexin domain containing 1	PLXDC1	NM_020405	3.12	0.01
Potassium inwardly-rectifying channel, subfamily J, member 8	KCNJ8	NM_004982	2.97	0.00
Placental growth factor	PGF	NM_002632	2.92	0.01
Pyrimidinergic receptor P2Y, G-protein coupled, 6	P2RY6	NM_176798	2.87	0.00
Glutamate receptor, ionotropic, N-methyl D-aspartate 2D	GRIN2D	NM_000836	2.83	0.01
Platelet-derived growth factor receptor, beta polypeptide	PDGFRB	NM_002609	2.82	0.00
Frizzled family receptor 10	FZD10	NM_007197	2.81	0.00
Tribbles homolog 3 (Drosophila)	TRIB3	NM_021158	2.81	0.01
Regulator of G-protein signalling 5	RGS5	NM_003617	2.79	0.00
Claudin 2	CLDN2	NM_001171092	2.75	0.02
Wingless-type MMTV integration site family member 2	WNT2	NM_003391	2.75	0.00
Uncharacterised LOC541471	LOC541471	NR_015395	2.73	0.01
Leukocyte immunoglobulin-like receptor, subfamily B, member 4	LILRB4	BC026309	2.71	0.01
Solute carrier family 4, sodium borate transporter, member 11	SLC4A11	NM_032034	2.67	0.01
Macrophage receptor with collagenous structure	MARCO	NM_006770	2.67	0.01
Vasorin	VASN	NM_138440	2.66	0.00
Transglutaminase 2	TGM2	NM_198951	2.60	0.00
Sulfatase 1	SULF1	NM_015170	2.58	0.02
Leucine rich repeat and Ig domain containing 1	LINGO1	NM_032808	2.57	0.00
SLAM family member 8	SLAMF8	NM_020125	2.52	0.03
Olfactory receptor, family 51, subfamily E, member 1	OR51E1	NM_152430	2.50	0.00
Gap junction protein, alpha 4, 37kDa	GJA4	NM_002060	2.50	0.00
Interleukin 13 receptor, alpha 2	IL13RA2	NM_000640	2.45	0.02
Regulator of G-protein signalling 16	RGS16	NM_002928	2.44	0.01
Fibronectin type III domain containing 1	FNDC1	NM_032532	2.39	0.02
Notch 3	NOTCH3	NM_000435	2.34	0.00
ArfGAP with dual PH domains 2	ADAP2	NM_018404	2.27	0.00
G protein-coupled receptor 4	GPR4	NM_005282	2.24	0.01

4.2.4 Validation of genes of interest

Microarray based differential analysis suffers from two weaknesses. First there is a high false positive rate of genes identified as being significantly differentially expressed, although this was ameliorated by the selection of genes greater than five times enriched in the tumour endothelium with a p-value < 0.05. Secondly it is unable to provide information about the absolute expression level of any of the genes identified, resulting in some being expressed differentially, but at such a minute level that they would be impossible to target.

RTqPCR was conducted on the eight selected candidate targets, in order to compare gene expression in colorectal cancer EC and healthy colon EC (n=8 for each) (Figure 4.1). Gene expression was normalised to both flotillin-2 (per cell expression level) and PECAM-1 (per endothelial cell expression level) in order to assess the level of enrichment of the target in the cancer endothelium (Table 4.5). Additionally target gene expression level in the cancer EC was compared to flotillin-2 expression, in order to ensure that genes were expressed at a high enough level to be of interest (Table 4.5). This investigation identified GRIN2D alone as having sufficient cancer enrichment and expression, to be taken forward for further investigation.

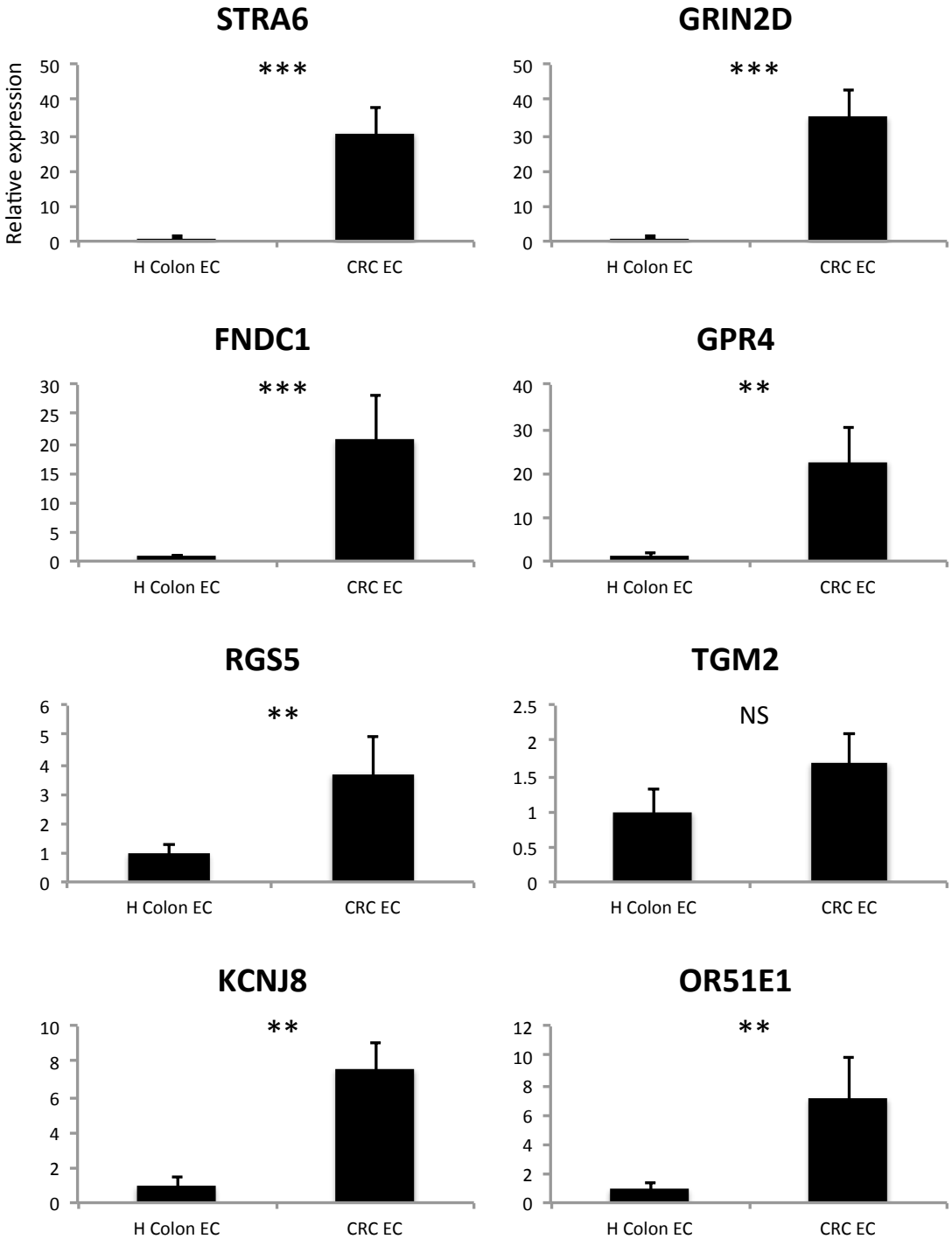

Figure 4.1. Validation of putative colorectal cancer vascular markers by RTqPCR. Quantitative real-time analysis of relative candidate target gene levels in endothelium isolated from malignant and healthy tissue. Gene expression levels were normalised to flotillin-2. Average gene expression ± SEM (n=8, Mann-Whitney U, *** $p<0.0001$, ** $p<0.001$, NS $p>0.05$).

Table 4.5. Selection of genes of interest for further investigation and validation based on gene enrichment and expression level in the tumour endothelial isolates

	Flotillin-2 vs. target fold expression change	PECAM vs. target fold expression change	Expression level relative to flotillin-2 (%)	Selected genes
STRA6	30.7	5.1	10.6	
GRIN2D	35.4	15.8	35.0	GRIN2D
FNDC1	20.5	2.4	16.9	
GPR4	22.7	8.8	17.3	
RGS5	3.7	1.0	109.1	
TGM2	1.7	0.5	841.7	
KCNJ8	7.5	6.25	4.4	
OR51E1	7.1	4.0	8.8	

Differential expression of GRIN2D was further validated on the protein level by immunohistochemistry (IHC) on formalin fixed paraffin embedded sections (Figure 4.2).

Immunohistochemistry is a semi-quantitative method to determine the expression and tissue localisation of a protein. This is achieved by first the removal of paraffin from the sections using a liquid in which paraffin is miscible, in this case, petroleum distillates (Histoclear), followed by a stepwise rehydration of the tissue with ethanol and water in varying combinations. This generates an environment within the tissue permissible to aqueous solutions. An EDTA solution is then used to restore the di-sulphide bonds and the three dimensional structure of proteins within the tissue, destroyed by formalin fixation and embedding. This permits the subsequent recognition and binding of antigens within the tissue to antibodies. First a primary antibody, recognising the target protein, is introduced, then a secondary antibody that recognises and binds the heavy chain of the primary antibody. The secondary antibody is conjugated to a

horseradish peroxidase, which catalyses a chromogenic peroxidase substrate to change colour and stain the location of antibody binding.

Sections of colorectal cancer and healthy colon were stained for PECAM-1 (a marker of endothelium) and GRIN2D by IHC. This analysis determined that the vessels in colorectal cancer stain strongly for GRIN2D, however, vessels in the healthy, marked by PECAM-1 staining do not stain for GRIN2D (Figure 4.2A and B). Additionally GRIN2D IHC staining was assessed by multi-organ tissue array analysis, in order to determine its global tumour and healthy tissue expression profile (Figure 4.2C). This involved staining 10 samples each, of 12 different tumour and matched healthy tissue sample for GRIN2D. The analysis identified GRIN2D to be positively expressed on the vessels of 40% of colorectal cancers, but only 10% of healthy colon samples. It was additionally expressed on a range of cancer and healthy tissues to a lesser extent. The fact that GRIN2D is expressed to a greater extent in cancerous tissues and in colon cancer in particular, is encouraging in that it suggests a potential for vessel specific targeting, but with careful monitoring for healthy tissue toxicity.

In order to investigate whether the expression of GRIN2D has any prognostic value in colorectal cancer, 90 colorectal tumours were stained for GRIN2D (Figure 4.3). Key clinical data for this cohort is shown in Table 4.6. The survival of patients with tumours positive or negative for GRIN2D staining was compared by log-ranks statistical analysis (Figure 4.3). This analysis determined that patients with positive vascular GRIN2D expression survived for longer than those without, though not to a significant level ($p=0.053$).

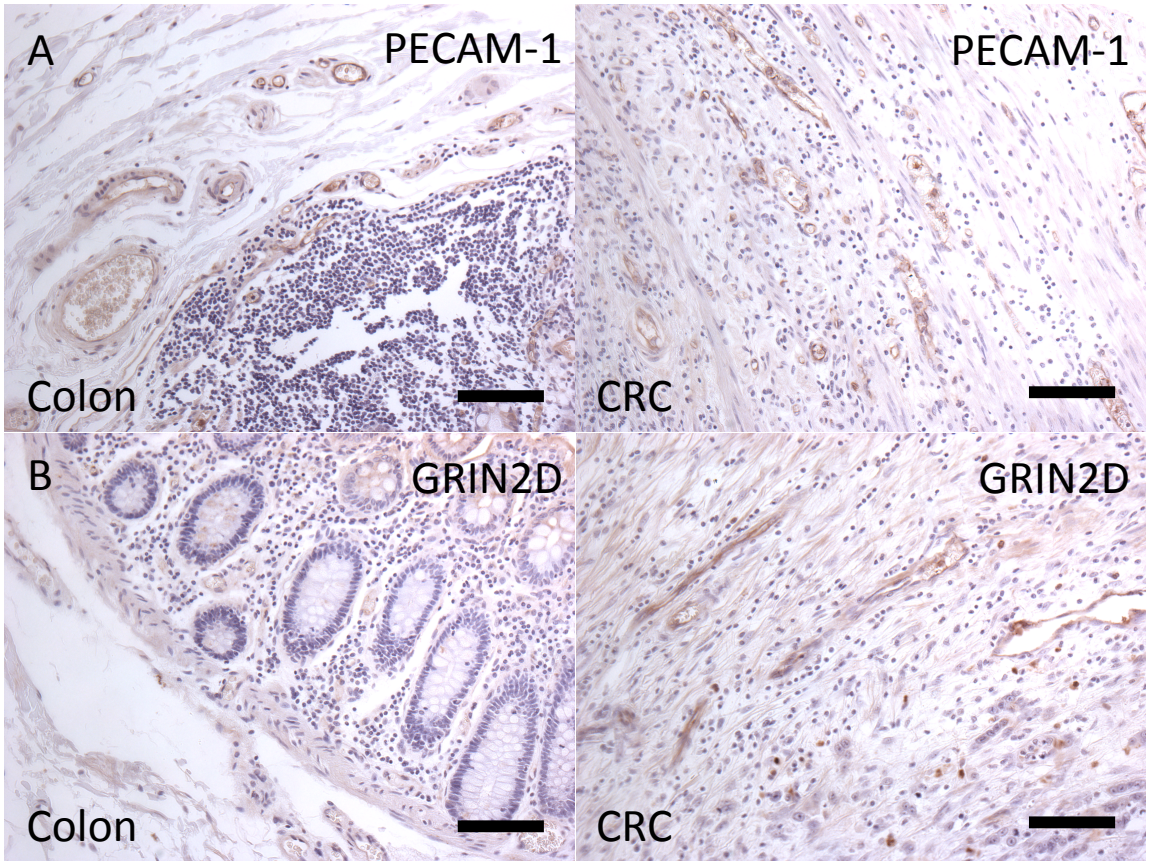

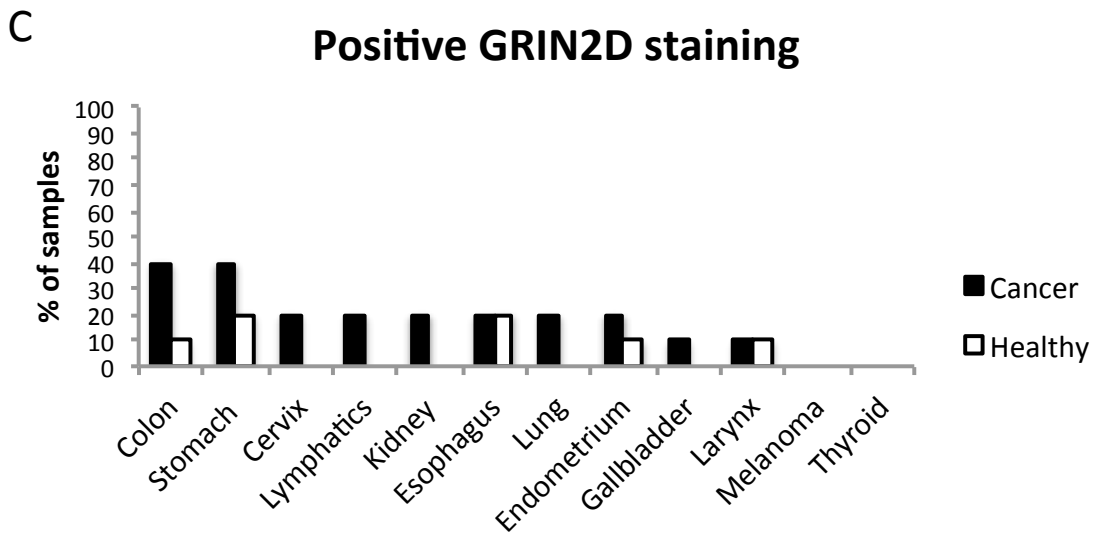

Figure 4.2. Confirmation of colon cancer specific enrichment of GRIN2D by immunohistochemistry. Representative images of A, PECAM and B, GRIN2D staining in healthy colon and colorectal cancer (scale bar = 50 μm). C, multi-organ tissue array analysis of GRIN2D expression, showing the frequency of positive GRIN2D vascular staining.

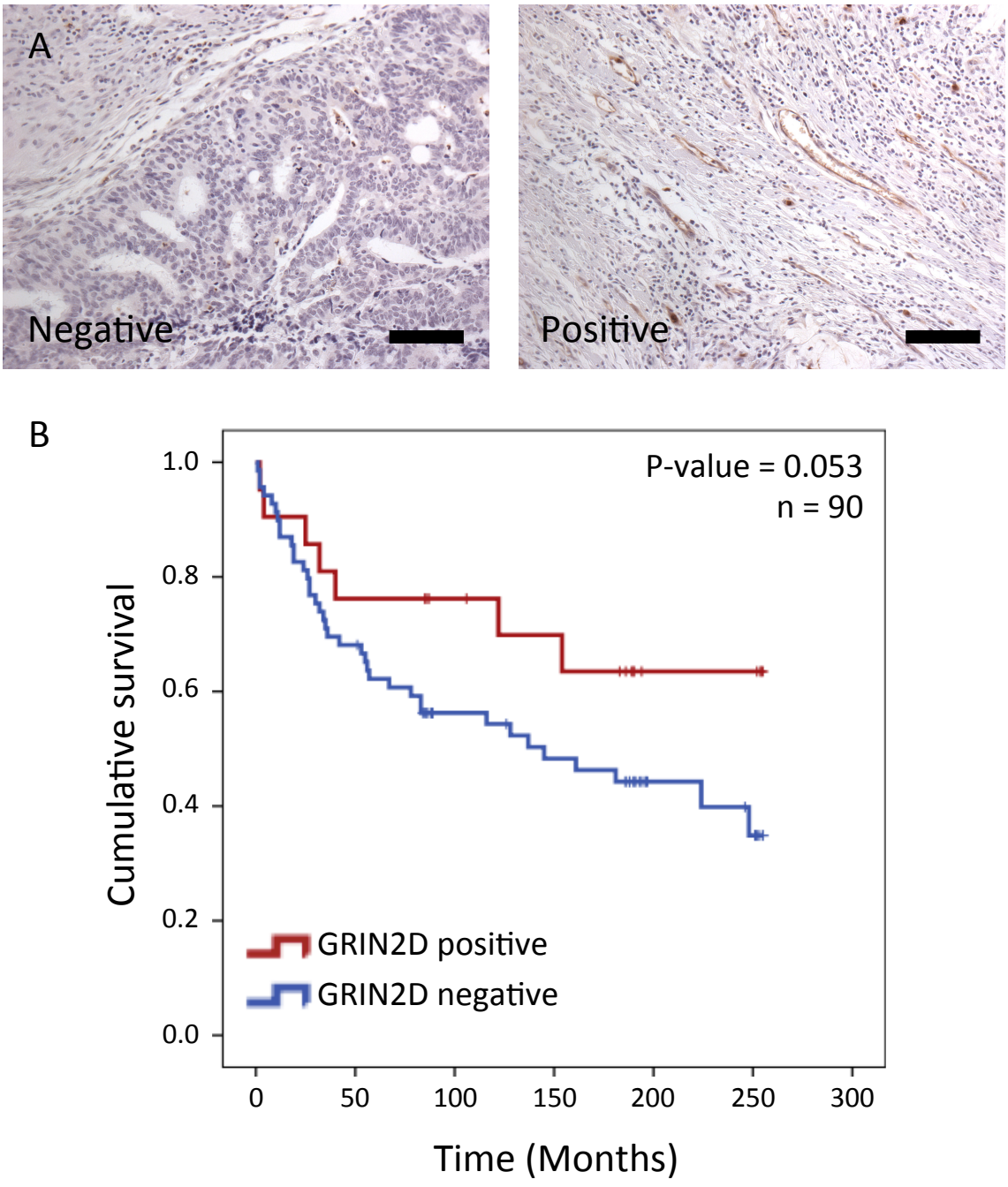

Figure 4.3. GRIN2D vascular expression is positively correlated with survival in colorectal cancer. A, representative images of positive and negative GRIN2D staining in CRC by IHC (scale bar = 50 μm). B, Kaplan-Meier analysis of survival in CRC with (red) or without (blue) GRIN2D vascular expression. Statistical analysis = Log-ranks test, P and N-numbers shown.

Table 4.6. Key clinical data for CRC cohort showing overall survival (OS).

Characteristics	N of patients	Median OS	Mean OS
All	90	87.5	112.8
Gender			
Male	65	86	107.2
Female	25	122	127.3
Age			
above 58	47	122	130.2
below or equal to 58	43	67	93.8
Stage			
I/II	44	157.5	148.5
III/IV	46	38	78.6
Tumour location			
Ascending colon	21	27	63.5
Descending colon	6	194	183
Sigmoid colon	31	84	96.6
Transverse colon	9	186	127.1
Cecum	4	102.5	109
Rectum	19	186	165.6
T-stage			
T2	8	187.5	160.5
T3	75	86	105.5
T4	7	122	136.3
N-stage			
N0	50	129.5	138.3
N1+	40	33	80.1
M-stage			
M0	75	116	126.3
M1	15	42	45.3
GRIN2D staining			
Positive	21	154	137.6
Negative	69	86	109.8

4.2.5 Analysis of the functional role in endothelium of GRIN2D

4.2.5.1 siRNA knockdown

In order to investigate the functional role GRIN2D plays in tumour endothelium, human umbilical cord vein endothelial cells (HUVEC) were transfected with small interfering RNA (siRNA) duplexes corresponding to GRIN2D, to selectively silence its expression. siRNA are double stranded RNA molecules of 20-25 base pairs and when introduced to a cell, are taken into the RNA interference (RNAi) pathway. This pathway evolved in eukaryotic cells as an anti-RNA virus response. When double stranded RNA, foreign to eukaryotic cells is detected, it is unwound to single-stranded RNA (ssRNA). One of these strands (in this case complementary to GRIN2D mRNA) is incorporated into the RNA-induced silencing complex (RISC), where it is used to guide the complex into binding with any complementary mRNA in the cell. The common outcome is the cleavage of the mRNA catalysed by Argonaute, a component of the RISC, thus achieving post-translational silencing of the target gene (or destruction of viral RNA).

4.2.5.2 RTqPCR and western blot GRIN2D silencing validation

Comparative RTqPCR for GRIN2D expression in cells transfected with siRNA duplexes, corresponding to GRIN2D in two locations or a scrambled non-mammalian sequence, was performed to assess the efficacy of siRNA for GRIN2D silencing (Figure 4.4A). This revealed a 60-70% reduction in GRIN2D expression in the presence of GRIN2D siRNA duplexes.

For a functional effect to be observed the protein level of GRIN2D must also be reduced. To ensure this was the case, western blot analysis of GRIN2D gene expression was

performed. In this assay proteins from the lysate of cells under investigation are sodium dodecyl sulphate (SDS) denatured and drawn through a polyacrylamide gel under a charge. Proteins are retarded by the acrylamide mesh, separating them based on their size. The separated proteins are then transferred from the gel to a PVDF membrane, again under a charge. This membrane then undergoes immunological probing for the gene of interest. It is first incubated with milk protein to block non-specific antibody binding, then incubated with an antibody recognising the gene of interest and finally washed and incubated with an antibody recognising the heavy chain of the first antibody, conjugated to horseradish peroxidase. A luminescent peroxidase substrate is then introduced to the membrane, causing the location of any proteins trapped on the membrane and recognised by the antibodies, to luminesce in a quantitative manner. The membrane is used to expose photosensitive film, the analysis of which permits the relative quantitation of protein expression between samples. By this method GRIN2D protein level was found to be reduced by 45-60% by treatment with GRIN2D siRNA duplexes (Figure 4.4B and C).

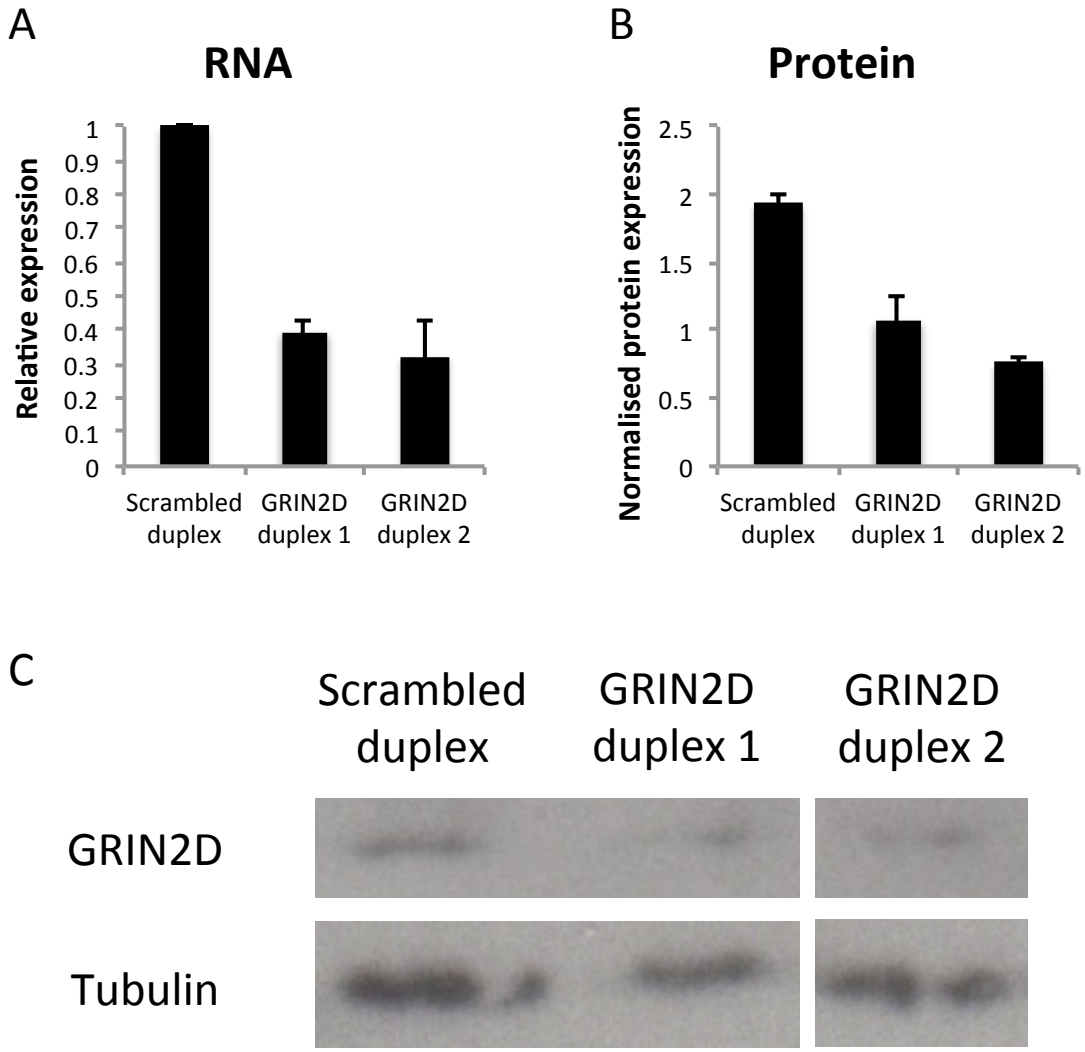

Figure 4.4. siRNA duplexes successfully knockdown GRIN2D expression on the RNA and protein level. Analysis of GRIN2D expression in three cords of HUVEC treated with a scrambled duplex or two GRIN2D targeting duplexes, by A, RTqPCR (normalised to flotillin-2) or B, western blot (normalised to Tubulin) (n=3, average expression ± SEM). C, representative western blot images (GRIN2D band - 70 kDa, Tubulin band – 55 kDa).

4.2.5.3 Matrigel tube forming assay

The cell-to-cell communication required for endothelial cells to differentiate into vessel tubes is vitally important for their healthy function. To assess the impact that the partial loss of GRIN2D expression has on this process, a matrigel tube-forming assay was performed. Endothelial cells are sparsely cultured in matrigel, a gelatinous protein mixture, secreted by Engelbreth-Holm-Swarm (EHS) mouse sarcoma cells that generates a growth matrix resembling the complex extracellular environment found in many tissues (209). Endothelial cells grown in this matrix form spiderweb like networks, reminisent of microvascular capillary systems (210). By assessing the complexity of network endothelial cells are able to form, their functionality can be determined. This is done by quantifying the number of nodes (network intersections) and sprouts per node, in this model of endothelial capillary formation. The capillary networks formed by endothelial cells from three HUVEC cords showed significant reduction in both the number of nodes ($p<0.001$) and sprouts per node ($p<0.001$) when treated with either GRIN2D siRNA duplex, compared to with the scrambled control duplex, suggesting GRIN2D plays some role in the endothelial capillary tube formation (Figure 4.5).

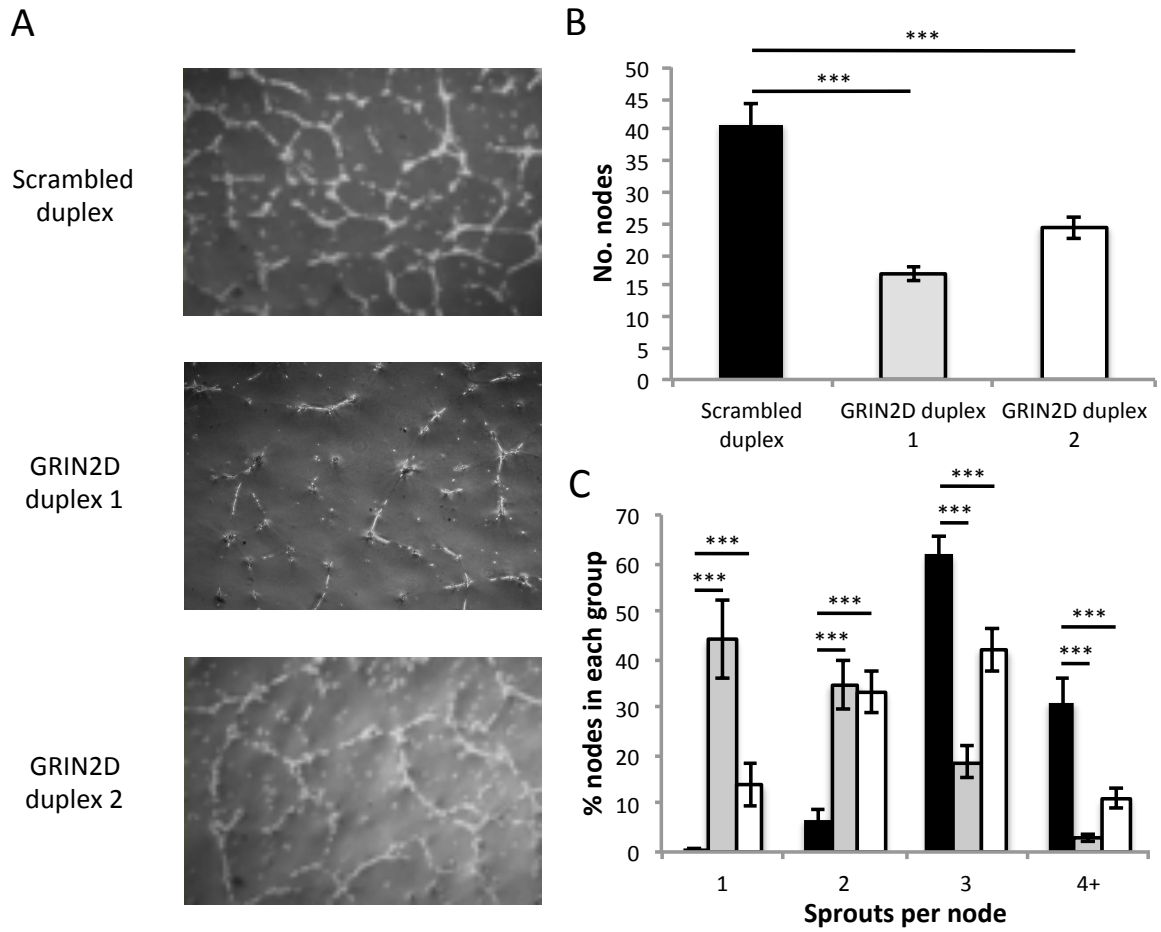

Figure 4.5. Loss of GRIN2D impairs endothelial matrigel tube formation. GRIN2D was knocked down by transfection of two siRNA duplexes into 3 separate HUVEC isolates. The cells were plated on matrigel and endothelial tube formation and integrity observed over 16 hours. A, representative images of tube formation in each condition. B, the average number of nodes per field of view ± SEM. C, the average number of sprouts per node ± SEM. (N=6 per condition [3] and isolate [3]) (Mann-Whitney U, *** $p<0.0001$).

4.2.5.4 Scratch wound assay

The speed of endothelial cell migration is an important indicator of functionality. To determine the effect GRIN2D knockdown has on endothelial migration, scratch wound assays were performed. In this assay, scratches are scored through a confluent monolayer of endothelial cells. Three scratches are scored from top to bottom and three from left to right, generating nine intersection sites into which endothelial cells will migrate, closing the scratch. By determining the percentage of the scratch wound still open at the point where the control duplex is 90% closed, the rate of endothelial migration can be compared. The percentage scratch wound closure was significantly reduced by GRIN2D knockdown with both duplexes, when compared to the scrambled control ($p<0.001$), suggesting that GRIN2D plays a significant role in endothelial migration (Figure 4.6).

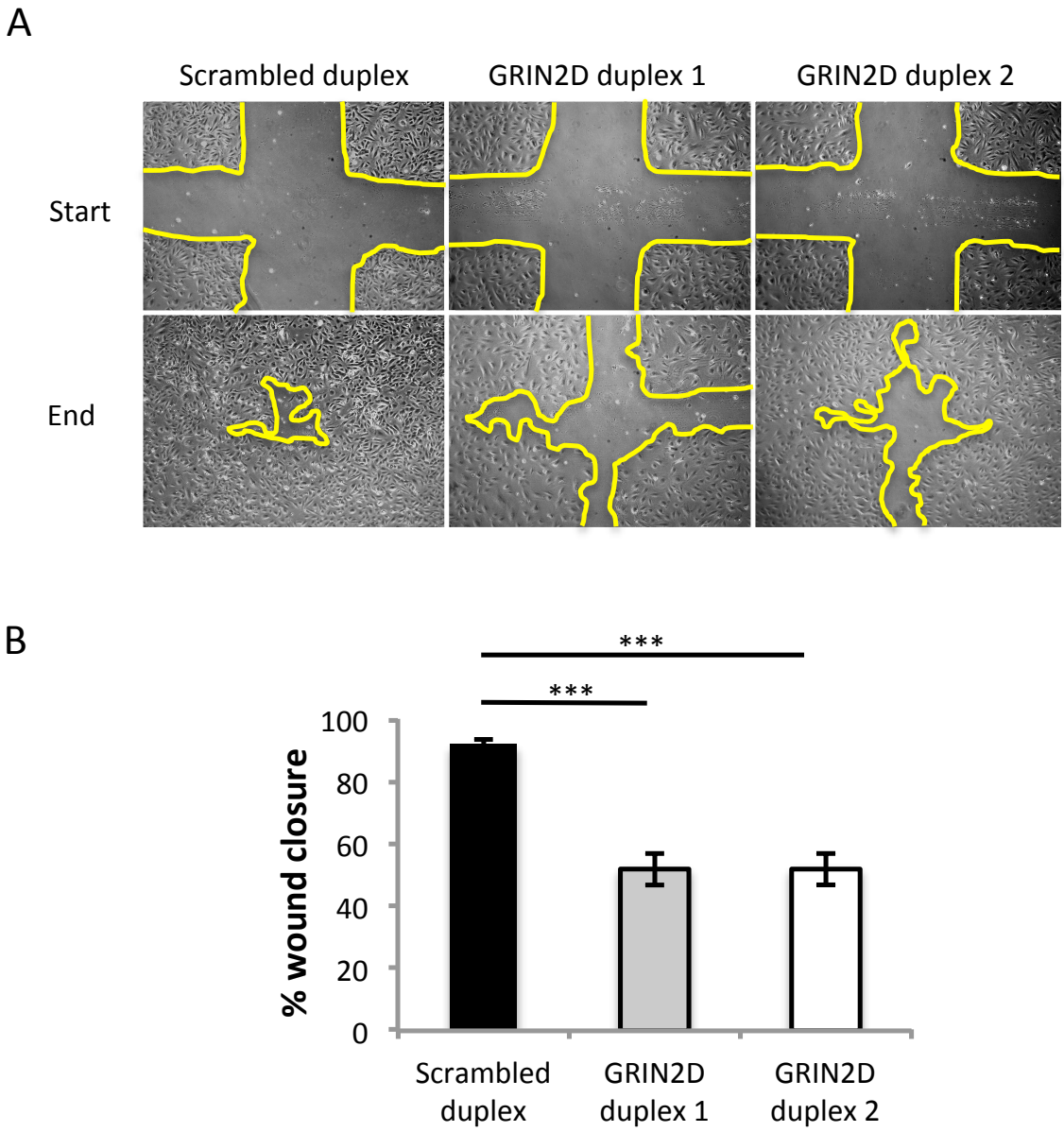

Figure 4.6. Loss of GRIN2D impairs scratch wound closure. GRIN2D was knocked down by transfection of two siRNA duplexes into 3 separate HUVEC isolates. The cells were plated, allowed to grow to confluence, the monolayer was scratched and wound closure observed at nine scratch intersections over time. A, representative images of wound closure from initial scratch to end-stage. B, quantification of percentage wound closure over the time course of the experiment ± SEM. (n=9 per condition [3] and isolate [3]) (Mann-Whitney U, *** $p<0.0001$).

4.2.5.5 Transfilter (modified Boyden chamber) assay

Endothelial migration takes many forms, the functionality of which the scratch wound assay alone cannot accurately assess. The transfilter assay tests the ability of the endothelial cell to transmigrate through a filter, stimulated by a growth factor and mitogen concentration gradient. In order to assess the effect the loss of GRIN2D has on transmigration, this assay was performed. The experimental set up is outlined in Figure 4.7A, briefly both sides of a membrane insert, with 8 μm pores, were gelatine coated generating a receptive environment for endothelial cells to cross the membrane. HUVEC were introduced on the upper side of the membrane in a low serum/ growth factor environment (M199 with 1% fetal calf serum (a source of the mitogens, sphingosine-1-phosphate [S1P] and lysophosphatidic acid [LPA]) and no brain extract (a source of FGF). On the lower side of the membrane a growth factor rich environment was set up (M199 with 10% FCS and 0.2% brain extract) creating a growth factor gradient across the membrane. HUVEC were allowed to migrate across this membrane for 16 hours, after which the cells on either side of the membrane were nuclear stained (with bisbenzamide) and quantified by fluorescent imaging. By determining the percentage of cells that have migrated across the membrane, endothelial transmigration can be assessed.

The percentage of cells that have migrated across the membrane was significantly reduced by GRIN2D knockdown with both duplexes when compared to the scrambled control ($p<0.001$), suggesting that GRIN2D plays a role in endothelial transmigration (Figure 4.7B).

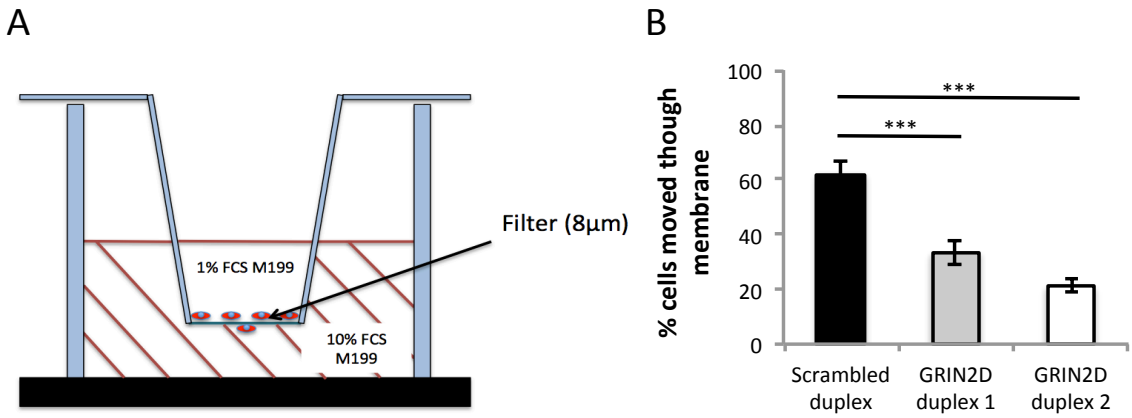

Figure 4.7. Loss of GRIN2D impairs endothelial cell transmigration and chemotaxis. GRIN2D was knocked down by transfection of two siRNA duplexes into 3 separate HUVEC isolates. The cells were subjected to the transfilter (modified Boyden chamber) assay the set up of which is shown in A. B, quantification of the average percentage of endothelial cells that have migrated through the filter, after 16 hours, per field of view ± SEM (n=6 per condition [3] and isolate [3]). (Mann-Whitney U, *** p<0.0001).

4.2.5.6 Acumen cell cytometry

Knockdown of genes important for cellular function can lead to a reduction in cell survival, proliferation and movement through the cell cycle, which could in turn effect cellular migration, chemotaxis and formation into a capillary-like network, in a manner not specific to those particular functions. In order to assess the effect GRIN2D knockdown has on the cell cycle, apoptosis and proliferation, Acumen cell cycle analysis was performed. Cells were sparsely plated into the wells of a 96 well plate, fixed with ethanol and stained for DNA content with propidium iodide (Figure 4.8A). The Acumen cell imager, by quantifying DNA content on a single cell basis, is able to split the cell population into G0/G1 phase cells, dead or dying cells (less nuclear material) and dividing cells (up to twice as much nuclear material) at each stage of the cell cycle. In this way the health of a cell population can be assessed, with a healthy population

profile shown in Figure 4.8B and an unhealthy (highly apoptotic) population profile shown in Figure 4.8C.

This assessment revealed no significant shift in population profile between the scrambled control duplex treated cells and those treated with either GRIN2D duplex, with all the profiles resembling that of the healthy population (Figure 4.8D, E and F). This suggests that loss of GRIN2D does not cause any cell cycle defect or loss of cell viability and proliferation, meaning that effects on endothelial cell migration, chemotaxis and formation into a capillary-like network are likely to be specific.

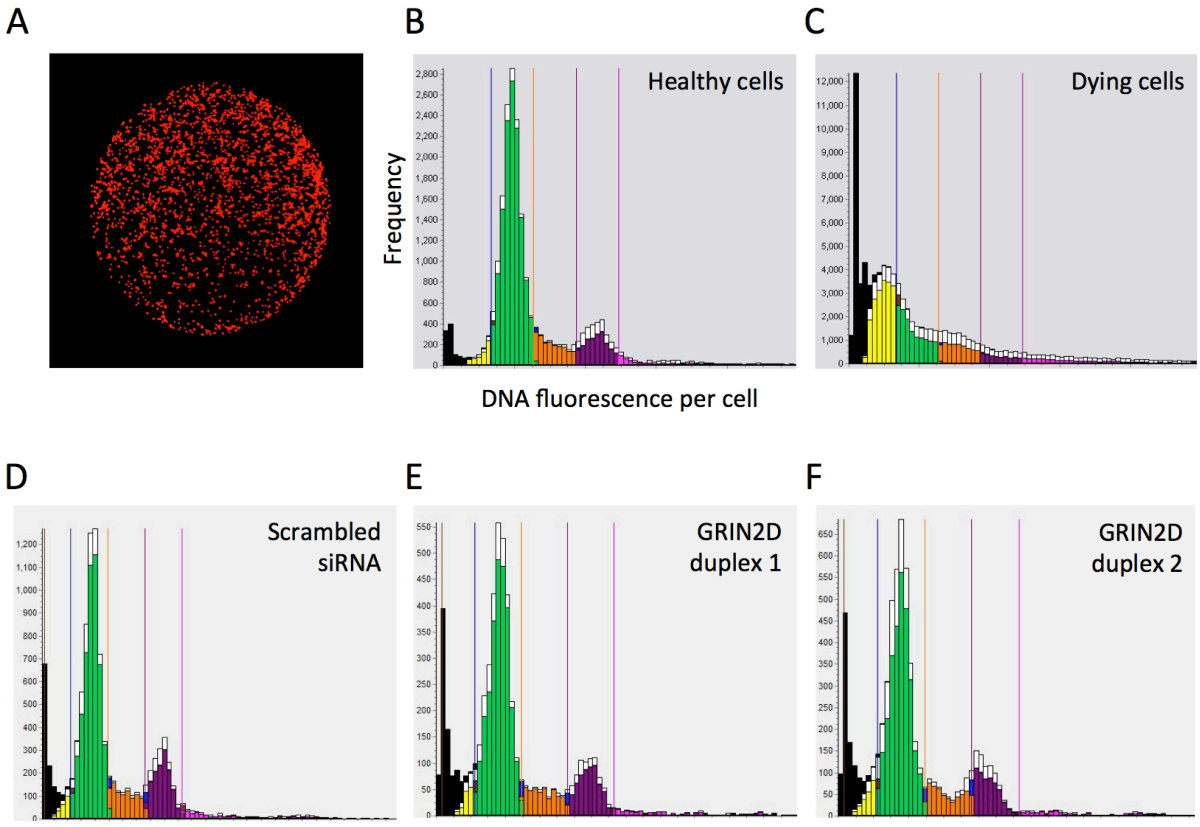

Figure 4.8. siRNA knockdown of GRIN2D in HUVEC does not affect cell viability, proliferation or progression through the cell cycle. siRNA treated cells were fluorescently labelled and imaged using the Acumen^{tm} cell imager (TTP Labtech). The cells were sorted by quantity of nuclear material into dead (black), apoptosing (yellow), G0/1-phase (green), S-phase (orange) and G2/M-phase (purple). A, representative image of fluorescently labelled cellular DNA. The histograms shown illustrate the proportion of cells at each phase in a plate of, B, healthy HUVEC, C, dying HUVEC, and HUVEC treated with either, D, scrambled siRNA, or E, GRIN2D siRNA duplex 1 and F, GRIN2D siRNA duplex 2.

4.3 Discussion

Microarray transcriptomic analysis on freshly isolated endothelium from colorectal cancer and matched healthy colon identified a panel of putative colorectal tumour endothelial markers. Of these the glutamate receptor GRIN2D emerged as the most interesting target. GRIN2D was shown to have vessel-restricted expression in colorectal cancer by RTqPCR and IHC analysis. Multi-organ tissue array analysis identified GRIN2D to be predominantly expressed in tumour tissue, particularly in colorectal malignancies, where its expression was shown to be associated with increased survival. *In vitro* analysis of GRIN2D's endothelial function showed it to be important in endothelial migration and capillary tube formation in matrigel.

GRIN2D is primarily studied as a neuronal ionotropic glutamate receptor, involved in long-term potentiation, which underlies certain types of learning and memory. GRIN2D is a component of the N-methyl-D aspartate (NMDA) receptor calcium channels, which are heteromers formed from a combination of GRIN1 and GRIN2 subunits (211). It is widely expressed within the brain, in particular the developing diencephalon, however, selective knockout mice develop normally both pre- and post-natally, with normal mating behaviour (212). There was no observed effect in motor activity or anxiety tests, however, due to the loss of function of certain NMDA receptors, mice showed altered emotional behaviour in forced swimming and light/dark box stress tests (213). This led to the suggestion of its role in the glutaminergic theory of schizophrenia, which has been a focus of GRIN2D research, reviewed in Moghaddam and Javitt, 2012 (214).

Neuronal and vascular cells share an embryonic stem cell lineage, leading to considerable cross-expression of endothelial and neuronal genes and many similarities in the processes that govern the modelling of vascular and neuronal architecture (215). With this in mind it is unsurprising that a traditionally neuronal glutamate receptor GRIN2D should be found to be expressed on endothelial cells.

GRIN2D's identity as a component of a calcium channel could be responsible for its observed role in angiogenesis. VEGF, a potent stimulatory growth factor of angiogenesis, promotes endothelial migration, proliferation and capillary formation in part via VEGF mediated calcium influx (216). Increased intracellular calcium concentration, observed or induced by arachidonic acid has been reported to promote endothelial migration and tube formation in angiogenesis assays (217,218). Loss of GRIN2D by siRNA knockdown results in reduced endothelial migration, tube formation and transmigration, which could be in part due to reduced calcium influx into the endothelial cells, curtailing the efficiency of growth factor mediated endothelial function, although this theory requires further investigation.

The functioning of GRIN2D in neuronal calcium channels is distinct from that of other NMDA receptor components, in that it promotes calcium influx over an extended period, mediating its role in long term potentiation (219,220). It is therefore easy to see how, by offering long-term calcium influx, the promotion of GRIN2D containing calcium channels in tumour endothelium could offer a survival advantage and even prime endothelial cells to respond to pro-angiogenic growth factor signalling within the tumour. Calcium flux and metabolism has been suggested as a target for anti-

angiogenic therapy (221) and targeted inhibition of GRIN2D could be a potential method for achieving this.

Multiple links have been described between glutamate receptor function and tumour biology, with knockdown of some non-GRIN2D glutamate receptor subunits resulting in both pro and anti-tumour effects (222). Additionally increased serum levels of glutamate have been reported as a marker of malignant potential in prostate cancer (223), where it has also been observed to be positively related to advancing Gleason grade (224). It has been proposed that this is due to glutamate acting to cause a genetic switch within the tumour, reducing the threshold for oncogenic k-ras signalling (225). This is of particular relevance in colorectal cancer as mutations in the k-ras oncogene is strongly implicated in the progression of colorectal cancer (226).

GRIN2D shows a promising tumour specific endothelial expression profile in a number of tumours, in particular colorectal cancer. However, it also appears to be expressed in a small subset of healthy tissues of the colon, stomach, esophagus and larynx as well as its reported expression throughout the brain and autonomic and enteric nervous systems (227). The integrity of the blood brain barrier (BBB) and other nervous system protective structures must be ensured and maintained to avoid potentially serious side effects from GRIN2D guided therapies. If the BBB is intact the safety of immunological therapies should still be maintained, as large proteins like antibodies, cannot pass through the tight endothelial junctions of the BBB (228). However, in 2-3% of cases of advanced CRC, patients develop brain metastases leading to disruption of the BBB (229). This could make targeting GRIN2D potentially unwise in this setting. With this in

mind, care will have to be taken in the selection of patients in which GRIN2D targeted therapies can be safely used.

Intriguingly GRIN2D expression in the vessels of colorectal cancer appears to be associated, albeit not quite significantly, to improved patient survival. The expression of tumour endothelial markers being associated with survival in this way is not without precedent. Expression of the tumour specific orphan receptor ELTD1 has been reported to be associated with improved survival in head and neck, colorectal and ovarian cancers (55). Increased expression of ROBO4, CLEC14A and ECSCR have also been associated with improvements in survival in non-small cell lung cancer (230). It has been suggested that the expression of these pro-angiogenic TEMs could be associated with vascular normalisation within tumours. Indeed ROBO4-Slit2 signalling has been implicated in the normalisation of VEGF induced chaotic vascular structures (231). This vascular normalisation could in turn lead to improved perfusion of the tumours leading to greater responsiveness to systematic blood-borne chemotherapeutics and therefore increased survival (55,230).

In conclusion GRIN2D is a promising vascular target in colorectal cancer for both treatment and prognostication. Endothelial function is impaired by siRNA-mediated disruption of gene function in *in vitro* angiogenesis assays. This effect may be due to reduced calcium flux within the endothelial cells, although this theory requires further investigation. The expression profile of GRIN2D throughout the body must be further assessed in order to ascertain the safety of systemic administration of GRIN2D targeted therapies.

Chapter Five

MCAM, LAMA4 and Other Pan-Tumour Endothelial Markers

5.1 Introduction

One of the difficulties encountered with identifying tumour endothelial markers from data derived from only one tumour type is one of considerable false positivity. However, as shown in chapter 4, it can be effective for the identification of cancer type specific markers, such as GRIN2D. In order to address this issue, data from microarray analysis of vessels from renal cell carcinoma and colorectal liver metastasis generated in chapter 3 were combined with the colorectal data discussed in chapter 4. With this analysis a pan-tumour endothelial marker expression profile was generated, hopefully improving the identification of targets, not just in CRC, but also RCC and CRM.

Approximately 271,000 new cases of renal cancer are diagnosed each year worldwide, 3% of all cancers, with the highest incidence rate found in North America (232). By far the most common form of kidney cancer is renal cell carcinoma (RCC), accounting for 90-95% of cases (232). Initial treatment is most commonly surgical, with this approach remaining the primary curative intervention (233). Unfortunately as RCC is often asymptomatic until the tumour is advanced or metastatic, curative surgical treatment is often not possible. Five year survival drops from 65-90% in operable cases to less than 10% in metastatic disease (234). It is therefore clear that new prognostic/diagnostic biomarkers for RCC are urgently needed.

Inoperable or recurrent RCC is difficult to treat with the success rate of traditional chemo or radiotherapy at 4-5% (235). Because of this, a multitude of alternative therapies have been trialled and shown efficacy in metastatic RCC (mRCC), including vascular endothelial growth factor (VEGF) targeted antiangiogenic therapies, sunitinib,

bevacizumab, sorafenib and axitinib (236). RCC being a cancer characteristic for and highly dependent on excessive VEGF production, due to the common loss of the tumour suppressor Von Hippel-Lindau (237) in clear cell RCC (ccRCC), anti-VEGF therapies have improved the outlook for mRCC (236). Despite this, 5-year survival remains low and antiangiogenic treatment relapse is very common (236). Because of this, it was decided that renal cell carcinoma would be an ideal tumour type, alongside colorectal cancer, in which to identify and target tumour vascular markers for therapy.

5.2 Results

5.2.1 Identification of a pan-tumour endothelial expression profile

As described in chapter 3 endothelial cells from renal cell carcinoma, colorectal carcinoma and liver metastasis from colorectal cancer were isolated and subjected to microarray analysis. Four comparison matrices were set up, RCC vs. Kidney, CRC vs. Colon, CRM vs. Colon and CRM vs. Liver. The CRM data was compared to the colon as well as the liver from which its vessels are derived, in order to set up a direct comparison between the markers induced by the colorectal primary tumour and the colorectal metastasis. This analysis identified multiple collagens consistently up-regulated within the three tumour types studied. Collagen type IV family members in particular were altered in their expression levels, whilst alpha 1 and 2 were up-regulated in the tumours, alpha 3, 4 and 5 were down-regulated (Table 5.1). Many matrix metallopeptidases were also modulated by exposure to the tumour environment. In particular MMP9, MMP12 and MMP14, whilst MMP7 and 11 were consistently up-regulated in the vessels of tumours derived from colorectal malignancy alone (Table 5.2).

Table 5.1. Collagen regulation across tissue types (Gene expression comparison shown as Log2 fold change).

Gene ID	Gene symbol	GenBank accession no.	RCC vs. Kidney	CRC vs. Colon	CRM vs. Colon	CRM vs. Liver
Collagen, type I, alpha 1	COL1A1	NM_000088	1.47	4.18	3.88	3.17
Collagen, type I, alpha 2	COL1A2	NM_000089	1.18	2.79	2.36	2.20
Collagen, type III, alpha 1	COL3A1	NM_000090	0.62	1.66	1.64	1.41
Collagen, type IV, alpha 1	COL4A1	NM_001845	1.85	2.86	3.13	1.70
Collagen, type IV, alpha 2	COL4A2	NM_001846	1.19	2.36	2.08	1.31
Collagen, type IV, alpha 3	COL4A3	NM_000091	-1.29	-0.36	-0.09	-0.63
Collagen, type IV, alpha 4	COL4A4	NM_000092	-1.29	-0.97	0.39	-1.48
Collagen, type IV, alpha 5	COL4A5	NM_033380	-1.32	-1.20	-2.67	-1.73
Collagen, type V, alpha 1	COL5A1	NM_000093	1.02	2.30	2.23	2.09
Collagen, type V, alpha 2	COL5A2	NM_000393	1.24	2.10	1.80	2.25
Collagen, type V, alpha 3	COL5A3	NM_015719	1.29	1.79	0.23	-0.19
Collagen, type VI, alpha 1	COL6A1	NM_001848	0.75	1.45	-0.27	-0.08
Collagen, type VI, alpha 2	COL6A2	NM_058175	1.71	0.23	0.97	0.25
Collagen, type VI, alpha 3	COL6A3	NM_004369	0.52	1.44	1.22	1.72
Collagen, type VI, alpha 6	COL6A6	NM_001102608	-0.42	0.07	-0.01	-1.93
Collagen, type VII, alpha 1	COL7A1	NM_000094	-1.39	2.00	1.22	1.15
Collagen, type VIII, alpha 1	COL8A1	NM_001850	2.09	2.28	2.94	1.31
Collagen, type VIII, alpha 2	COL8A2	NM_005202	0.73	0.93	0.56	1.26
Collagen, type IX, alpha 1	COL9A1	NM_001851	0.11	1.08	0.24	0.40
Collagen, type IX, alpha 3	COL9A3	NM_001853	0.29	-0.19	1.07	1.70
Collagen, type X, alpha 1	COL10A1	NM_000493	-0.05	1.69	3.03	2.40
Collagen, type XII, alpha 1	COL12A1	NM_004370	0.75	3.13	1.53	1.03
Collagen, type XIV, alpha 1	COL14A1	NM_021110	0.34	1.54	0.75	-0.09
Collagen, type XV, alpha 1	COL15A1	NM_001855	1.18	2.56	1.73	1.23
Collagen, type XVI, alpha 1	COL16A1	NM_001856	0.50	0.48	0.55	1.11
Collagen, type XVII, alpha 1	COL17A1	NM_000494	-0.37	-0.39	-0.81	2.49
Collagen, type XVIII, alpha 1	COL18A1	NM_030582	0.65	2.42	2.01	1.08
Collagen, type XXI, alpha 1	COL21A1	NM_030820	2.39	-0.84	-0.36	-1.29
Collagen, type XXII, alpha 1	COL22A1	NM_152888	-0.39	0.47	0.40	1.01
Collagen, type XXIII, alpha 1	COL23A1	NM_173465	1.53	0.10	0.15	0.08

Table 5.2. Matrix metallopeptidase regulation across tissue types (Gene expression comparison shown as Log2 fold change).

Gene ID	Gene symbol	GenBank accession no.	RCC vs. Kidney	CRC vs. Colon	CRM vs. Colon	CRM vs. Liver
Matrix metallopeptidase 1	MMP1	NM_002421	0.16	4.49	-0.57	2.12
Matrix metallopeptidase 2	MMP2	NM_004530	0.63	1.51	-0.80	-0.32
Matrix metallopeptidase 3	MMP3	NM_002422	0.02	5.72	-1.66	0.75
Matrix metallopeptidase 7	MMP7	NM_002423	-1.01	5.54	6.25	1.78
Matrix metallopeptidase 9	MMP9	NM_004994	3.60	4.10	5.03	2.98
Matrix metallopeptidase 10	MMP10	NM_002425	-0.01	2.54	-0.06	0.69
Matrix metallopeptidase 11	MMP11	NM_005940	0.28	3.25	3.16	4.70
Matrix metallopeptidase 12	MMP12	NM_002426	0.68	4.86	3.79	5.76
Matrix metallopeptidase 13	MMP13	NM_002427	0.28	1.18	-0.11	0.26
Matrix metallopeptidase 14	MMP14	NM_004995	0.87	1.94	1.77	1.58
Matrix metallopeptidase 16	MMP16	NM_005941	1.03	0.56	0.81	0.50
Matrix metallopeptidase 23B	MMP23B	NM_006983	0.13	0.38	1.14	0.44

In order to generate a shortlist of consistently up-regulated tumour endothelial markers (TEMs), comparative Venn analysis was performed on genes 2 fold up-regulated in the cancer with a p-value < 0.001, from each of the four comparison matrices, together with a list of known endothelial genes identified previously by *in silico* analysis (59) (Figure 5.1). From this analysis a shortlist of key genes of interest was generated (Table 5.3). This list included a number of well-known pan-tumour endothelial markers such as angiopoietin 2, lysyl oxidase, apelin and neuropilin, validating the approach as a method of identifying tumour endothelial markers. One of the most consistently up-regulated genes in this analysis was Laminin-alpha-4 (LAMA4) a component of the laminin complex, a major non-collagenous constituent of the basal lamina. The recently identified endothelial receptor for LAMA4, melanoma cell adhesion molecule (MCAM) (238) was also identified by this analysis as consistently up-regulated in cancer. It was therefore decided to investigate these two interacting proteins further.

A list of consistently down-regulated genes from the analysis was also generated (Table 5.4), which could be of interest therapeutically, potentially to restore normality to the tumour and its vessels via gene therapy, for example. However, for the purposes of this investigation, genes up-regulated in tumour vessels were the focus.

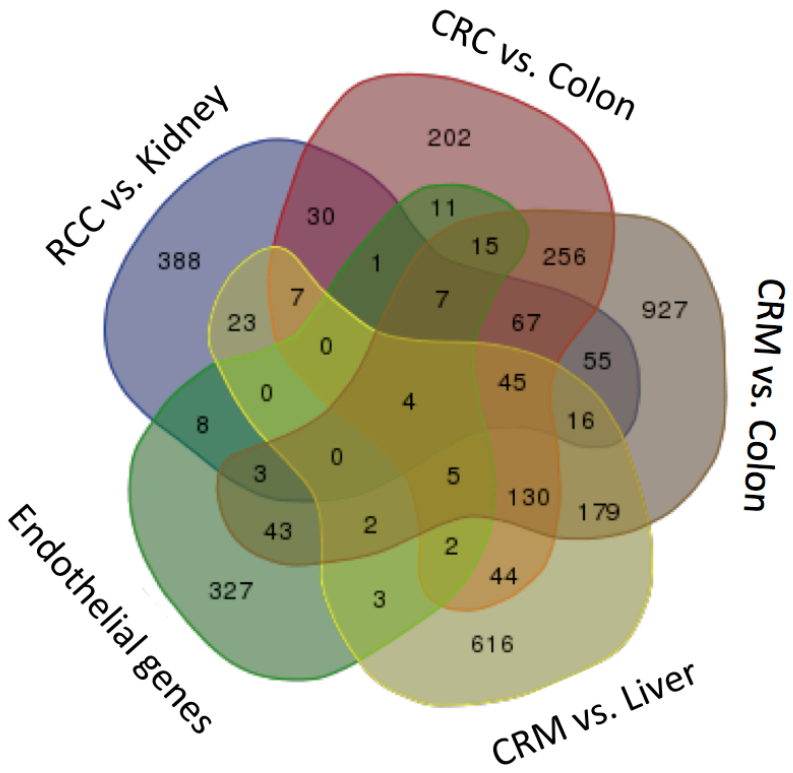

Figure 5.1. Venn diagram showing the commonality of genes at least 2 fold up-regulated in four tumour vs. healthy tissue analyses and present in a list of known endothelial restricted genes.

Table 5.3. Consistently up-regulated vascular genes across cancer types (gene expression comparison shown as Log2 fold change).

Gene ID	Gene symbol	GenBank accession No.	RCC vs Kidney	CRC vs Colon	CRM vs Colon	CRM vs Liver	Gene ontology
Lysyl oxidase	LOX	NM_002317	2.80	1.20	1.00	1.86	EX and IC
Angiopoietin 2	ANGPT2	NM_001147	2.50	3.40	2.48	1.22	EX
Laminin, alpha 4	LAMA4	NM_001105206	2.41	1.50	1.53	1.75	EX
Melanoma cell adhesion molecule	MCAM	NM_006500	2.38	1.70	1.43	-0.51	PM
Regulator of G-protein signaling 5	RGS5	NM_003617	2.24	2.79	1.22	-1.40	PM
Matrix metallopeptidase 1	MMP1	NM_002421	0.16	4.49	-0.57	2.12	EX
Endothelial cell-specific molecule 1	ESM1	NM_007036	0.91	2.63	1.37	-0.17	EX
Transglutaminase 2	TGM2	NM_198951	-0.32	2.60	2.36	1.54	IC and PM
Serpin peptidase inhibitor, clade H, 1	SERPINH1	NM_001207014	-0.04	2.09	2.06	1.04	EX and IC
Biglycan	BGN	NM_001711	0.92	1.29	3.75	0.03	EX
Neuropilin 1	NRP1	NM_001024629	0.66	1.23	2.37	0.25	PM
Coagulation factor II (thrombin) receptor	F2R	NM_001992	1.18	1.42	2.12	1.07	PM
Troponin C type 2 (fast)	TNNC2	NM_003279	-0.26	1.28	1.11	3.38	IC
Serpin peptidase inhibitor, clade B, 5	SERPINB5	NM_002639	-0.33	1.12	0.35	2.82	EX
Apelin	APLN	NM_017413	1.34	1.98	1.20	0.30	EX
Protease, serine, 23	PRSS23	NM_007173	1.02	1.53	0.65	0.68	IC
Serpin peptidase inhibitor, clade E, 1	SERPINE1	NM_000602	1.09	0.85	1.81	0.71	EX and PM
Secreted protein, acidic, cysteine-rich	SPARC	NM_003118	0.47	1.39	1.64	-0.10	EX
Sushi-repeat containing protein, X-linked 2	SRPX2	NM_014467	-0.62	1.22	1.11	1.92	EX and IC
Peroxidasin homolog (Drosophila)	PXDN	NM_012293	1.36	1.20	1.44	0.68	EX
Calcitonin receptor-like	CALCRL	NM_005795	1.26	1.03	1.42	-0.08	PM
Chemokine (C-C motif) ligand 20	CCL20	NM_004591	1.25	1.04	1.29	0.08	EX
Follistatin-like 1	FSTL1	NM_007085	0.69	1.48	1.44	1.03	EX
Transcription factor 4	TCF4	NM_003199	1.05	1.41	1.15	-1.02	IC
Lectin, galactoside-binding, soluble, 1	LGALS1	NM_002305	1.10	1.25	1.35	0.66	EX and IC
Vimentin	VIM	NM_003380	1.01	0.50	1.01	-0.89	IC and PM

Table 5.4. Consistently down-regulated vascular genes across cancer types (gene expression comparison shown as Log2 fold change).

Gene ID	Gene Symbol	GeneBank accession no.	RCC vs Kidney	CRC vs Colon	CRM vs Colon	CRM vs Liver	Gene ontology
Interleukin 1 receptor-like 1	IL1RL1	NM_016232	-2.68	-1.30	-1.17	-1.01	EX and PM
Tissue factor pathway inhibitor 2	TFPI2	NM_006528	-1.98	1.63	2.18	-2.78	EX
Rho-related BTB domain containing 3	RHOBTB3	NM_014899	-1.42	-0.81	-1.40	0.22	IC
Serum/glucocorticoid regulated kinase 1	SGK1	NM_005627	-1.36	-0.44	1.20	-1.02	PM and IC
Endomucin	EMCN	NM_016242	-1.30	0.51	0.36	-2.33	PM and IC
Hedgehog interacting protein	HHIP	NM_022475	-0.34	-2.53	-1.57	-1.20	PM
Multimerin 1	MMRN1	NM_007351	2.24	-2.00	-2.01	-2.18	EX
Leukemia inhibitory factor receptor alpha	LIFR	NM_002310	-0.58	-1.95	-1.06	-3.01	EX and PM
Ectonucleotide pyrophosphatase	ENPP2	NM_006209	0.54	-1.55	-1.08	-1.40	EX and PM
Serum deprivation response	SDPR	NM_004657	0.32	-1.46	-0.78	-2.32	PM and IC
G protein-coupled receptor 126	GPR126	NM_020455	1.28	-1.37	-2.11	-1.28	PM
BMX non-receptor tyrosine kinase	BMX	NM_001721	0.78	-1.21	-0.98	-1.73	PM and IC
UDP-glucose 6-dehydrogenase	UGDH	NM_003359	-0.43	-1.09	-1.60	0.82	IC
Metallothionein 2A	MT2A	NM_005953	-0.37	-0.10	-1.39	-1.16	IC
Complement component 7	C7	NM_000587	-0.94	-1.00	1.37	-2.53	EX and PM
Sushi-repeat containing protein, X-linked	SRPX	NM_006307	-0.01	-1.13	-0.61	-1.77	EX and PM
Junctional adhesion molecule 2	JAM2	AK056079	0.21	-1.02	-0.80	-1.75	PM
Aldehyde dehydrogenase 1 family, A1	ALDH1A1	NM_000689	-0.17	-1.12	-0.55	-1.64	IC

5.2.2 Validation of MCAM and LAMA4 as tumour endothelial markers

In order to confirm the findings of the microarray analysis, RTqPCR was performed to assess mRNA expression levels of MCAM and LAMA4 in endothelial isolates from RCC (n=8), CRC (n=8) and CRM (n=6) and associated healthy tissues (n=8, 8, 6). This analysis showed a pronounced and consistent up-regulation of both genes in the endothelium of the cancers when compared to the matched healthy tissues (Figure 5.2).

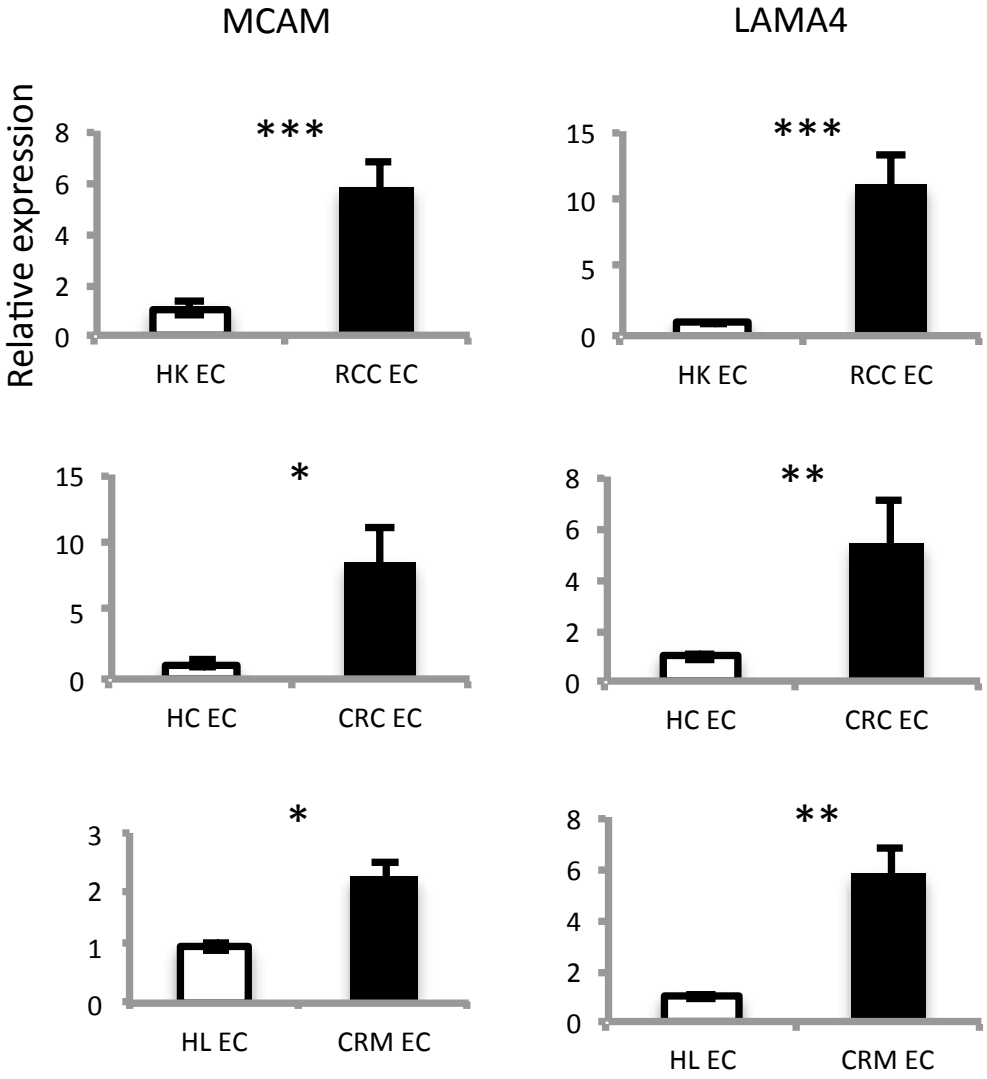

Figure 5.2: Confirmation of cancer specific enrichment of MCAM and LAMA4 by RTqPCR on endothelial isolates from RCC, (n = 8), CRC, (n = 8), CRM, (n = 6) and associated healthy tissues (n = 8,8,6). Mean expression standardised to flotillin-2, ± SEM. Mann-Whitney U test, *** $p < 0.001$, ** $p < 0.01$, * $p < 0.05$).

The identity of these genes as markers of tumour endothelium was further confirmed by semi-quantitative analysis of their protein expression level by immunohistochemistry (IHC), compared to that of the pan-endothelial marker PECAM-1 (Figure 5.3). Vessels of both RCC and CRC strongly stained for MCAM and LAMA4, while the vessels of the associated healthy kidney and colon did not stain, or stained only weakly at equivalent antibody concentrations. This was particularly apparent in healthy kidney tissue where PECAM-1 was strongly stained within the glomerulus, a highly vascular structure, whereas neither MCAM nor LAMA4 staining was detected in glomeruli. Immunohistochemical staining for both targets was absent in a small cohort of colorectal liver metastases probed (n=6, data not shown).

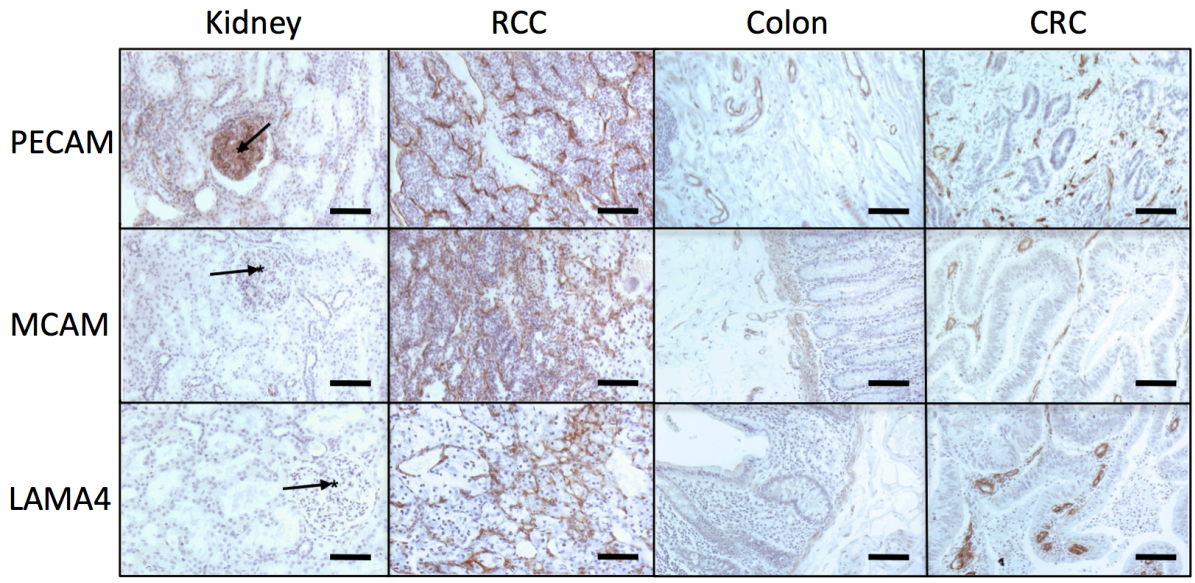

Figure 5.3. Confirmation of cancer specific enrichment of MCAM and LAMA4 by immunohistochemistry (IHC). Representative images of kidney (arrows show glomeruli), RCC, colon and CRC stained for PECAM (endothelial marker), MCAM and LAMA4, scale bar = 50 μm.

In order to identify the tissue specific expression profile of MCAM and LAMA4, 10 samples each of 18 common cancers and associated healthy tissues were stained and scored for strength of staining (Figure 5.4). Both MCAM and LAMA4 demonstrated markedly specific vascular expression profiles, with vessels the primary source of staining in all tissues other than melanoma, where MCAM expression was primarily found on the tumour cells (data not shown). Of note, 90% of kidney tumours showed strong vascular staining for MCAM, in excess of any healthy tissue and most cancerous tissues examined, highlighting MCAM as a promising vascular target in RCC. LAMA4 on the other hand was shown to be highly expressed in a broad range of both tumour and healthy tissues (Figure 5.4).

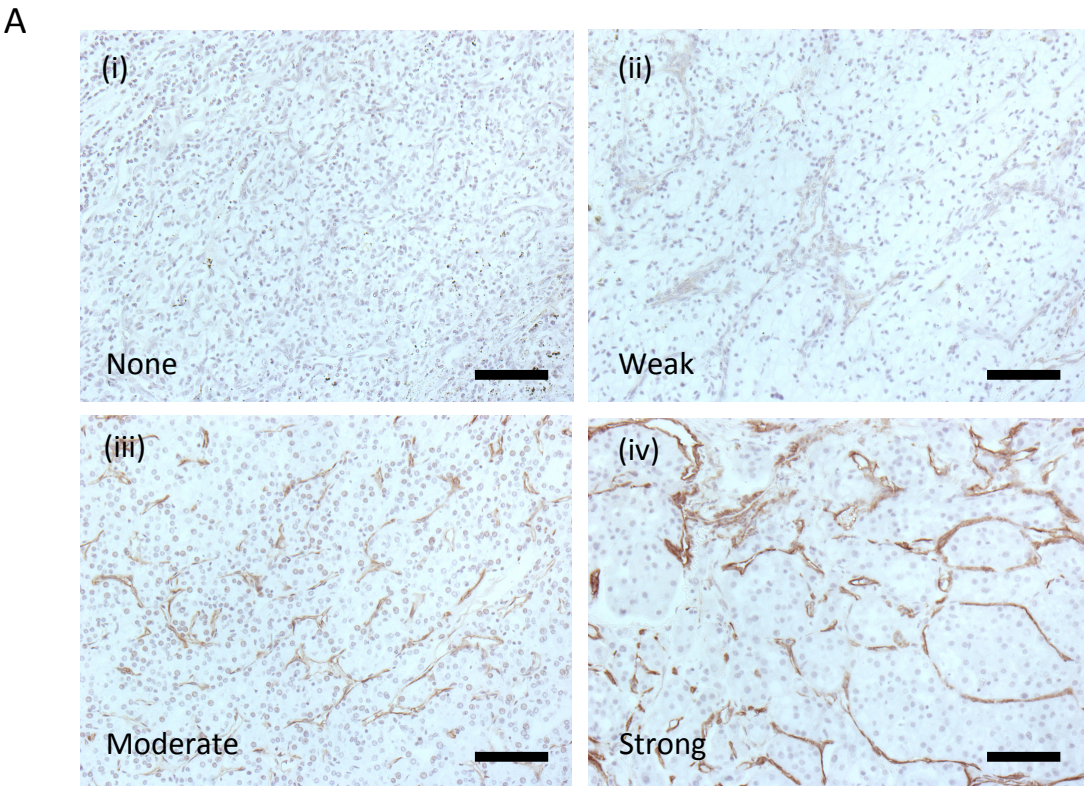

Figure 5.4. MCAM expression is specifically enriched on the vasculature of renal cancer. A, representative images of MCAM IHC staining on renal cell carcinoma demonstrative of scoring used for analysis, scale bar = 50 μm.

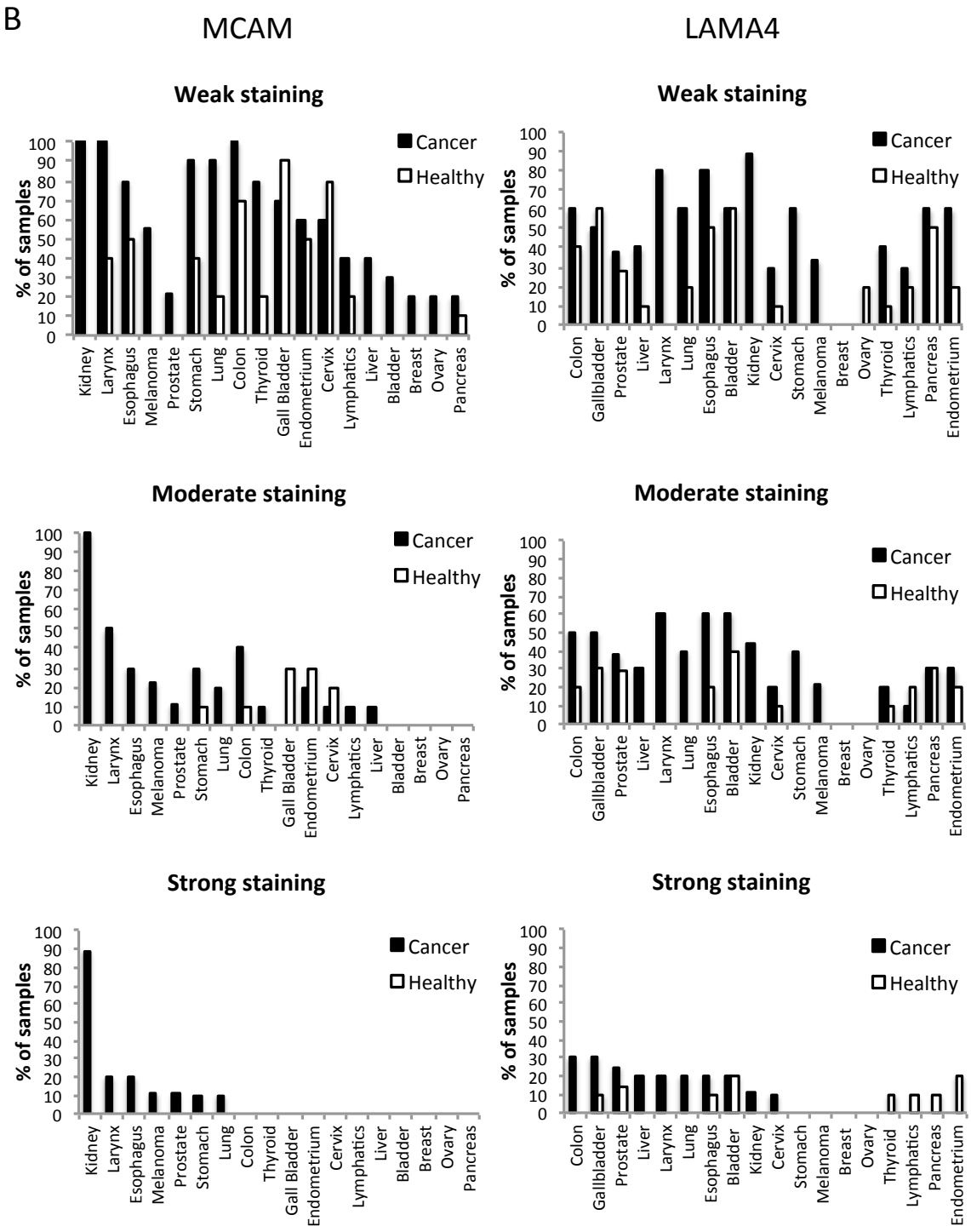

Figure 5.4. B, multi-organ tissue and cancer array analysis of MCAM and LAMA4 expression by IHC. The proportion of tissues matching or exceeding the weak, moderate or strong staining thresholds is shown.

5.2.3 MCAM expression is induced by vascular endothelial growth factor (VEGF)

MCAM expression on tumour vessels appears to be highly RCC specific. High VEGF expression, due to the loss of the tumour suppressor Von-Hippel-Lindau (VHL), is common in cases of clear cell RCC (237) as previously discussed. In order to investigate whether enhanced VEGF production within the tumour could be the cause of high MCAM expression, isolated human umbilical cord vein endothelium (HUVEC) and commercially purchased human dermal micro-vascular endothelial cells (HDMEC) were exposed to recombinant VEGF. Six HUVEC isolates and two multisource HDMEC isolates, each used in triplicate, were serum starved for 16 hours and then cultured with or without 100 ng/ml recombinant VEGF for 24 hours, before being harvested. RTqPCR and western blot analysis for both cell types showed that MCAM was significantly up-regulated by VEGF (Mann-Whitney U test, $p<0.01$) (Figure 5.5).

Clear cell RCC alone is characteristic for high VEGF expression and all the RCC tumours in the multi-organ expression analysis were clear cell. In order to investigate whether MCAM expression is specific for ccRCC, tissues from multiple other types of renal malignancy were stained by IHC. This analysis revealed that a far greater proportion of clear cell tumours (61%, n=64) stained strongly for MCAM than transitional cell (47%, n=15), carcinoma sarcomatodes (33%, n=6), squamous cell (14%, n=7) or papillary cell (13%, n=8) (Table 5.5). This result supports the suggestion that VEGF is playing a part in enhancing MCAM expression in ccRCC. Additionally this result suggested that ccRCC should be the focus of investigation.

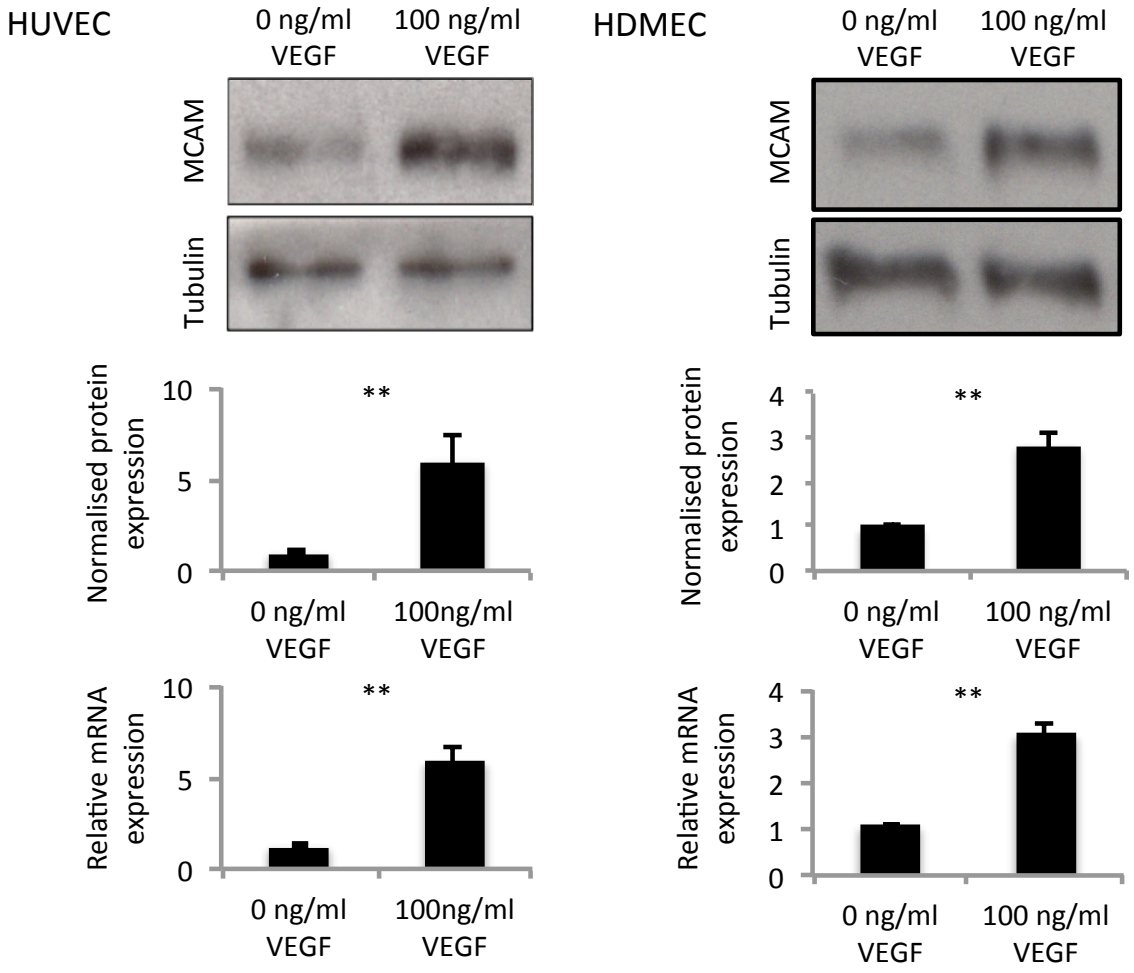

Figure 5.5. VEGF significantly induces MCAM expression in endothelial cells. HUVEC isolates (n=6) and HDMEC (n=6) were serum and growth factor starved for 16 hours, then cultured with serum depleted media ± 100 ng/ml recombinant human VEGF (hVEGF), MCAM expression was determined by western blot and RTqPCR. Confidence limits ± SEM, statistical analysis: Mann-Whitney U test, ** $p<0.01$ for both western blot and RTqPCR analysis. Western blot: MCAM band – 120 kDa, tubulin band – 55 kDa.

Table 5.5. Key clinical data for different types of kidney cancer and metastasis.

Characteristics	Clear cell	Transitional cell	Papillary cell	Squamous cell	Sarcomatodes
Tumours	64	15	8	7	6
Gender					
Male	50	13	7	5	2
Female	14	2	1	2	4
Age					
Above 60	29	11	0	2	2
Below 60	35	4	8	5	4
T-stage					
No information	30	0	0	0	1
T1	23	14	8	4	0
T2	8	1	0	2	4
T3	3	0	0	1	1
M-stage					
M0	56	15	7	7	5
M1	8	0	1	0	1
MCAM staining					
Strong	39	7	1	1	2
Weak	25	8	7	6	4
% strong staining	**60.94**	**46.67**	**12.50**	**14.29**	**33.33**
Metastasis	15	2	2	2	1
Gender					
Male	13	0	2	2	1
Female	2	2	0	0	0
Age					
Above 60	11	2	0	2	1
Below 60	4	0	2	0	0
Location				0	
Adrenal gland	3	0	0	0	0
Bone	1	0	0	0	0
Lymph node	4	2	2	2	0
Lung	3	0	0	0	0
Thyroid	1	0	0	0	0
Intestine	1	0	0	0	0
Spleen	0	0	0	0	1
Retroperitoneum	2	0	0	0	0
MCAM staining					
Strong	11	0	2	1	0
Weak	4	2	0	1	1
% strong staining	**73.33**	**0.00**	**100.00**	**50.00**	**0.00**

5.2.4 Identification of strong MCAM and LAMA4 expression as potent adverse prognostic indicators in RCC

In order to investigate whether the strong expression of MCAM and LAMA4 in the vessels of many RCC and CRC tumours could have some prognostic value, excised tissue from cohorts of ccRCC (n=81[cohort 1], 48 [cohort 2], n=47 [cohort 3]) and CRC (n=90) were stained by IHC for each marker and semi-quantitatively scored. Demographic information is shown for each cohort in Tables 5.6 (RCC cohort 1), 5.7 (RCC cohort 2), 5.8 (RCC cohort 3) and 5.9 (CRC cohort).

For effective investigation of prognostic linkage to marker expression, the analytical tools must be sensitive to the full range of marker expression within the cohort. As the multi-organ tissue array staining for MCAM resulted in 90% of renal cell carcinoma samples staining strongly, the antibody concentration was titrated down from 0.6 to 0.3 μg/ml, to a level where a range of MCAM staining in RCC could be observed. 0.6 μg/ml was used for the results listed in Figures 5.3 and 5.4, 0.3 μg/ml was used for all other IHC analyses.

Each cohort was split into tumours exhibiting strong or weak marker staining, as judged by three independent scorers. Thresholds were set as described in Figure 5.4 (weak = none/weak, strong = moderate/strong). Tumour marker staining was correlated with patient survival by Kaplan-Meier analysis (Figure 5.6). This analysis identified a significant decrease in survival in patients whose tumours exhibited strong MCAM and LAMA4 staining, in both RCC cohort 1 (log-ranks-p=0.001 & 0.0005 respectively) and cohort 2 (p=0.08 & 0.001 respectively) (Figure 5.6). In patients with tumours exhibiting strong staining for both MCAM and LAMA4 together, this effect was more pronounced, with only 18% surviving to date, versus 75% in tumours that were

not strongly stained for either marker, in RCC cohort 1 and 27% vs. 81% in RCC cohort 2 ($p<0.0005$, both cohorts) (Figure 5.6). In the CRC cohort there was no significant association between survival and strong MCAM ($p=0.809$) or LAMA4 ($p=0.353$) expression alone or when co-expressed ($p=0.713$) (Figure 5.6). This suggests that MCAM and LAMA4 play a unique, tumour-specific role in ccRCC patient survival.

No significant survival effect was observed in RCC cohort 3, with the exception of where the markers were co-expressed ($p=0.013$). RCC cohorts 1 and 2 are primarily made up non-metastatic tumours, with only five with metastasis across the two cohorts and survival to last check up is 64% and 66% respectively (Tables 5.6 and 5.7). These types of cohort are ideal for looking at survival effects, as the potential for a separation in survival between two groups is great. RCC cohort 3 is entirely made up of metastatic tumours and survival to last check up is 21% (Table 5.8). It is therefore reasonable to suggest that a single marker survival effect is not seen as too few patients survive. This does however, suggest that prognostication using MCAM and LAMA4 marker expression will find its greatest utility in early-stage disease.

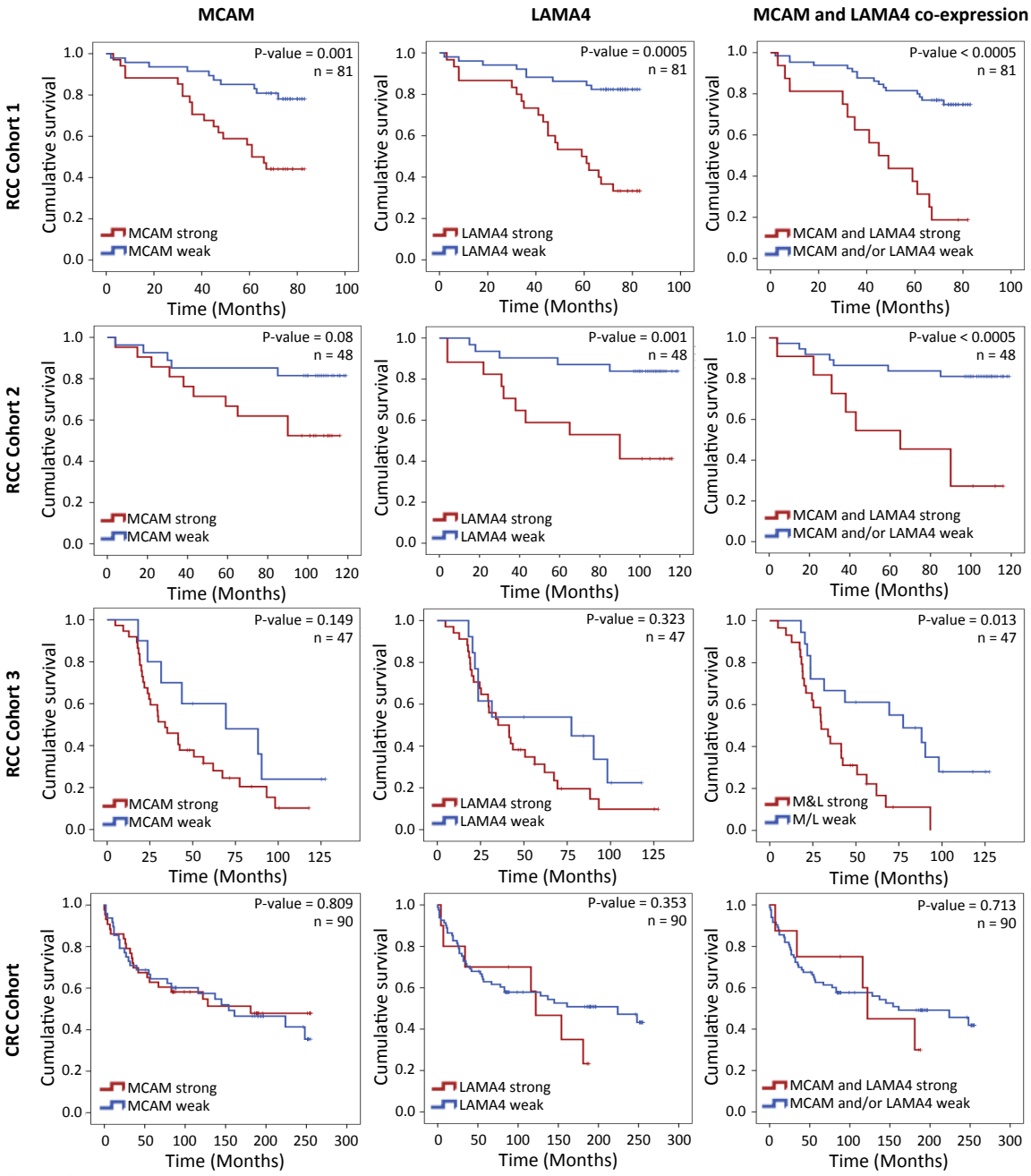

Figure 5.6. High MCAM and LAMA4 tumour vessel expression has a significant detrimental effect on the survival of RCC patients but not CRC patients. Kaplan-Meier survival analysis of patients, from RCC cohort 1,2 and 3 and the CRC cohort, with strong vs. weak staining for MCAM, LAMA4 and marker co-expression. Statistical analysis: Log-ranks test, p-values and n-numbers for each test are shown. Crosses mark censored cases.

Table 5.6. Key clinical data for clear cell RCC cohort 1, showing overall survival (OS).

Characteristics	N of patients	Median OS	Mean OS
All	81	69.5	63.7
Gender			
Male	48	71	65.2
Female	33	68	61.6
Age			
Above /=60	41	69	65.1
Below 60	40	70	62.3
Grade			
G1	30	72	64.3
G1-2	10	66	59.4
G2	26	71	64.2
G2-3	4	68	61.8
G3/4	11	70	67.5
Stage			
No information	4	-	-
I	55	69.5	66.1
II	16	71	59.3
III	4	63.5	58.0
IV	2	69.5	69.5
T-stage			
No information	2	-	-
T1a	34	70	66.2
T1b	24	69	61.9
T2a	13	70	57.8
T2b	3	76	76.0
T3	5	68	62.0
M-stage			
M0	79	69.5	63.5
M1	2	69.5	69.5
MCAM staining			
Strong	34	71	67.2
Weak	47	69	61.4
LAMA4 staining			
Strong	30	72	66.0
Weak	51	69	61.8
MCAM and LAMA4 co-staining			
Both strong	16	69	62.3
Both weak	33	68	56.5
MCAM strong LAMA4 weak	18	73.5	73.5
MCAM weak LAMA4 strong	14	74	69.7

Table 5.7. Key clinical data for clear cell RCC cohort 2, showing overall survival (OS).

Characteristics	N of patients	Median OS	Mean OS
All	48	104	86.9
Gender			
Male	35	104	81.5
Female	13	110	101.5
Age			
Above 58	26	103.5	80.9
Below 58	22	104.5	94.04
T-stage			
T1a	9	108	97.3
T1b	12	102	86.8
T2a	7	105	96
T2b	3	115	83
T3a	15	97	80.8
T3b	1	101	101
T4	1	22	22
M-stage			
M0	45	104	86.7
M1	3	110	90.3
MCAM staining			
High	21	97	77.6
Low	27	105	94.2
LAMA4 staining			
High	17	90	71.7
Low	31	105	96.1
MCAM and LAMA4 co-staining			
MCAM and LAMA4 strong	11	65	64.7
MCAM and LAMA4 weak	21	105	98.1
MCAM strong LAMA4 weak	10	103.5	91.8
MCAM weak LAMA4 strong	6	107.5	80.3

Table 5.8. Key clinical data for clear cell RCC cohort 3, showing overall survival (OS).

Characteristics	N of patients	Median OS	Mean OS
All	47	41.50	48.02
Gender			
Male	37	43.67	53.18
Female	10	24.48	28.97
Age			
Above 60	27	67.82	68.30
Below 60	20	56.37	53.41
T-stage			
No information	7		
T1	6	61.83	58.51
T2	1	127.47	127.47
T3	31	29.60	37.66
T4	2	32.77	32.77
M-stage			
M0	0		
M1	16	48.37	59.37
M2	18	29.37	39.24
M3	13	29.90	41.51
MCAM staining			
High	37	33.87	42.96
Low	10	59.68	66.76
LAMA4 staining			
High	34	38.32	44.09
Low	13	49.97	58.31
MCAM and LAMA4 co-staining			
MCAM and LAMA4 strong	29	29.90	36.04
MCAM and LAMA4 weak	5	31.57	42.71
MCAM strong, LAMA4 weak	8	80.95	68.05
MCAM weak, LAMA4 strong	5	88.20	90.81

Table 5.9. Key clinical data for the CRC cohort, showing overall survival (OS).

Characteristics	N of patients	Median OS	Mean OS
All	90	87.5	112.8
Gender			
Male	65	86	107.2
Female	25	122	127.3
Age			
Above 58	47	122	130.2
Below 58	43	67	93.8
Stage			
I/II	44	157.5	148.5
III/IV	46	38	78.6
Tumour location			
Ascending colon	21	27	63.5
Descending colon	6	194	183
Sigmoid colon	31	84	96.6
Transverse colon	9	186	127.1
Cecum	4	102.5	109
Rectum	19	186	165.6
T-stage			
T2	8	187.5	160.5
T3	75	86	105.5
T4	7	122	136.3
N-stage			
N0	50	129.5	138.3
N1+	40	33	80.1
M-stage			
M0	75	116	126.3
M1	15	42	45.3
MCAM staining			
Strong	42	86	108.6
Weak	48	89	115.6
LAMA4 staining			
Strong	10	119	108
Weak	80	86	113.4
MCAM and LAMA4 co-staining			
MCAM and LAMA4 strong	7	122	115.1
MCAM and LAMA4 weak	45	89	118.1
MCAM strong LAMA4 weak	35	85	108
MCAM weak LAMA4 strong	3	116	91.3

Multivariate cox-regression analysis on the largest RCC cohort, cohort 1, identified MCAM (p=0.006), LAMA4 (p=0.007) individually and in combination (p=0.002) as independent risk factors for reduced survival in patients with tumours exhibiting strong staining, independent of gender, age, histopathological tumour grade or T-stage (Table 5.10). This analysis additionally identified a considerably greater risk of death in patients exhibiting strong MCAM and LAMA4 expression: MCAM, odds ratio 3.4, confidence interval 1.4-8.1; LAMA4, OR 3.3, CI 1.4-7.9; Co-expression, OR 4.1, CI 1.7-10 (Table 5.10).

Table 5.10. Multivariate analysis (Cox regression) of prognostic markers in RCC cohort 1 (n = 81*),* censored cases n = 52 (64.2%)*.* $p < 0.05$ are in bold.

Prognostic factor	Relative Risk Exp(B)	95% Confidence Interval	P-value M and L	P-value MCAM	P-value LAMA4
M and L co-expression (high vs. low)	4.102	1.690-9.954	**0.002**		
MCAM (high vs. low)	3.402	1.419-8.157		**0.006**	
LAMA4 (high vs. low)	3.297	1.379-7.884			**0.007**
Sex (female vs. male)	0.624	0.270-1.442	0.27	0.164	0.835
Age (over 60 vs. under 60)	1.811	0.780-3.862	0.076	0.058	0.246
Grade (G2 and above vs. G1)	2.233	0.881-5.660	0.091	0.319	0.223
T-stage (T2 and above vs. T1)	2.363	0.923-6.049	0.073	**0.002**	**0.041**

5.2.5 MCAM and LAMA4 expression is enhanced in locally invasive and metastatic disease

Metastatic disease is the area of most therapeutic need for renal cell carcinoma, survival is lowest and there is the greatest need for new, systemic therapies. A tumour vascular target would ideally have utility in this setting. In order to investigate the expression of MCAM and LAMA4 in metastatic disease, tumours from ccRCC cohorts 1, 2 and 3 were grouped based on their metastatic status. This revealed that the proportion of metastatic tumours exhibiting strong marker staining is significantly greater than in tumours with no known metastases (76% vs. 41%-MCAM, 68% vs. 36%-LAMA4, chi-squared-$p<0.001$) (Figure 5.7A). It should be borne in mind however, that the majority metastatic tumours are from one cohort and non-metastatic tumours from another and possible differences in tissue preparation may have affected the result. An additional analysis, grouping the tumours based on T-stage found that both markers are significantly enriched in tumours exhibiting greater local invasion (chi-squared-$p<0.001$) (Figure 5.7B). In the case of metastatic disease it is not just the primary tumour that must be treated, but also the metastases, therefore MCAM staining in metastases from clear cell RCC tumours was investigated (Figure 5.7C). This analysis revealed that 73% of clear cell RCC metastases (n=15) exhibit strong MCAM staining regardless of metastasis location (Table 5.5). MCAM expression was additionally observed in metastases from papillary and squamous cell RCC, however, sample number (n=2,2) was too low to make any significant conclusions (Table 5.5). This data collectively identifies MCAM and LAMA4 as markers of advanced disease and MCAM as an ideal target for the treatment of metastatic renal cell carcinomas of the clear cell type.

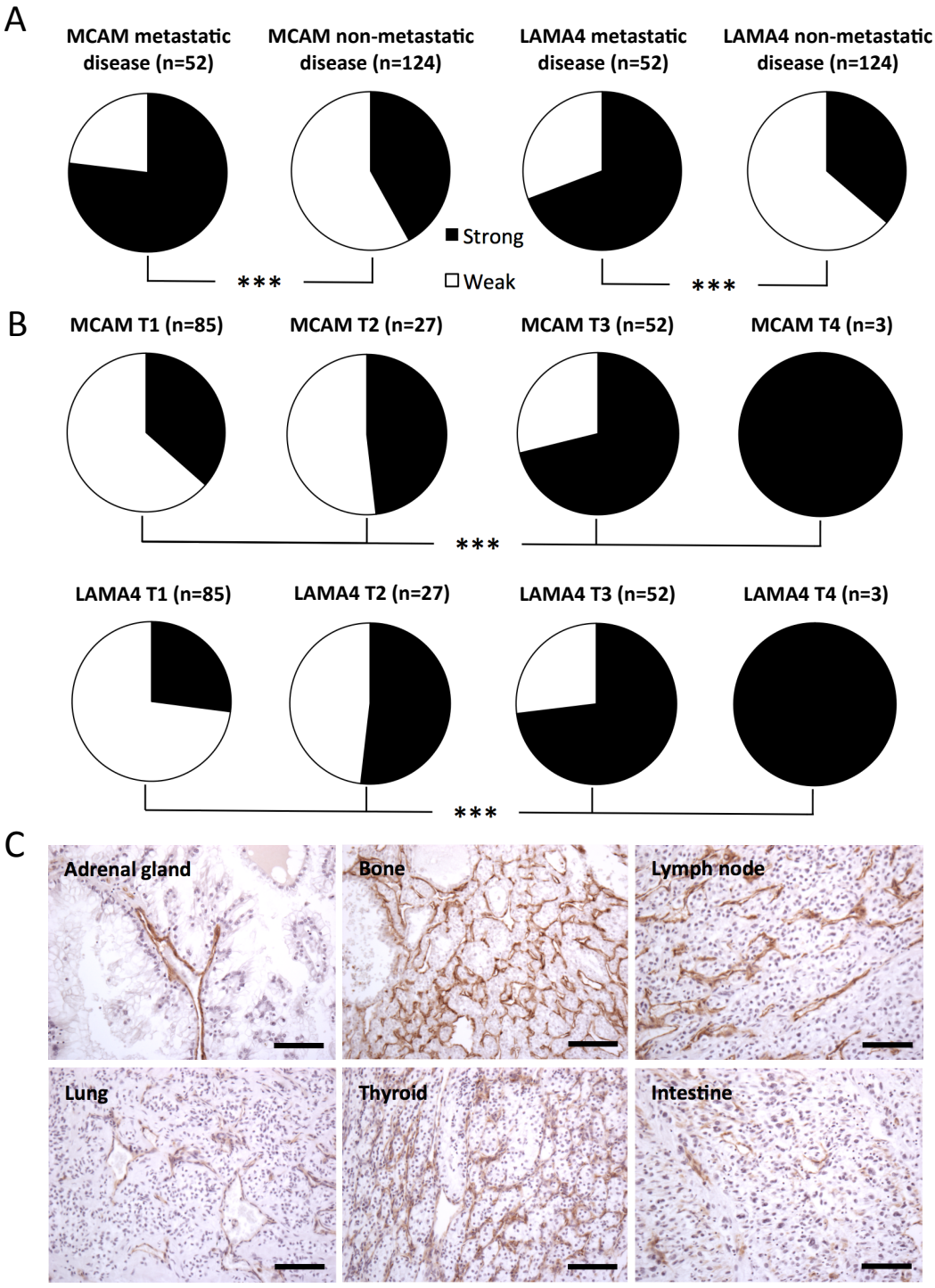

Figure 5.7. MCAM and LAMA4 expression is enhanced in metastatic and locally advanced clear cell RCC. A, pie-chart proportional representation of strong (black) vs. weak (white) marker expression in metastatic and non-metastatic RCC, determined by IHC on RCC cohorts 1,2 and 3. Statistical analysis: Chi-squared, *** $p<0.001$. B, pie-chart proportional representation of strong (black) vs. weak (white) marker expression at different RCC T-stages, determined by IHC on RCC cohorts 1,2 and 3. Statistical analysis: Chi-squared, *** $p<0.001$. C, representative images of MCAM staining in clear cell RCC metastases to various organs, generated by IHC. Scale bar = 50 μm.

5.2.6 Monoclonal anti-MCAM antibodies specifically localise to murine RCC tumour vessels

The abundance and specificity of MCAM expression in renal tumours opens the possibility of using it as a targeting ligand for therapeutic agents. In order to investigate this potential utility, the localisation of a monoclonal rat anti-MCAM antibody was determined, following intravenous injection into murine renal cell carcinoma (RENCA) tumour bearing mice. The RENCA model was chosen as the tumours have previously been shown to express VEGF at a high level (160), closely modelling the majority of human renal cell cancers. Additionally subcutaneous RENCA tumours were shown to strongly express MCAM on their vessels by immunofluorescence (Figure 5.8A), identifying it as an ideal model for use in this situation. Immunofluorescence works on the same principle as immunohistochemistry, with the exception that a fluorophore, rather than an HRP-activated chromogen, is used to mark the expression of the target protein, which is quantified by fluorescence microscopy.

An hour after antibody infusion, the mice were culled, the organs harvested and then processed for frozen sectioning. Tissues from the RENCA tumour, stomach, heart, liver, colon, kidney, skin and lung from two mice were probed for PECAM-1 (vessels) and also fluorescently labelled anti-Rat IgGs, to detect localised anti-MCAM antibodies. In order to quantify the fluorescence emanating from localised anti-MCAM antibody within the vessels of each tissue, images were taken and processed in Image J. A mask was generated to select only the vessels within the tissue as a region of interest, using the green (PECAM) channel. The average optical density of the red (localised anti-MCAM antibody) channel was then quantified within this region of interest. This

analysis demonstrated an at least 25 fold greater localisation of antibody in the vessels of the RENCA tumours than any other tissue probed (Figures 5.8B and C). This finding suggests that renal cell carcinoma therapies could potentially use anti-MCAM antibodies to localise therapeutics to the tumour vasculature specifically, permitting a functional anticancer effect.

Figure 5.8. A monoclonal anti-MCAM antibody specifically localises to murine RCC tumour vessels. A, triple immunofluorescent staining of a murine RCC (RENCA) tumour for; PECAM (green), MCAM (red) and DAPI (blue). Scale bar = 25 μm. B & C, 20 μg of MCAM monoclonal antibody was intravenously injected into RENCA tumour bearing mice 1 hour prior to cull. The tumour and selected organs were collected. Frozen sections were stained with anti-rat IgGs (red), PECAM (green) and DAPI (blue). B, the average optical density of fluorescence detected in the anti-rat IgG (red) channel, within regions of vascular (PECAM) staining was quantified. The tissue from two mice was assessed, with six regions of interest randomly selected for each organ and mice (n=12), confidence limits ± SEM. C, representative images of MCAM monoclonal antibody localisation. Scale bar = 12.5 μm.

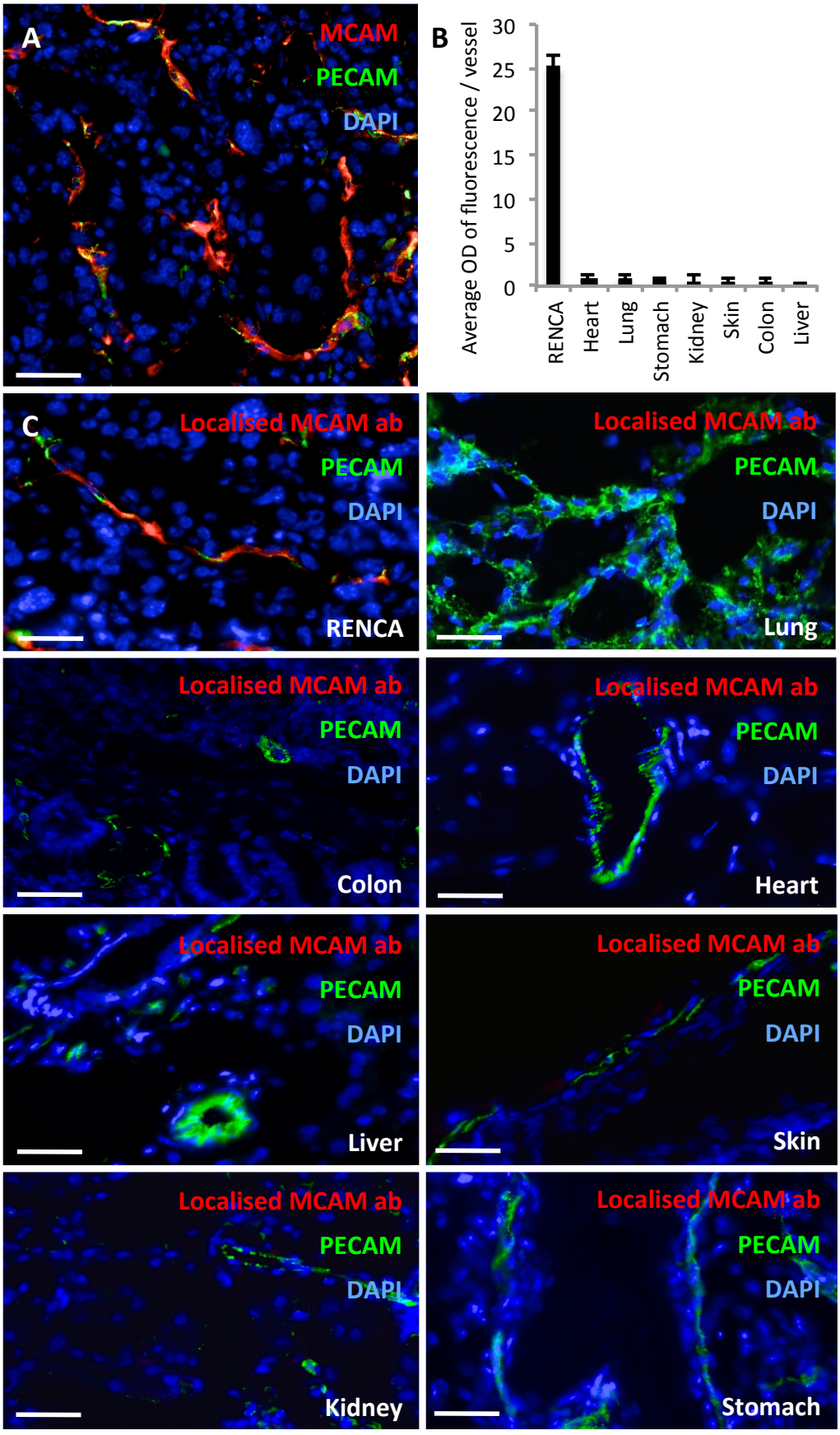
A
MCAM
PECAM
DAPI
B
Average OD of fluorescence / vessel
30
25
20
15
10
5
0
RENCA
Heart
Lung
Stomach
Kidney
Skin
Colon
Liver
C
Localised MCAM ab
PECAM
DAPI
RENCA
Lung
Colon
Heart
Liver
Skin
Kidney
Stomach

5.3 Discussion

The aim of this study was to identify vascular markers with pan-tumour expression and demonstrate their utility as specific ligands against which to target immunological therapies. This study identified MCAM and LAMA4 as promising markers with specific overexpression in endothelial isolates from both colorectal and renal malignancies. A significant link between high expression of these markers and poor patient survival, invasive local disease and metastasis, was demonstrated in RCC, but not CRC. MCAM expression was found to be highly enriched in the vessels of clear cell RCC, in excess of other tumour and healthy tissues, possibly due to VEGF induction demonstrated in this study. This data highlighted MCAM as a potential specific target in renal cell carcinoma and this utility was demonstrated by specific localisation of MCAM monoclonal antibodies to the tumour vessels in a model of RCC.

Our comparative analysis of vessels derived from colorectal carcinoma (CRC), colorectal liver metastasis (CRM) and renal cell carcinoma (RCC) with patient matched healthy tissues, identified a small group of endothelial genes consistently up-regulated in these tumours. Many of these genes are stimulatory to angiogenesis and tumour invasion, such as LOX (239), MCAM (240), LAMA4 (241), NRP1 (242), MMP1 (243), APLN (244) and SPARC (245) suggesting a signature characterised by active angiogenesis.

One of the most consistent pan-tumour endothelial markers in our analysis was laminin alpha 4 (LAMA4) an extracellular matrix glycoprotein and component of the laminin complex. Laminins are made up of three chains, alpha, beta and gamma and have been implicated in a wide variety of cellular processes from cell attachment and differentiation, to influences on cell shape and movement, maintenance of tissue phenotype, and promotion of tissue survival (246). The function of individual laminin chains is poorly understood, however, LAMA4, a constituent of laminin-8, 9 and 14 (247), has been shown to have an endothelial specific expression pattern and also to promote angiogenesis (241). LAMA4 has been shown to co-distribute and interact with integrins αvβ3, α3β1, and together with α6β1 mediate endothelial cell-LAMA4 interactions and blood vessel formation (241).

The exact role LAMA4 plays in cancer is unclear. In this study it was shown to be strongly up-regulated on tumour blood vessels in colorectal and renal malignancies when compared to surrounding non-malignant tissue. Its tissue distribution appears to be diverse when more broadly investigated however, appearing in both healthy and tumour tissues. This analysis suggests that using LAMA4 as a target for cancer therapy could be problematic. This study did, however, demonstrate a highly significant link between LAMA4 expression in RCC and poor patient survival, which was not shared in CRC. A strong association between LAMA4 expression and both metastasis and local invasion was also shown. LAMA4 has previously been associated with increased tumour invasion and metastasis in hepatocellular carcinoma (248), the transition from premalignant to malignant breast carcinomas and reduced relapse-free survival in estrogen receptor negative breast cancer patients (249), marking LAMA4 as a useful

prognostic marker in certain cancers, not least renal cell carcinoma. A recombinant form of the LAMA4 chain containing laminin-411 (laminin-8) has been reported to have an anti-adhesive effect on RCC cells grown on fibronectin (250). This report, combined with our observations suggests a potential mechanism in which heightened vascular LAMA4 might impair RCC tumour adhesion and thereby increase metastasis, negatively impacting patient survival. The functional relevance of this mechanism warrants further investigation.

This study also identified MCAM as a potent vascular marker in clear cell renal cell carcinoma. The role of MCAM on the vascular endothelium is poorly understood, but it is thought to promote angiogenesis (240) and act as a co-receptor for VEGFR-2, thus enhancing endothelial migration and micro-vessel formation (251). Endothelial conditional knock out of MCAM in mice, results in impaired vessel formation in VEGF-dependent angiogenesis assays (251). MCAM is also thought to play a role in cell-to-cell junctions and vascular permeability (252). Besides this, MCAM over expression has been associated with pro-survival signalling including protein kinase B (PKB) phosphorylation and down-regulation of BCL2-Associated Agonist Of Cell Death (BAD) expression (253). It is therefore plausible that up-regulation of MCAM in tumor vessels could act as a survival mechanism, as well as impacting on angiogenesis and vascular integrity.

MCAM was first identified as a marker on the carcinoma cells of malignant melanoma, emerging as a potential prognostic indicator of cancer progression (254). MCAM expression has also been reported on the carcinoma cells of prostate (255), breast

(256) and ovarian cancer (257), suggesting that MCAM could be a widely expressed tumour antigen. However, in this study, MCAM expression was only occasionally observed on the tumour cells of tissue examined, with MCAM expression being almost exclusively reserved to tumour vessels in all malignancies aside from melanoma, calling into question the relative importance of tumour and endothelial cell MCAM expression in these malignancies.

A significant association was demonstrated in this study, between high vascular MCAM expression and poor RCC patient survival, increased metastasis and increased local invasion. Heightened MCAM mRNA expression has previously been reported in bulk tumour tissue from patients with RCC, with the highest levels observed in metastatic disease, indicating a direct correlation between increasing MCAM expression and disease progression (258), partially corroborating our observations. We further this finding by highlighting vascular MCAM as key to this process and demonstrating a direct survival impact. High MCAM expression has additionally been associated with poor survival in patients with non-small cell lung adenocarcinoma (but not squamous cell carcinoma) (259). This data highlights MCAM as an important prognostic marker in cancer, in particular ccRCC, where co-expression with its recently identified extracellular ligand LAMA4 (238), was shown to be highly predictive of very poor patient survival. This observation suggests that the expression and interaction of MCAM and LAMA4 could be highly significant in RCC progression and should be further investigated. MCAM interaction with the LAMA4 containing laminin-9 complex has been shown to promote migration of tumour cells when associated with α6β1 integrin

(260), but the importance of this interaction for endothelial cell or cancer biology is unknown.

Multi-tissue analysis identified MCAM as highly specific to RCC in its expression. Whilst it is present in other tissues, its expression in ccRCC vessels is greatly in excess. This study identified VEGF-mediated induction of MCAM in endothelial cells as a potential explanation for this. This is the first study to demonstrate that VEGF, a growth factor highly expressed in ccRCC (237), will induce MCAM expression in endothelial cells. The regulation of MCAM on vessels is poorly understood. The expression of MCAM in HUVEC was found to be up-regulated by culture with media conditioned with a hepatoma cell line (240), however, the exact mechanism was not determined. Tumour necrosis factor has been reported to induce the formation of a soluble form of MCAM in various cell types including endothelium (261,262). Of note, insulin-like growth factor-binding protein 4 (IGFBP-4) has been reported to induce MCAM in renal cell carcinoma. IGFBP-4 transfected renal tumour cells were found to exhibit enhanced cell growth, invasion and motility, as well as enhancing MCAM expression (263). However, as has been discussed, in this study MCAM expression was primarily observed on tumour vasculature, with no discernable RCC tumour cell expression, so the significance of IGFBP-4 induced MCAM expression on RCC tumour cells in human cancer, is unclear.

Non-metastatic renal tumours are primarily treated by nephrectomy and whilst tumour vascular targeting could be of use in this setting, as adjuvant therapy to downsize the tumour prior to removal, or as a post-operative maintenance therapy, this approach is likely to have most therapeutic impact in the metastatic setting

The finding that MCAM, a cell surface glycoprotein, was highly specific to RCC vessels and expressed at its highest level in the metastatic setting, an area of great therapeutic need, marked it out as an ideal target for anti-cancer immunological therapies. This study demonstrates this utility by showing that a monoclonal anti-MCAM antibody will specifically localise to the vessels of a murine model of RCC, accumulating in the tumour at at least 25 fold greater density. This constitutes a striking level of antibody specificity to cancer, in excess of other successful tumour localisation studies (91,261). It should be noted, however, that no control antibody was used in this investigation. It is therefore possible that the specificity of the anti-MCAM antibody was not exclusively the result of the differential expression of MCAM in the tumour vs. healthy tissue sites, but was instead mediated by tumour exclusive, non-specific binding, or by environmental factors, such as poor drainage within the tumour, leading to the accumulation of the antibody in this site. The use of an isotype control would determine whether this was the case and therefore this form of control should be used in any further validation of this approach in the future.

A number of successes in anti-cancer cell targeting using antibodies have been achieved including FDA approved ADCs brentuximab vedotin in Hodgkins lymphoma (264) and trastuzumab emtansine in breast cancer (265). However, as mentioned in the main introduction the targeting of tumour blood vessels does offer a number of advantages; the blood vessels are easily accessible for ligand targeting; up to 100 tumour cells are dependent on a single endothelial cell (3) for survival, making the vessels an extremely efficient target; the vasculature is thought to be more genetically stable and so more homogenous in terms of marker expression (7) and finally therapeutics disrupting the vessels have been shown to cause preferential lysis in the core of large tumour (266), a

region poorly treated by antiangiogenics and traditional chemotherapeutics (44). This study therefore identifies and validates MCAM as a new ligand with which to specifically target therapeutics against renal cell carcinoma vessels, potentially improving treatment of this malignancy.

Chapter Six

An *In Vivo* Breast Cancer Model of Sunitinib Resistance

6.1 Introduction

Breast cancer is the leading cause of cancer in women, accounting for a quarter of cases (267). Survival in the developed world is generally good with 80-90% survival to 5 years (267), although survival is highly dependent on the type and stage of disease. Stage 1, 2 and 3 cancers have reasonably good prognosis, being primarily treated with a combination of surgery, chemotherapy, radiation and targeted therapy, however, the situation changes drastically with stage 4, metastatic cancer. Stage 4 cancer is treated with a similar combination of therapies, however, surgery is often not curative and other treatments focus on tumour maintenance rather than cure. In this setting 10-year survival is between 5-10% depending on the effectiveness of therapy (202).

One of the major factors governing treatment efficacy is the cancer marker expression profile. 80% of breast tumours are highly dependent on estrogen and/or progesterone for their survival and can be well-managed using hormone blocking therapies. These inhibit the progesterone and estrogen receptors (tamoxifen) or block the production of the hormones (anastrozole / letrozole) (268,269). 25-30% of breast cancers overexpress the human epidermal growth factor receptor 2 (HER2) and can be targeted with a HER2 monoclonal blocking antibody therapy (trastuzumab) (270). This therapy very effectively prevents growth factor activation of the HER2 receptor inhibiting cancer growth, leading to an overall survival in this cohort of over 95% (270). However, there is a small cohort (~14%) negative for both hormone receptors and HER2, which are far harder to treat (271). It is triple negative breast cancers (TNBC), particularly in

the metastatic setting, where there is most interest in the use of anti-angiogenic therapies.

Sunitinib malate is a multi-target oral tyrosine kinase receptor (RTK) inhibitor (Table 6.1) (272). Among its targets are the pro-angiogenic platelet derived growth factor receptors alpha and beta as well as the vascular endothelial growth factor receptors on endothelial cells. It additionally inhibits the tumourgenic KIT receptor, colony stimulating factor type 1 receptor (CSF-1R), glial cell line neutrophic factor receptor (RET) and fms-like tyrosine kinase receptor-3 (FLT-3) on tumour cells (Table 6.1). The therapy therefore targets both the tumour and vascular compartments.

Table 6.1. IC_{50} values for sunitinib inhibition of receptor tyrosine kinases (272).

Kinase	Sunitinib drug IC_{50} (nM)
VEGFR1	15 ± 1
VEGFR2	38 ± 11
VEGFR3	30 ± 6
PDGFRα	69 ± 15
PDGFRβ	55 ± 1
CSF-1R	35 ± 6
Flt-3	21 ± 5
Kit	1-10
Ret	224
FGF-R1	675 ± 69
Src	1000
Abl	610
CDK1	2600

Initial phase II clinical trial results, for the use of sunitinib as a monotherapy to treat metastatic breast cancer, were encouraging (152,273). However, subsequent phase II and III clinical trials in both the metastatic and triple negative setting have not achieved their objectives of prolonged survival compared with standard-of-care (274,275),

although some efficacy has been reported in combination with docetaxel (276). This has lead Pfizer to discontinue multiple clinical trials involving sunitinib in breast cancer. Efforts continue however, to broaden its use into breast cancer therapy, in combination with crizotinib, in clinical trials (Information retrieved from: http://clinicaltrials.gov and http://www.cancer.gov [accessed: 18.8.2015]).

A weakly responsive tumour type appeared the ideal model with which to investigate sunitinib drug resistance, as it should rapidly display resistant activity. Sunitinib resistance in breast cancer has not been extensively investigated, although intrinsic resistance to devascularisation and enhancement of lung tumour cell seeding has been reported (174). The 4T1 tumour is a murine stage 4 (metastatic) breast cancer, that faithfully models the pattern of human metastasis (186). It represents a major target of interest for sunitinib treatment, metastatic breast cancer, and was therefore selected for this investigation. Triple negative tumours have been generated from 4T1 cells by cell selection (277), although the strain used for this investigation was not from this background. This study did however, suggest that 4T1 tumour cells are heterogeneous in their marker expression, with a considerable population of triple negative cells (277), modelling the initial stages of TNBC encountered in the clinic. The 4T1 tumour was derived from Balb/c mice allowing a syngeneic, immuno-competent model of breast cancer to be generated that can be inoculated orthotopically into the mammary fat pad, providing a faithful model of metastatic breast cancer. In this model the full range of resistance mechanisms can be investigated. In this chapter the effects sunitinib has on metastasis and tumour vascular patterning are reported.

6.2 Results

6.2.1 Production of 4T1-luc cells

In order to generate a tumour cell line that permits bioluminescent imaging and quantification of tumour growth and metastasis, 4T1 cells were virally transduced to express the firefly luciferase gene. The MSCV-puro-luc plasmid was used for this purpose (Figure 6.1). When introduced into a cell, this plasmid leads to the expression of both the luciferase and puromycin resistance genes.

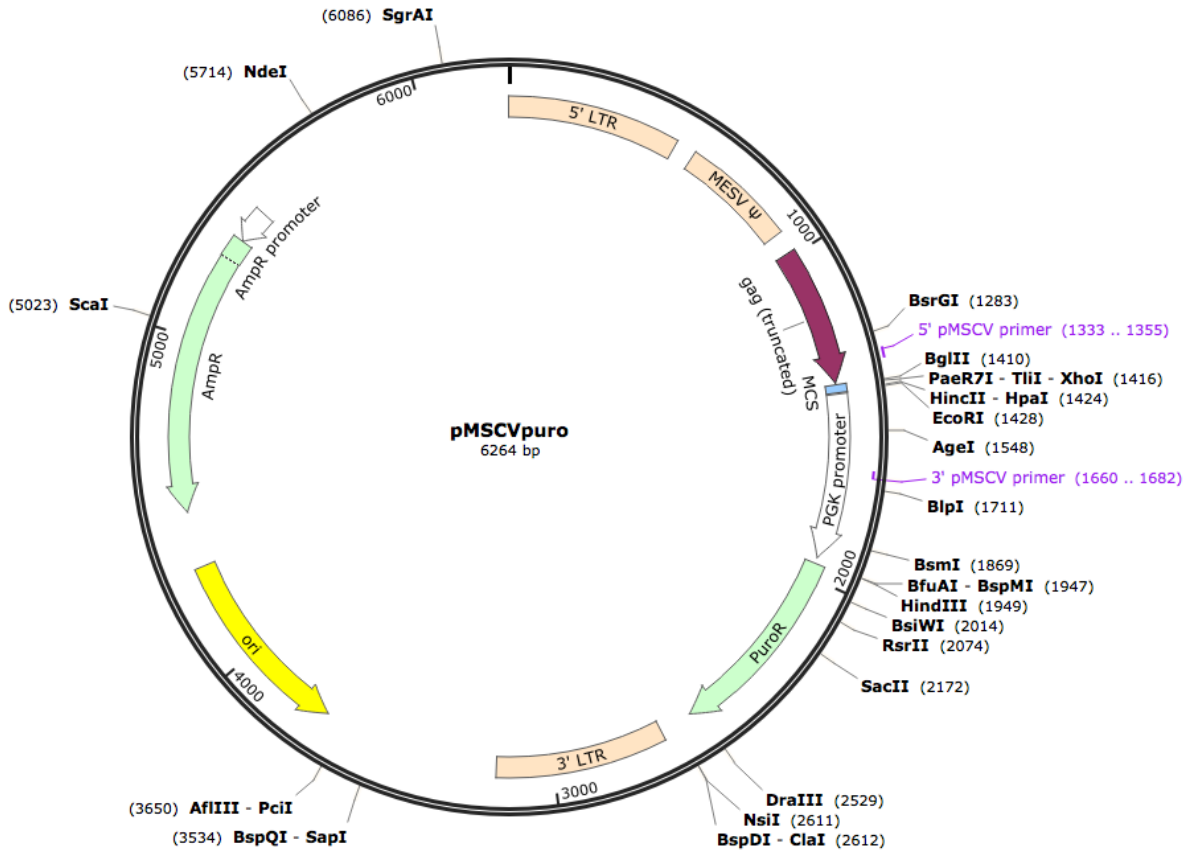

Figure 6.1. Map of the of the MSCVpuro plasmid used for retroviral transduction of the luciferase gene into 4T1 cells. The luciferase gene is inserted between the EcoRI and XhoI restriction sites. Image reproduced with permission (www.snapgene.com/resources).

Puromycin is an antibiotic that inhibits protein synthesis and is therefore toxic to many cells, including mammalian. Puromycin resistance was therefore used as a selectable marker for cells with successful transduction of the plasmid. The inherent puromycin tolerance of the 4T1 cells was determined by culturing them with between 0.16 and 20 μg/ml puromycin and then assessing cell viability after 72 hours, using the MTS assay. In this assay MTS, a yellow tetrazole, is added to the cells. Viable, metabolically active, cells reduce this compound to purple formazan, which has an absorbance maximum of 490 nm. By determining the absorbance of the solution at 490 nm after 4 hours of incubation, relative cell viability can be quantified. In this way it was determined that between 2 and 10 μg/ml puromycin would be suitable for selection (Figure 6.2A).

The MSCV-puro-luc plasmid was packaged by Phoenix-Ampho cells into retroviral particles, which were released into cultured media over time. This media was then supplemented with polybrene, to promote viral uptake, and introduced to 4T1 cells. The cells were centrifuged in a plate spinner with the viral media for 1 hour, before being washed and new media applied, containing between 2 and 10 μg/ml puromycin. Cells were selected for 48 hours after which cell viability was determined by assessment under the microscope (Figure 6.2B). It was found that transduced cells treated with 2-8 μg/ml puromycin had good viability whilst untranduced cells cultured with 2 μg/ml were almost entirely dead. Transduced 4T1 cells were cultured with puromycin for 2 further passages, after which the luminosity of the cells was determined by bioluminescent imaging with the CCD camera of the IVIS machine (Figure 6.2C and D). D-luciferin was introduced to the cells. The luciferase enzyme produced by the cells catalyses the reaction converting this substrate to L-luciferin,

releasing a photon of light. By this method it was determined that cells selected with 8 μg/ml puromycin were brightest, with over 275 fold greater luminosity than blank 4T1 cells (Figure 6.2D) and were therefore expanded over 2 passages and frozen down for murine tumour inoculation.

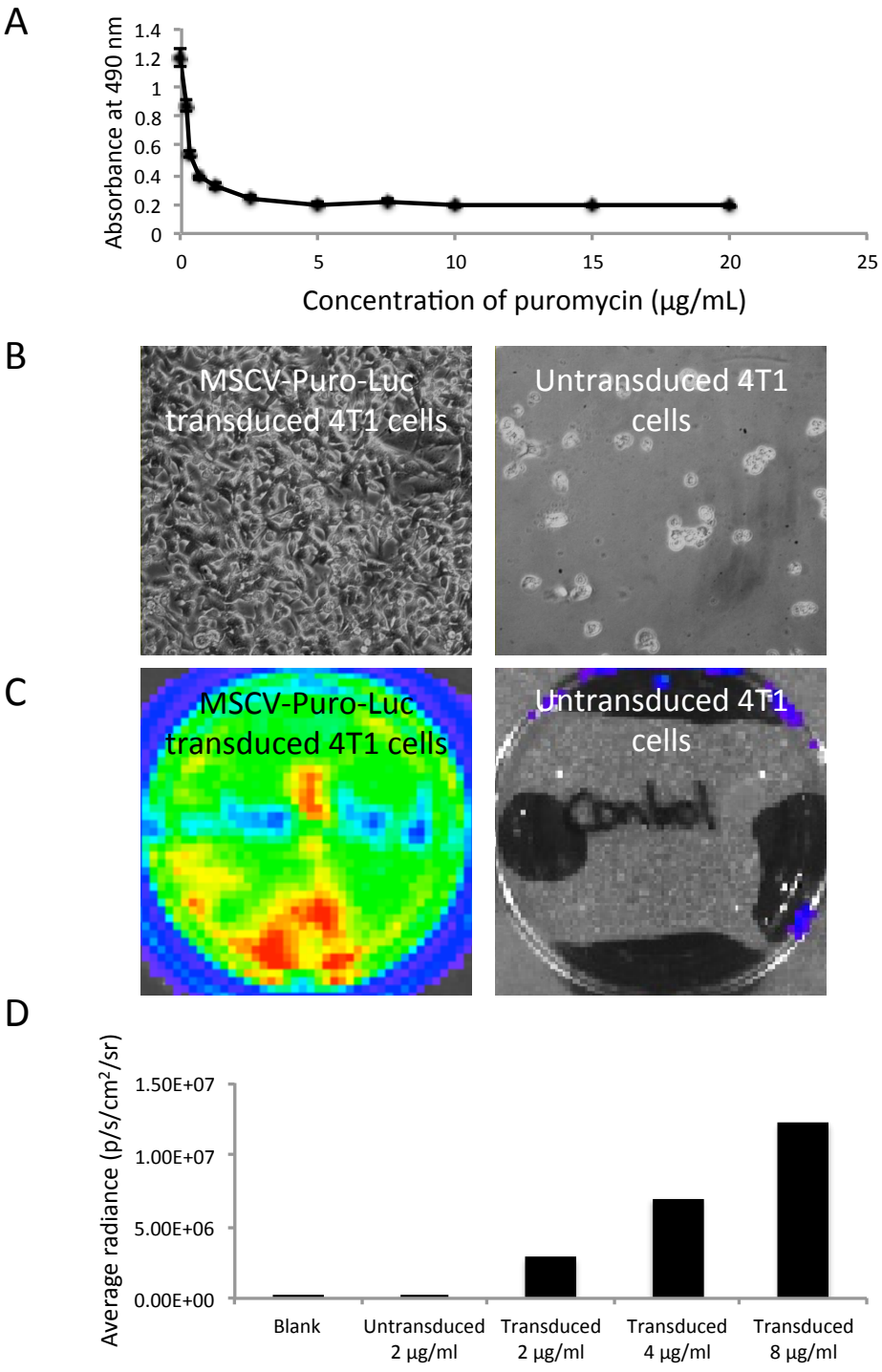

Figure 6.2. Retroviral transduction of the MSCV-puro-luc plasmid into 4T1 cells and puromycin selection. A, 4T1 cells were treated with 0.16-20 µg/ml puromycin and subjected to the MTS cell viability assay. Absorbance of the resultant solution, from cells treated with each concentration of puromycin is shown (mean ±SEM). 4T1 cells were transduced with the MSCV-puro-luc plasmid and selected with 8 µg/ml puromycin. Images showing the apparent cell viability, B, and bioluminoscity, C, of transduced versus untransduced cells are provided. D, quantitation of bioluminescence in transduced and untransduced 4T1 cells under selection with 0-8 µg/ml puromycin.

6.2.2 4T1 tumour growth under sunitinib treatment

4T1-luc cells were revived from liquid nitrogen storage and grown for 2 days. 2.5 ×10^5 4T1-luc cells were injected, in optimem, into the 3rd mammary fat pad of female Balb/c mice. The tumours were grown for 7 days prior to the commencement of treatment with 40 mg/kg sunitinib, or vehicle only control. Once tumours reached 1300 mm^3 in size, mice were culled and tumour collected (Figure 6.3).

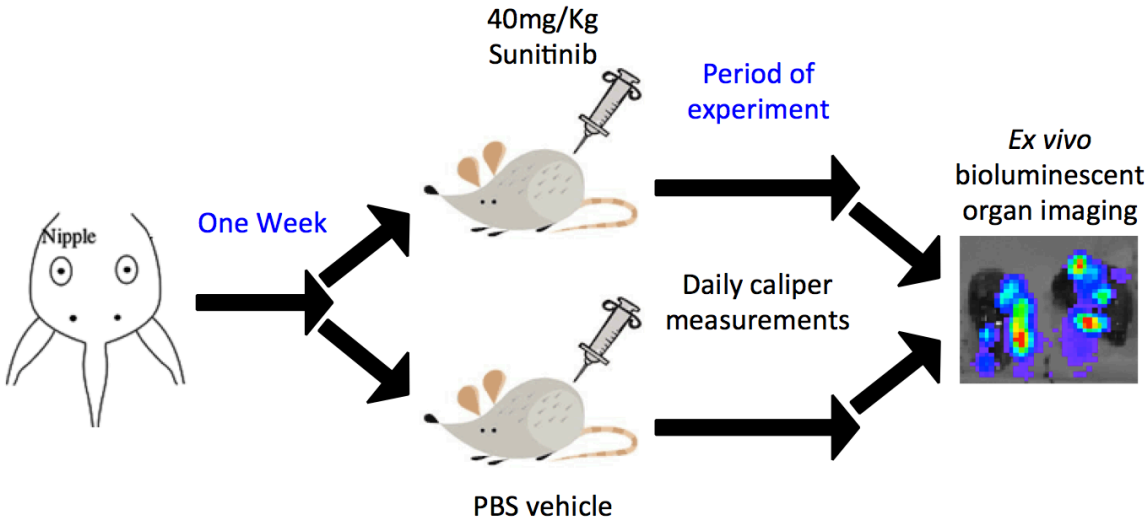

Figure 6.3. Experimental set up for sunitinib drug trial. 2.5 × 10^5 4T1 cells were injected into the third mammary fat pad of female Balb/C mice. The tumours were grown for 1 week, prior to drug treatment. Tumours were measured daily by calipers for the period of the experiment, then culled, with selected organs subjected to *ex vivo* imaging.

Daily caliper measurements were performed to track the development of these tumours over time. This analysis revealed that whilst untreated tumours grew at a fairly linear rate throughout the experiment, sunitinib treated tumours appeared to fall

into two groups. Some showed no response to sunitinib treatment and shared a similar growth profile with the untreated tumours. These were classified as non-responsive, whilst others appeared to have retarded growth for the first 9 days, after which the tumours started to grow at a similar rate to the other two groups (Figure 6.4A). In order to determine whether these two treated groups could be considered distinct, the distribution of tumour sizes at day 8, the point of greatest disparity between responsive and non-responsive tumour growth, was investigated for this and subsequent experiments (Figure 6.4B). This analysis revealed that whilst the untreated tumours appeared to follow a close to normal distribution, the treated group had two populations, one considerably smaller than the vast majority of untreated tumours (responsive) and the other with similar tumour size and distribution to the untreated group (non-responsive). The best point of distinction between the two groups appeared to be whether they were larger or smaller than 250 mm^3 at day 8, therefore this cut-off point was selected. Of note, the term "responsive", used here and later in the manuscript, refers to the cohort from which the tumour is derived, based on its growth pattern, not its current resistance status. Therefore "responsive" tumours collected at 1300 mm^3 display sunitinib resistant behavior, but only after an initial sensitive phase.

Broadly this experiment generated 3 cohorts of tumours, (i) naïve/ untreated, (ii) those that show no response to sunitinib, modelling innate resistance and (iii) those that after an initial sensitive period become resistant to sunitinib growth inhibition, mirroring the response pattern of acquired or adaptive resistance, encountered in the clinic.

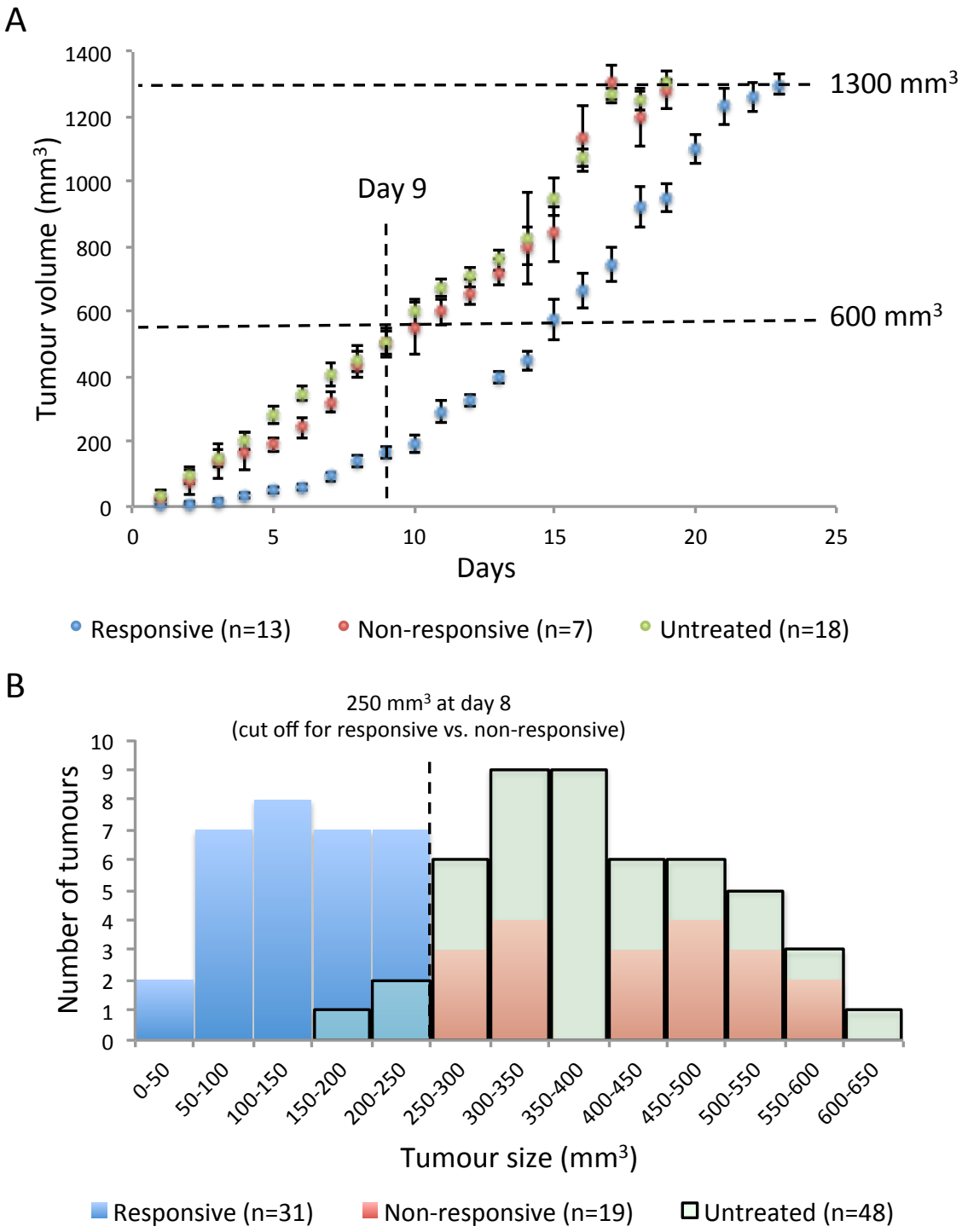

Figure 6.4. Sunitinib therapy bisects the treated group into responsive and non-responsive cohorts. A, Tumour growth curves from the initial sunitinib drug trials, with endpoint set at 1300 mm³. Measurements begin one week after tumour inoculation and on the day sunitinib treatment began. Subsequent experimental endpoints were set based on these growth curves and there intersections with this data are shown. B, histogram plot showing the distribution of tumour sizes at day 8 of treatment. Sunitinib treated tumours exceeding 250 mm³ in size were identified as falling into the non-responsive cohort.

In order to investigate the process of resistance further, it was decided to harvest tumours at key time and size points for further analysis. The tumours of a cohort of 15 treated and 15 untreated mice were collected at day 9 (the end of the treatment sensitive period in the responsive group) (Figure 6.5A) and at 600 mm^3 (a size point at which all initially responsive tumours are growing at the same rate as their untreated counterparts (Figure 6.5B). Of note, in each experiment there was a roughly 60-40% split between responsive to non-responsive tumours and by log-ranks statistical analysis it was determined that sunitinib treatment had a significant effect on the time it took responsive tumours to grow to both 600 mm^3 and 1300mm^3, versus non-responsive or untreated tumours, confirming that sunitinib has a significant, if transient, effect on tumour growth, restricted to the responsive group (Figures 6.5B and C).

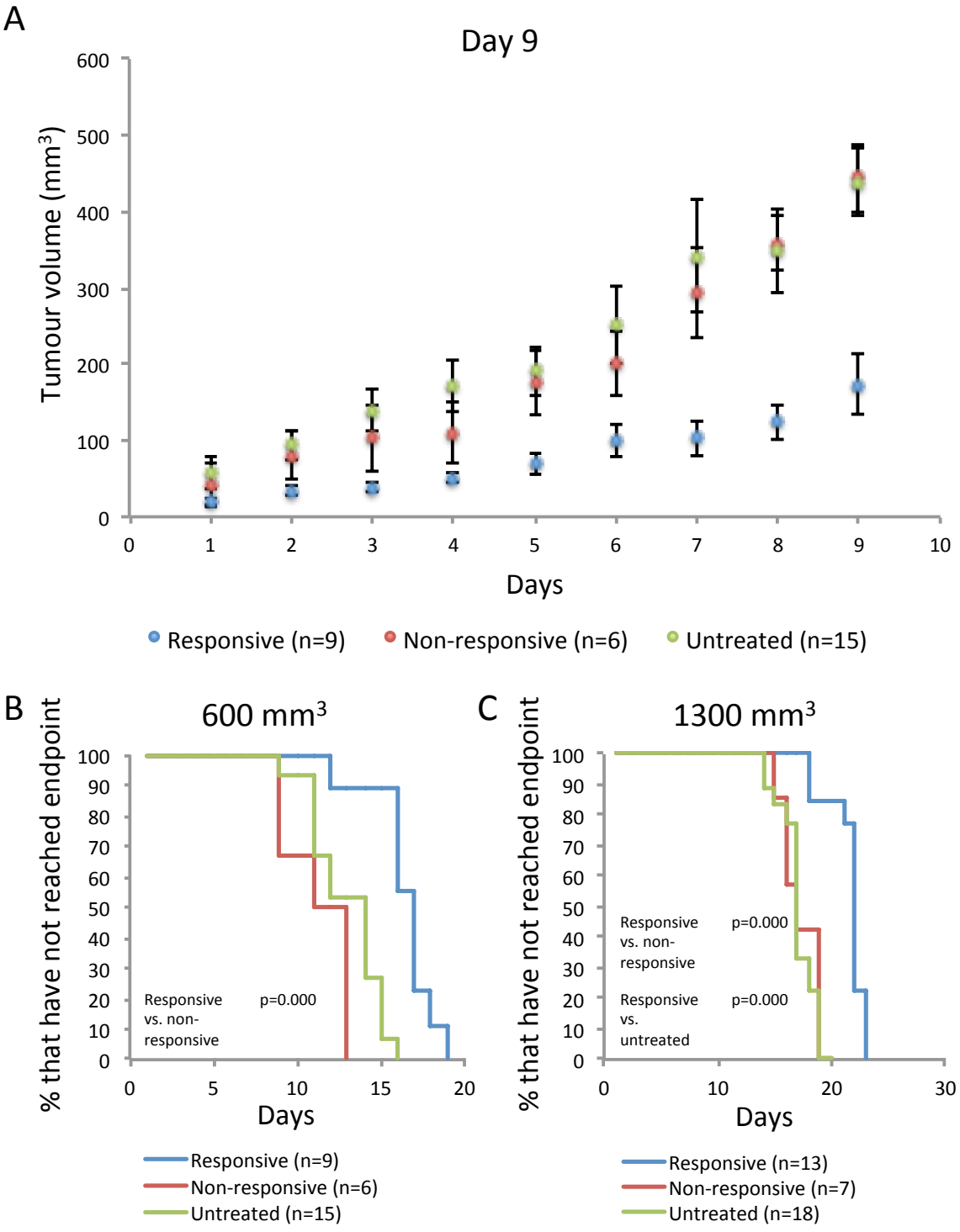

Figure 6.5. Sunitinib treatment significantly retards growth of responsive tumours. A, growth curves for tumours grown to the day 9 endpoint (mean ± SEM). B & C, Kaplan-Meier comparative analysis of time to endpoint of tumours grown to 600 mm^3 and 1300 mm^3. Log ranks statistical analysis of significant results is shown.

6.2.3 Differential sunitinib mediated effects on tumour vascular patterning

Tumours collected at either day 9, 600 mm^3 or 1300 mm^3 in size where assessed both macro- and microscopically for effects of sunitinib treatment on vascular patterning (Figure 6.6). This assessment revealed distinct patterns of vascularisation in each cohort. Untreated tumours appeared macroscopically well vascularised throughout the experiment (Figure 6.6A) and showed modest increases in vascularity (% of microscopic tumour area PECAM-1 positive) (Figure 6.6B). Responsive sunitinib treated tumours appeared macroscopically avascular at day 9, by 600mm^3 they had an apparent avascular core, possibly derived from growth up to day 9, around which was a crest of greater vascularity (post day 9 growth) which by 1300 mm^3 had encompassed the entire outside of the tumour. Of note the yellow hue clearly observable on all responsive day 9 tumours, which was presumably derived from the accumulation of sunitinib in the tumours, due to the drug being yellow in colour, had disappeared by 600 mm^3 in the majority of cases (all but one, data not shown), suggesting that the drug had been removed by some process or could not gain entry to the core of the tumour at this time point, contributing to drug resistance (Figure 6.6A). Possibly due to the maintenance of an avascular core, average microscopic vascular density in the responsive group was consistently less than the untreated group (Figure 6.6B). Intriguingly the non-responsive cohort appeared to split into two groups, one macroscopically resembling the responsive group (day 9 n=3, 600 mm^3 n=2, 1300 mm^3 n=?) and another macroscopically resembling the untreated group (day 9 n=3, 600 mm^3 n=4, 1300 mm^3 n=?). This hinted at a possible further subdivision of cohorts, in that some non-responsive tumours did not respond to sunitinib at all and appeared to be untreated, whilst others showed signs of sunitinib induced vascular inhibition, but

continued to grow regardless, possibly due to support from their surrounding environment (Figure 6.6A). Microscopic assessment of vascular density suggested that non-responsive tumours had an intermediate level of vascularity, between the responsive and untreated groups, possibly due to the pooling of data from the two non-responsive groups (Figure 6.6B). This subdivision of the non-responsive cohort, based on macroscopic appearance, was not taken forward for further investigation, firstly because it would have resulted in the n-numbers of an already small cohort being further diminished, and secondly because based on macroscopic assessment alone it was impossible to divide the 1300 mm^3 tumours as they all bear roughly the same appearance. In a larger investigation it may be possible to reliably subdivide these groups by microscopic assessment of vascular patterning. Assessment of the comparative level of vascularity found in the outer and core regions of 600 mm^3 tumours supported observations made on the macroscopic level, in that untreated tumours have a consistent level of vascularity, responsive tumours have a clear reduction of vascularity in the core of the tumour with non-responsive tumours resembling either one or the other of these groups (Figure 6.6C). By this method it may be possible in the future to divide the groups reliably at each time and size point for further investigation of the different mechanisms behind innate resistance.

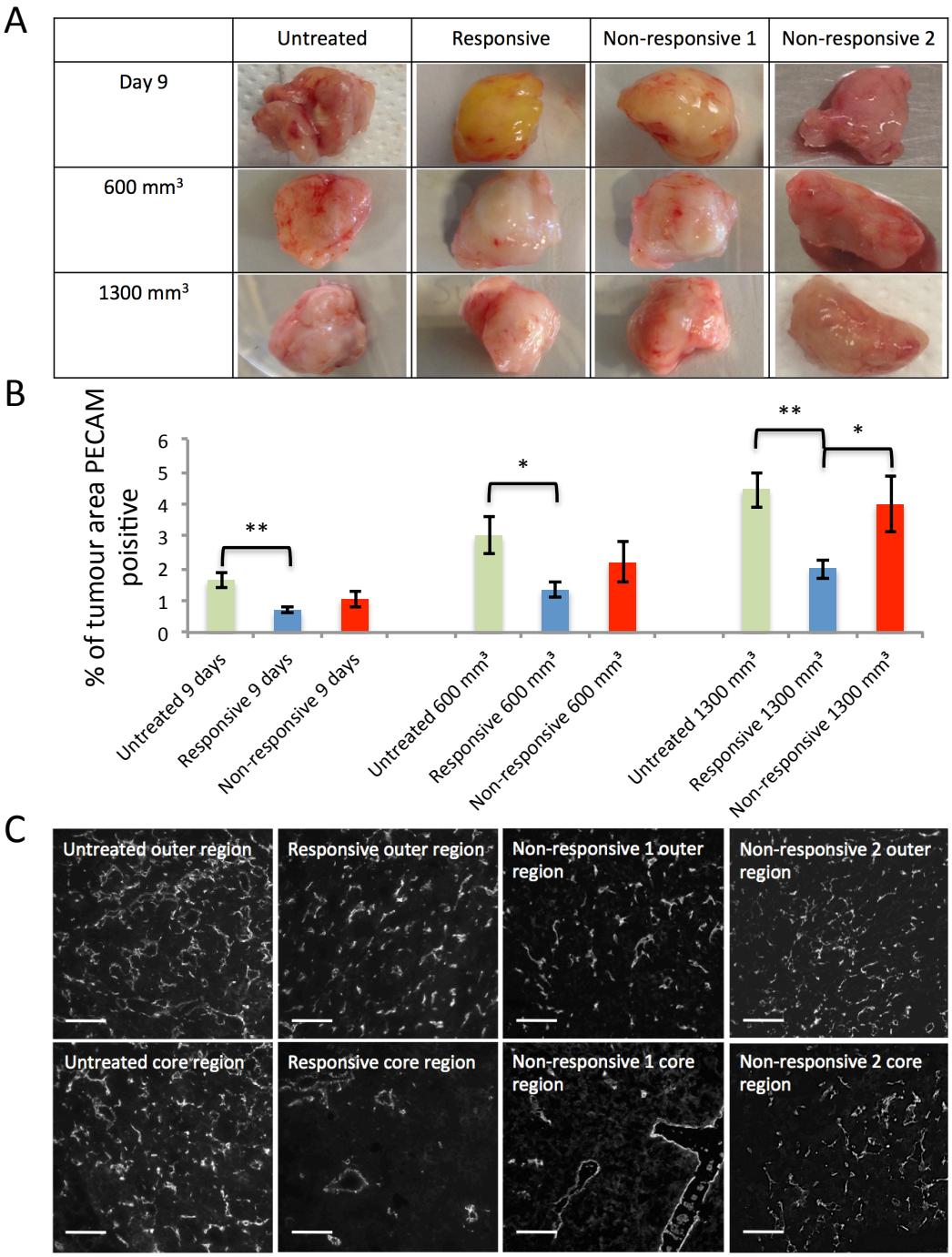

Figure 6.6. Sunitinib treatment reduces vascularity and impacts the vascular patterning of 4T1 tumours. A, representative images of tumours from each cohort and experimental endpoint, showing macroscopic vascular patterning, not to scale. B, bar chart of vascular density of tumours from each cohort and experimental endpoint, determined by the average percentage of PECAM-1 immunofluorescent staining across 5-6 fields of view (mean ± SEM, Mann-Whitney, ** $p<0.01$, * $p<0.05$, n-numbers as displayed in Figure 6.5). C, representative images of immunofluorescent PECAM-1 staining in the core and outer regions of tumours, from each cohort of tumours taken at 600 mm^3. Scale bar = 50 µm.

6.2.4 Sunitinib enhances metastasis in innately resistant tumours

Anti-angiogenic drugs have been reported to enhance tumour metastasis in certain circumstances (149). The utility of *ex vivo* bioluminescent imaging of resected organs for signs of metastasis was investigated as a reliable method for quantifying metastasis. Key sites of 4T1 metastasis (the liver, lungs and spleen) were probed by both *ex vivo* bioluminescent imaging and H&E staining (Figure 6.7A and B). For details of both approaches see sections 2.7.3 to 2.7.5). The apparent metastatic burden, from 10 mice where tumours had been harvested at 1300 mm^3, was quantified by each method and correlated. There was a good level of correlation of metastatic burden between the two approaches on a individual organ level, although it must be noted that this correlation was not shared between organs (Figure 6.7C). The ratio of apparent metastasis quantified in the direct, but time consuming, H&E manner and the indirect, but rapid, bioluminescent manner, varies between organs, likely due to differences in the size, density and absorbance of the tissues.

As bioluminescent imaging appeared to provide metastasis quantification consistent with more conventional pathological staining methods, but in a fraction of the time, it was selected as the method by which the metastatic burden of the mice of each treatment/response cohort was quantified and compared.

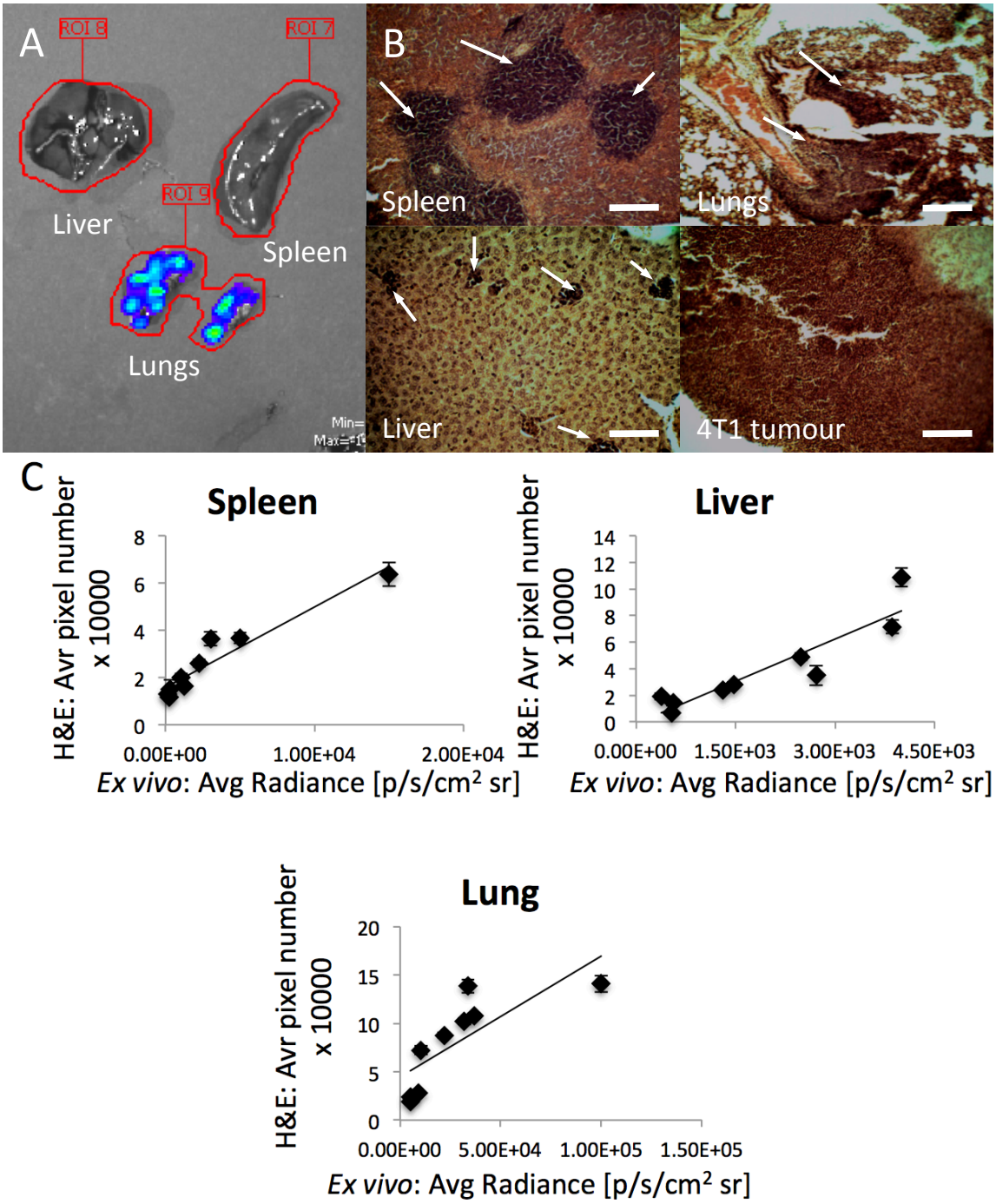

Figure 6.7. *Ex vivo* bioluminescent imaging and H&E staining correlate as methods to determine metastatic tumour burden. A, representative image of liver, spleen and lung whole organs undergoing bioluminescent imaging by the IVIS (overlay of blue-green-red colouring represents bioluminescence of increasing intensity. B, representative images of H&E staining of 4T1 tumour and metastasis in spleen, lungs and liver (metastasis marked by white arrows). Scale bar = 100 µm. C, correlation between metastatic burden, as determined by measurement of average metastatic area across 6 fields of view, in organs stained by H&E and by whole organ bioluminescent pixel density, in spleen, liver and lung tissues (mean ± SEM, n=10).

This analysis revealed that the liver and lungs of mice with non-responsive primary tumours developed a significantly greater metastatic burden, compared to those of both responsive and untreated cohorts at 1300 mm^3, whereas in the spleen, the untreated cohort developed the greatest metastatic burden (Figure 6.8). Of note this shift is only observed at the later time-point. At day 9, metastasis from untreated tumours is greater than either treated group. This suggests that sunitinib initially inhibited metastasis, possibly by blocking the development of vasculature and lymphatics, however, in the non-responsive group this inhibition was not only overcome, but reversed (Figure 6.8).

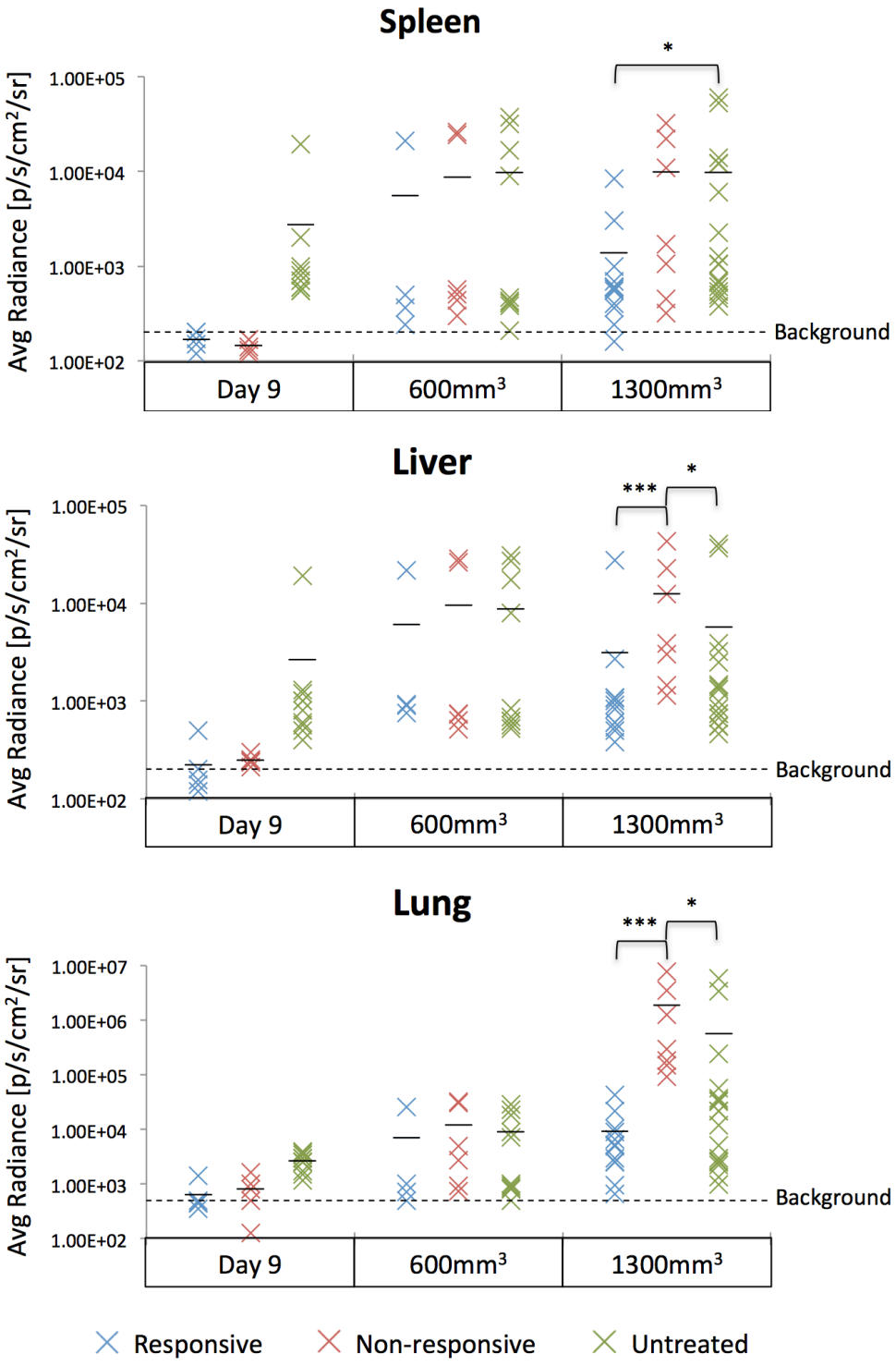

Figure 6.8. Sunitinib treatment enhances 4T1 tumour metastasis, but only in the innately resistant setting. Distribution plots of bioluminescence from each organ, cohort and experimental endpoint. The level of background auto-fluorescence measured by imaging of organs from mice with no tumour is also displayed. Statistical analysis: Mann-Whitney, *** $p<0.001$, * $p<0.05$. N-numbers: Day 9, responsive (R)=5, non-responsive (NR)=5, untreated (UT)=10; 600mm³, R=4, NR=6, UT=10; 1300mm³, R=12, NR=7, UT=17.

6.3 Discussion

4T1 tumour cells engineered to express luciferase were used to set up a model of breast cancer tumour growth and metastasis. The effect daily sunitinib treatment had on these tumours was investigated. This study identified 4T1 tumours responding to treatment in 3 distinct manners. One group were initially sensitive to therapy, with retarded tumour growth for the first 9 days of treatment, after which tumour growth followed the same rate as the untreated cohort. These tumours displayed marked devascularisation during the period of inhibition, and evidence of revascularisation once insensitive. This cohort additionally displayed significantly reduced metastasis over the period of the experiment. A second cohort, showed complete insensitivity to the sunitinib treatment, with no growth retardation or vascular patterning effects, relative to the untreated cohort. A third group again showed no growth rate response, however, the tumours did show evidence of devascularisation in response to sunitinib treatment, on both the macro and microscopic levels. Additionally the pooled growth insensitive tumour cohorts displayed significantly enhanced metastatic growth in the liver and lungs. In conclusion a model of sunitinib resistance in metastatic breast cancer has been set up, with cohorts displaying both acquired and innate resistance. A key finding was that sunitinib does enhance metastasis but only in the innately resistant setting.

The presence of 3 groups of tumours showing differing responses to sunitinib treatment could be seen as surprising. A genetically identical (albeit heterogeneous) population of 4T1 cells were injected into another genetically identical population of Balb/c mice. The natural variance observed in any tumour experiment is usually

explained by slight differences in tumour cell placement and other factors that then impact on how well it thrives. These factors are likely to be playing a part in the segregation of the populations based on size, however, as is explored in this chapter, the difference in the populations goes beyond tumour size. 20-27% of treated tumours showed no devascularisation or growth inhibition in response to sunitinib, while another 13-20% grew at the same rate as the untreated group, despite showing signs of devascularisation. The genetic and environmental factors underlying this response profile warrant investigation and could provide insight into the factors leading to resistance, which could have clinical utility.

The existence of a cohort of tumours displaying no response to sunitinib is well established in the clinic. A recent phase III clinical trial investigating sunitinib in combination with docetaxel as a treatment for advanced breast cancer, reported a response rate of only 55% (276), while (278) reported an objective response rate of 11% with sunitinib used as a monotherapy in HER2-negative advanced breast cancer. The identification of markers that will allow the prediction of which tumours are likely to respond to sunitinib, has the potential to considerably improve the use and effectiveness of this drug and this is one of the focuses of investigation in chapter 7.

62% of treated tumours did respond to sunitinib, resulting in devascularisation and tumour growth retardation. However, this effect was only maintained for 9 days of treatment, after which their growth resumed unabated and a crest of vascularised tumour tissue formed around the avascular core. Broadly this group model another form of resistance observed in the clinic, acquired resistance (279). Another one of the

focuses of chapter 7 is the investigation of the molecular profile of tumours exhibiting this form of resistance, so that strategies designed to slow or circumvent this resistance can be formulated.

The presence of tumour metastases are one of the major risk factors for death in all cancers and anti-angiogenic therapies, including sunitinib have been implicated in increasing the risk of this eventuality, as previously discussed. This may seem counter-intuitive, as sunitinib has been shown to not only block vascular angiogenesis, but also through the inhibition of vascular endothelial growth factor 3 (VEGFR-3), lymph-angiogenesis. Sunitinib effectively shuts down two of the major routes to metastasis for a tumour, however, both Yin *et al*., 2014 (280) and Welti *et al*., 2012 (174), report enhanced lung metastasis and tumour infiltration in models of breast cancer. Admittedly the tumour cells in Welti *et al*., 2012 (174) were injected intra-venously, therefore were already circulating and did not have to escape the tumour. The observations detailed in this chapter add to the story. Metastasis was significantly enhanced to the liver and lungs by sunitinib treatment at the 1300 mm^3 stage, but only in the innately resistant cohort. The majority of this cohort displayed no devascularisation and therefore the anti-metastatic effects of inhibiting vascular and lymph angiogenesis would likely not apply. The question therefore is, why once circulating, do the tumour cells more readily infiltrate other organs, under the influence of sunitinib. A number of potential mechanisms have been suggested. The up-regulation of angiogenesis and metastasis associated cytokines and growth factors in response to treatment (281), the mobilisation of bone-marrow derived cells discussed in chapter one could generate a pre-metastatic niche (282), host micro-environmental

responses to cellular inhibition or injury (283), could promote tumour metastasis, in a similar manner to that reported with radiation or chemotherapeutic agents (284-286) and finally high dose treatment with sunitinib has been reported to lead to pericyte depletion, likely through PDGF signalling inhibition, in lung vasculature, which is correlated with enhanced breast tumour seeding (174). This latter observation is supported by pericyte depletion studies in which they found that loss of pericytes in advanced tumours, inhibited growth but enhanced lung metastasis (287).

It should be noted that the usual human dosing for sunitinib is 37.5 mg / day, and as the average human body weight is 62 kg (288), the 40 mg/kg sunitinib treatment of the mice used in this investigation and many other studies, (174,289,290), is clearly in great excess. This factor could be leading to systematic effects, such as pericyte depletion, that are not observed in the clinic. Therefore metastatic effects identified in animal models require validation in the human setting.

The sunitinib responsive cohort displays unchanged or reduced metastasis relative to the untreated cohort at the 1300 mm^3 stage. This suggests that the inhibited vascularisation and tumour growth, experienced up to day 9, did retard the progress of metastasis in this group. In support of this Weidner *et al*., 1991 (291) report a strong independent link between micro-vascular density and metastasis in invasive breast cancer. This is supported by the observation of no significant metastasis in the treated group at day 9, relative to the untreated group. After this point tumour cells do escape and colonise the spleen, liver and lungs and continued sunitinib treatment does not appear to inhibit this. However, the initial retardation experienced up to day 9 means

that by the time the primary tumour is 1300 mm^3 in size, the development of metastases is still lagging behind the untreated cohort.

The broad pattern of the data is, where primary tumour growth is retarded and vascular production inhibited, metastasis is slowed by sunitinib therapy. On the other hand when the primary tumour is non-responsive to treatment the presence of sunitinib enhances the tumour metastasis, possibly due to pericyte depletion in the target organs or host pro-metastatic micro-environmental responses to treatment. This data further highlights the need for reliable markers for the prediction of sunitinib response, as inappropriate treatment could potentially not only waste time and money, but also enhance metastasis.

Chapter Seven

The Molecular Profile of Breast Cancer Sunitinib Drug Resistance

7.1 Introduction

The investigation of tumour growth and metastasis in a model of sunitinib drug resistance in breast cancer, detailed in chapter 6, generated three cohorts divided by their response to the drug. (i) A naïve cohort never treated with the drug (termed-untreated), (ii) a cohort treated with sunitinib that initially showed drug induced tumour stasis for 9 days, after which the tumours grew at a similar rate to the naïve cohort, but with reduced metastasis (modelling acquired resistance and termed responsive) and (iii) a cohort treated with sunitinib that showed no tumour growth response and grew at a similar rate to the naïve cohort but with enhanced metastasis (modelling innate resistance and termed non-responsive).

This chapter presents data from high throughput microarray transcriptomic analysis of both the tumours and the tumour vessels (the primary target of therapy), from each of these cohorts and downstream validation of the findings. This investigation attempts to elucidate the molecular profile of acquired and innate resistance to sunitinib, in this model of metastatic breast cancer.

7.2 Results

7.2.1 Murine tumour endothelial isolation and microarray analysis

In order to investigate the impact sunitinib therapy has on the tumour vessels, endothelium was isolated from the untreated, responsive and non-responsive cohorts, using magnetic beads. Sheep anti-rat coated dynabeads were coupled with rat anti-mouse PECAM-1 antibodies and used to rosette and magnetically isolate endothelium from collagenase V digested 4T1 tumours (Figure 7.1). PECAM-1 is also a marker of a small subset of leukocytes, therefore RTqPCR was performed on the isolates to confirm specific endothelial enrichment. Relative expression of markers of leukocytes (CD11b), macrophages (CD68), epithelial cells (EPCAM), smooth muscle cells (PDGFRA) and endothelium (PECAM), was assessed between matched endothelial isolates and endothelial depleted fractions, by RTqPCR. This analysis confirmed that PECAM expression alone was enriched 25-30 fold in the endothelial isolates, suggesting a very good level of endothelial enrichment (Figure 7.1).

Two tumour bulk samples each, from the responsive and untreated cohorts harvested at day 9 and 600 mm^3, along with four representative endothelial isolate samples and bulk samples from each of the responsive, non-responsive and untreated cohorts taken at 1300 mm^3, were selected for microarray transcriptomic analysis (individual growth curves shown in Figure 7.2).

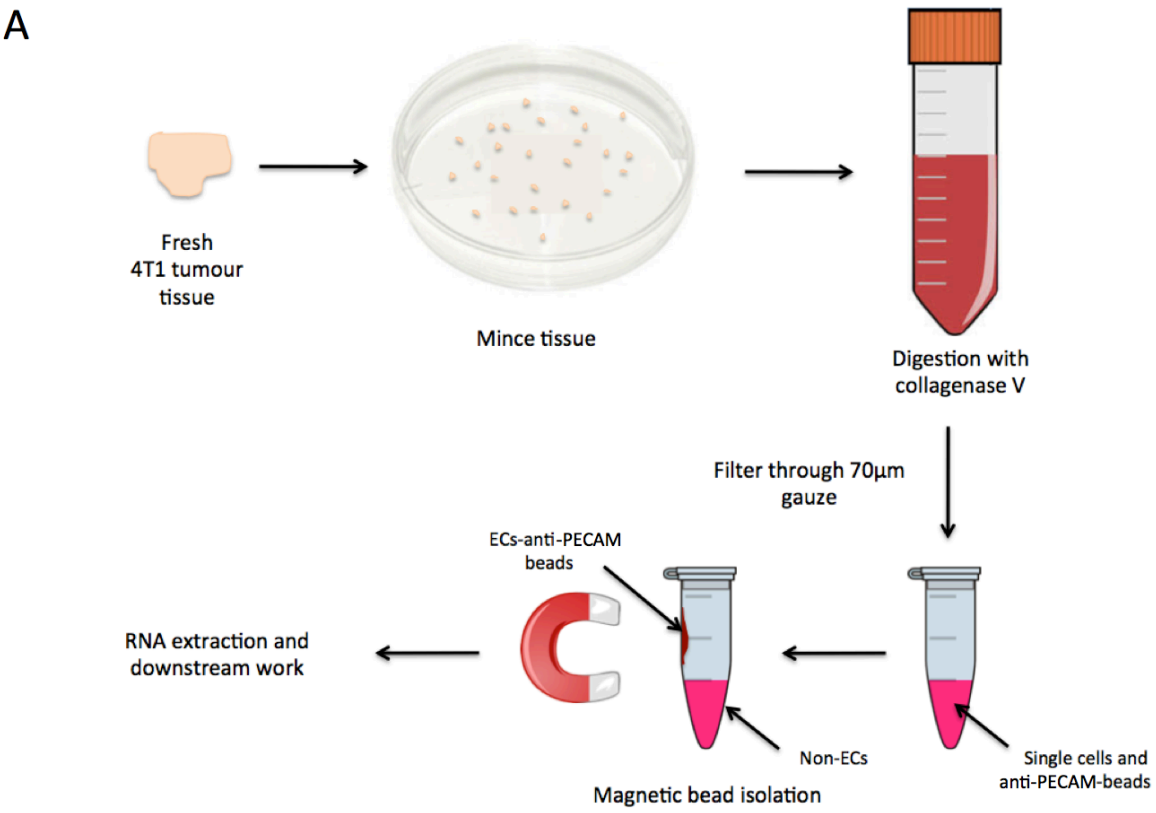

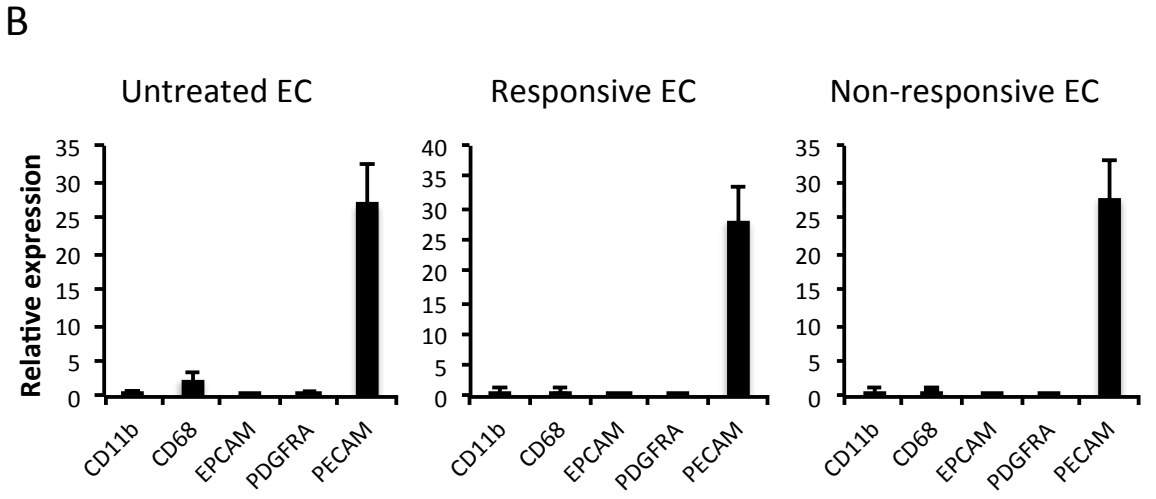

Figure 7.1. Endothelial isolation from murine breast tumours. A, workflow of the main steps involved in the murine endothelial cell isolation procedure. B, RTqPCR for markers of leukocytes (CD11b), macrophages (CD68), epithelium (EPCAM), smooth muscle (PDGFRA) and endothelium (PECAM) in the endothelial isolates (EC) from responsive, untreated and non-responsive tumours (n=4,4,4) standardised to β-actin (a house keeping gene) and normalised for marker expression to matched bulk tissue. Mean fold change of marker expression between the endothelial and bulk fraction is shown ± SEM.

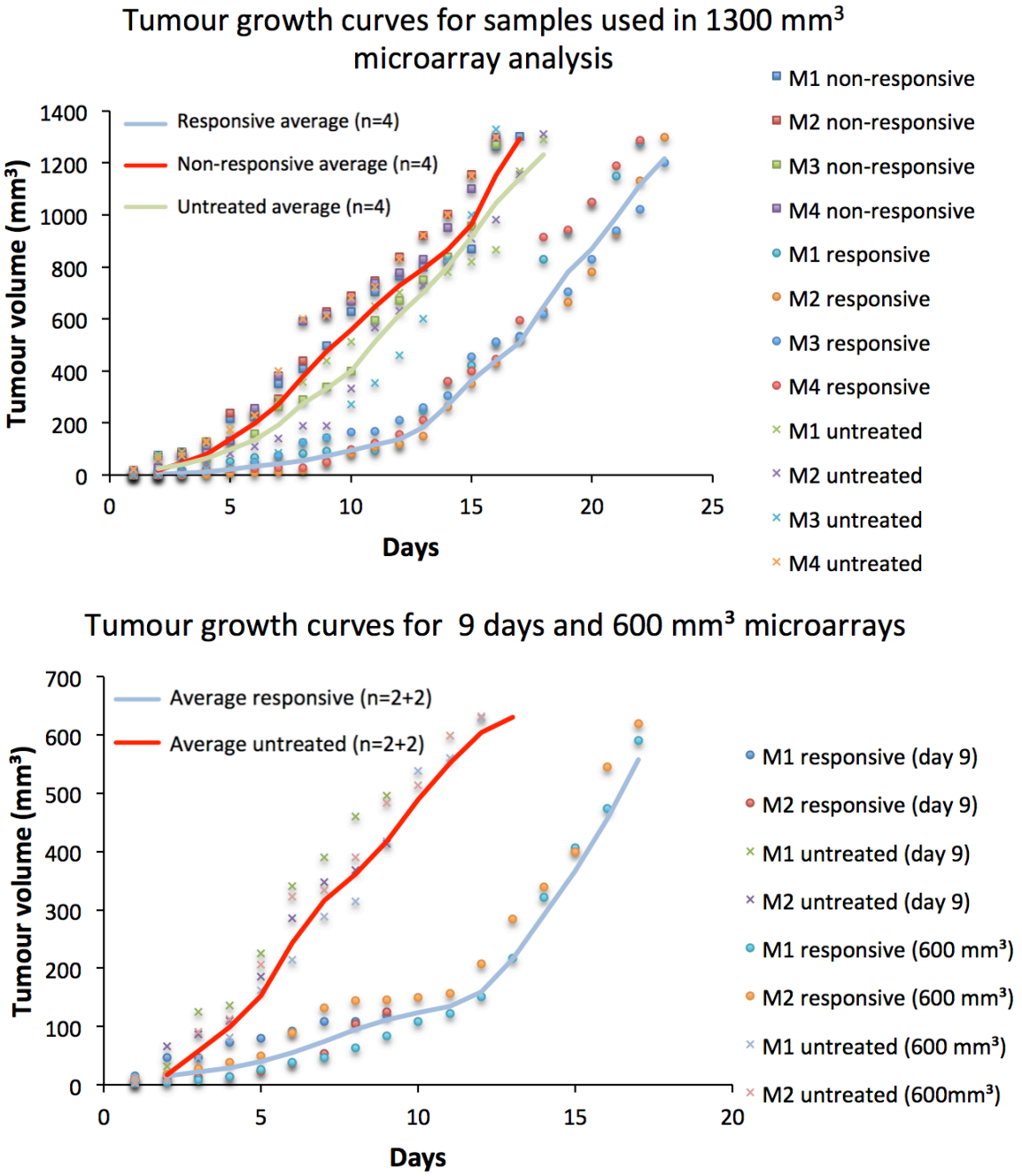

Figure 7.2. Representative tumours from the non-responsive (square), responsive (circle) and untreated (cross) group at each time period, were subjected to microarray transcriptomic analysis. Graphs showing individual tumour growth data points and mean tumour size of the selected tumours over the period of the experiment. N-numbers for each experiment are shown.

7.2.2 The impact of sunitinib treatment on tumour and endothelial gene expression

Microarray analysis of the selected samples facilitated the transcriptional characterisation of the tumour and associated endothelium, from naïve (untreated), innately resistant (non-responsive) and adaptively resistant (responsive) tumours, at key stages of resistance acquisition (day 9, 600 mm^3 and 1300 mm^3). This was done by the investigation of the comparative expression profile between these cohorts, of genes known (or predicted by the Qiagen Ingenuity pathway prediction software database, on stringent settings) to be associated with sunitinib response (Tables 7.1 and 7.2), metastasis (Tables 7.3 and 7.4), and endothelial migration and angiogenesis (Tables 7.5 and 7.6). Gene expression in the signaling pathways of selected targets of sunitinib drug activity (VEGFR-1&2, PDGFR-α&β and FLT3) was also investigated (Appendix figures A, B and C).

7.2.2.1 Comparative analysis of genes associated with sunitinib response

In order to characterise the responsiveness of the tumours and associated endothelium to sunitinib therapy, during the course of the experiment, on a transcriptomic level, a list of genes associated with sunitinib response was collated as described previously and their expression analysed between arrays.

This analysis revealed that at day 9, tumours from the "responsive" cohort do indeed display an expression profile in line with that predicted of response to sunitinib therapy, when compared to the untreated cohort. Five out of six genes with expression >2 fold changed, are altered in line with predicted sunitinib response (Table 7.1). This response profile is lost however, at later time points, in line the loss of sunitinib

induced growth retardation in the “responsive” cohort, discussed in chapter 6 (Table 7.1).

This analysis when applied to endothelial isolates from the responsive, non-responsive and untreated cohorts, at 1300 mm^3 agreed with the bulk tumour data, as regards the “responsive” (but now having acquired resistance) group, showing no obvious sensitivity to sunitinib treatment, in terms of gene expression (Table 7.2). Conversely, gene expression of sunitinib target genes is reduced in the non-responsive cohort, relative to the responsive cohort, suggesting that despite displaying innate resistance from the outset of the experiment, in terms of growth profile, on the transcriptomic level the endothelium of this cohort were more sensitive to sunitinib treatment than the “responsive” cohort (Table 7.2).

Table 7.1. Expression change of genes on which sunitinib has a predicted effect, in tumour bulk harvested at each time-point

Gene ID	Gene symbol	GeneBank accession no.	Predicted sunitinib effect	Responsive vs. Untreated 9 days	Responsive vs. Untreated 600 mm^3	Responsive vs. Untreated W 1300 mm^3
kit oncogene	KIT	NM_001122733	Downregulated	-2.33	-0.78	0.27
platelet derived growth factor receptor, beta	PDGFRB	NM_001146268	Downregulated	-2.11	-0.41	-0.60
CD69 antigen	CD69	NM_001033122	Downregulated	-2.00	0.47	0.47
interleukin 2 receptor, alpha	IL2RA	NM_008367	Downregulated	-1.28	-0.24	0.99
Janus kinase 2	JAK2	NM_008413	Downregulated	0.40	1.41	0.07
phosphofructokinase, muscle	PFKM	NM_021514	Downregulated	1.06	-0.61	-0.05
vascular endothelial growth factor A	VEGFA	NM_001025250	Upregulated	1.18	-0.25	0.01

Table 7.2. Expression change of genes on which sunitinib has a predicted effect, in EC isolates from tumours harvested at 1300 mm^3

Gene ID	Gene symbol	GeneBank accession no.	Predicted sunitinib effect	Non-responsive vs. Untreated EC	Responsive vs. Untreated EC	Non-responsive vs. Responsive EC
chemokine (C-X-C motif) ligand 3	CXCL3	NM_203320	Downregulated	-1.97	-0.35	-1.62
FMS-like tyrosine kinase 1	FLT1	AK005502	Downregulated	0.04	0.89	-1.84
kinase insert domain protein receptor	KDR	NM_010612	Downregulated	0.26	1.04	-1.18
FMS-like tyrosine kinase 3	FLT3	AK045865	Downregulated	0.34	-0.01	-1.04
ret proto-oncogene	RET	NM_001080780	Downregulated	0.60	1.26	-0.41
baculoviral IAP repeat-containing 5	BIRC5	NM_001012273	Downregulated	1.15	0.20	0.45
BCL2-like 11 (apoptosis facilitator)	BCL2L11	NM_207680	Upregulated	1.30	-0.33	0.39

7.2.2.2 Comparative analysis of genes expression in sunitinib targeted pathways

An analysis of the pattern of expression of genes downstream of selected sunitinib targeted pathways (VEGFR-1&2, PDGFR-α&β), broadly agrees with but also recapitulates the findings of section 7.2.2.1. This analysis is therefore briefly mentioned here, but is further discussed in the appendix. Using similar comparison matrices to those mentioned previously, it was determined that expression of genes downstream of each of the selected targeted pathways were modulated in line with predicted response to sunitinib (Appendix figures A, B and C (i)), at day 9, in bulk tumour samples from the responsive cohort, when compared to the untreated cohort (Appendix figures A, B and C (ii:1)). This modulation was lost at later stages (Appendix figures A, B and C (ii:2&3)), concurrent with the loss of tumour growth retardation reported in chapter 6 and in agreement with the patturn of gene expression reported for genes associated with sunitinib response (section 7.2.2.1). This suggests that these initially "responsive" tumours acquired resistance, accelerating tumour growth and vascularisation, via a loss of sensitivity in sunitinib targeted pathways. Conversely, at the 1300 mm^3 tumour stage, gene expression in the non-responsive cohort, when compared with both the responsive and untreated cohorts, was still modulated in line with response to sunitinib (Appendix figures A, B and C (ii:4-8)). This was particularly apparent in the VEGFR-1&2 pathways (Appendix figure A (ii:4-8)). This finding is in agreement with that reported for the expression of sunitinib response genes (section 7.2.2.1), suggesting that these "innately resistant" tumours are still sensitive to sunitinib therapy as regards its gene expression modulatory activity, but maintain tumour growth and vascularity, potentially via alternative unaffected mechanisms.

7.2.2.3 Comparative analysis of genes associated with metastasis

Besides effects on tumour growth and vascularisation, metastasis was significantly affected by sunitinib treatment and response, as discussed in chapter 6. In order to investigate this on a molecular level, a list of genes known to enhance metastasis was compiled from the Ingenuity online database, and their expression analysed between arrays (Table 7.3 and 7.4). Metastasis signalling in the responsive tumours appears to be quite strongly inhibited at day 9, when compared to the untreated cohort at the same time period (Table 7.3). Fifteen known or predicted pro-metastatic genes were >2 fold down-regulated by sunitinib treatment at this stage. Five pro-metastatic genes were >2 fold up-regulated at this stage in the treated tumours, however, the pattern of signalling was primarily inhibitory to metastasis. This expression pattern was progressively reversed at subsequent harvesting points, with a third of >2 fold altered pro-metastatic genes up-regulated at 600 mm^3 and three quarters at 1300 mm^3. In the non-responsive cohort too the majority of pro-metastatic genes >2 fold altered were up-regulated at 1300 mm^3, when compared to the untreated cohort (Table 7.4). Intriguingly however, when comparing the two treated cohorts, it was the responsive group that displayed the more pro-metastatic profile, with five genes stimulatory to metastasis, up-regulated in the responsive group, over the non-responsive cohort. This data overall agrees with the observed metastatic profile of the tumours explored in chapter 6, with sunitinib initially inhibiting metastasis up to day 9, and even 600 mm^3, but by 1300 mm^3 metastasis and the signalling for it, was enhanced by sunitinib treatment. The strong metastatic signalling in tumours of the "responsive" cohort is in disagreement with the chapter 6 metastatic profile data (Figure 6.8). Metastasis, as assessed by IVIS imaging, was reduced in this cohort relative to non-responsive and

untreated tumours, however, according to transcriptomic analysis at the 1300 mm^3 stage, signaling for metastasis was enhanced in this cohort above the other two groups. This begs the question, had the mice been left for longer, would the level of metastasis in the initially responsive cohort have caught up or even overtaken that of the non-responsive cohort?

Table 7.3. Expression change of genes that enhance metastasis in tumour bulk harvested at each time-point.

Gene ID	Gene symbol	GeneBank accession no.	Effect of metastasis	Responsive vs. Untreated 9 days	Responsive vs. Untreated 600 mm^3	Responsive vs. Untreated 1300 mm^3
bone morphogenetic protein 2	BMP2	NM_007553	Increased	-3.30	-0.45	-1.05
snail homolog 2 (Drosophila)	SNAI2	NM_011415	Increased	-2.91	0.08	0.46
ubiquitin D	UBD	NM_023137	Increased	-2.06	0.72	0.04
thymus cell antigen 1, theta	THY1	NM_009382	Increased	-1.98	-0.67	0.19
collagen triple helix repeat containing 1	CTHRC1	NM_026778	Increased	-1.37	-0.71	-0.70
nitric oxide synthase 3, endothelial cell	NOS3	NM_008713	Increased	-1.34	-0.32	-0.24
angiopoietin-like 4	ANGPTL4	NM_020581	Increased	-1.32	-1.04	0.22
heparanase	HPSE	NM_152803	Increased	-1.30	-0.18	-0.21
O-6-methylguanine-DNA methyltransferase	MGMT	NM_008598	Increased	-1.28	-0.52	-0.08
tumor necrosis factor (ligand) superfamily, 11	TNFSF11	NM_011613	Increased	-1.27	0.29	0.36
zeta-chain (TCR) associated protein kinase	ZAP70	NM_009539	Increased	-1.27	0.19	0.89
CD274 antigen	CD274	NM_021893	Increased	-1.25	-0.21	0.00
Fyn proto-oncogene	FYN	NM_001122893	Increased	-1.13	-0.35	-0.08
tumor necrosis factor	TNF	NM_013693	Increased	-1.11	-0.30	0.96
chemokine (C-X-C motif) receptor 4	CXCR4	NM_009911	Increased	-1.07	-0.73	0.00
matrix metallopeptidase 2	MMP2	NM_008610	Increased	-0.29	-1.14	-0.40
chemokine (C-X-C motif) ligand 1	CXCL1	NM_008176	Increased	0.25	1.08	0.77
TOX high mobility group box family member 4	TOX4	NM_023434	Increased	0.31	-0.02	1.95
chemokine (C-X-C motif) ligand 3	CXCL3	NM_203320	Increased	0.40	1.41	0.07
lysyl oxidase	LOX	NM_010728	Increased	0.41	-1.05	-0.29
c-fos induced growth factor	FIGF	NM_010216	Increased	0.42	-1.21	-0.36
syndecan binding protein	SDCBP	AK014678	Increased	0.60	-0.06	1.11
leukotriene B4 receptor 2	LTB4R2	NM_020490	Increased	0.74	-0.69	1.29
CD151 antigen	CD151	NM_009842	Increased	1.03	0.13	0.21
inositol hexaphosphate kinase 2	IP6K2	NM_029634	Increased	1.05	-0.15	0.04
chemokine (C-X-C motif) ligand 5	CXCL5	NM_009141	Increased	1.07	0.32	0.04
S100 calcium binding protein A4	S100A4	NM_011311	Increased	1.13	0.38	0.33
bone morphogenetic protein 7	BMP7	NM_007557	Increased	2.34	-0.14	0.54

Table 7.4. Expression change of genes that enhance metastasis in tumour bulk harvested at 1300 mm^3.

Gene ID	Gene symbol	GeneBank accession no.	Effect of metastasis	Non-responsive vs. Untreated W	Responsive vs. Untreated W	Non-responsive vs. Responsive W
zinc finger E-box binding homeobox 1	ZEB1	NM_011546	Increased	-1.33	-0.40	-0.90
leukotriene B4 receptor 2	LTB4R2	NM_020490	Increased	-1.01	1.29	-2.04
insulin-like growth factor 1	IGF1	NM_010512	Increased	-0.74	0.10	-1.62
bone morphogenetic protein 2	BMP2	NM_007553	Increased	-0.02	-1.05	0.91
TOX high mobility group box family member 4	TOX4	NM_023434	Increased	-0.02	1.95	-3.94
cadherin 2	CDH2	NM_007664	Increased	0.05	0.29	-1.01
neurotrophic tyrosine kinase, receptor, type 2	NTRK2	NM_001025074	Increased	0.35	0.64	-1.74
syndecan binding protein	SDCBP	AK014678	Increased	0.77	1.11	-0.51
netrin 1	NTN1	NM_008744	Increased	1.01	0.30	0.52
CD44 antigen	CD44	NM_009851	Increased	1.02	0.17	-0.35
Notch gene homolog 1 (Drosophila)	NOTCH1	NM_008714	Increased	1.16	0.75	0.40
ubiquitin D	UBD	NM_023137	Increased	1.23	0.04	1.17
melanoma cell adhesion molecule	MCAM	NM_023061	Increased	1.27	-0.05	0.31
chemokine (C-X-C motif) ligand 5	CXCL5	NM_009141	Increased	1.55	0.04	1.52

7.2.2.4 Comparative analysis of genes associated with endothelial migration

One of the major targets of sunitinib therapy is angiogenesis. In order to explore the effect sunitinib treatment had on pro-angiogenic gene expression over the course of the experiment, a list of genes known to enhance endothelial migration (a key component of angiogenesis) was compiled from the Ingenuity online database, and their expression investigated in each of the comparison matrices used previously. At day 9 pro-angiogenic signalling was primarily inhibited in the responsive group versus the untreated group, with the majority of >2 fold altered genes being down-regulated at this stage, presumably in response to sunitinib angiogenesis inhibition (Table 7.5). This pattern of inhibition was lost at later time points, with even a few pro-angiogenic genes showing enhanced expression in the treated group. However, there was no obvious pattern of angiogenic signalling maintained between tumours harvested at 600 and 1300 mm^3. This data is in agreement with the observed vascularisation patterns reported in chapter 6 for the responsive cohort, with a greater level of vascularization signalled for by pro-angiogenic gene expression at later time points. At 1300 mm^3 genes stimulatory to endothelial migration were both up and down-regulated in the endothelium of non-responsive tumours, versus the untreated cohort (Table 7.6). This suggests that despite the observed similarity in tumour growth and vascularisation between the groups, the methods of vascularisation could be quite distinct. This observation suggests that despite sensitivity to sunitinib signalling inhibition potentially being maintained, as reported in Table 7.2, the use of alternative angiogenic pathways permits the continued growth and vascularisation of this cohort. The responsive group on the other-hand displayed an endothelial expression pattern primarily stimulatory to endothelial migration with the expression of pro-angiogenic

molecules, such as endothelial cell specific adhesion molecule (ESAM), endothelin 1 (EDN1) and pleiotrophin (PTN) enhanced versus the untreated group. The same pattern was observed when comparing expression profiles with the non-responsive cohort. Endothelial migration signalling appears to be enhanced in the responsive group at the 1300 mm^3, beyond that found in the other cohorts, but not via the same alternative pathways utilised by the non-responsive group.

Table 7.5. Expression change of genes that enhance endothelial migration in tumour bulk harvested at each time-point.

Gene ID	Gene symbol	GeneBank accession no.	Effect on endothelial migration	Responsive vs. Untreated 9 days	Responsive vs. Untreated 600 mm^3	Responsive vs. Untreated 1300 mm^3
tenascin N	TNN	NM_177839	Increased	-3.45	-0.42	-0.14
bone morphogenetic protein 2	BMP2	NM_007553	Increased	-3.30	-0.45	-1.05
matrix metallopeptidase 13	MMP13	NM_008607	Increased	-2.90	1.24	-0.75
wingless-related MMTV integration site 5A	WNT5A	NM_009524	Increased	-2.86	-0.36	0.17
endothelial cell-specific adhesion molecule	ESAM	NM_027102	Increased	-2.62	-0.29	-1.08
integrin alpha 9	ITGA9	NM_133721	Increased	-2.33	0.20	-0.47
EGF-like domain 7	EGFL7	NM_178444	Increased	-2.00	-0.38	-0.42
elastin	ELN	NM_007925	Increased	-1.65	-1.04	-0.15
growth arrest specific 6	GAS6	NM_019521	Increased	-1.64	-0.75	0.12
phosphoinositide-3-kinase, catalytic, gamma	PIK3CG	NM_020272	Increased	-1.63	-0.46	-0.34
tumor necrosis factor (ligand) superfamily, 10	TNFSF10	NM_009425	Increased	-1.62	1.01	-0.03
tachykinin 1	TAC1	NM_009311	Increased	-1.60	0.35	0.01
insulin-like growth factor binding protein 3	IGFBP3	NM_008343	Increased	-1.59	-0.79	-0.43
Rac/Cdc42 guanine nucleotide exchange factor 6	ARHGEF6	NM_152801	Increased	-1.52	-0.08	0.18
sphingosine-1-phosphate receptor 3	S1PR3	NM_010101	Increased	-1.50	-1.03	0.16
sphingosine-1-phosphate receptor 1	S1PR1	NM_007901	Increased	-1.44	-0.70	-0.96
endothelial-specific receptor tyrosine kinase	TEK	NM_013690	Increased	-1.42	-0.45	-0.38
nitric oxide synthase 3, endothelial cell	NOS3	NM_008713	Increased	-1.34	-0.32	-0.24
heparanase	HPSE	NM_152803	Increased	-1.30	-0.18	-0.21
chemokine (C-C motif) ligand 5	CCL5	NM_013653	Increased	-1.25	-0.15	0.43
phosphodiesterase 2A, cGMP-stimulated	PDE2A	NM_001143848	Increased	-1.21	-0.77	-0.62
protein kinase D1	PRKD1	NM_008858	Increased	-1.13	-0.07	-0.51
GATA binding protein 1	GATA1	NM_008089	Increased	-0.82	-1.45	-0.60
pleiotrophin	PTN	NM_008973	Increased	-0.34	-0.15	3.23
matrix metallopeptidase 2	MMP2	NM_008610	Increased	-0.29	-1.14	-0.40
chemokine (C-X-C motif) ligand 1	CXCL1	NM_008176	Increased	0.25	1.08	0.77
teratocarcinoma-derived growth factor 1	TDGF1	NM_011562	Increased	0.30	0.56	1.03
lysyl oxidase	LOX	NM_010728	Increased	0.41	-1.05	-0.29
c-fos induced growth factor	FIGF	NM_010216	Increased	0.42	-1.21	-0.36
gastrin releasing peptide	GRP	NM_175012	Increased	0.49	0.47	-2.22
syndecan 4	SDC4	NM_011521	Increased	0.73	-0.55	1.01
adrenomedullin	ADM	NM_009627	Increased	0.78	-1.31	0.10
CD151 antigen	CD151	NM_009842	Increased	1.03	0.13	0.21
angiopoietin 1	ANGPT1	NM_009640	Increased	1.77	0.15	-0.19
colony stimulating factor 2	CSF2	NM_009969	Increased	1.80	0.28	0.06
kininogen 1	KNG1	NM_001102411	Increased	2.58	-0.08	-0.09
calcitonin/calcitonin-related polypeptide, alpha	CALCA	NM_001033954	Increased	2.73	-0.08	0.67

Table 7.6. Expression change of genes that enhance endothelial migration in EC isolates from tumours harvested at 1300 mm^3.

Gene ID	Gene symbol	GeneBank accession no.	Effect on endothelial migration	Non-responsive vs. Untreated EC	Responsive vs. Untreated EC	Non-responsive vs. Responsive EC
leptin	LEP	NM_008493	Increased	-2.24	-0.11	-2.08
interleukin 17A	IL17A	NM_010552	Increased	-1.91	-0.54	-1.29
colony stimulating factor 2	CSF2	NM_009969	Increased	-1.53	-0.90	-0.56
prostaglandin-endoperoxide synthase 2	PTGS2	NM_011198	Increased	-1.42	-0.46	-0.97
chemokine (C-X-C motif) ligand 1	CXCL1	NM_008176	Increased	-1.31	-0.39	-0.91
sphingosine-1-phosphate receptor 3	S1PR3	NM_010101	Increased	-1.31	0.10	-1.41
hyaluronan synthase 3	HAS3	NM_008217	Increased	-1.16	0.04	-1.16
GATA binding protein 1	GATA1	NM_008089	Increased	-1.14	-0.78	-0.31
elastin	ELN	NM_007925	Increased	-1.07	0.02	-1.07
thrombomodulin	THBD	NM_009378	Increased	-0.79	0.68	-1.49
protein tyrosine phosphatase 4a3	PTP4A3	NM_008975	Increased	-0.78	0.22	-1.00
SH2 domain protein 2A	SH2D2A	NM_021309	Increased	-0.76	0.02	-1.96
bone morphogenetic protein 6	BMP6	NM_007556	Increased	-0.70	0.49	-1.12
phosphodiesterase 2A, cGMP-stimulated	PDE2A	NM_001143848	Increased	-0.64	0.52	-1.15
placental growth factor	PGF	NM_008827	Increased	-0.61	0.39	-1.01
homeobox A9	HOXA9	NM_010456	Increased	-0.44	0.05	-1.44
secreted acidic cysteine rich glycoprotein	SPARC	NM_009242	Increased	-0.38	0.57	-1.60
endothelial cell-specific adhesion molecule	ESAM	NM_027102	Increased	-0.35	1.07	-1.45
endothelial-specific receptor tyrosine kinase	TEK	NM_013690	Increased	-0.26	0.81	-1.14
nitric oxide synthase 3, endothelial cell	NOS3	NM_008713	Increased	-0.22	0.78	-1.11
pleckstrin homology domain containing, G5	PLEKHG5	NM_001004156	Increased	-0.07	0.51	-1.27
chemokine (C-X-C motif) ligand 12	CXCL12	NM_001012477	Increased	0.05	0.86	-2.14
phospholipase C, gamma 1	PLCG1	AK169695	Increased	0.06	0.15	-1.05
endothelin 1	EDN1	NM_010104	Increased	0.07	1.02	-1.00
5-hydroxytryptamine (serotonin) receptor 6	HTR6	NM_021358	Increased	0.14	0.18	-1.21
insulin-like growth factor binding protein 3	IGFBP3	NM_008343	Increased	0.21	0.57	-1.60
BMX non-receptor tyrosine kinase	BMX	NM_009759	Increased	0.47	0.24	-1.47
gastrin releasing peptide	GRP	NM_175012	Increased	0.49	-0.73	1.05
melanoma cell adhesion molecule	MCAM	NM_023061	Increased	0.87	0.69	-1.08
insulin-like growth factor 1	IGF1	NM_010512	Increased	0.89	0.15	-1.87
mechanistic target of rapamycin	MTOR	NM_020009	Increased	1.03	0.18	-0.01
arachidonate 12-lipoxygenase	ALOX12	NM_007440	Increased	1.06	0.63	-0.15
nuclear factor of activated T cells C3	NFATC3	NM_010901	Increased	1.12	-0.11	0.06
integrin alpha 4	ITGA4	NM_010576	Increased	1.12	-0.07	-0.05
5-hydroxytryptamine (serotonin) receptor 7	HTR7	FM178516	Increased	1.15	0.28	0.22
tenascin N	TNN	NM_177839	Increased	1.17	0.32	0.88
activating transcription factor 2	ATF2	NM_001025093	Increased	1.18	0.03	0.01
heparanase	HPSE	NM_152803	Increased	1.19	0.43	0.74
pleiotrophin	PTN	NM_008973	Increased	1.19	1.54	-0.45
collagen and calcium binding EGF domains 1	CCBE1	NM_178793	Increased	1.22	-0.09	0.25
inhibitor of DNA binding 1	ID1	NM_010495	Increased	1.28	0.67	0.58
teratocarcinoma-derived growth factor 1	TDGF1	NM_011562	Increased	1.89	0.05	-0.13

7.2.3 The selection and validation of acquired resistance markers

In order to investigate and validate this observed up-regulation of sunitinib targeted pathways and angiogenesis in general, in the vessels of the initially responsive cohort, after resistance has been acquired, a matrix comparing responsive tumour endothelium to untreated tumour endothelium was set up. This analysis identified a strikingly large number of angiogenic genes >2 fold up-regulated in the responsive group, such as the prolactin receptor (PRLR), aquaporin 1 (AQP1), angiopoietin 2 (ANGPT2), the duffy blood group receptor (DARC), multimerin 2 (MMRN2) among others (Table 7.7). Interestingly the RET proto-oncogene and VEGF receptor 2, targets of sunitinib inhibition were also both up-regulated in the responsive group, possibly suggesting a mechanism of resistance by the up-regulation of the target genes (Table 7.7).

Table 7.7. Genes significantly enriched in the endothelial isolates from responsive vs. untreated tumours harvested at 1300 mm^3.

Gene ID	Gene Symbol	GeneBank accession no.	Fold change	P-value
Prolactin receptor	PRLR	NM_011169	4.32	0.01
Pleiotrophin	PTN	NM_008973	2.91	0.01
Aquaporin 1	AQP1	NM_007472	2.76	0.00
Ret proto-oncogene	RET	NM_001080780	2.40	0.00
Angiopoietin 2	ANGPT2	NM_007426	2.34	0.00
Duffy blood group, chemokine receptor	DARC	NM_010045	2.30	0.01
Leptin receptor	LEPR	NM_001122899	2.30	0.00
Endothelial cell surface expressed chemotaxis regulator	ECSCR	NM_001033141	2.25	0.00
Tetraspanin 7	TSPAN7	NM_019634	2.25	0.00
Stanniocalcin 2	STC2	NM_011491	2.12	0.00
Endothelial cell-specific adhesion molecule	ESAM	NM_027102	2.10	0.00
Multimerin 2	MMRN2	NM_153127	2.06	0.00
Kinase insert domain protein receptor	KDR (VEGFR2)	NM_010612	2.06	0.00
Endothelin 1	EDN1	NM_010104	2.03	0.00

In order to validate the differential expression of the 14 candidate genes arising from the microarray analysis (Table 7.7), RTqPCR analysis comparing the expression level of each of these genes between responsive EC and untreated EC, used for the microarray analysis, was performed (Table 7.8). Genes of interest warranting further investigation must be suitably enriched in the responsive cohort compared to the untreated cohort EC, as well as being sufficiently expressed to realistically have an impact of cellular behaviour. Candidate selection was therefore based on fold expression change, normalised to β-actin (per cell level) and PECAM-1 (per endothelial cell level), as well as on gene expression level relative to β-actin. Genes identified by RTqPCR analysis, with a fold enrichment of >3 times and expressed at >5% of the expression level of β-actin, were taken forward (Table 7.8). This left ANGPT2, AQP1, DARC, MMRN2, PRLR and VEGFR2, as the key genes of interest for further investigation.

Table 7.8. Selection of genes of interest for further analysis by RTqPCR, in EC isolates from responsive vs. untreated tumours, harvested at 1300 mm^3 (n=4). Selected genes (green) exhibit >3 fold enrichment in responsive tumours standardised to both β-actin and PECAM and have > 5% of the expression of β-actin. Rejected genes, highlighted red.

Identified targets	β-actin vs. target fold expression change	PECAM vs. target fold expression change	Expression level relative to β-actin (%)	Selected genes
ANGPT2	5.75	3.57	41.39	ANGPT2
AQP1	4.93	4.19	240.42	AQP1
DARC	6.79	5.66	30.83	DARC
ECSCR	1.86	1.70	0.89	
EDN 1	3.04	2.41	1.98	
ESAM	2.49	1.74	10.33	
LEPR	5.44	3.75	2.26	
MMRN2	3.23	2.59	11.58	MMRN2
PRLR	9.81	10.20	5.23	PRLR
PTN	2.25	2.72	0.01	
RET	9.02	7.85	0.27	
STC2	27.22	18.02	0.04	
TSPAN7	0.50	0.64	0.03	
VEGFR2	4.69	3.49	11.65	VEGFR2

7.2.4 Expression changes of candidate markers of acquired resistance over time

In order to investigate the expression of the candidate genes at key stages of tumour development, in the full set of isolates of different cohorts, RTqPCR was performed on endothelial isolates from day 9, 600 mm^3 and 1300 mm^3, in the responsive, non-responsive and untreated cohorts (Figure 7.3). This analysis revealed a significant shift in the expression of all the candidate genes, except for PRLR, between the responsive and untreated tumour endothelium at 1300 mm^3. Aquaporin-1 alone however, had an additional significant shift in expression between the responsive and non-responsive cohorts at 1300 mm^3, marking it out as a key distinguishing gene, enriched in the responsive cohort alone, at this time point. Interestingly the expression of each of the candidate genes is only significantly up-regulated in the responsive cohort at the 1300 mm^3 stage, suggesting a distinct change has occurred in the tumour vessel transcriptome at this stage compared to other stages.

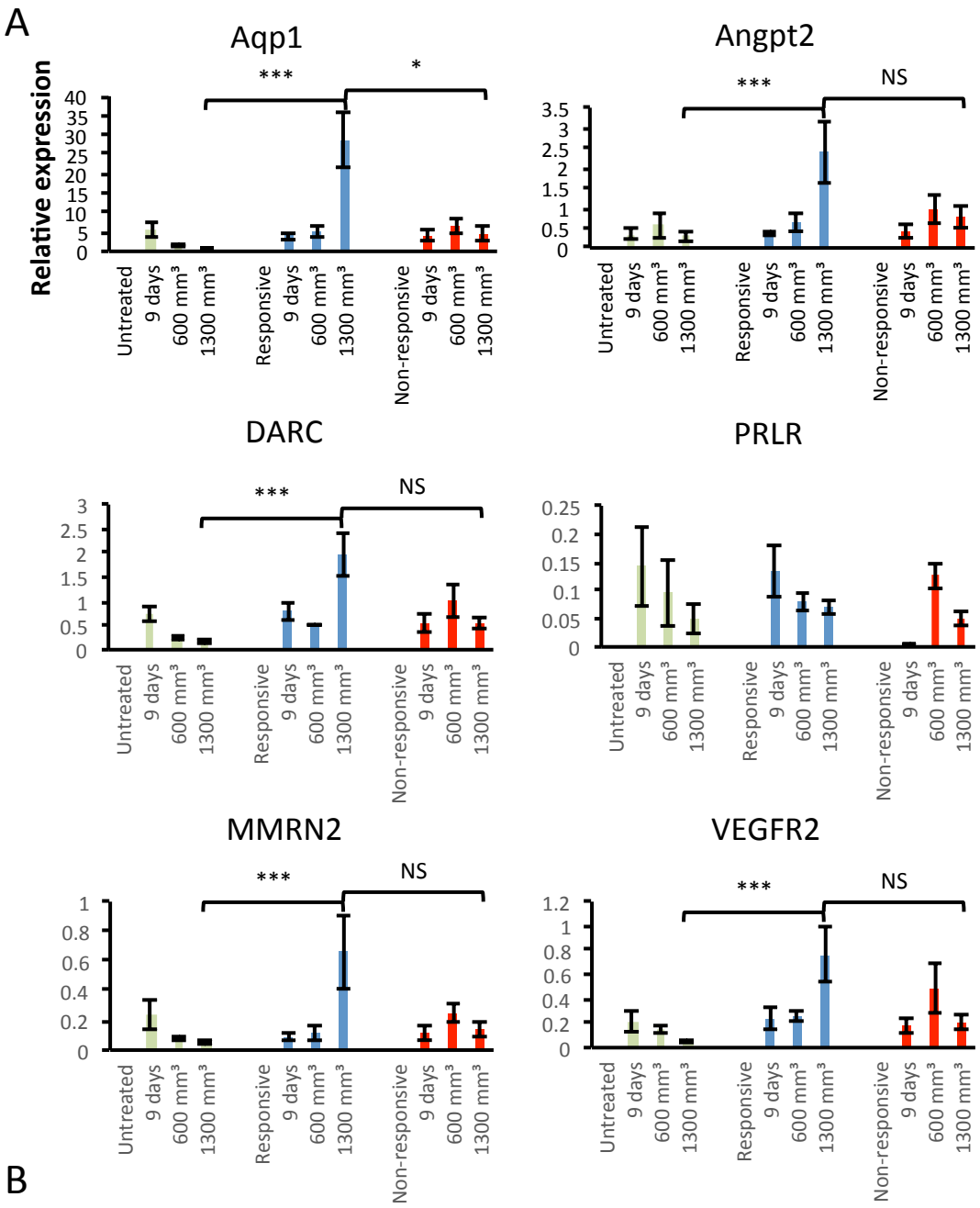

B

	Responsive	Non-responsive	Untreated
Day 9	5	5	10
600 mm^3	4	6	10
1300 mm^3	13	7	18

Figure 7.3. Aquaporin is significantly enriched in the vessels of responsive tumours over those of untreated and non-responsive tumours. A, RTqPCR for the relative expression of the six genes of interest in endothelial isolates from untreated, responsive and non-responsive tumours harvested at 9 days, 600 mm^3 and 1300 mm^3 (mean expression ±SEM, *** $p<0.001$, * $p<0.05$, NS – Not Significant, Mann-Whitney). B, N-numbers for each group used in the analysis.

7.2.5 Validation of aquaporin on the protein level

In order to further validate aquaporin as a specific marker of acquired resistance on the protein level, immunohistochemistry and immunofluorescence was conducted, comparing marker expression in sections cut from responsive, non-responsive and untreated cohort tumours, harvested at day 9, 600 mm^3 and 1300 mm^3. The analysis compared the optical density of marker fluorescence (green channel), normalised to the PECAM-1 fluorescence (red channel), between the groups of tumour samples. In this way it was confirmed that AQP1 was enriched in the vessels of responsive tumours specifically at the 1300 mm^3 stage (Figure 7.4).

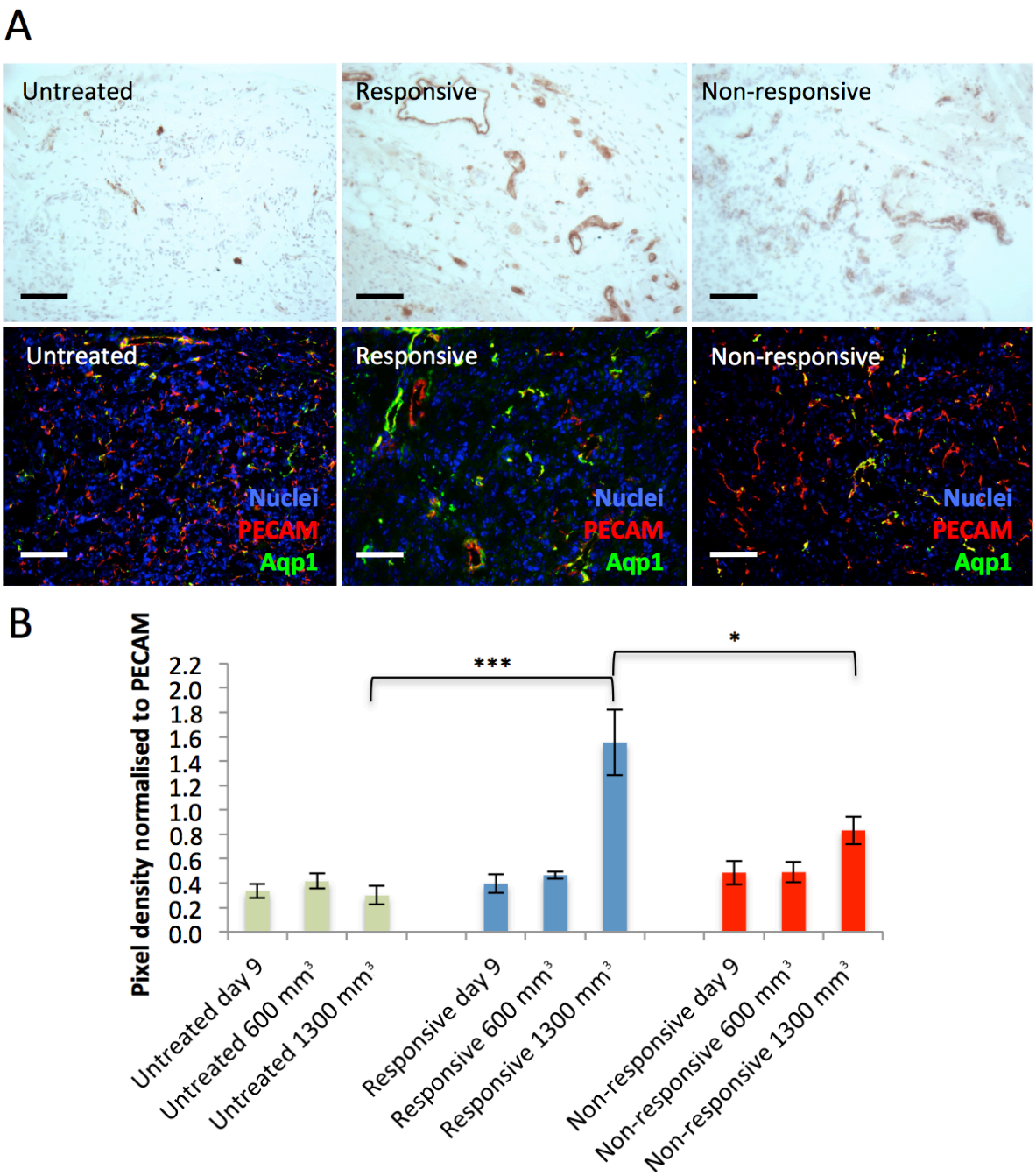

Figure 7.4. Aquaporin is significantly enriched in the vessels of responsive tumours over those of untreated and non-responsive tumours on the protein level. A, representative images of AQP1 staining in untreated, responsive and non-responsive tumours by IHC and IF. Tumours triple stained by IF for DAPI (nuclei, blue), PECAM-1 (vessels, red) and AQP1 (green). B, quantitation of pixel density of staining by IF for AQP1 standardised to PECAM-1 staining (mean ± SEM, *** $p<0.001$, * $p<0.05$, Mann-Whitney, n-numbers [see Figure 7.3B], 6 fields of view each)

7.3 Discussion

A key requirement in the drive to improve the use of antiangiogenic therapies is to understand the processes by which drug resistance is acquired. This chapter presents data from an exploration of the processes, used by two groups of sunitinib treated tumours, showing distinct resistance profiles. In tumours that showed initial growth retardation in response to treatment, signalling within the tumour was altered during the sensitive period, in a manner closely matching that predicted of sunitinib treatment. Sunitinib target or responsive genes were inhibited and both metastatic and angiogenic signalling reduced, relative to untreated tumours. After this period of roughly 9 days, the tumours started to grow at a rate roughly matching that of the untreated cohort and at this point signalling changed. The inhibition of the VEGF, PDGF and FLT-3 pathways was lost and both endothelial migration and metastasis signalling was progressively enhanced. This profile was suggestive of an acquired loss of sensitivity to sunitinib therapy after day 9, in both tumour growth rate and signalling. In tumours that didn't show sensitivity to sunitinib therapy in terms of growth rate from the outset, this effect was not observed. Even at the latest size-point, 1300 mm^3, the tumours still appeared to be sensitive to sunitinib therapy. Sunitinib target genes were still inhibited, however, metastasis and endothelial migration signalling in general was not. This suggests that this cohort of tumours utilised a separate, uninhibited mechanism for continued tumour growth and metastasis and therefore had an innate resistance to sunitinib therapy. Intriguingly direct transcriptomic comparisons of the initially responsive and non-responsive cohorts, revealed that the acquired resistance of the responsive group was not gained via the same mechanism by which the non-responsive tumours

achieved innate resistance, but rather by a separate mechanism that involved the up-regulation of a number pro-angiogenic genes in the endothelium. Some of these genes are known to be targeted by sunitinib for inhibition. Further analysis of this phenomenon revealed that the up-regulation of aquaporin 1 was characteristic of tumours displaying acquired resistance.

7.3.1 Innate resistance

Innate resistance to antiangiogenic therapies, has been suggested to occur due to the development of tumour dependence on uninhibited mechanisms of growth and vascularisation. This is thought not to be in response to therapy, but due to incidental selective pressures exerted by the tumour microenvironment (149). This appears to be broadly what has occurred in the non-responsive group. Transcriptomic profiling of non-responsive versus untreated endothelium at 1300 mm^3 suggested that a quite distinct method of angiogenesis was favored in each group.

The expression of nine pro-angiogenic genes were at least 2 fold enhanced in the untreated cohort, including leptin (LEP), the reduction of which, significantly correlates with response to sunitinib in RCC and prostate cancer (292,293), chemokine ligand-1 (CXCL1), the release of which is induced by VEGF signalling (294) and S1P receptor 3, an endothelial mitogen receptor that operates synergistically with PDGFR-β and is known to be down-regulated by sunitinib treatment in breast cancer (295). This profile is suggestive of active sunitinib inhibition in the non-responsive tumours.

The expression of twelve other proangiogenic genes however, was enhanced in the non-responsive tumours, including pleiotrophin (PTN), an angiogenic cytokine, highly

expressed in 60% of breast cancers (296). Additionally the expression of PTN has been shown to be specifically enhanced in response to VEGF signalling blockade, in three separate pre-clinical tumour models (296), suggesting that it may form part of an adaptive response to VEGF targeted therapies. Intriguingly PTN is additionally up-regulated in the vessels of initially responsive tumours at 1300 mm^3. This suggests that PTN may be playing an important role in mediating the evasion of sunitinib angiogenic blockade in both cohorts, either as an acquired resistance mechanism in the responsive group, or an innate one in the non-responsive group. However, the analyses detailed in this chapter did not show PTN to be highly expressed in the 4T1 tumours. Despite this, the role of PTN in breast cancer resistance to sunitinib warrants further investigation. Mechanistic target of rapamycin (mTOR), a pro-angiogenic protein kinase, whose phosphorylation is known to be inhibited by sunitinib (297), is also up-regulated in the non-responsive cohort. MTOR is known to enhance pro-angiogenic hypoxia inducible factor (HIF) signalling (298) and therefore may also be playing a role in mediating sunitinib resistance. This result suggests that sunitinib treatment of breast cancer could be improved by co-treatment with mTOR inhibitors, temsirolimus and everolimus.

This expression data suggests that despite sunitinib targeted genes being inhibited in the non-responsive cohort, angiogenesis and tumour growth was maintained by the up-regulation of alternative pathways to angiogenesis. This rendered the tumour innately resistant to sunitinib induced angiogenic blockade.

7.3.2 Acquired resistance

Whereas innately resistant tumours appeared to display a distinct angiogenic expression profile, leading to insensitivity to sunitinib treatment, tumours that displayed acquired resistance in this investigation, instead showed initial responsiveness, characterised by the inhibition of key sunitinib targeted pathways, followed by a gradual reversal of this inhibition. As discussed this resulted not in a transition to the alternate angiogenic profile of the non-responsive cohort, but rather a loss of sensitivity in the targeted pathways to sunitinib blockade, leading to constitutive activation. This resulted in this cohort developing an expression profile progressively more similar to the untreated cohort. This finding is not without precedent, Sakai *et al*., 2013 (299) generated a sunitinib resistant RCC cell line, through prolonged treatment with sunitinib. They found that the cells acquired resistance via the constitutive activation of target signal transduction pathways. It is plausible that this phenomenon is due to mutations in the target pathways, leaving them immune to sunitinib inhibition. This offers a survival benefit to the cells affected and is propagated throughout the tumour. This mechanism of acquired resistance has been observed in gastrointestinal tumours treated with sunitinib, but only after approximately a year of response (300). It is unlikely however that 9 days is sufficient for tumours to have acquired such mutations.

The loss of sunitinib signalling sensitivity was coupled in the tumour with the up-regulation of a number of pro-angiogenic genes. RTqPCR, IHC and IF validation of this profile, identified AQP1, ANGPT2, DARC, MMRN2 and VEGFR2, to be significantly up-

regulated at 1300 mm^3, in the responsive cohort alone and enhanced AQP1 expression to be a distinct marker of acquired resistance in this experiment.

7.3.3 AQP1 in acquired resistance to sunitinib

AQP1 is a widely expressed cell surface water channel, important for water transfer in the kidney (301), but with a key function in many cells including endothelium, allowing the rapid transit of water across the plasma membrane, facilitating the increase in cellular volume critical for cell proliferation (302). The up-regulation of AQP1 has been reported in murine kidney tumours after acquired resistance to sunitinib therapy (303) as well as in instances of pathological neovascularisation accompanying liver cirrhosis (304). AQP1 has also been reported to be involved in fibroblast growth factor FGF induced endothelial invasion (304). This could potentially implicate AQP1 expression as a surrogate marker of enhanced FGF signalling, in resistant tumour vessels. FGF is a pro-angiogenic growth factor, the signalling of which is not inhibited by sunitinib therapy and has been implicated in antiangiogenic resistance (156). If FGF signalling were active in the resistant tumours it would suggest that the initially responsive cohort acquired resistance not just via constitutive activation of target pathways, but also via the up-regulation of alternative angiogenic pathways. The expression of AQP1 in human breast tumours receiving sunitinib therapy, warrants investigation to determine whether it is a novel marker of acquired anti-angiogenic resistance.

Chapter Eight

Concluding Remarks

This thesis has detailed the transcriptomic analysis of the tumour vascular expression profile of colorectal and renal cancers and colorectal metastases to the liver. This has resulted in the identification of two potential tumour vascular targets, MCAM and GRIN2D, and three potential, tumour type specific, prognostic markers, MCAM, LAMA4 and GRIN2D. With further work, these markers could be used to develop both ligand-targeted therapies and diagnostic tests.

In addition the behaviour of breast tumours displaying acquired and innate resistance to the anti-angiogenic therapy, sunitinib, was investigated and revealed that innately resistant tumours display enhanced metastasis when treated with sunitinib, highlighting the need for reliable markers of resistance. Transcriptomic analysis of the tumour and vascular expression profiles in these cancers, identified a number of potential markers of resistance including PTN, mTOR, and AQP1. The validation of these markers is at an early stage, but with further investigation they could be used diagnostically to guide therapy selection and therapeutically to circumvent resistance to sunitinib in breast cancer.

Besides these key findings that will hopefully contribute to cancer treatment and prognostication in the future, other results contained within this thesis also contribute to the understanding of cancer and how vascular-targeted therapies might be used. The tumour vasculature is a highly promising target for anti-cancer therapy, given its key role in tumour development. It is also a difficult target however. It is a non-cancerous component of the tumour, which was initially seen as an advantage, suggesting it would be less adaptive than the tumour cells (8). This has been found to not be the case however. These “normal” cells are distorted structurally, behaviourally and in terms of

their expression profile by the extreme environment, of hypoxia, hypoglycaemia, acidity and a multitude of other factors encountered in the tumour. Analysis of the pan-tumour endothelial expression profile, described in chapter 5, demonstrates this effect well. A spectrum of different factors are thought to transcriptionally regulate the genes identified in this analysis. Cytokine signalling from infiltrating immune cells appears to be responsible for the up-regulation of many of the identified genes. ANGPT2 has been shown to be induced by tumour necrosis factor alpha (TNF-α) (305); ESM1 by TNF-α and interleukin 1 beta (IL1-β) (306); FSTL1 by IL1-β (307); CCL20 by TNF and interferon-gamma (IFN-γ) (308); TGM2 by IFN-γ (309) and BGN, SPARC and VIM by transforming growth factor beta (TGF-β) (310-312). In addition the activation of hypoxia inducible factors (HIFs) have been shown to regulate both LOX and RGS5 expression (313,314). Interestingly RGS5 itself regulates the expression of the thrombin receptor F2R (also known as PAR-1) (315), another gene consistently up-regulated within the analysis. This suggests that F2R may be up-regulated in this setting as a downstream result of hypoxia induced RGS5 activation. Activation by tumour-derived growth factors is also thought to be a key regulator of tumour endothelial markers (TEMs) and indeed as discussed in chapter 5, MCAM expression is regulated by VEGF.

It is not only the intrinsic tumour environment that impacts on this expression profile, but also the changes induced by therapeutic intervention. As described in chapter 7, the vasculature of different groups of breast tumours, challenged by sunitinib angiogenic blockade, respond in quite distinct manners. Some are inhibited, but acquire resistance through a loss of sensitivity to treatment blockade over time. This is possibly induced

by a crisis point being reached within the tumour where it can't develop sufficient vessels to grow, one or a group of endothelial cells adapt to the therapy, are selectively favoured and vascularise the tumour. Some other tumours do not respond to the blockade at all, have intrinsically developed a dependence of non-blockaded pathways to growth and therefore have not gone through any crisis or selection and so still show signs of sensitivity to sunitinib blockade.

This data highlights the vasculature as an extremely heterogeneous and adaptive compartment of the tumour. To achieve treatment efficacy considerable work is required to find the optimal indication for a therapy. As was shown in chapter 5, MCAM is highly expressed in the vessels of clear cell RCC, but to a far lesser extent in other renal malignancies, or even other architectures of RCC. GRIN2D also appears to be expressed to the greatest extent in colorectal and stomach cancers, but even then only in 40% of cases. Only 62% of breast tumours examined in chapter 6 responded to sunitinib therapy and response has been reported to be even lower in the clinic (276,278). These findings all suggest that research should be focused on developing new therapies, optimal in different indications, but also marrying these and existing therapies with diagnostic tests that can reliably predict response.

The investigation of the survival impact of TEMs identified in this thesis, illustrated another interesting aspect of tumour vessel behavior. Namely the existence of TEMs predictive of more or less aggressive tumours. High expression of MCAM and LAMA4 on ccRCC tumour vessels is very strongly predictive of poor survival, more advanced and aggressive tumours and enhanced metastasis. On the other hand GRIN2D

expression on the vessels CRC was associated with enhanced survival. This dichotomy can be explained by the differing functions of the TEMs involved, as discussed in chapters 4 and 5. Briefly, MCAM is an adhesion molecule known to promote endothelial cell motility and tumour vessel invasion (251), but also reported to be expressed on some tumour cells, therefore its expression on vessels could promote extravasation, leading to enhanced metastasis. LAMA4, besides potentially operating synergistically with MCAM, has also been reported to promote tumour cell invasion via the interaction with various integrins. GRIN2D, on the other hand, is a dedicated ion channel and glutamate receptor, which as reported in this thesis, is involved in functional vessel formation *in vitro*. Its expression could therefore be a marker of more functional vessel formation, enhancing tumour perfusion and chemotherapy infiltration, as reported for ROBO4-Slit2 signalling (231).

CLEC14a, a tumour vessel associated adhesion molecule, reported to mediate endothelial cell attachment to the extracellular matrix via multimerin-2 in a manner akin to MCAM and LAMA4 (316), is reported to enhance survival in non-small-cell lung cancer (230), for an as yet undetermined reason. This suggests that it will be no simple matter to dissect pro- and anti-survival TEMs into groups. The impact of a TEM on survival is an important determination to make however, from a therapeutic point of view, as well as prognostic. Tumour vascular targeting has the potential to achieve rapid tumour regression, however, given the adaptive and heterogeneous nature of the tumour vasculature, this may result in the selection and revascularisation of the tumour with vessels not expressing the target. In the case of an anti-survival target, this could result in a down-staged tumour optimised for further treatment, a hope for

MCAM targeted therapies. If targeting a pro-survival marker however, the treatment could result in a tumour with decreased perfusion, or other factors not conducive to survival, depending on the nature of the target, which could reduce the therapeutic's operational synergy with other anti-cancer treatments. Given that cancer vessel targeted agents cannot themselves destroy the tumour, the productive combination of these therapeutics with cancer-cell-targeted agents is critical for success [reviewed in (1)].

This thesis describes the identification of vascular markers of potential use in cancer treatment, prognostication and prediction of therapy resistance, but there is much work still to do to realise the optimal utility of these findings.

Appendix

Wragg et al., publications

Used as a basis for Chapter One, General Introduction:

Chapter 3
Vascular Targeting Approaches to Treat Cancer

Joseph W. Wragg and Roy Bicknell

ELSEVIER

Available online at www.sciencedirect.com

ScienceDirect

EJSO 40 (2014) 133–136

EJSO the Journal of Cancer Surgery

www.ejso.com

For debate

Vaccination against tumour blood vessels in colorectal cancer

H.J.M. Ferguson [a,b,*], J. Wragg [a], T. Ismail [b], R. Bicknell, Prof.[a]

[a] *School of Immunity and Infection and Cancer Studies, Institute for Biomedical Research, College of Medical and Dental Sciences, University of Birmingham, Edgbaston, Birmingham B15 2TT, UK*

[b] *Department of Colorectal Surgery, Queen Elizabeth Hospital, Mindelsohn Way, Birmingham B15 2TH, UK*

Accepted 25 November 2013

Available online 13 December 2013

Microcirculation
The Official Journal of the Microcirculatory Society, Inc., the British Microcirculation Society, and the Australia & New Zealand Microcirculation Society

DOI:10.1111/micc.12119

Invited Review

Shear Stress Regulated Gene Expression and Angiogenesis in Vascular Endothelium

JOSEPH W. WRAGG,* SARAH DURANT,* HELEN M. MCGETTRICK,† KLARKE M. SAMPLE,* STUART EGGINTON,‡ AND ROY BICKNELL*

*Angiogenesis Group, Centre for Cardiovascular Sciences, Institute for Biomedical Research, Schools of Immunity and Infection and Cancer Sciences, College of Medical and Dental Sciences, University of Birmingham, Birmingham, UK; †Centre for Cardiovascular Sciences, Institute for Biomedical Research, Schools of Immunity and Infection and Cancer Sciences, College of Medical and Dental Sciences, University of Birmingham, Birmingham, UK; ‡School of Biomedical Sciences, Faculty of Biological Sciences, University of Leeds, Leeds, UK
Address for correspondence: Roy Bicknell, Angiogenesis Group, Centre for Cardiovascular Sciences, Institute for Biomedical Research, Schools of Immunity and Infection and Cancer Sciences, College of Medical and Dental Sciences, University of Birmingham, Birmingham, UK.
E-mail: r.bicknell@bham.ac.uk

Received 6 December 2013; accepted 22 January 2014.

NEXT GENERATION SEQUENCING

Next-generation transcriptomic analysis in cancer vascular research

Joseph W. Wragg and Roy Bicknell
University of Birmingham

Therapeutics, Targets, and Chemical Biology

Cancer Research

MCAM and LAMA4 Are Highly Enriched in Tumor Blood Vessels of Renal Cell Carcinoma and Predict Patient Outcome

Joseph W. Wragg[1], Jonathan P. Finnity[1], Jane A. Anderson[2], Henry J.M. Ferguson[1], Emilio Porfiri[2,3], Rupesh I. Bhatt[3], Paul G. Murray[2], Victoria L. Heath[1], and Roy Bicknell[1]

Supplementary section to 7.2.2 "The impact of sunitinib treatment on tumour and endothelial gene expression."

Comparative analysis of the microarray data (generated as described in section 7.2.1), facilitated the *in silico* investigation of changes in signalling of key sunitinib targeted pathways, (VEGFR-1&2, PDGFR-α&β and FLT3, Appendix figures A, B and C respectively). The Qiagen Ingenuity pathway prediction software was used to generate a predicted expression change profile within each of the pathways, upon the inhibition of VEGFR-1&2, PDGFR-α&β and FLT3 (the supposed effect of sunitinib activity), (Appendix figures A, B and C (i)). This was then compared with the observed gene expression changes between arrays. This investigation identified genes >2 fold changed and with a Benjamini and Hochberg 1995 (317) adjusted P-value < 0.05, in the following comparison matrices; bulk tissue and endothelium from the responsive versus untreated, non-responsive versus untreated and responsive versus non-responsive cohorts at 1300 mm^3 (Appendix figures A, B and C (ii)). The 2 vs. 2 comparison matrices generated from the day 9 and 600 mm^3 responsive and untreated cohorts, were also included in this pathway analysis, however, due to their reduced n-numbers they are suboptimal for this setting (due to inferior p-values), therefore the selection threshold was set to >2 fold gene expression change and unadjusted p-value <0.05.

This analysis revealed that at day 9 signalling of each of the pathways in the responsive cohort broadly resembled that predicted from sunitinib treatment, suggesting that at this stage the tumours were sensitive to sunitinib (Appendix figures A, B and C (ii:1)).

Sunitinib inhibition of each of the pathways was lost however, in the responsive versus untreated cohort at the 600 and 1300 mm^3 size points (Appendix figures A, B and C (ii:2&3)), suggesting that by this point the tumour had become resistant to sunitinib therapy. This data supports the pattern of tumour sensitivity reported for the responsive group in chapter 6. The non-responsive cohort on the other hand, when its expression profile was compared to that of the untreated group, displayed sensitivity to sunitinib treatment at 1300 mm^3, in either the bulk, or endothelial fractions, or both. Additionally when comparing the two treated cohorts, the responsive group consistently showed greater activation of each pathway than the non-responsive group at 1300 mm^3 (Appendix figures A, B and C (ii:4-8)).

This data broadly agrees with the pattern of response reported in section 7.2.2 adding a supplementary level of detail as regards the effect of sunitinib treatment on the expression of genes downstream of the drug's target receptors. It should be noted that changes to gene expression don't necessarily translate to changes in the activity of the gene product. For genuine activity analysis the phosphorylation state of downstream target would have to be assessed (eg. by western blot analysis). However, the analysis detailed in this supplementary section does provide some insight into the effect of sunitinib treatment and resistance on downstream players in targeted signalling pathways, guiding future analysis of this area, via RNA and protein based assays.

Appendix figures A, B and C: Tumour and vascular signalling is differentially affected by sunitinib therapy in different cohorts and timepoints. Injenuity software pathway predictions of signalling in the A, VEGFR-1&2, B, PDGFR-α&β and C, FLT-3 pathways. (i) Predicted effect of sunitinib therapy on the signalling pathway. Activity of the target receptors were reduced in silico (in line with predicted sunitinib activity) (green) and downstream genes predicted to be upregulated (red), downregulated (blue), or where there is conflicting data (yellow), by this intervention are shown. Greater intensity of colour denotes a greater predicted fold change in expression. (ii) Effects on the signalling pathways in different cohorts, timepoints and comparison matrices, formulated from microarray data of genes >2 fold changed and with a Benjamini & Hochberg, 1995 (317) adjusted P-value < 0.05. Genes upregulated (red) and downregulated (green) in these analyses are shown. Greater intensity of colour denotes a greater fold change in expression.
The functional linkage of genes in the pathways to one another is illustrated. Arrows between genes denote one gene enhancing the activity of the other. Flat ended lines between genes denote one gene inhibiting the activity of the other. Lines with no ending denote a connection between two genes where the effect of this connection on gene activity is not conclusively known.

Appendix figure A(i)

VEGF signalling pathway

Predicted response to sunitinib treatment

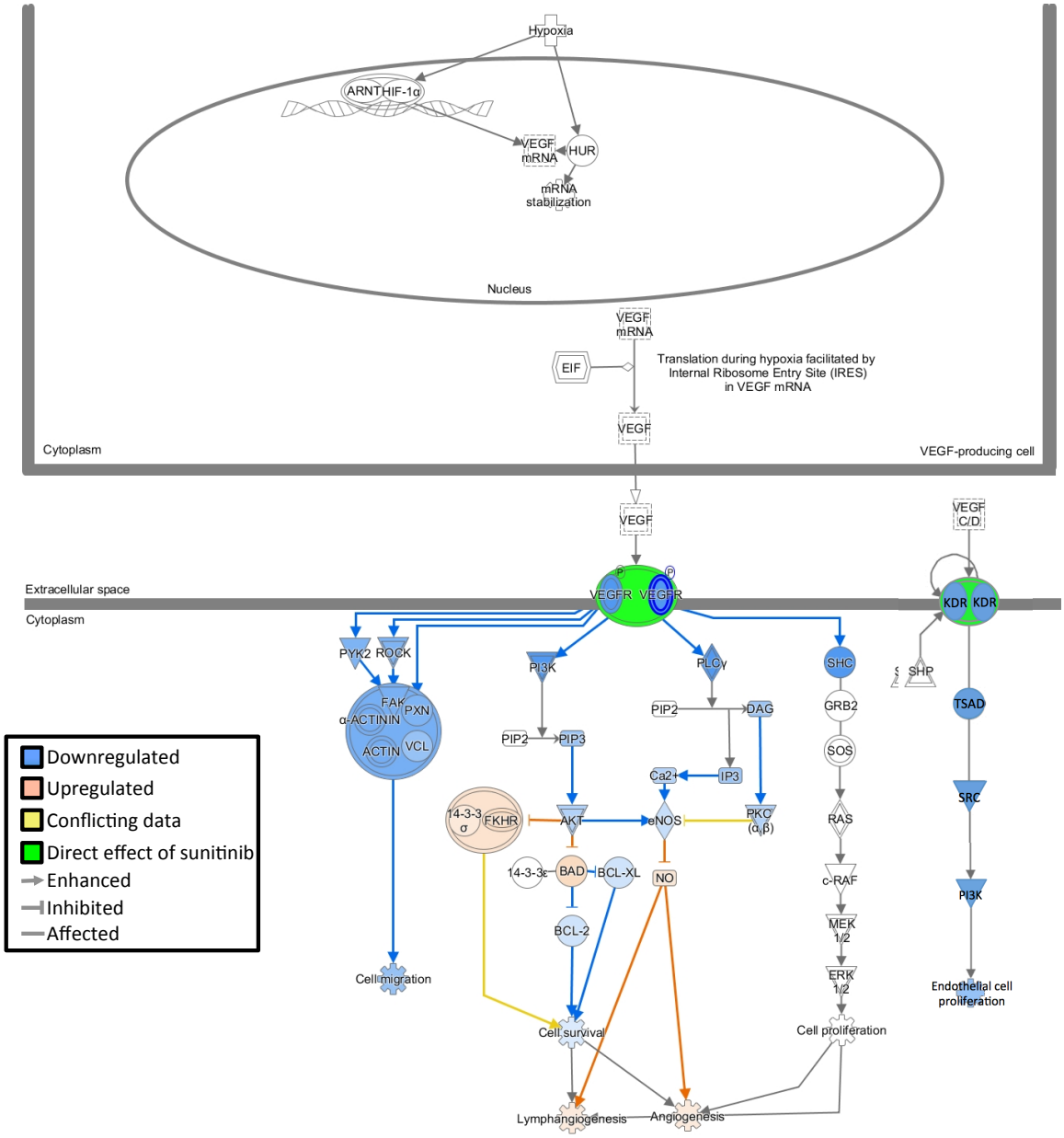

Appendix figure A(ii:1)

VEGF signalling pathway

Responsive vs. untreated day 9 bulk

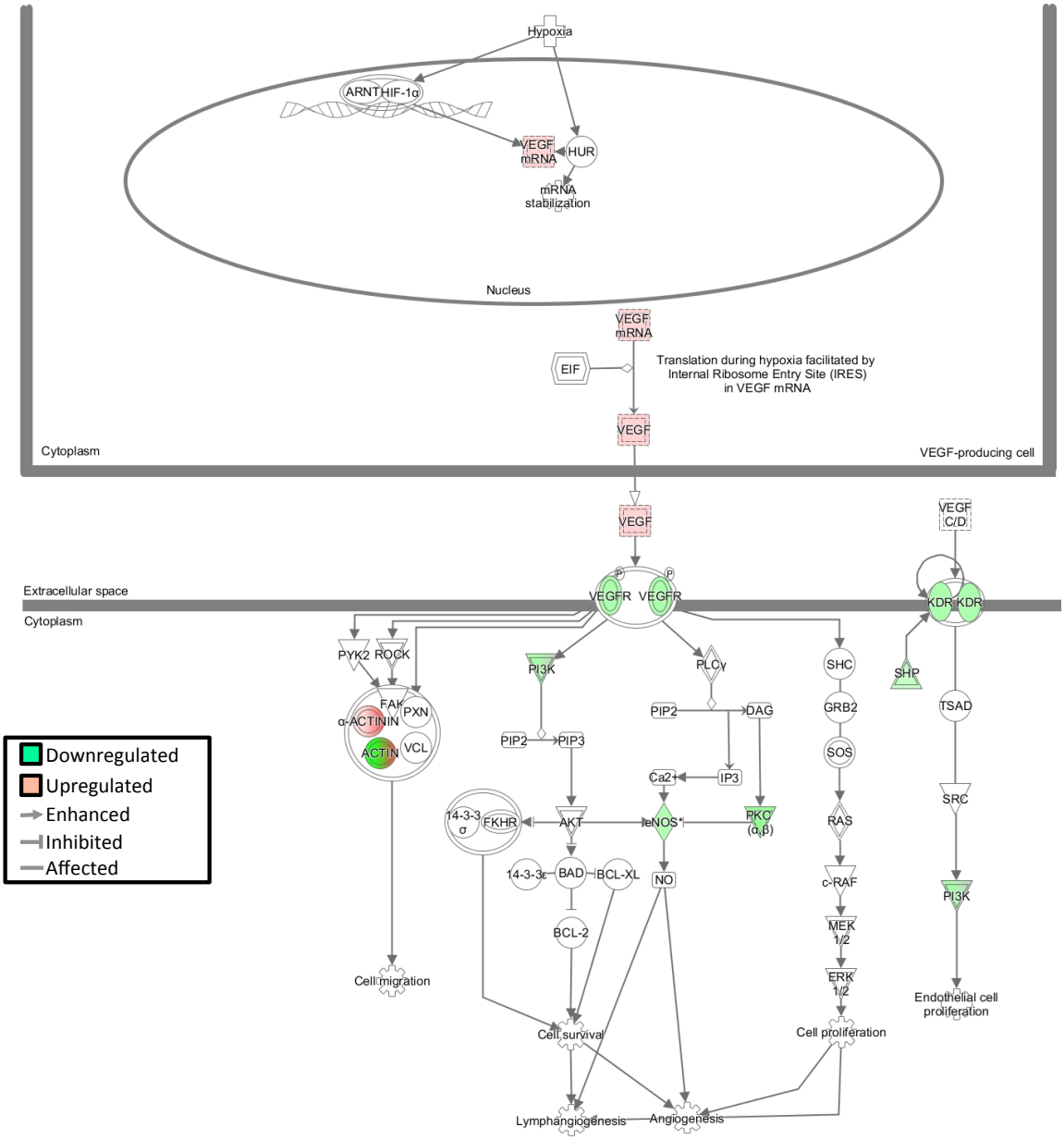

Appendix figure A(ii:2)

VEGF signalling pathway

Responsive vs. untreated 600 mm^3 bulk

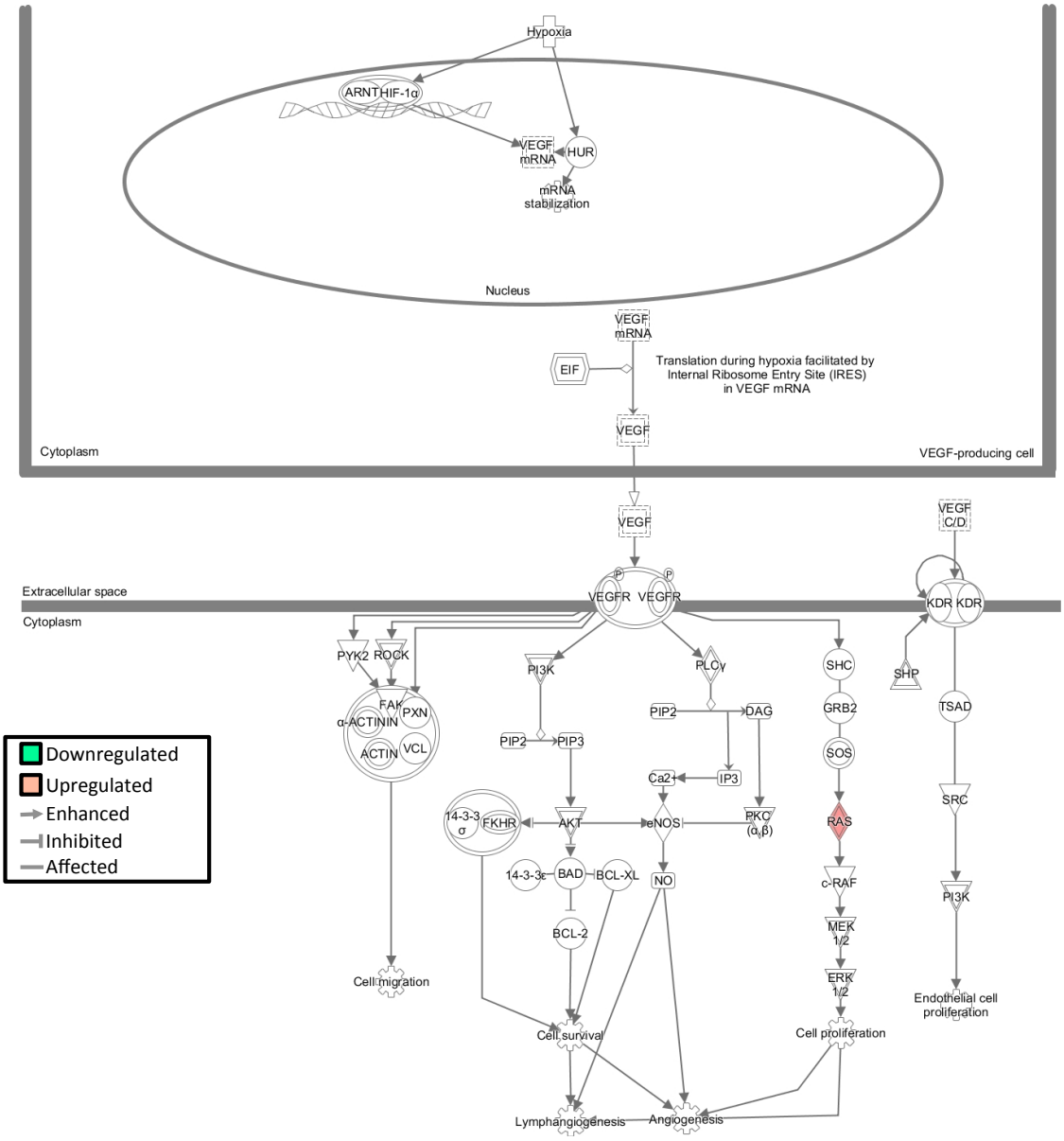

Appendix figure A(ii:3)

VEGF signalling pathway

Responsive vs. untreated 1300 mm^3 bulk

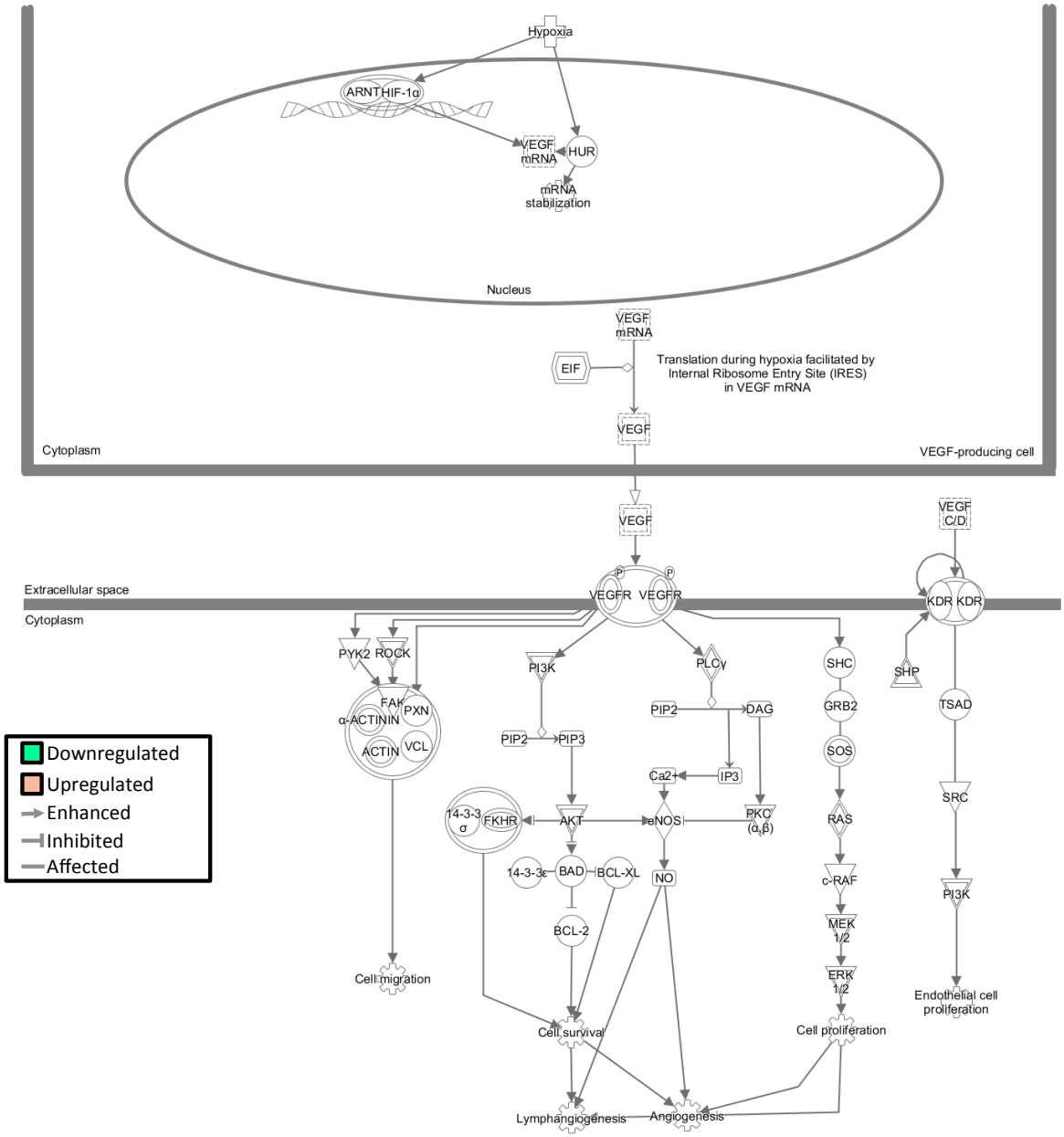

Appendix figure A(ii:4)

VEGF signalling pathway

Non-responsive vs. untreated 1300 mm^3 bulk

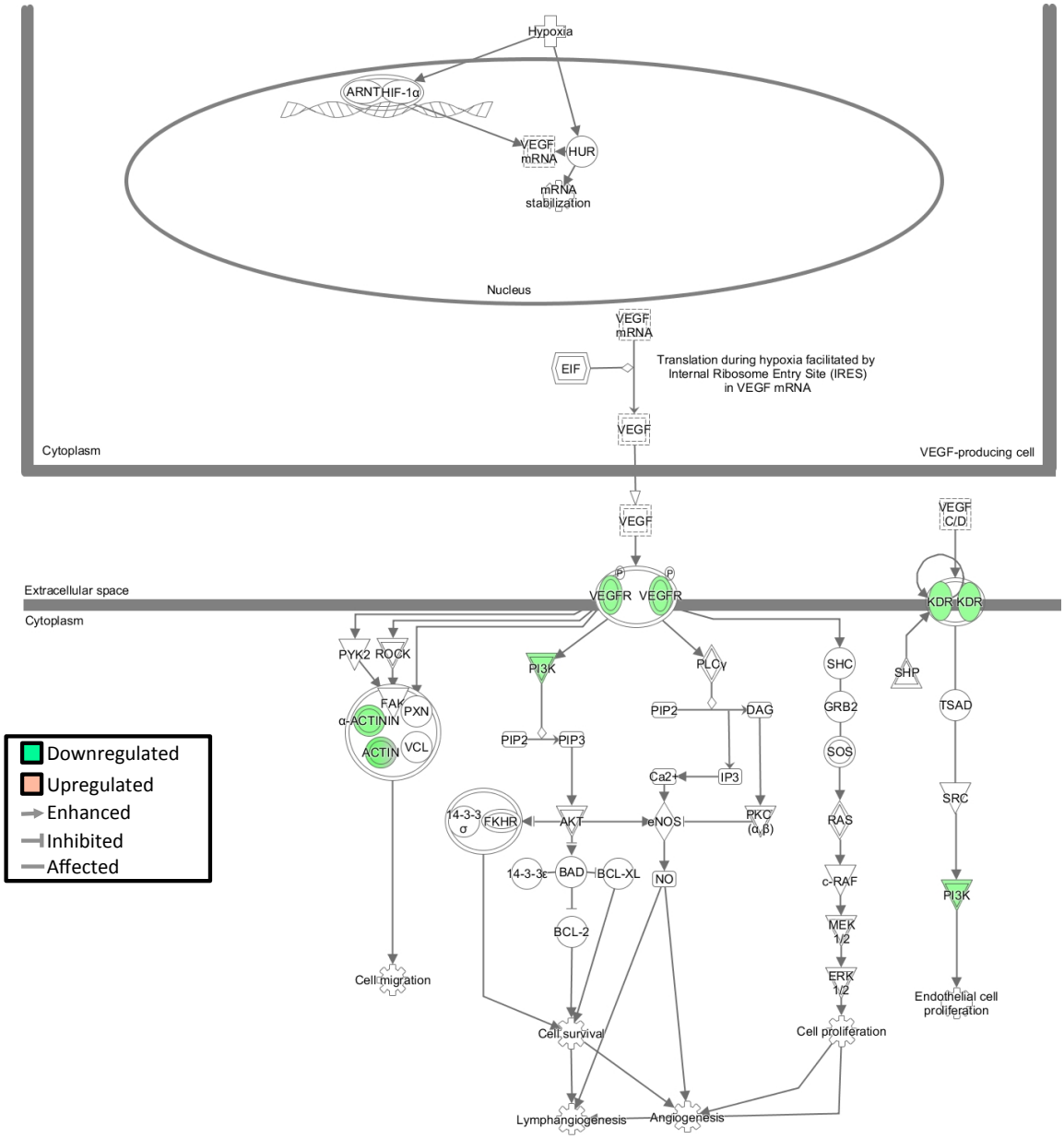

Appendix figure A(ii:5)

VEGF signalling pathway

Responsive vs. Non-responsive 1300 mm^3 bulk

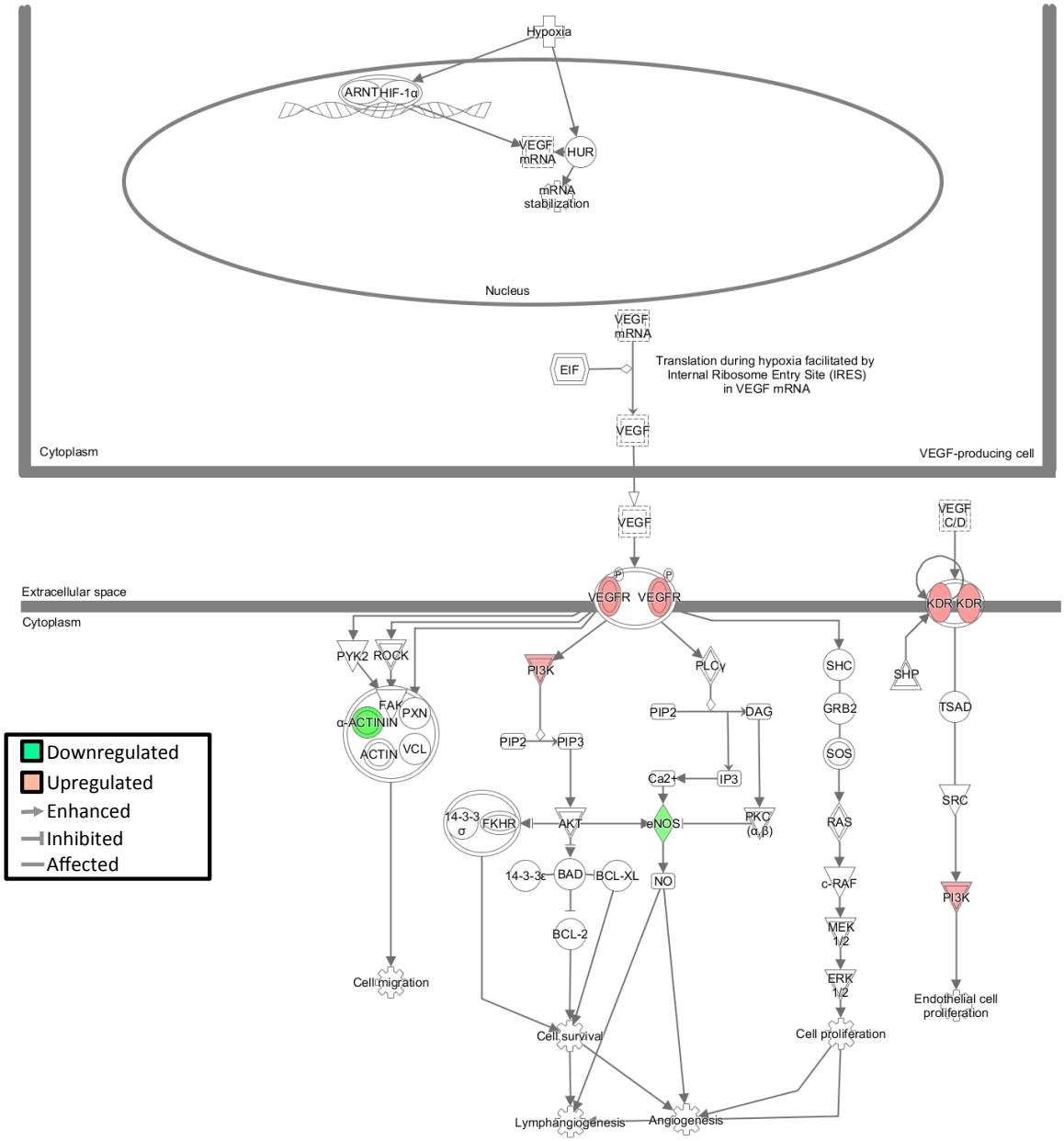

Appendix figure A(ii:6)

VEGF signalling pathway

Responsive vs. untreated 1300 mm^3 EC

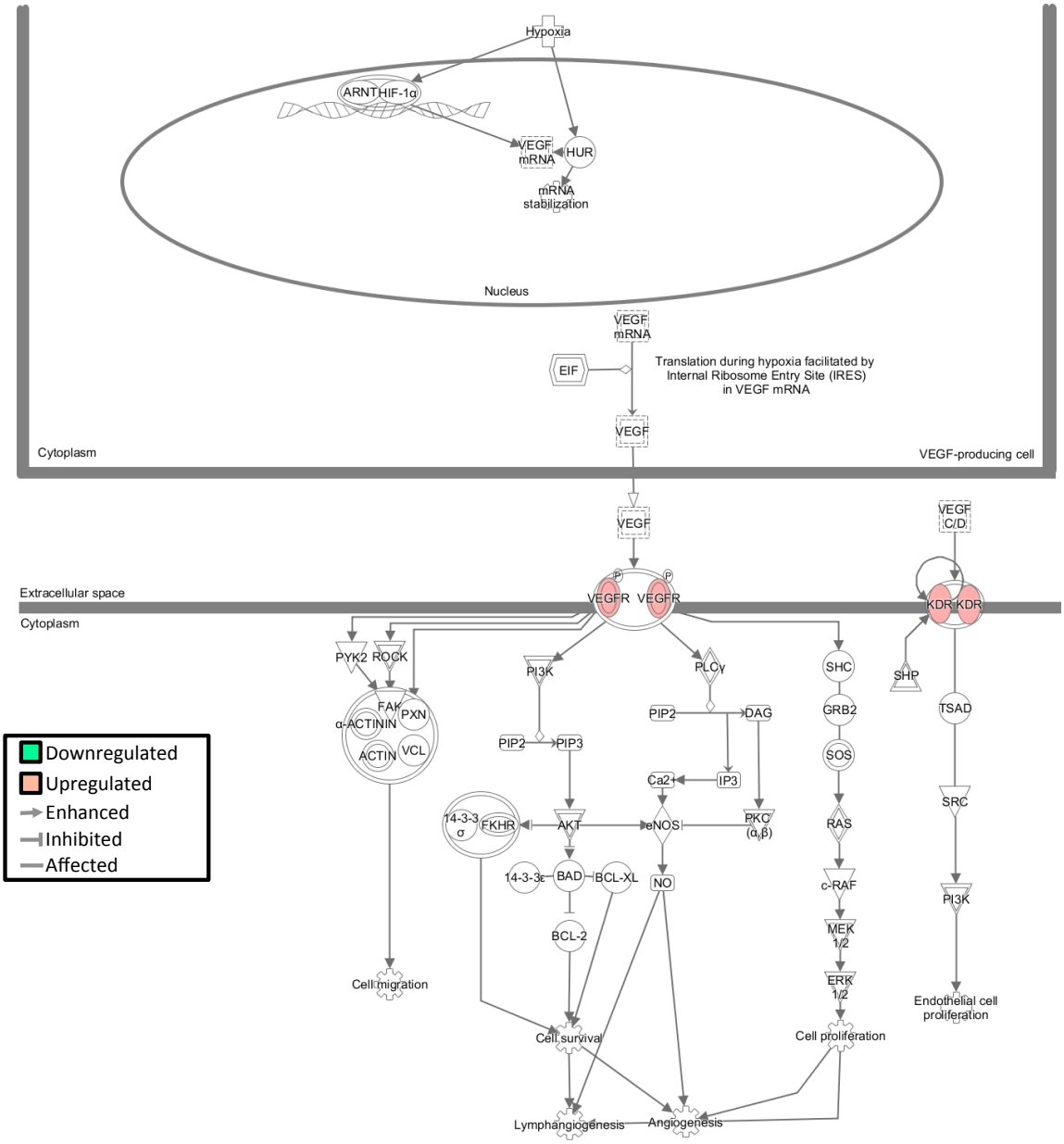

Appendix figure A(ii:7)

VEGF signalling pathway

Non-responsive vs. untreated 1300 mm^3 EC

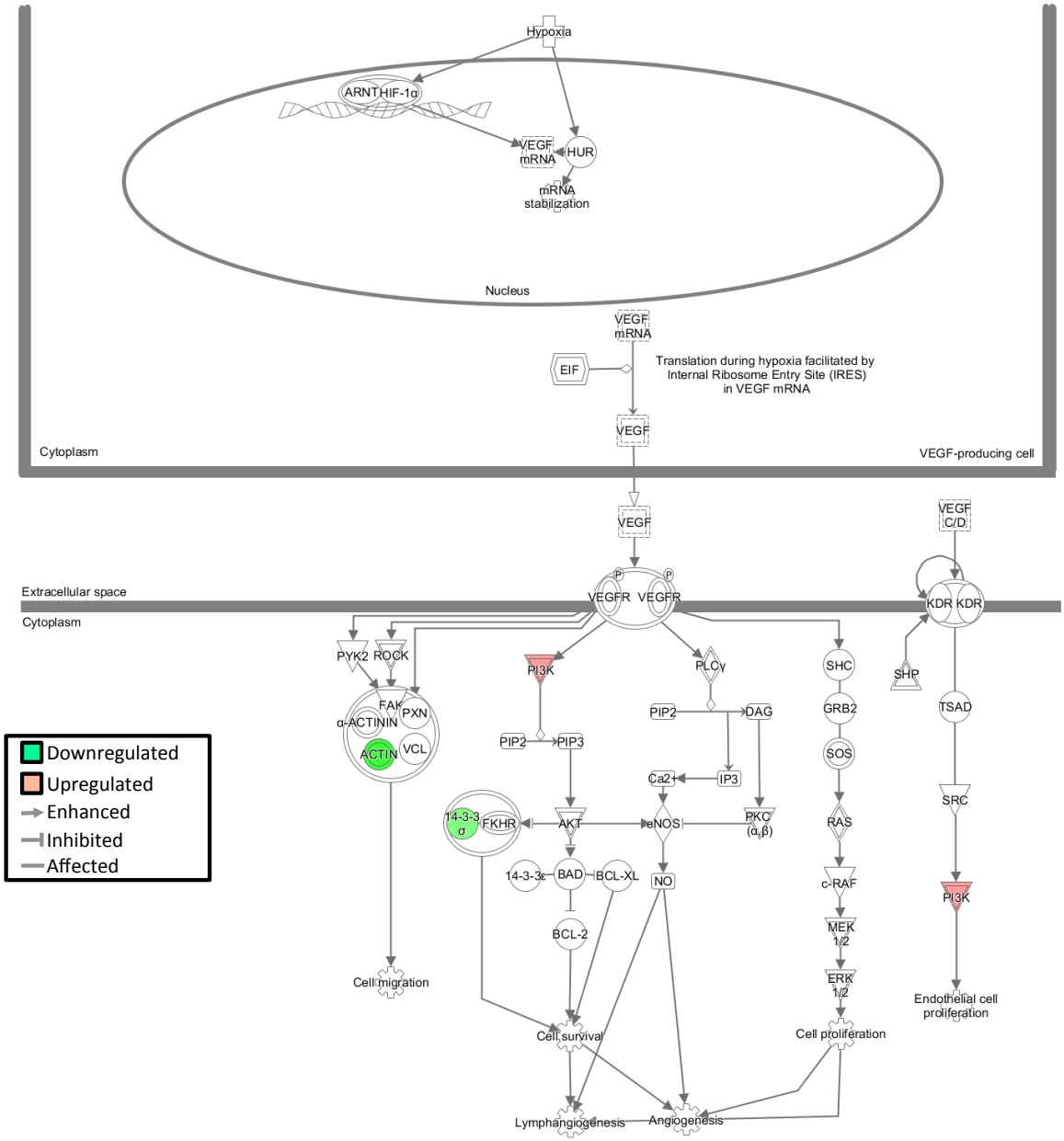

Appendix figure A(ii:8)

VEGF signalling pathway

Responsive vs. Non-responsive 1300 mm^3 EC

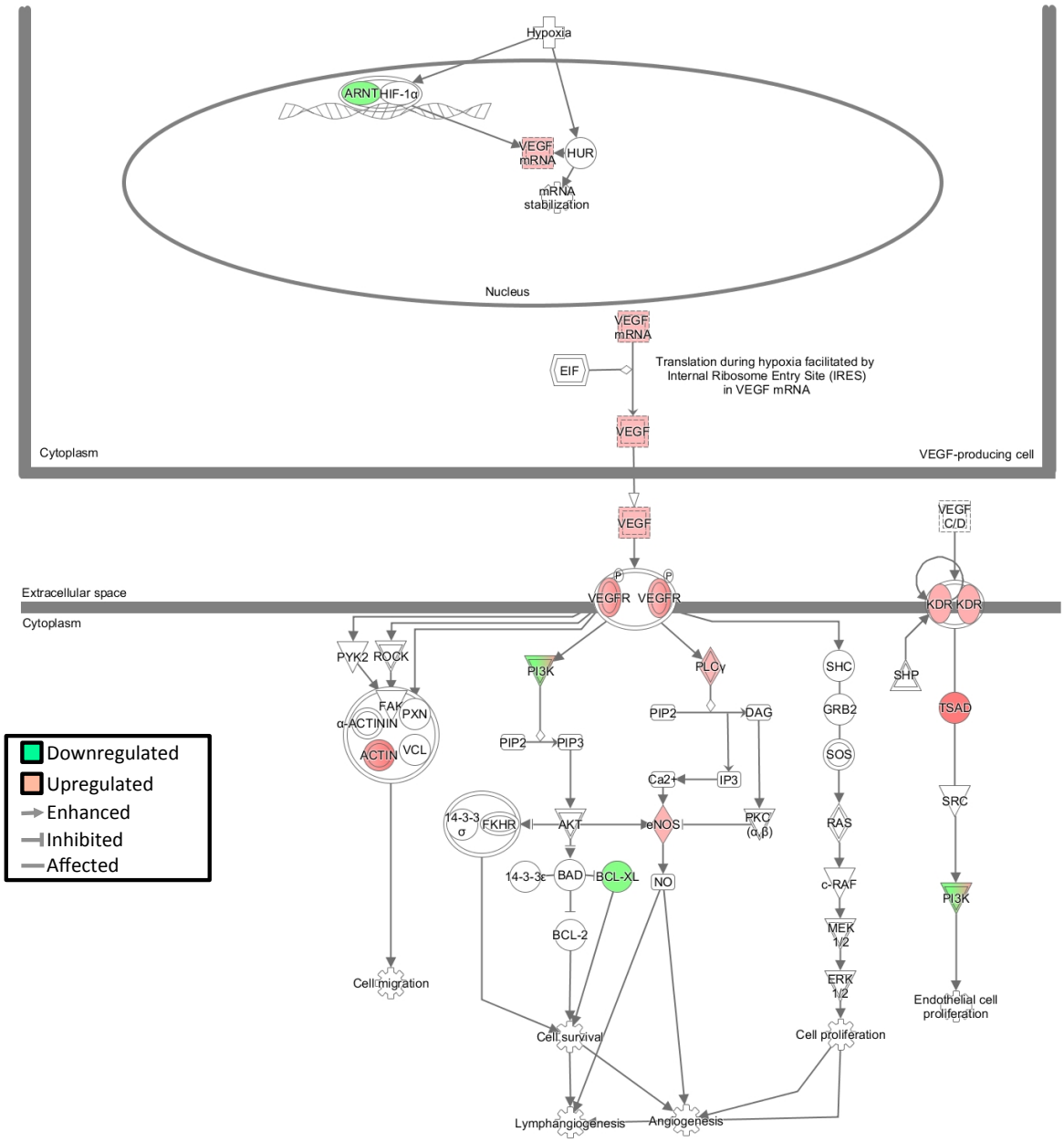

Appendix figure B(i)

PDGF signalling pathway

Predicted response to sunitinib treatment

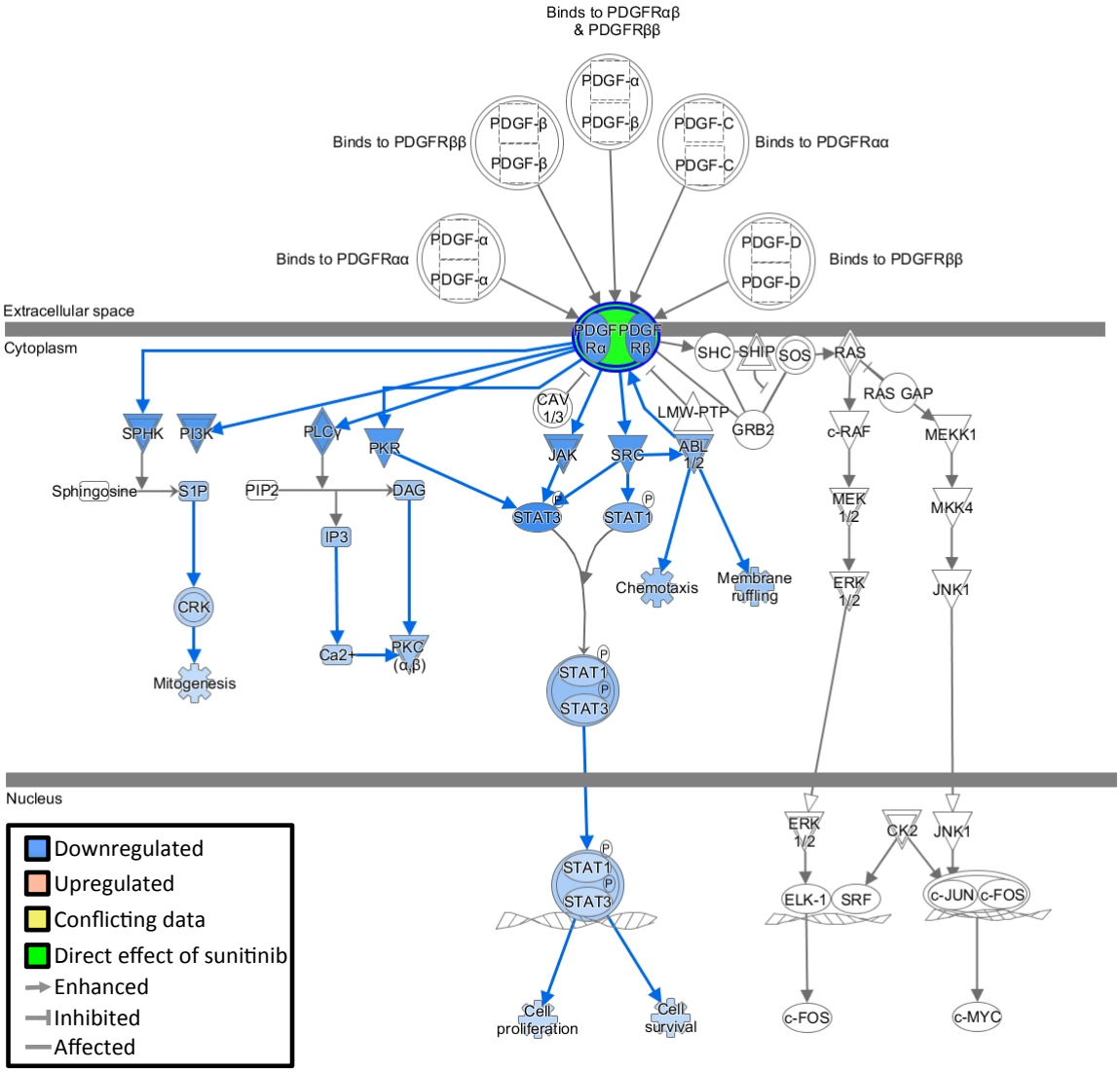

Appendix figure B(ii:1)

PDGF signalling pathway

Responsive vs. untreated day 9 bulk

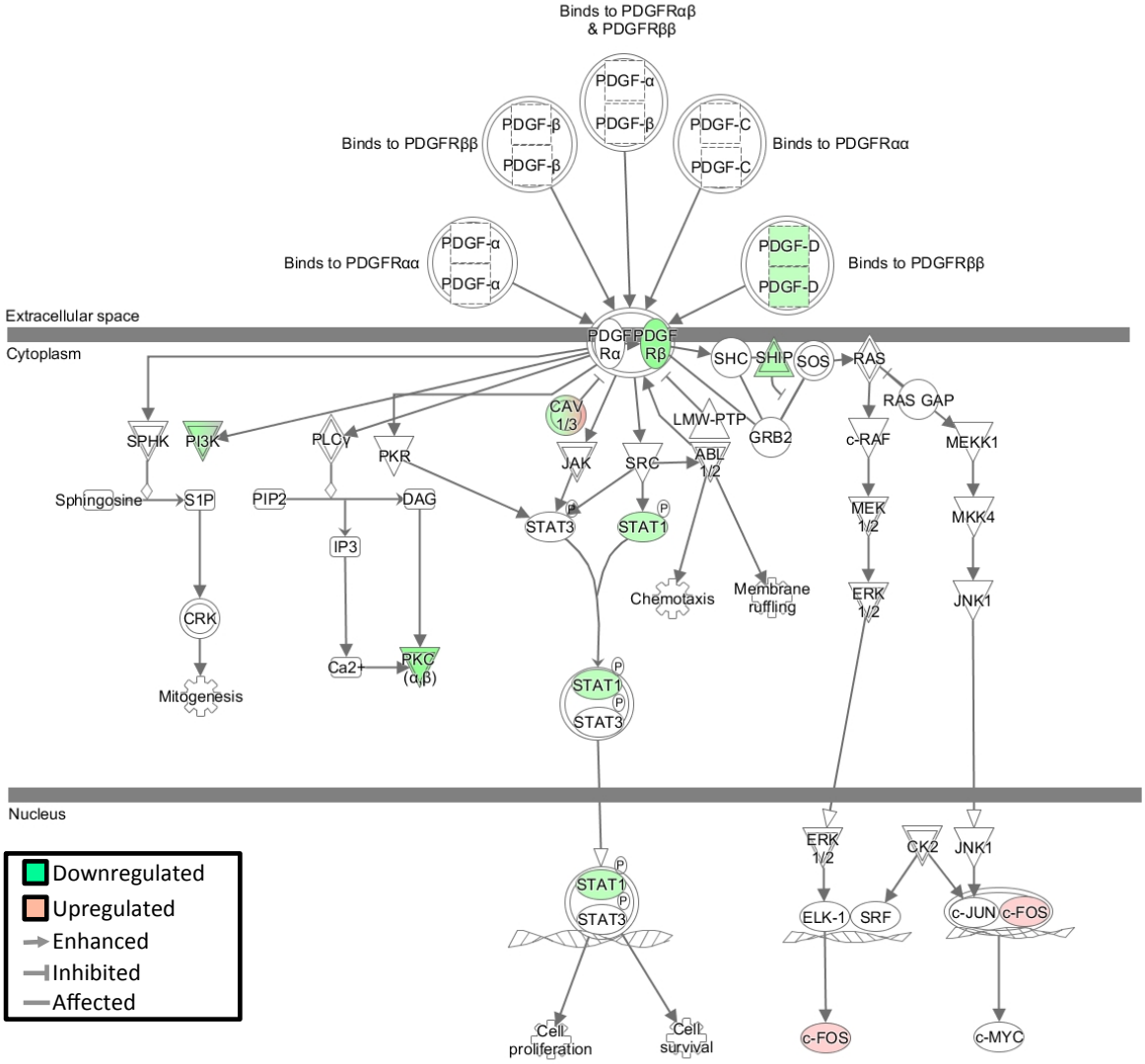

Appendix figure B(ii:2)

PDGF signalling pathway

Responsive vs. untreated 600 mm^3 bulk

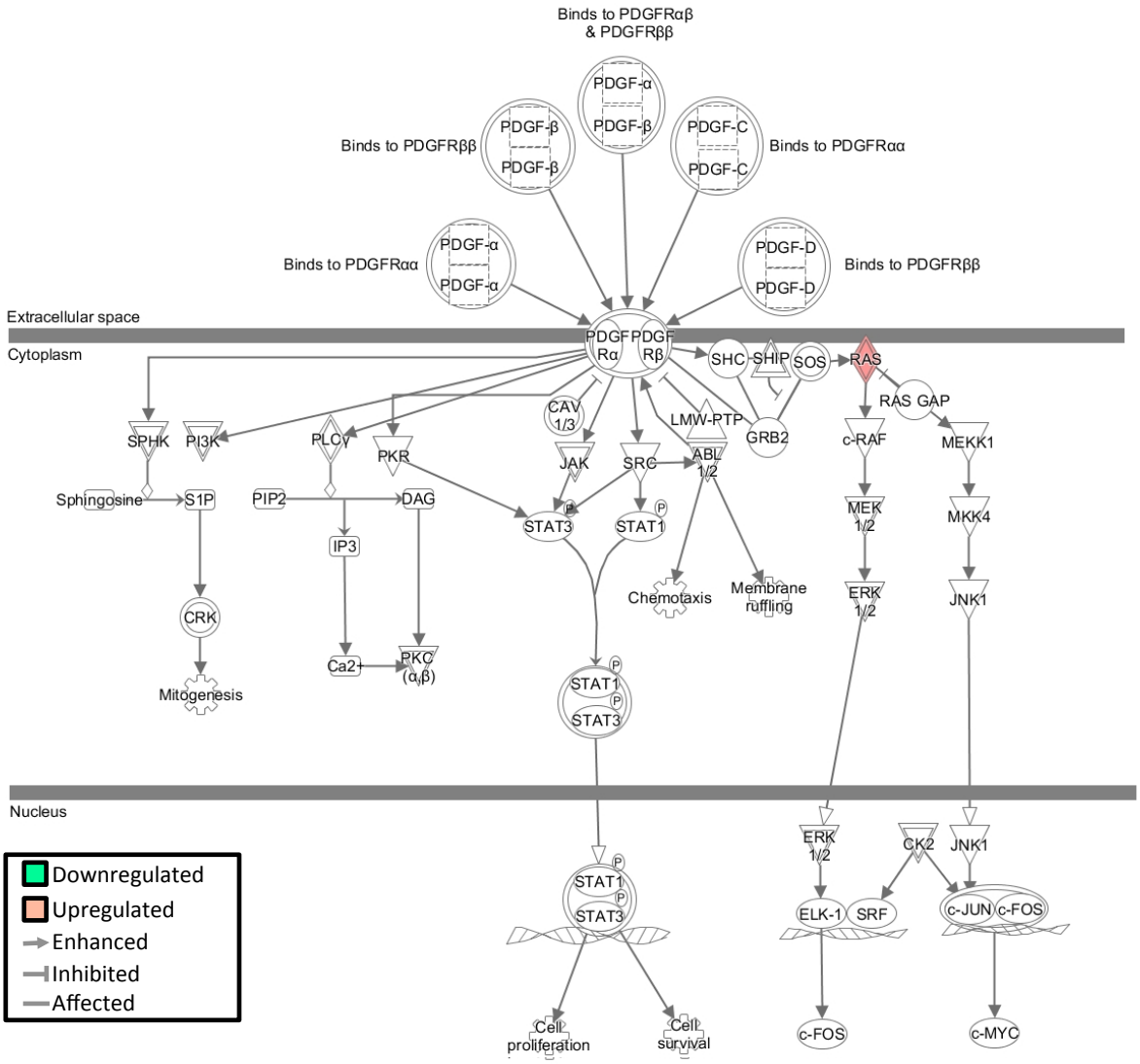

Appendix figure B(ii:3)

PDGF signalling pathway

Responsive vs. untreated 1300 mm^3 bulk

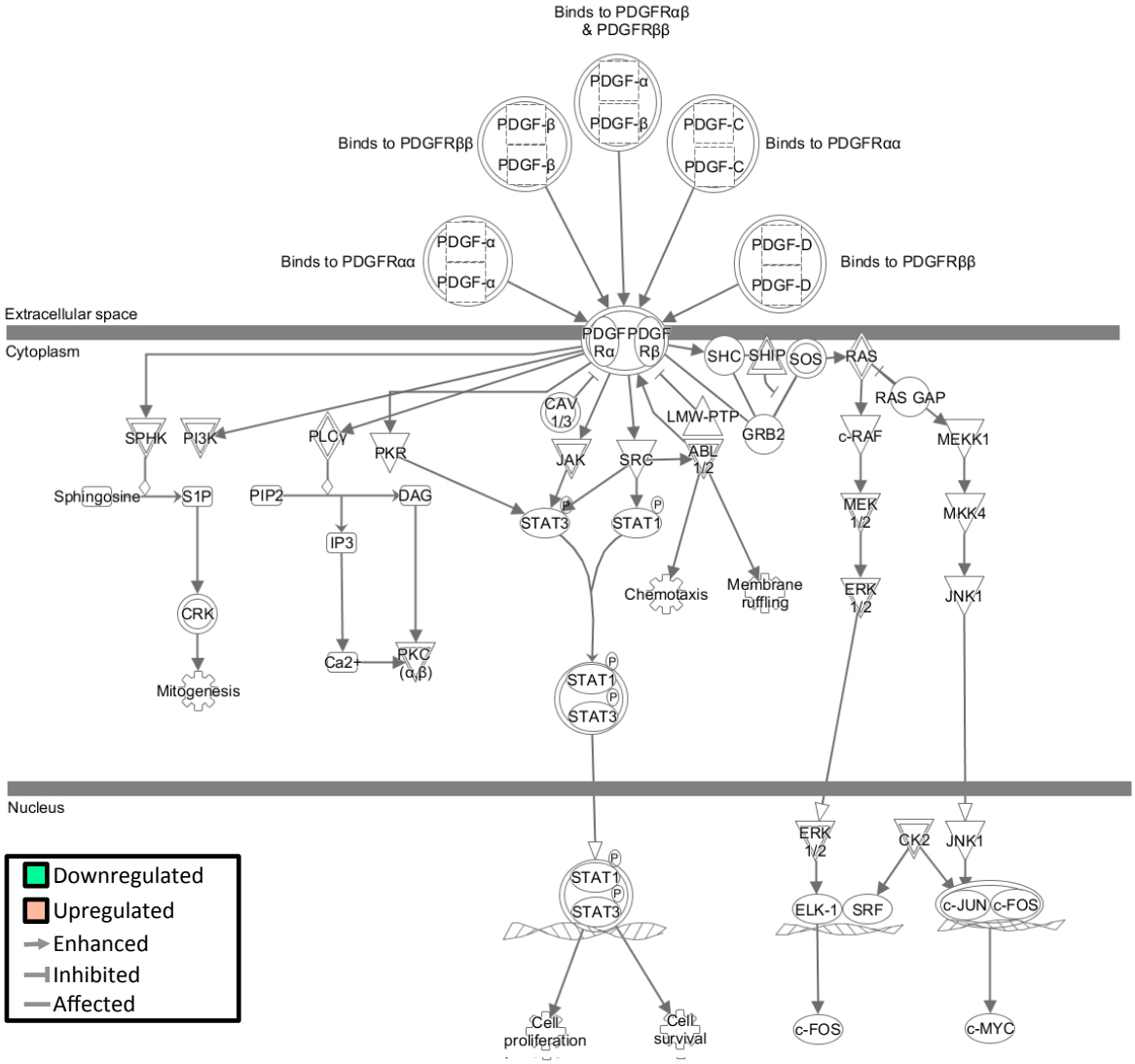

Appendix figure B(ii:4)

PDGF signalling pathway

Non-responsive vs. untreated 1300 mm^3 bulk

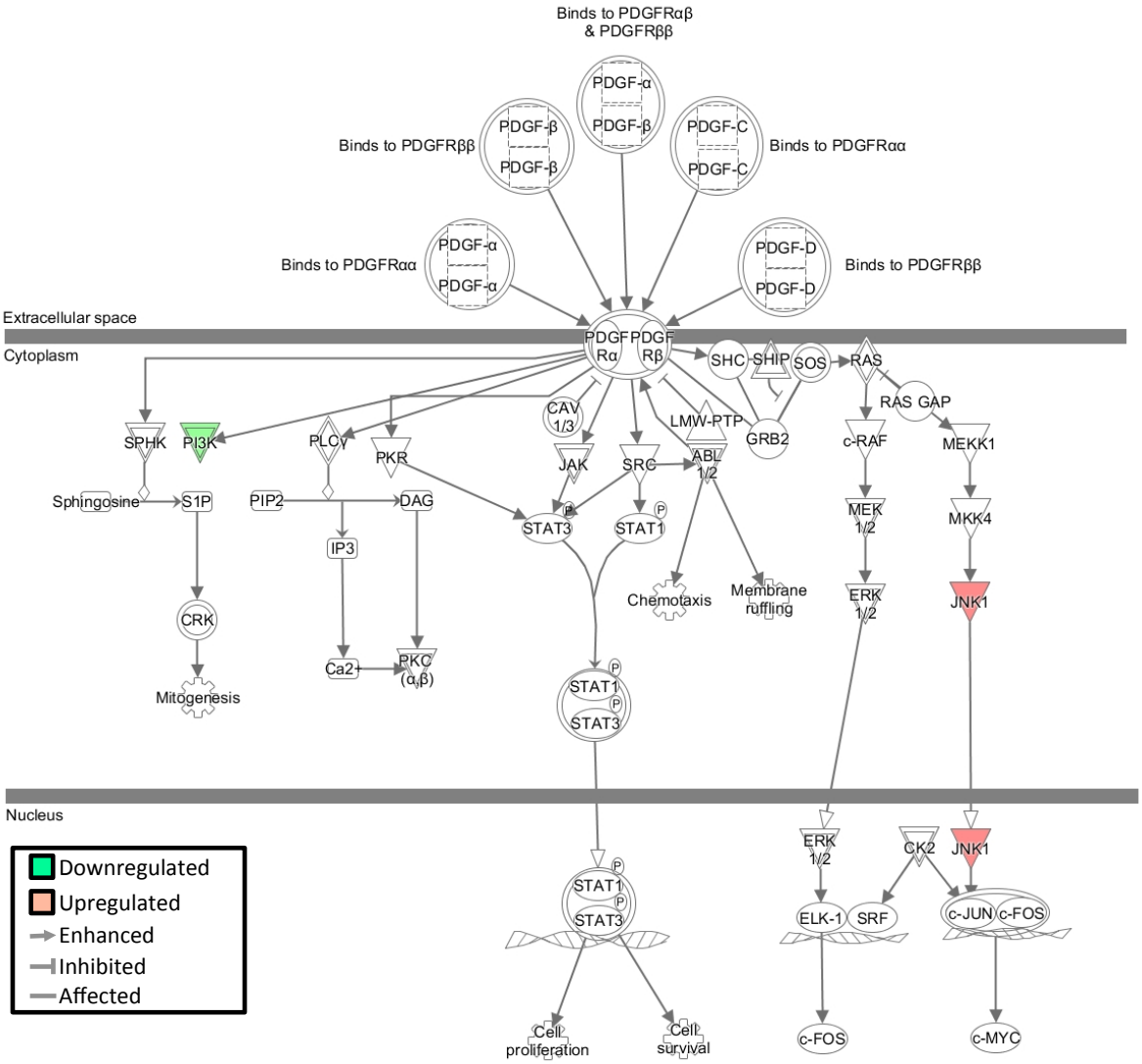

Appendix figure B(ii:5)

PDGF signalling pathway

Responsive vs. Non-responsive 1300 mm^3 bulk

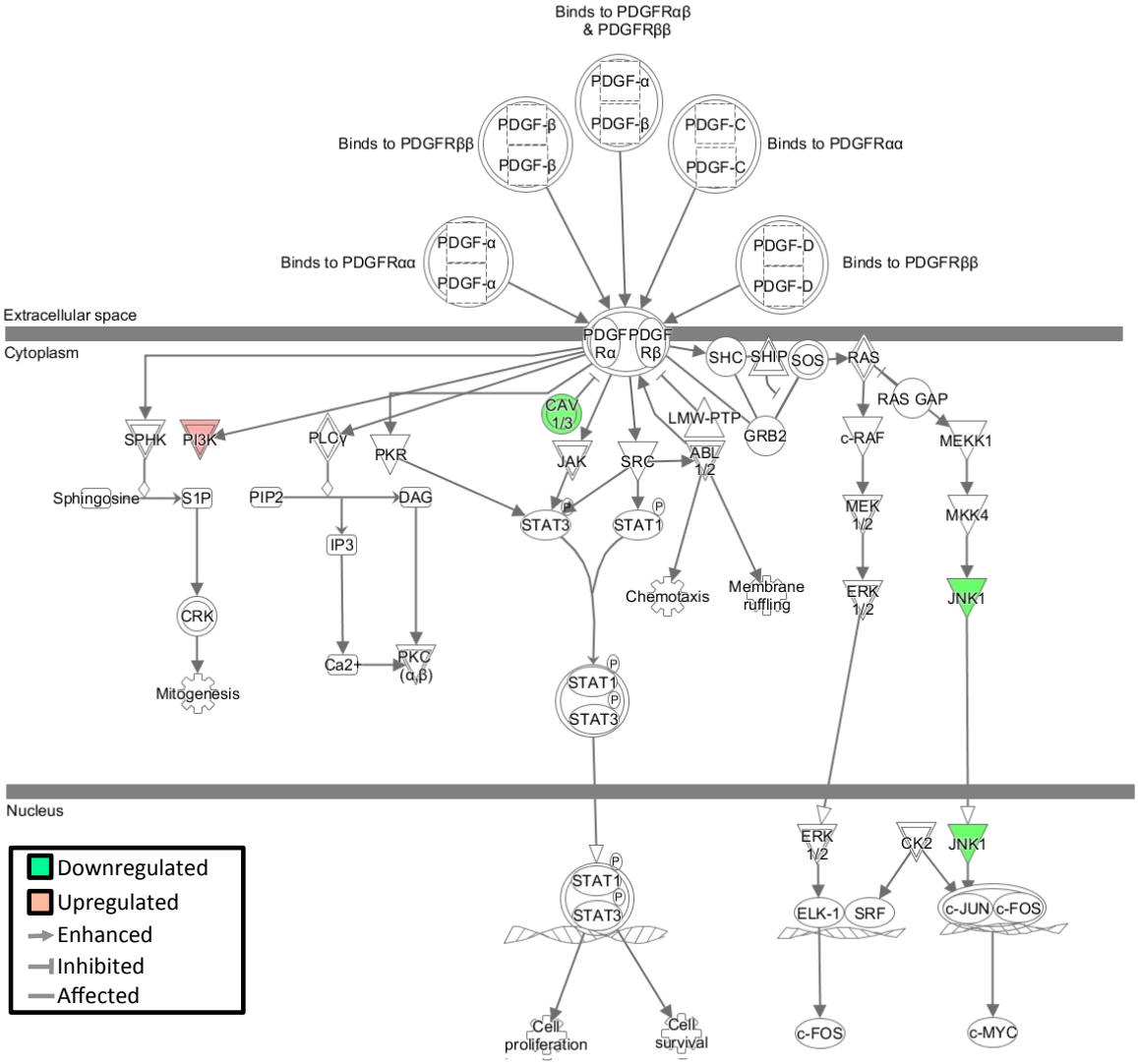

Appendix figure B(ii:6)

PDGF signalling pathway

Responsive vs. untreated 1300 mm^3 EC

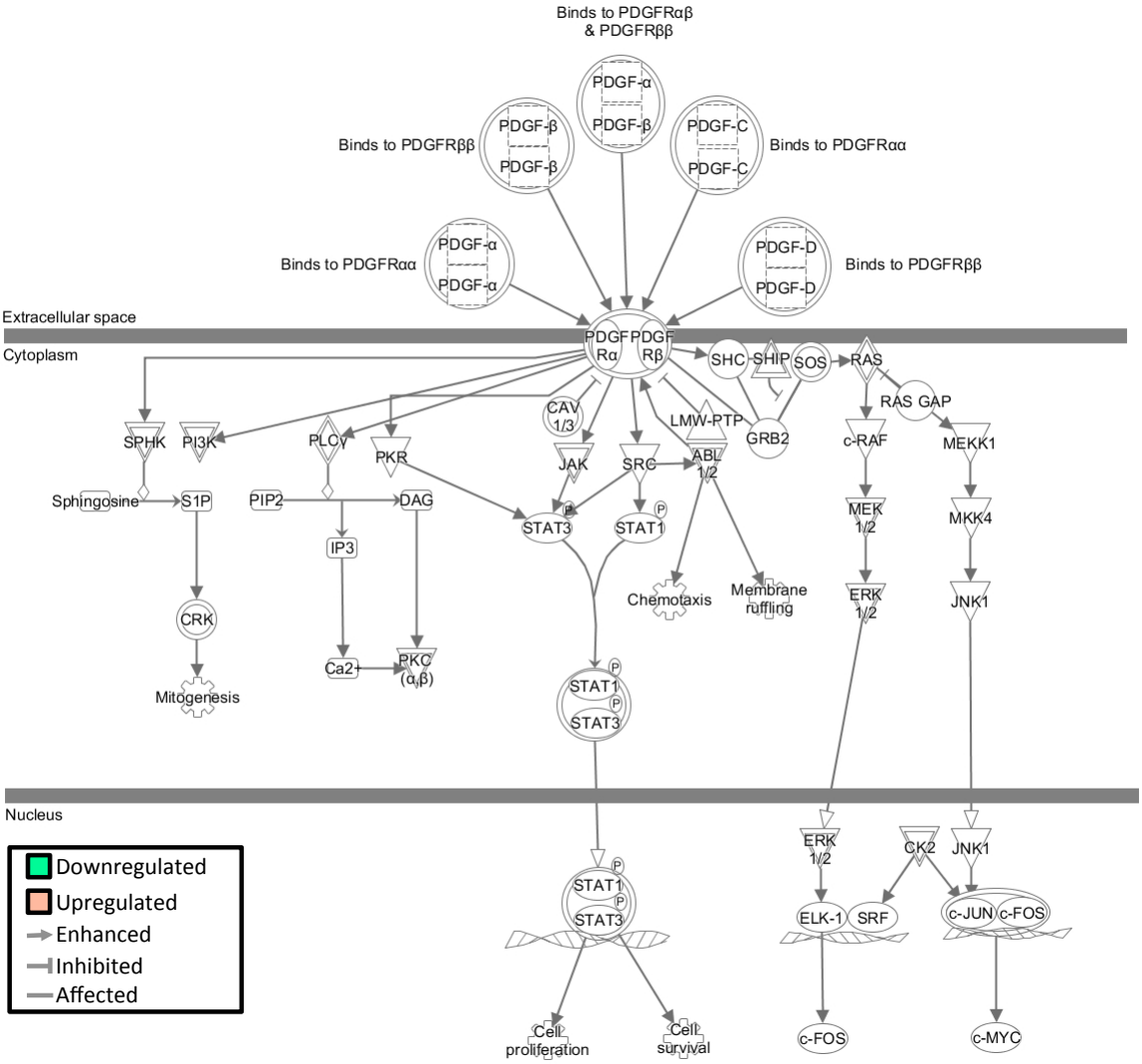

Appendix figure B(ii:7)

PDGF signalling pathway

Non-responsive vs. untreated 1300 mm^3 EC

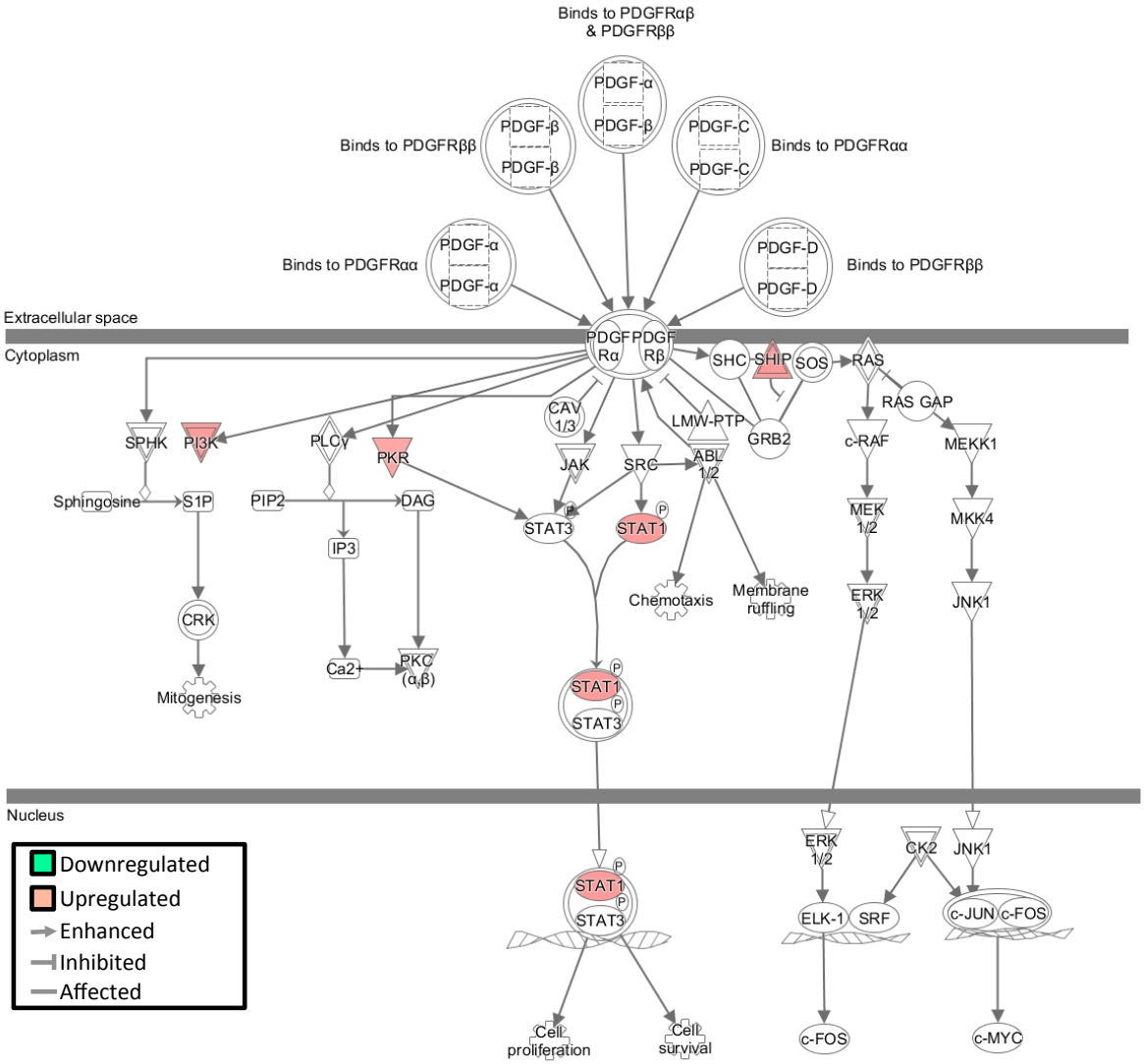

Appendix figure B(ii:8)

PDGF signalling pathway

Responsive vs. Non-responsive 1300 mm^3 EC

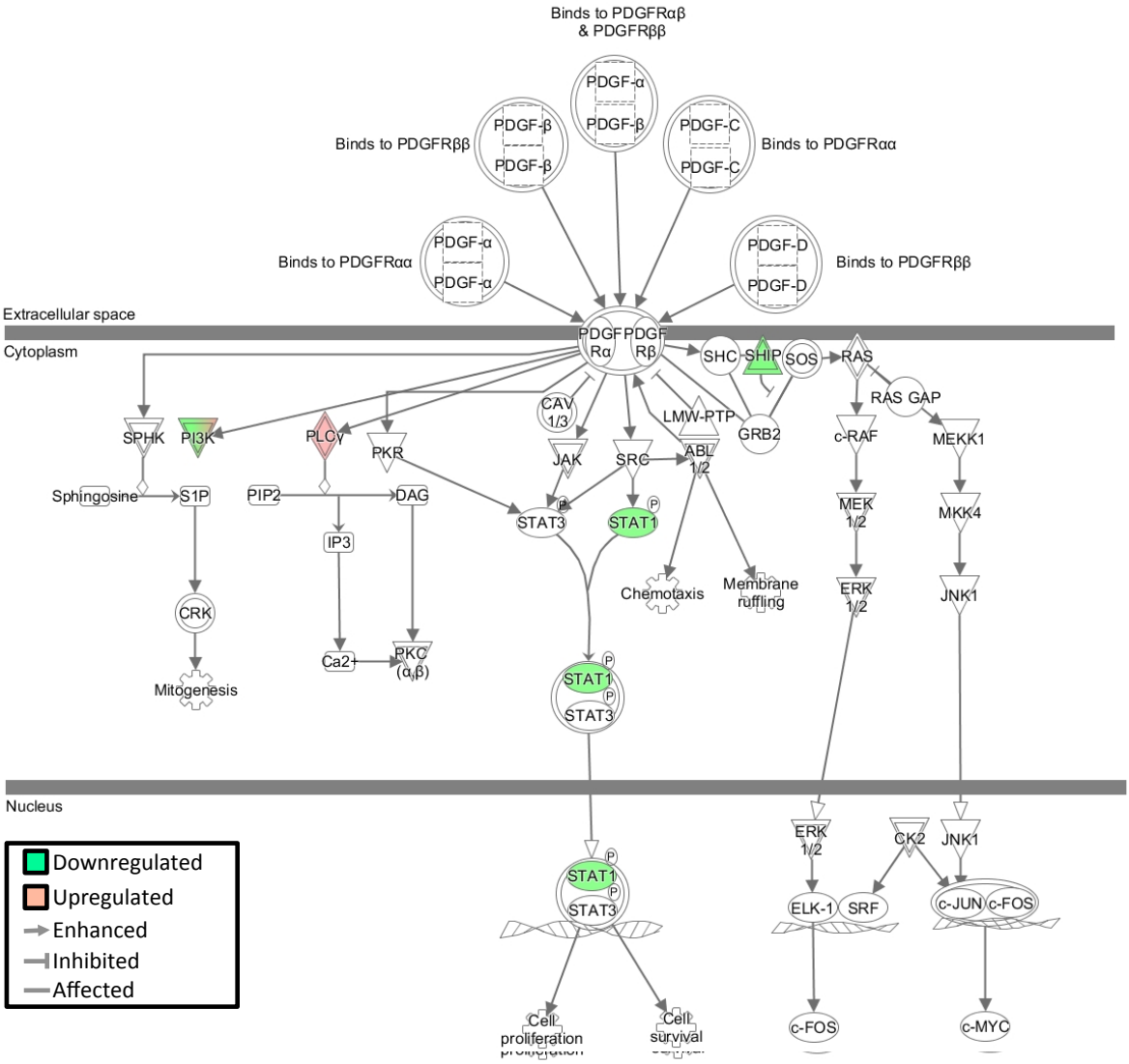

Appendix figure C(i)

FLT3 signalling pathway

Predicted response to sunitinib treatment

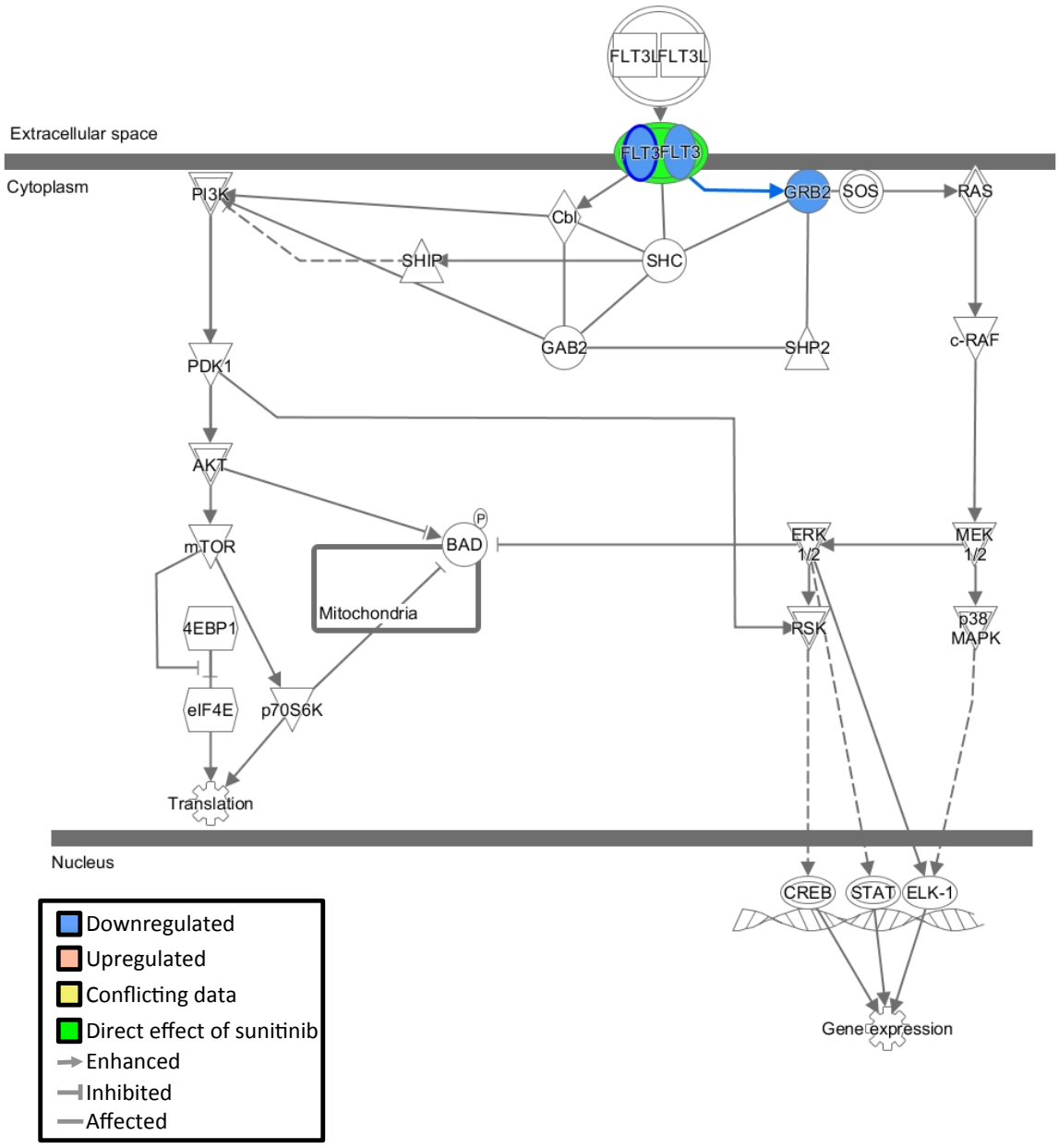

Appendix figure C(ii:1)

FLT3 signalling pathway

Responsive vs. untreated day 9 bulk

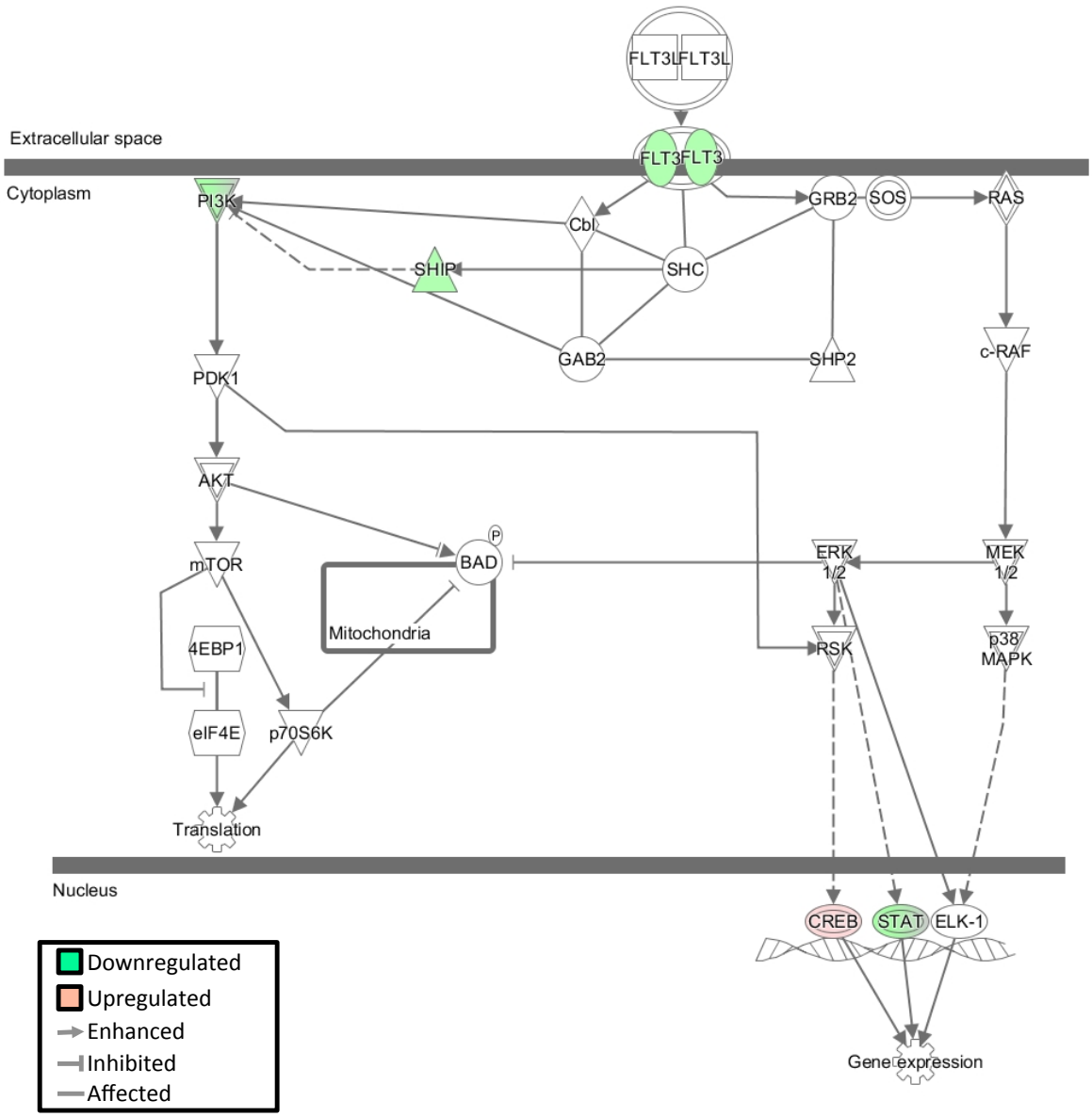

Appendix figure C(ii:2)

FLT3 signalling pathway

Responsive vs. untreated 600 mm^3 bulk

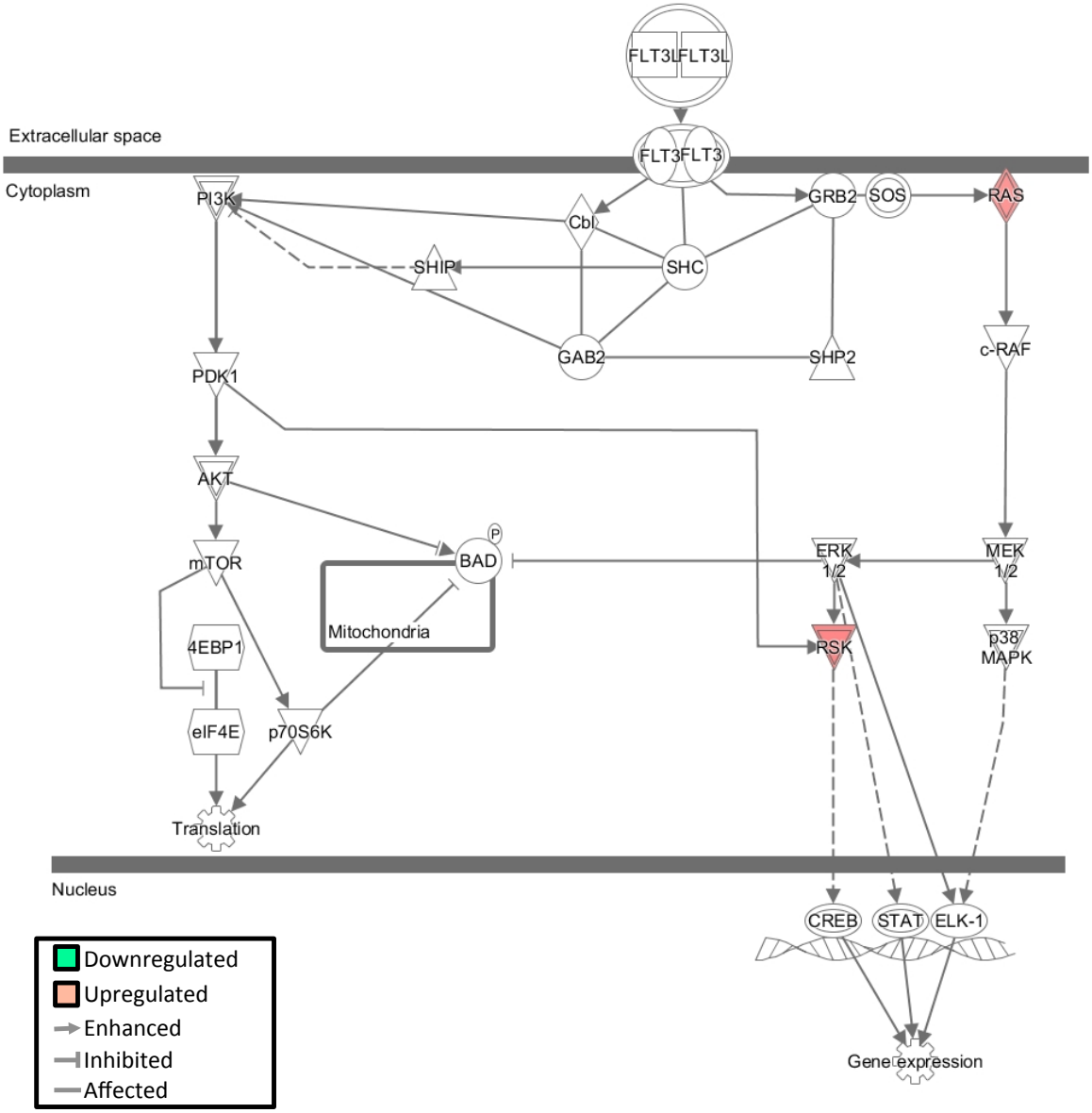

Appendix figure C(ii:3)

FLT3 signalling pathway

Responsive vs. untreated 1300 mm^3 bulk

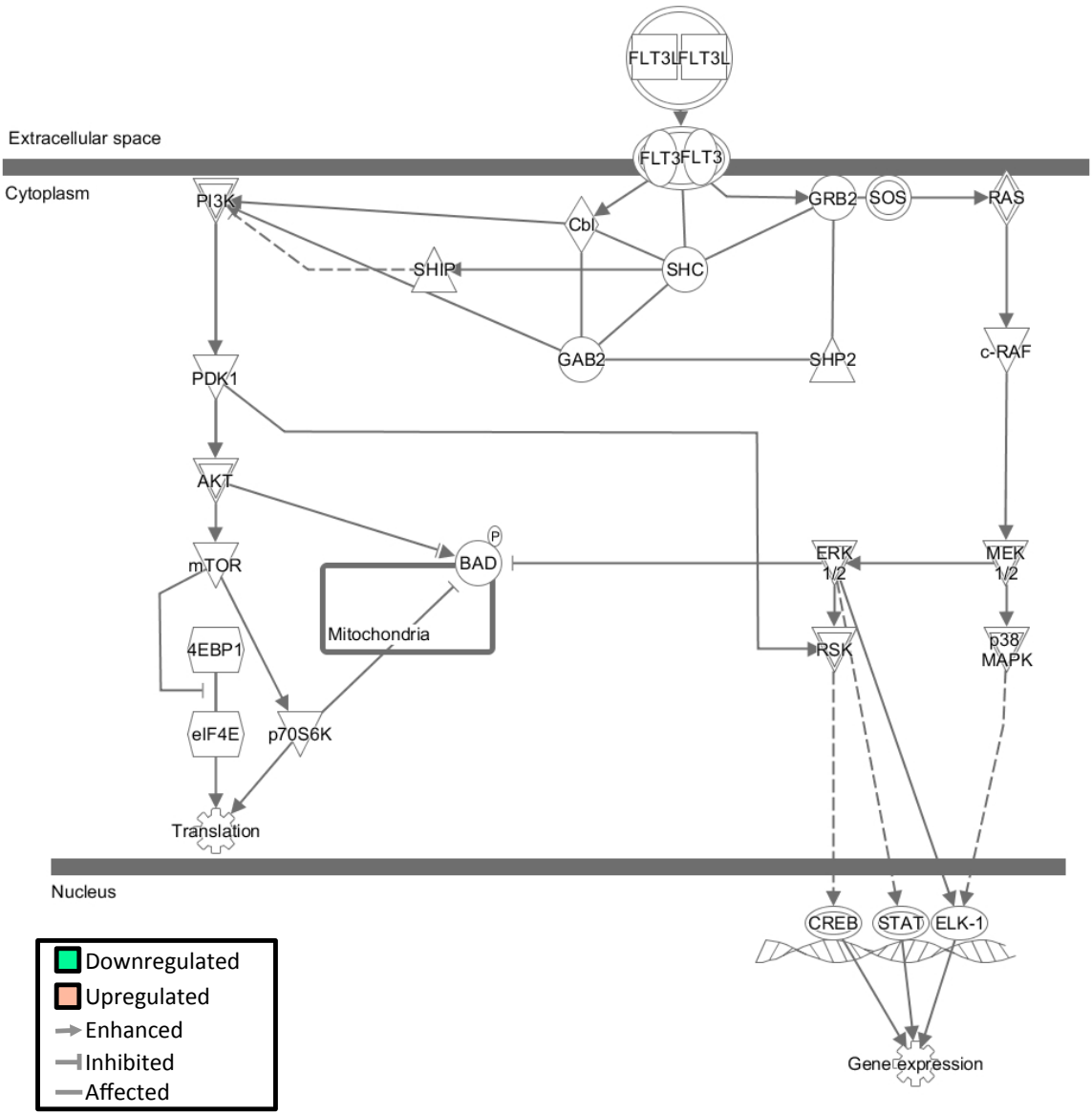

Appendix figure C(ii:4)

FLT3 signalling pathway

Non-responsive vs. untreated 1300 mm^3 bulk

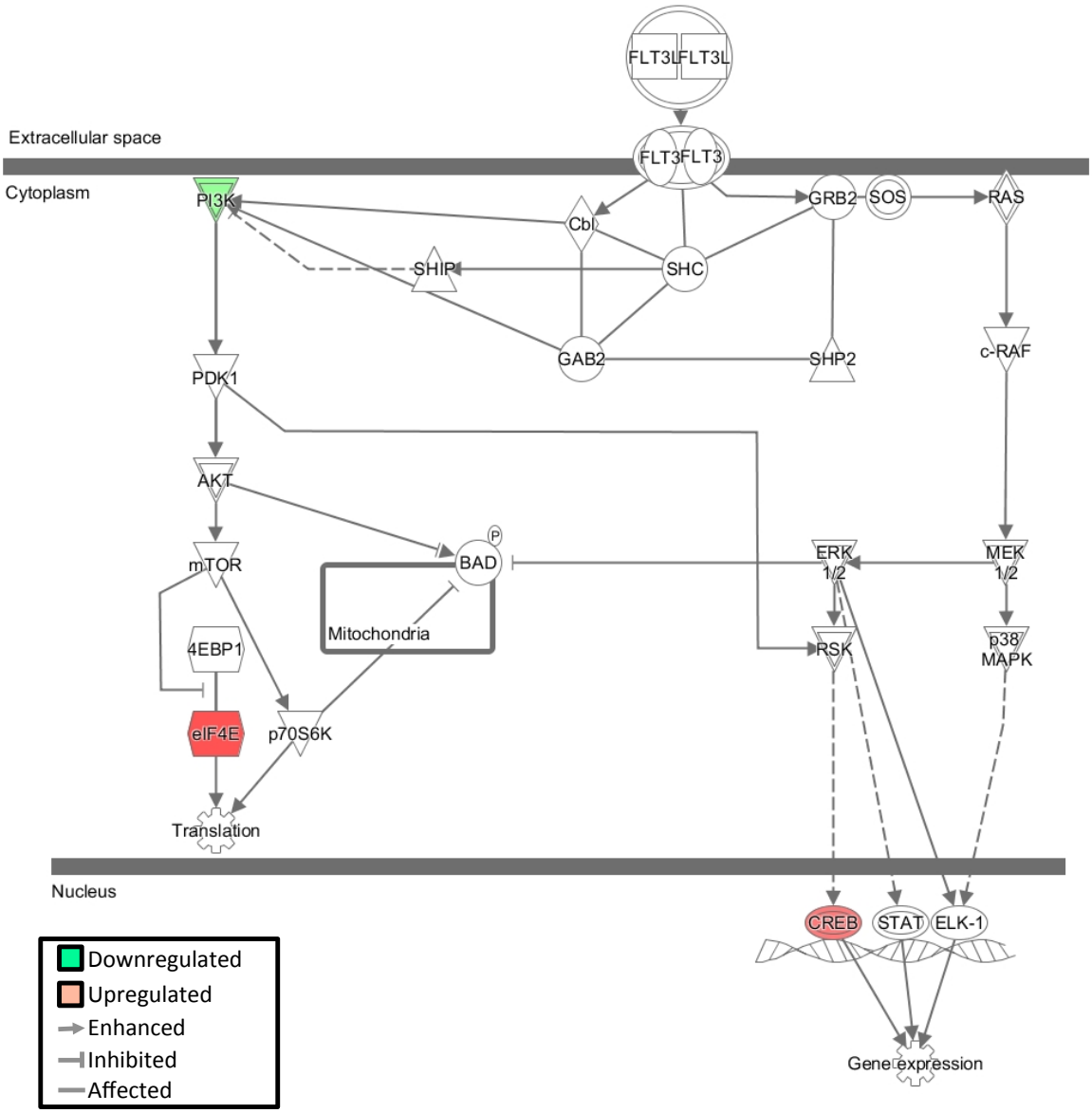

Appendix figure C(ii:5)

FLT3 signalling pathway

Responsive vs. Non-responsive 1300 mm^3 bulk

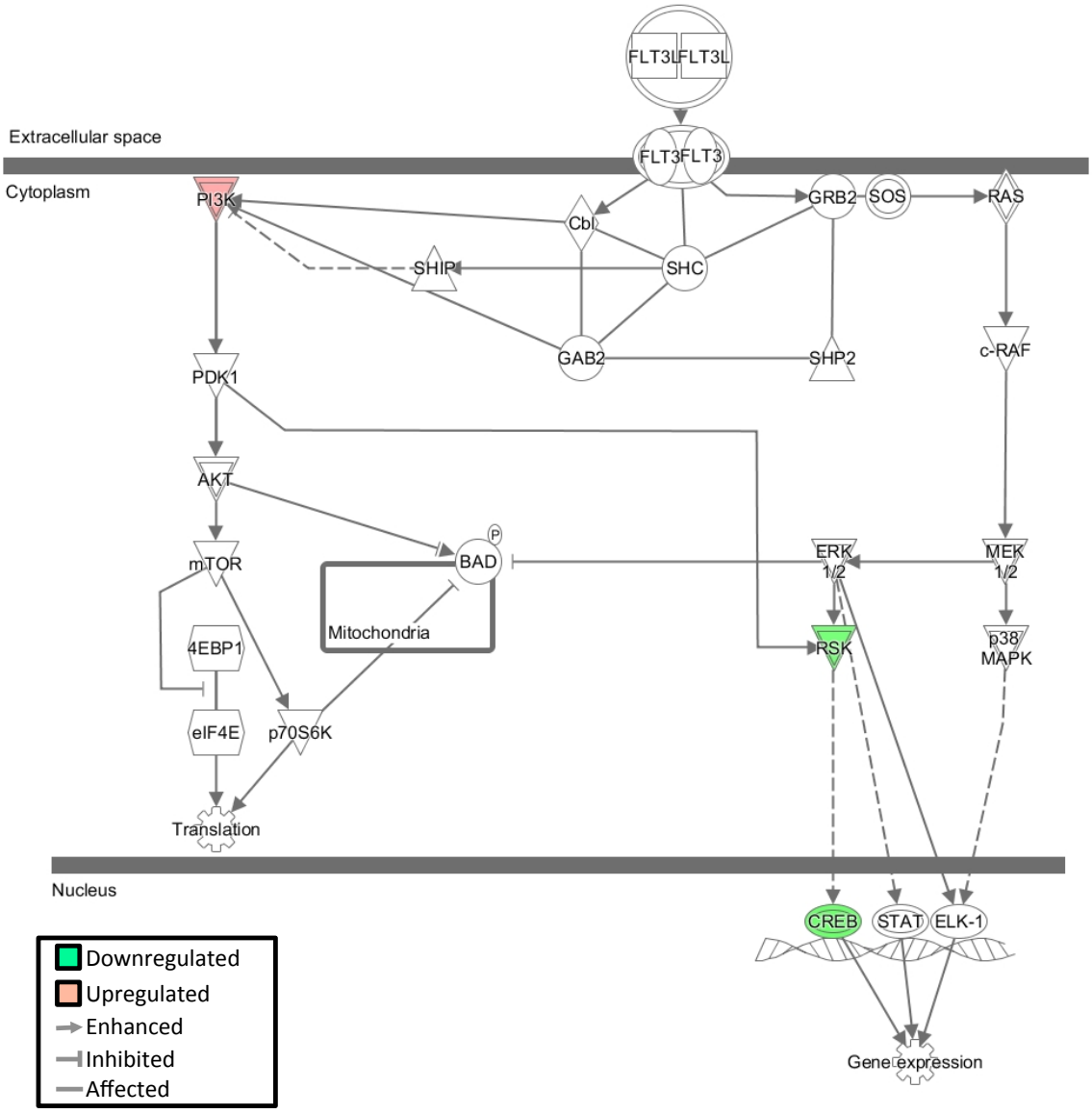

Appendix figure C(ii:6)

FLT3 signalling pathway

Responsive vs. untreated 1300 mm^3 EC

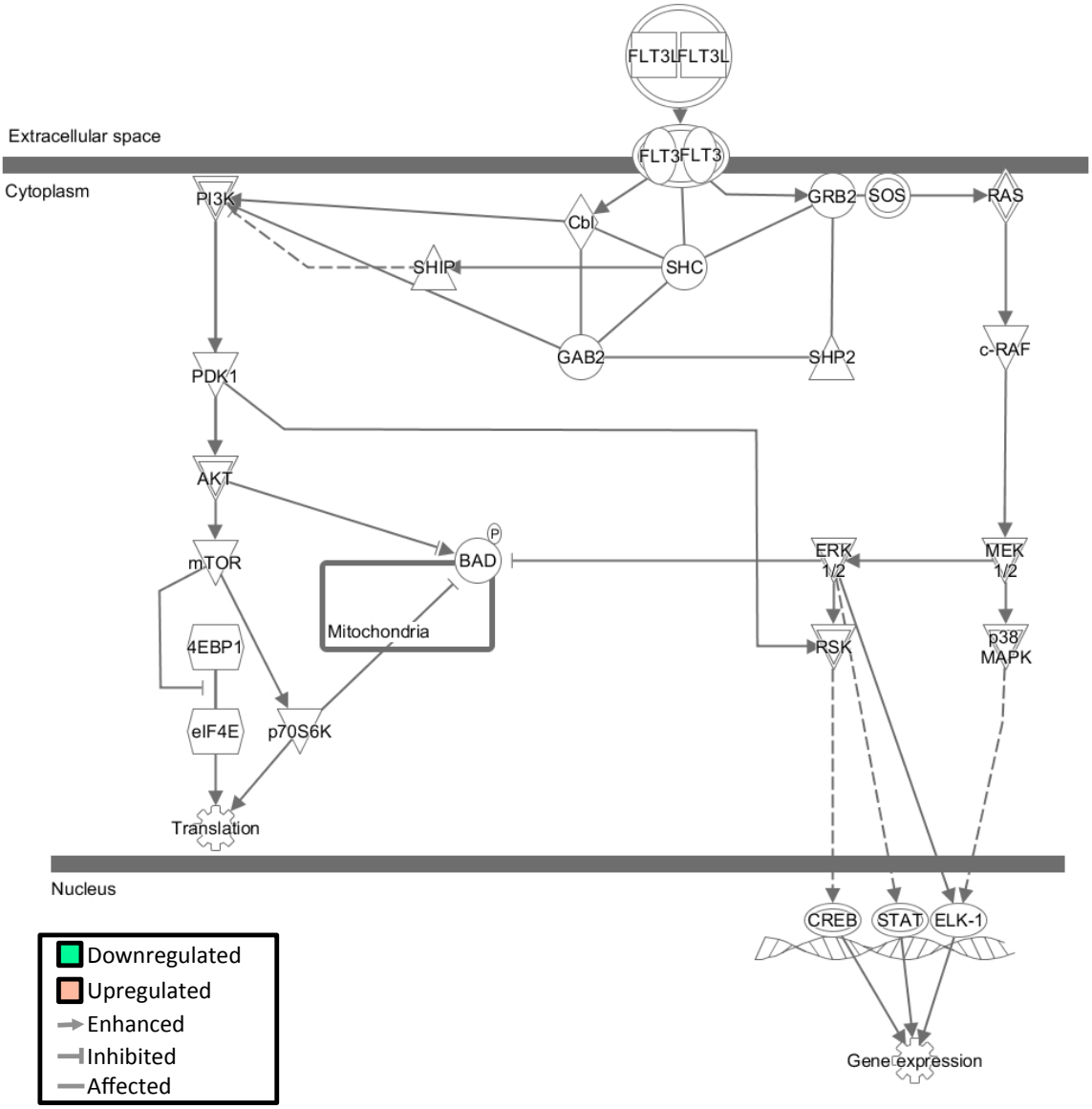

Appendix figure C(ii:7)

FLT3 signalling pathway

Non-responsive vs. untreated 1300 mm^3 EC

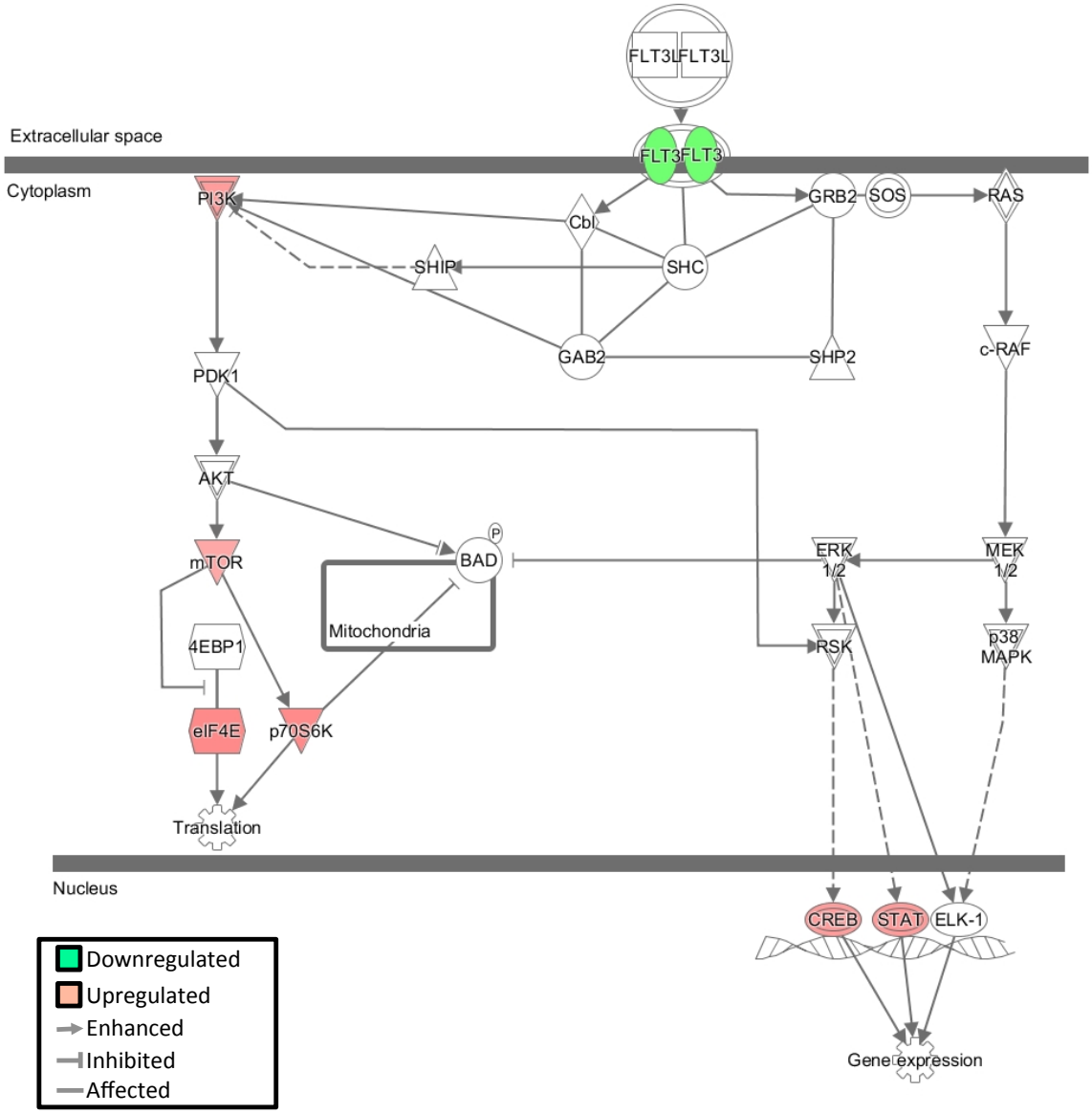

Appendix figure C(ii:8)

FLT3 signalling pathway

Responsive vs. Non-responsive 1300 mm^3 EC

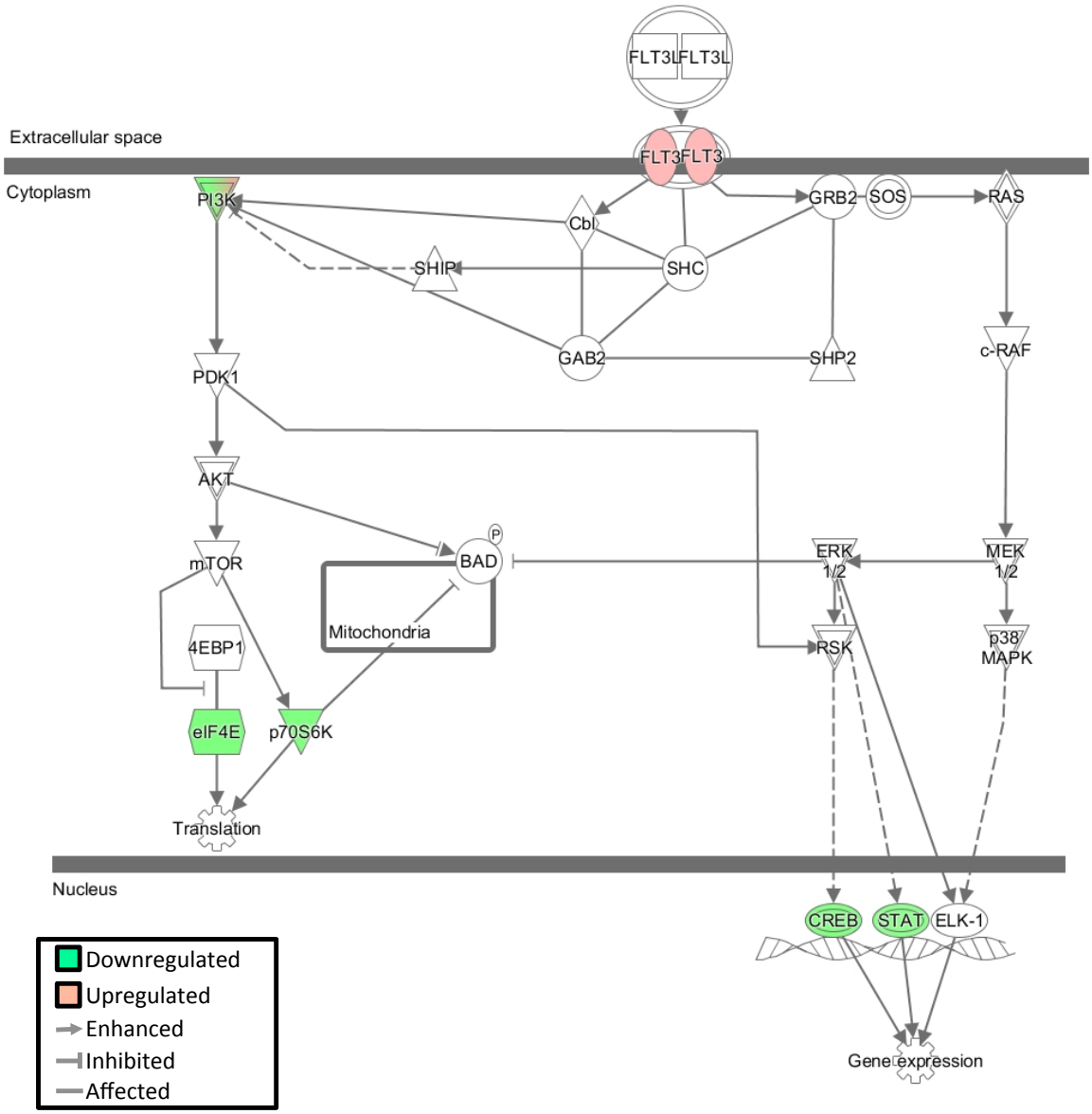

References

1. Wragg JW, Bicknell R. Vascular Targeting Approaches to Treat Cancer. In: Bae YH, Mrsny RJ, Park K, editors. Cancer Targeted Drug Delivery. New York, NY: Springer New York; 2013. pp. 59–95.

2. Bosslet K, Straub R, Blumrich M, Czech J, Gerken M, Sperker B, et al. Elucidation of the mechanism enabling tumor selective prodrug monotherapy. Cancer Res. 1998 Mar 15;58(6):1195–201.

3. Hajitou A, Pasqualini R, Arap W. Vascular targeting: recent advances and therapeutic perspectives. Trends Cardiovasc Med. Elsevier; 2006 Apr;16(3):80–8.

4. Jain RK. Transport of molecules in the tumor interstitium: a review. Cancer Res. 1987 Jun 15;47(12):3039–51.

5. Folli S, Pèlegrin A, Chalandon Y, Yao X, Buchegger F, Lienard D, et al. Tumor-necrosis factor can enhance radio-antibody uptake in human colon carcinoma xenografts by increasing vascular permeability. Int J Cancer. 1993 Mar 12;53(5):829–36.

6. Folkman J. Tumor angiogenesis: therapeutic implications. N Engl J Med. 1971 Nov 18;285(21):1182–6.

7. St Croix B, Rago C, Velculescu V, Traverso G, Romans KE, Montgomery E, et al. Genes expressed in human tumor endothelium. Science. 2000 Aug 18;289(5482):1197–202.

8. Kolonin M, Pasqualini R, Arap W. Molecular addresses in blood vessels as targets for therapy. Curr Opin Chem Biol. 2001 Jun;5(3):308–13.

9. Carmeliet P, Jain RK. Molecular mechanisms and clinical applications of angiogenesis. Nature. Nature Publishing Group; 2011 May 19;473(7347):298–307.

10. Berquin IM, Edwards IJ, Kridel SJ, Chen YQ. Polyunsaturated fatty acid metabolism in prostate cancer. Cancer Metastasis Rev. 2011 Dec;30(3-4):295–309.

11. Folkman J, Cole P, Zimmerman S. Tumor behavior in isolated perfused organs: in vitro growth and metastases of biopsy material in rabbit thyroid and canine intestinal segment. Annals of Surgery. 1966 Sep;164(3):491–502.

12. Tannock IF. Population kinetics of carcinoma cells, capillary endothelial cells, and fibroblasts in a transplanted mouse mammary tumor. Cancer Res.

American Association for Cancer Research; 1970 Oct;30(10):2470–6.

13. Konerding MA, Fait E, Gaumann A. 3D microvascular architecture of pre-cancerous lesions and invasive carcinomas of the colon. British Journal of Cancer. 2001 May 18;84(10):1354–62.

14. Siemann DW, Horsman MR. Vascular targeted therapies in oncology. Cell Tissue Res. 2009 Jan;335(1):241–8.

15. van Beijnum JR. Gene expression of tumor angiogenesis dissected: specific targeting of colon cancer angiogenic vasculature. Blood. 2006 Oct 1;108(7):2339–48.

16. Follin F. De la cryptorchidie chez l'homme. Mem Soc Biol. 1852.

17. Woglom WH. A Critique of Tumor Resistance. Cancer Res. American Association for Cancer Research; 1922 Oct 1;7(4):283–311.

18. Denekamp J, Hill SA, Hobson B. Vascular occlusion and tumour cell death. Eur J Cancer Clin Oncol. 1983 Feb;19(2):271–5.

19. Denekamp J, Hobson B. Endothelial-cell proliferation in experimental tumours. British Journal of Cancer. 1982 Nov;46(5):711–20.

20. Denekamp J. Vascular attack as a therapeutic strategy for cancer. Cancer Metastasis Rev. 1990 Nov;9(3):267–82.

21. Nihei Y, Suzuki M, Okano A, Tsuji T, Akiyama Y, Tsuruo T, et al. Evaluation of antivascular and antimitotic effects of tubulin binding agents in solid tumor therapy. Jpn J Cancer Res. 1999 Dec;90(12):1387–95.

22. Baguley BC, Holdaway KM, Thomsen LL, Zhuang L, Zwi LJ. Inhibition of growth of colon 38 adenocarcinoma by vinblastine and colchicine: evidence for a vascular mechanism. Eur J Cancer. 1991;27(4):482–7.

23. Dark GG, Hill SA, Prise VE, Tozer GM, Pettit GR, Chaplin DJ. Combretastatin A-4, an agent that displays potent and selective toxicity toward tumor vasculature. Cancer Res. 1997 May 15;57(10):1829–34.

24. Beauregard DA, Thelwall PE, Chaplin DJ, Hill SA, Adams GE, Brindle KM. Magnetic resonance imaging and spectroscopy of combretastatin A4 prodrug-induced disruption of tumour perfusion and energetic status. British Journal of Cancer. 1998 Jun;77(11):1761–7.

25. Horsman MR, Ehrnrooth E, Ladekarl M, Overgaard J. The effect of combretastatin A-4 disodium phosphate in a C3H mouse mammary carcinoma and a variety of murine spontaneous tumors. Int J Radiat Oncol Biol Phys. 1998 Nov 1;42(4):895–8.

26. Malcontenti-Wilson C, Muralidharan V, Skinner S, Christohi C, Sherris D, OBrien PE. Combretastatin A4 prodrug study of effect on the growth and the microvasculature of colorectal liver metastases in a murine model. Clin Cancer Res. 2001 Apr;7(4):1052–60.

27. Tozer GM, Prise VE, Wilson J, Locke RJ, Vojnovic B, Stratford MR, et al. Combretastatin A-4 phosphate as a tumor vascular-targeting agent: early effects in tumors and normal tissues. Cancer Res. 1999 Apr 1;59(7):1626–34.

28. Sosa JA, Elisei R, Jarzab B, Bal CS, Koussis H, Gramza AW, et al. A randomized phase II/III trial of a tumor vascular disrupting agent fosbretabulin tromethamine (CA4P) with carboplatin (C) and paclitaxel (P) in anaplastic thyroid cancer (ATC): Final survival analysis for the FACT trial. J Clin Oncol. 2011;29.

29. Blaschuk OW, Rowlands TM. Cadherins as modulators of angiogenesis and the structural integrity of blood vessels. Cancer Metastasis Rev. 2000;19(1-2):1–5.

30. Vestweber D, Winderlich M, Cagna G, Nottebaum AF. Cell adhesion dynamics at endothelial junctions: VE-cadherin as a major player. Trends in Cell Biology. 2009 Jan;19(1):8–15.

31. Kelland L. Drug evaluation: ADH-1, an N-cadherin antagonist targeting cancer vascularization. Curr Opin Mol Ther. 2007 Feb;9(1):86–91.

32. Li H, Price DK, Figg WD. ADH1, an N-cadherin inhibitor, evaluated in preclinical models of angiogenesis and androgen-independent prostate cancer. Anticancer Drugs. 2007 Jun;18(5):563–8.

33. Mariotti A, Perotti A, Sessa C, Rüegg C. Expert Opin Investig Drugs. 2007 Apr;16(4):451–65.

34. Perotti A, Sessa C, Mancuso A, Noberasco C, Cresta S, Locatelli A, et al. Clinical and pharmacological phase I evaluation of Exherin (ADH-1), a selective anti-N-cadherin peptide in patients with N-cadherin-expressing soli... - PubMed - NCBI. Annals of Oncology. 2009 Jan 19;20(4):741–5.

35. Yarom N, Stewart D, Malik R, Wells J, Avruch L, Jonker DJ. Phase I clinical trial of Exherin (ADH-1) in patients with advanced solid tumors. Curr Clin Pharmacol. 2013 Feb 1;8(1):81–8.

36. Blakey DC, Westwood FR, Walker M, Hughes GD, Davis PD, Ashton SE, et al. Antitumor activity of the novel vascular targeting agent ZD6126 in a panel of tumor models. Clin Cancer Res. 2002 Jun;8(6):1974–83.

37. Goertz DE, Yu JL, Kerbel RS, Burns PN, Foster FS. High-frequency Doppler ultrasound monitors the effects of antivascular therapy on tumor blood flow. Cancer Res. 2002 Nov 15;62(22):6371–5.

38. Davis PD, Dougherty GJ, Blakey DC, Galbraith SM, Tozer GM, Holder AL, et al. ZD6126: a novel vascular-targeting agent that causes selective destruction of tumor vasculature. Cancer Res. 2002 Dec 15;62(24):7247–53.

39. Davis IA, Kennel SJ. Radioimmunotherapy using vascular targeted 213Bi: the role of tumor necrosis factor alpha in the development of pulmonary fibrosis. Clin Cancer Res. 1999 Oct;5(10 Suppl):3160s–3164s.

40. Siemann DW, Rojiani AM. Antitumor efficacy of conventional anticancer drugs is enhanced by the vascular targeting agent ZD6126. Int J Radiat Oncol Biol Phys. 2002 Dec 1;54(5):1512–7.

41. Goto H, Yano S, Zhang H, Matsumori Y, Ogawa H, Blakey DC, et al. Activity of a new vascular targeting agent, ZD6126, in pulmonary metastases by human lung adenocarcinoma in nude mice. Cancer Res. 2002 Jul 1;62(13):3711–5.

42. Lippert JW. Vascular disrupting agents. Bioorg Med Chem. 2007 Jan 15;15(2):605–15.

43. Gould S, Westwood FR, Curwen JO, Ashton SE, Roberts DW, Lovick SC, et al. Effect of pretreatment with atenolol and nifedipine on ZD6126-induced cardiac toxicity in rats. J Natl Cancer Inst. 2007 Nov 21;99(22):1724–8.

44. Thorpe PE. Vascular targeting agents as cancer therapeutics. Clin Cancer Res. 2004 Jan 15;10(2):415–27.

45. Burrows FJ, Thorpe PE. Eradication of large solid tumors in mice with an immunotoxin directed against tumor vasculature. Proceedings of the National Academy of Sciences of the United States of America. 1993 Oct 1;90(19):8996–9000.

46. Kubitza M, Hickey L, Roberts WG. International Journal of Experimental Pathology. Wiley-Blackwell; 1999 Jan 1;80(1):1.

47. Carnemolla B, Balza E, Siri A, Zardi L, Nicotra MR, Bigotti A, et al. A tumor-associated fibronectin isoform generated by alternative splicing of messenger RNA precursors. J Cell Biol. 1989 Mar;108(3):1139–48.

48. Carnemolla B, Neri D, Castellani P, Leprini A, Neri G, Pini A, et al. Phage antibodies with pan-species recognition of the oncofoetal angiogenesis marker fibronectin ED-B domain. Int J Cancer. 1996 Nov 4;68(3):397–405.

49. Castellani P, Borsi L, Carnemolla B, Birò A, Dorcaratto A, Viale GL, et al. Differentiation between high- and low-grade astrocytoma using a human recombinant antibody to the extra domain-B of fibronectin. Am J Pathol. 2002 Nov;161(5):1695–700.

50. Neri D, Carnemolla B, Nissim A, Leprini A, Querzè G, Balza E, et al. Targeting by affinity-matured recombinant antibody fragments of an angiogenesis

associated fibronectin isoform. Nat Biotechnol. 1997 Nov;15(12):1271–5.

51. Birchler MT, Milisavlijevic D, Pfaltz M, Neri D, Odermatt B, Schmid S, et al. Expression of the extra domain B of fibronectin, a marker of angiogenesis, in head and neck tumors. Laryngoscope. John Wiley & Sons, Inc; 2003 Jul;113(7):1231–7.

52. Schliemann C, Wiedmer A, Pedretti M, Szczepanowski M, Klapper W, Neri D. Three clinical-stage tumor targeting antibodies reveal differential expression of oncofetal fibronectin and tenascin-C isoforms in human lymphoma. Leuk Res. Elsevier; 2009 Dec;33(12):1718–22.

53. Sauer S, Erba PA, Petrini M, Menrad A, Giovannoni L, Grana C, et al. Expression of the oncofetal ED-B-containing fibronectin isoform in hematologic tumors enables ED-B-targeted 131I-L19SIP radioimmunotherapy in Hodgkin lymphoma patients. Blood. 2009 Mar 5;113(10):2265–74.

54. Wallgard E, Larsson E, He L, Hellstrom M, Armulik A, Nisancioglu MH, et al. Identification of a core set of 58 gene transcripts with broad and specific expression in the microvasculature. Arteriosclerosis, Thrombosis, and Vascular Biology. 2008 Jul 23;28(8):1469–76.

55. Masiero M, Simões FC, Han HD, Snell C, Peterkin T, Bridges E, et al. A core human primary tumor angiogenesis signature identifies the endothelial orphan receptor ELTD1 as a key regulator of angiogenesis. Cancer Cell. 2013 Aug;24(2):229–41.

56. Huminiecki L, Bicknell R. In silico cloning of novel endothelial-specific genes. Genome Res. 2000 Nov;10(11):1796–806.

57. Huminiecki L, Gorn M, Suchting S, Poulsom R, Bicknell R. Magic roundabout is a new member of the roundabout receptor family that is endothelial specific and expressed at sites of active angiogenesis. Genomics. 2002 Apr;79(4):547–52.

58. Sullivan DC, Huminiecki L, Moore JW, Boyle JJ, Poulsom R, Creamer D, et al. EndoPDI, a novel protein-disulfide isomerase-like protein that is preferentially expressed in endothelial cells acts as a stress survival factor. J Biol Chem. 2003 Nov 21;278(47):47079–88.

59. Herbert JM, Stekel D, Sanderson S, Heath VL, Bicknell R. A novel method of differential gene expression analysis using multiple cDNA libraries applied to the identification of tumour endothelial genes. BMC Genomics. 2008;9(1):153.

60. Trepel M, Arap W, Pasqualini R. In vivo phage display and vascular heterogeneity: implications for targeted medicine. Curr Opin Chem Biol. 2002 Jun;6(3):399–404.

61. Arap W, Kolonin MG, Trepel M, Lahdenranta J, Cardó-Vila M, Giordano RJ, et al. Steps toward mapping the human vasculature by phage display. Nat Med. 2002

Feb;8(2):121–7.

62. Essler M, Ruoslahti E. Molecular specialization of breast vasculature: a breast-homing phage-displayed peptide binds to aminopeptidase P in breast vasculature. Proceedings of the National Academy of Sciences of the United States of America. 2002 Feb 19;99(4):2252–7.

63. Ruan W, Sassoon A, An F, Simko JP, Liu B. Identification of clinically significant tumor antigens by selecting phage antibody library on tumor cells in situ using laser capture microdissection. Mol Cell Proteomics. 2006 Dec;5(12):2364–73.

64. Mutuberria R, Satijn S, Huijbers A, Van Der Linden E, Lichtenbeld H, Chames P, et al. Isolation of human antibodies to tumor-associated endothelial cell markers by in vitro human endothelial cell selection with phage display libraries. J Immunol Methods. 2004 Apr;287(1-2):31–47.

65. Oh P, Li Y, Yu J, Durr E, Krasinska KM, Carver LA, et al. Subtractive proteomic mapping of the endothelial surface in lung and solid tumours for tissue-specific therapy. Nature. 2004 Jun 10;429(6992):629–35.

66. Rybak J-N, Ettorre A, Kaissling B, Giavazzi R, Neri D, Elia G. In vivo protein biotinylation for identification of organ-specific antigens accessible from the vasculature. Nat Meth. 2005 Apr;2(4):291–8.

67. Castronovo V, Waltregny D, Kischel P, Roesli C, Elia G, Rybak J-N, et al. A chemical proteomics approach for the identification of accessible antigens expressed in human kidney cancer. Mol Cell Proteomics. 2006 Nov;5(11):2083–91.

68. Sana TR, Janatpour MJ, Sathe M, McEvoy LM, McClanahan TK. Microarray analysis of primary endothelial cells challenged with different inflammatory and immune cytokines. Cytokine. 2005 Feb 17.

69. Engelse MA, Laurens N, Verloop RE, Koolwijk P, van Hinsbergh VWM. Differential gene expression analysis of tubule forming and non-tubule forming endothelial cells: CDC42GAP as a counter-regulator in tubule formation. Angiogenesis. Springer Netherlands; 11(2):153–67.

70. Wragg JW, Durant S, McGettrick HM, Sample KM, Egginton S, Bicknell R. Shear stress regulated gene expression and angiogenesis in vascular endothelium. Microcirculation. 2014 May 22;21(4):290–300.

71. Sumanas S, Jorniak T, Lin S. Identification of novel vascular endothelial-specific genes by the microarray analysis of the zebrafish cloche mutants. Blood. 2005 Jul 15;106(2):534–41.

72. Weber GJ, Choe SE, Dooley KA, Paffett-Lugassy NN, Zhou Y, Zon LI. Mutant-specific gene programs in the zebrafish. Blood. 2005 Jul 15;106(2):521–30.

73. del Toro R, Prahst C, Mathivet T, Siegfried G, Kaminker JS, Larrivee B, et al. Identification and functional analysis of endothelial tip cell-enriched genes. Blood. 2010 Nov 11;116(19):4025–33.

74. Carson-Walter EB, Watkins DN, Nanda A, Vogelstein B, Kinzler KW, St Croix B. Cell surface tumor endothelial markers are conserved in mice and humans. Cancer Res. 2001 Sep 15;61(18):6649–55.

75. St Croix B, Rago C, Velculescu V, Traverso G, Romans KE, Montgomery E, et al. Genes expressed in human tumor endothelium. Science. 2000 Aug 18;289(5482):1197–202.

76. Seaman S, Stevens J, Yang MY, Logsdon D, Graff-Cherry C, St Croix B. Genes that distinguish physiological and pathological angiogenesis. Cancer Cell. Elsevier; 2007 Jun;11(6):539–54.

77. Zhang HT, Gorn M, Smith K, Graham AP, Lau KK, Bicknell R. Transcriptional profiling of human microvascular endothelial cells in the proliferative and quiescent state using cDNA arrays. Angiogenesis. 1999;3(3):211–9.

78. Ho M, Yang E, Matcuk G, Deng D, Sampas N, Tsalenko A, et al. Identification of endothelial cell genes by combined database mining and microarray analysis. Physiol Genomics. 2003 May 13;13(3):249–62.

79. Ghilardi C, Chiorino G, Dossi R, Nagy Z, Giavazzi R, Bani M. Identification of novel vascular markers through gene expression profiling of tumor-derived endothelium. BMC Genomics. BioMed Central Ltd; 2008 Apr 30;9(1):201.

80. Zhuang X, Herbert JMJ, Lodhia P, Bradford J, Turner AM, Newby PM, et al. Identification of novel vascular targets in lung cancer. British Journal of Cancer. 2014 Dec 23;112(3):485–94.

81. Lohr M, Haas S, Bechstein W, Karrasch M, Mescheder A, Meyer I, et al. First-line treatment of inoperable pancreatic adenocarcinoma with lipid complexed paclitaxel nanoparticles plus gemcitabine compared with gemcitabine monotherapy. A prospective RCT - phase II study. ASCO Meeting Abstracts. 2008 May 20;26(15_suppl):4618.

82. Awada A, Bondarenko IN, Bonneterre J, Nowara E, Ferrero JM, Bakshi AV, et al. A randomized controlled phase II trial of a novel composition of paclitaxel embedded into neutral and cationic lipids targeting tumor endothelial cells in advanced triple-negative breast cancer (TNBC). Annals of Oncology. 2014 Mar 25;25(4):824–31.

83. Carnemolla B, Borsi L, Balza E, Castellani P, Meazza R, Berndt A, et al. Enhancement of the antitumor properties of interleukin-2 by its targeted delivery to the tumor blood vessel extracellular matrix. Blood. 2002 Mar 1;99(5):1659–65.

84. Wagner K, Schulz P, Scholz A, Wiedenmann B, Menrad A. The targeted immunocytokine L19-IL2 efficiently inhibits the growth of orthotopic pancreatic cancer. Clinical Cancer Research. 2008 Aug 1;14(15):4951–60.

85. Johannsen M, Roemer A, Spitaleri G, Curigliano G, Giovannoni L, Menssen HD, et al. Phase I/II study of the tumor-targeting human L19-IL2 monoclonal antibody-cytokine fusion protein in patients with advanced renal cell carcinoma. ASCO Meeting Abstracts. 2008 May 20;26(15_suppl):16032.

86. Weide B, Eigentler TK, Romanini A, de Braud FG, Giovannoni L, Neri D, et al. Tumor-targeting human L19IL2 monoclonal antibody-cytokine fusion protein in combination with DTIC in chemotherapy-naïve stage IV melanoma patients. ASCO Annual Meeting. 2010 [cited 2015 Sep 11]. Available from: http://meetinglibrary.asco.org/content/41442-74

87. Nilsson F, Kosmehl H, Zardi L, Neri D. Targeted delivery of tissue factor to the ED-B domain of fibronectin, a marker of angiogenesis, mediates the infarction of solid tumors in mice. Cancer Res. 2001 Jan 15;61(2):711–6.

88. Gafner V, Trachsel E, Neri D. An engineered antibody-interleukin-12 fusion protein with enhanced tumor vascular targeting properties. Int J Cancer. 2006 Nov 1;119(9):2205–12.

89. Villa A, Trachsel E, Kaspar M, Schliemann C, Sommavilla R, Rybak J-N, et al. A high-affinity human monoclonal antibody specific to the alternatively spliced EDA domain of fibronectin efficiently targets tumor neo-vasculature in vivo. Int J Cancer. 2008 Jun 1;122(11):2405–13.

90. Fonsatti E, Altomonte M, Arslan P, Maio M. Endoglin (CD105): a target for anti-angiogenetic cancer therapy. Curr Drug Targets. 2003 May;4(4):291–6.

91. Brack SS, Silacci M, Birchler M, Neri D. Tumor-targeting properties of novel antibodies specific to the large isoform of tenascin-C. Clin Cancer Res. 2006 May 15;12(10):3200–8.

92. Liu C, Huang H, Doñate F, Dickinson C, Santucci R, El-Sheikh A, et al. Prostate-specific membrane antigen directed selective thrombotic infarction of tumors. Cancer Res. 2002 Oct 1;62(19):5470–5.

93. Tsunoda S, Ohizumi I, Matsui J, Koizumi K, Wakai Y, Makimoto H, et al. Specific binding of TES-23 antibody to tumour vascular endothelium in mice, rats and human cancer tissue: a novel drug carrier for cancer targeting therapy. British Journal of Cancer. 1999 Dec;81(7):1155–61.

94. Koivunen E, Pasqualini R, Arap W, Valtanen H, Rainisalo A, Medina OP, et al. Tumor targeting with a selective gelatinase inhibitor. Nat Biotechnol. 1999 Aug 1;17(8):768–74.

95. Zhaofei Liu FWXC. Integrin αvβ3-Targeted Cancer Therapy. Drug development

research. NIH Public Access; 2008;69(6):329.

96. Ran S, Gao B, Duffy S, Watkins L, Rote N, Thorpe PE. Infarction of solid Hodgkin's tumors in mice by antibody-directed targeting of tissue factor to tumor vasculature. Cancer Res. 1998 Oct 15;58(20):4646–53.

97. Bhaskar V, Law DA, Ibsen E, Breinberg D, Cass KM, DuBridge RB, et al. E-selectin up-regulation allows for targeted drug delivery in prostate cancer. Cancer Res. 2003 Oct 1;63(19):6387–94.

98. Rho S-S, Choi H-J, Min J-K, Lee H-W, Park H, Park H, et al. Clec14a is specifically expressed in endothelial cells and mediates cell to cell adhesion. Biochemical and Biophysical Research Communications. 2011 Jan;404(1):103–8.

99. Mura M, Swain RK, Zhuang X, Vorschmitt H, Reynolds G, Durant S, et al. Identification and angiogenic role of the novel tumor endothelial marker CLEC14A. Oncogene. 2012 Jan 19;31(3):293–305.

100. Brady J, Neal J, Sadakar N, Gasque P. Human endosialin (tumor endothelial marker 1) is abundantly expressed in highly malignant and invasive brain tumors. J Neuropathol Exp Neurol. 2004 Dec;63(12):1274–83.

101. Ran S, He J, Huang X, Soares M, Scothorn D, Thorpe PE. Antitumor effects of a monoclonal antibody that binds anionic phospholipids on the surface of tumor blood vessels in mice. Clin Cancer Res. 2005 Feb 15;11(4):1551–62.

102. Hu Z, Sun Y, Garen A. Targeting tumor vasculature endothelial cells and tumor cells for immunotherapy of human melanoma in a mouse xenograft model. Proceedings of the National Academy of Sciences of the United States of America. 1999 Jul 6;96(14):8161–6.

103. Huang X, Molema G, King S, Watkins L, Edgington TS, Thorpe PE. Tumor infarction in mice by antibody-directed targeting of tissue factor to tumor vasculature. Science. 1997 Jan 24;275(5299):547–50.

104. Ramakrishnan S, Olson TA, Bautch VL, Mohanraj D. Vascular endothelial growth factor-toxin conjugate specifically inhibits KDR/flk-1-positive endothelial cell proliferation in vitro and angiogenesis in vivo. Cancer Res. 1996 Mar 15;56(6):1324–30.

105. Arora N, Masood R, Zheng T, Cai J, Smith DL, Gill PS. Vascular endothelial growth factor chimeric toxin is highly active against endothelial cells. Cancer Res. 1999 Jan 1;59(1):183–8.

106. Zhang Y-F, Wang J-C, Bian D-Y, Zhang X, Zhang Q. Targeted delivery of RGD-modified liposomes encapsulating both combretastatin A-4 and doxorubicin for tumor therapy: in vitro and in vivo studies. European Journal of Pharmaceutics and Biopharmaceutics. 2010 Mar;74(3):467–73.

107. Schuch G. EndoTAG-1. MediGene. Curr Opin Investig Drugs. 2005 Dec;6(12):1259–65.

108. Corti A, Ponzoni M. Tumor vascular targeting with tumor necrosis factor alpha and chemotherapeutic drugs. Ann N Y Acad Sci. 2004 Dec;1028:104–12.

109. Hood JD, Cheresh DA. Targeted delivery of mutant Raf kinase to neovessels causes tumor regression. Cold Spring Harb Symp Quant Biol. 2002;67:285–91.

110. Arap W, Haedicke W, Bernasconi M, Kain R, Rajotte D, Krajewski S, et al. Targeting the prostate for destruction through a vascular address. Proceedings of the National Academy of Sciences of the United States of America. 2002 Feb 5;99(3):1527–31.

111. Tijink BM, Neri D, Leemans CR, Budde M, Dinkelborg LM, Stigter-van Walsum M, et al. Radioimmunotherapy of head and neck cancer xenografts using 131I-labeled antibody L19-SIP for selective targeting of tumor vasculature. J Nucl Med. 2006 Jul;47(7):1127–35.

112. Kennel SJ, Chappell LL, Dadachova K, Brechbiel MW, Lankford TK, Davis IA, et al. Evaluation of 225Ac for vascular targeted radioimmunotherapy of lung tumors. Cancer Biotherapy & Radiopharmaceuticals. 2000 Jun;15(3):235–44.

113. Fukumura D, Xavier R, Sugiura T, Chen Y, Park EC, Lu N, et al. Tumor induction of VEGF promoter activity in stromal cells. Cell. 1998 Sep 18;94(6):715–25.

114. Tonini T, Rossi F, Claudio PP. Molecular basis of angiogenesis and cancer. - Google Search. Oncogene. 2003 Sep 29;22(42):6549–56.

115. Carmeliet P, Jain RK. Angiogenesis in cancer and other diseases. Nature. 2000 Sep 14;407(6801):249–57.

116. Erber R. Combined inhibition of VEGF and PDGF signaling enforces tumor vessel regression by interfering with pericyte-mediated endothelial cell survival mechanisms. FASEB J. Federation of American Societies for Experimental Biology; 2004 Feb;18(2):338–40.

117. Carmeliet P, Dor Y, Herbert JM, Fukumura D, Brusselmans K, Dewerchin M, et al. Role of HIF-1alpha in hypoxia-mediated apoptosis, cell proliferation and tumour angiogenesis. Nature. 1998 Jul 30;394(6692):485–90.

118. Semenza GL. Hypoxia-inducible factor 1: master regulator of O2 homeostasis. Curr Opin Genet Dev. 1998 Oct;8(5):588–94.

119. Siemann DW. Vascular targeting agents. Horizons in Cancer Therapeutics From Bench to Bedside. 2002;3(2):4–15.

120. Folkman J. Anti-angiogenesis: new concept for therapy of solid tumors. Annals of Surgery. 1972 Mar;175(3):409–16.

121. Presta LG, Chen H, O'Connor SJ, Chisholm V, Meng YG, Krummen L, et al. Humanization of an anti-vascular endothelial growth factor monoclonal antibody for the therapy of solid tumors and other disorders. Cancer Res. 1997 Oct 15;57(20):4593–9.

122. Muller YA, Chen Y, Christinger HW, Li B, Cunningham BC, Lowman HB, et al. VEGF and the Fab fragment of a humanized neutralizing antibody: crystal structure of the complex at 2.4 å resolution and mutational analysis of the interface. Structure. Elsevier; 1998 Sep;6(9):1153–67.

123. Yang JC, Haworth L, Sherry RM, Hwu P, Schwartzentruber DJ, Topalian SL, et al. A randomized trial of bevacizumab, an anti-vascular endothelial growth factor antibody, for metastatic renal cancer. N Engl J Med. 2003 Jul 31;349(5):427–34.

124. Hurwitz H, Fehrenbacher L, Novotny W, Cartwright T, Hainsworth J, Heim W, et al. Bevacizumab plus irinotecan, fluorouracil, and leucovorin for metastatic colorectal cancer. N Engl J Med. 2004 Jun 3;350(23):2335–42.

125. Miller K, Wang M, Gralow J, Dickler M, Cobleigh M, Perez EA, et al. Paclitaxel plus Bevacizumab versus Paclitaxel Alone for Metastatic Breast Cancer. N Engl J Med. 2007 Dec 27;357(26):2666–76.

126. Sandler A, Gray R, Perry MC, Brahmer J, Schiller JH, Dowlati A, et al. Paclitaxel-carboplatin alone or with bevacizumab for non-small-cell lung cancer. N Engl J Med. 2006 Dec 14;355(24):2542–50.

127. Jain RK. Normalizing tumor vasculature with anti-angiogenic therapy: A new paradigm for combination therapy. Nat Med. Nature Publishing Group; 2001 Sep 1;7(9):987–9.

128. Carmeliet P, Jain RK. Principles and mechanisms of vessel normalization for cancer and other angiogenic diseases. Nature Reviews Drug Discovery. Nature Publishing Group; 2011 Jun 1;10(6):417–27.

129. Goel S, Wong AH-K, Jain RK. Vascular normalization as a therapeutic strategy for malignant and nonmalignant disease. Cold Spring Harb Perspect Med. 2012 Mar;2(3):a006486.

130. Duda DG, Willett CG, Ancukiewicz M, di Tomaso E, Shah M, Czito BG, et al. Plasma soluble VEGFR-1 is a potential dual biomarker of response and toxicity for bevacizumab with chemoradiation in locally advanced rectal cancer. The Oncologist. AlphaMed Press; 2010;15(6):577–83.

131. Van der Veldt AAM, Lubberink M, Bahce I, Walraven M, de Boer MP, Greuter HNJM, et al. Rapid decrease in delivery of chemotherapy to tumors after anti-VEGF therapy: implications for scheduling of anti-angiogenic drugs. Cancer Cell. 2012 Jan;21(1):82–91.

132. Riley K. Press Announcements - FDA Commissioner announces Avastin decision.

2011 [cited 2016 Feb 13]. Available from: http://www.fda.gov/NewsEvents/Newsroom/PressAnnouncements/ucm280536.htm

133. Prewett M, Huber J, Li Y, Santiago A, O'Connor W, King K, et al. Antivascular endothelial growth factor receptor (fetal liver kinase 1) monoclonal antibody inhibits tumor angiogenesis and growth of several mouse and human tumors. Cancer Res. 1999 Oct 15;59(20):5209–18.

134. Kunkel P, Ulbricht U, Bohlen P, Brockmann MA, Fillbrandt R, Stavrou D, et al. Inhibition of glioma angiogenesis and growth in vivo by systemic treatment with a monoclonal antibody against vascular endothelial growth factor receptor-2. Cancer Res. 2001 Sep 15;61(18):6624–8.

135. Sweeney P, Karashima T, Kim S-J, Kedar D, Mian B, Huang S, et al. Anti-vascular endothelial growth factor receptor 2 antibody reduces tumorigenicity and metastasis in orthotopic prostate cancer xenografts via induction of endothelial cell apoptosis and reduction of endothelial cell matrix metalloproteinase type 9 production. Clin Cancer Res. 2002 Aug;8(8):2714–24.

136. Wilke H, Clingan P, Ananda S, Kurteva G, Suuroja T, Folprecht G, et al. RAINBOW: A global, phase III, randomized, double-blind study of ramucirumab plus paclitaxel versus placebo plus paclitaxel in the treatment of metastatic gastroesophageal junction (GEJ) and gastric adenocarcinoma following disease progression on first-line platinum- and fluoropyrimidine-containing combination therapy rainbow IMCL CP12-0922 (I4T-IE-JVBE). Annals of Oncology. Oxford University Press; 2014 Jun 17;25(suppl 2):ii106–7.

137. Fuchs CS, Tomasek J, Cho JY, Filip D, Passalacqua R, Goswami C, et al. Abstract LB-67: REGARD: A phase III, randomized, double-blind trial of ramucirumab and best supportive care (BSC) versus placebo and BSC in the treatment of metastatic gastric or gastroesophageal junction (GEJ) adenocarcinoma following disease progression on first-line p. Cancer Res. 2014 Nov 18;73(8 Supplement):LB–67–LB–67.

138. Garon EB, Ciuleanu TE, Arrieta O, Prabhash K, Syrigos KN, Goksel T, et al. Ramucirumab plus docetaxel versus placebo plus docetaxel for second-line treatment of stage IV non-small-cell lung cancer after disease progression on platinum-based therapy (REVEL): a multicentre, double-blind, randomised phase 3 trial. The Lancet. Elsevier; 2014 Aug;384(9944):665–73.

139. Holash J, Davis S, Papadopoulos N, Croll SD, Ho L, Russell M, et al. VEGF-Trap: A VEGF blocker with potent antitumor effects. PNAS. National Acad Sciences; 2002 Aug 20;99(17):11393–8.

140. Saishin Y, Saishin Y, Takahashi K, Lima e Silva R, Hylton D, Rudge JS, et al. VEGF-TRAP(R1R2) suppresses choroidal neovascularization and VEGF-induced breakdown of the blood-retinal barrier. J Cell Physiol. 2003 May;195(2):241–8.

141. Browning DJ, Kaiser PK, Rosenfeld PJ, Stewart MW. Aflibercept for age-related macular degeneration: a game-changer or quiet addition? Am J Ophthalmol. 2012 Aug;154(2):222–6.

142. Ramlau R, Gorbunova V, Ciuleanu TE, Novello S, Ozguroglu M, Goksel T, et al. Aflibercept and Docetaxel versus Docetaxel alone after platinum failure in patients with advanced or metastatic non-small-cell lung cancer: a randomized, controlled phase III trial. JCO. 2012 Oct 10;30(29):3640–7.

143. Wang T-F, Lockhart AC. Aflibercept in the treatment of metastatic colorectal cancer. Clin Med Insights Oncol. 2012;6:19–30.

144. Van Cutsem E, Tabernero J, Lakomy R, Prenen H, Prausová J, Macarulla T, et al. Addition of aflibercept to fluorouracil, leucovorin, and irinotecan improves survival in a phase III randomized trial in patients with metastatic colorectal cancer previously treated with an oxaliplatin-based regimen. J Clin Oncol. 2012 Oct 1;30(28):3499–506.

145. Kumar R, Harrington LE, Hopper TM, Miller CG, Onori JA, Cheung M, et al. Correlation of anti-tumor and anti-angiogenic activity of VEGFR inhibitors with inhibition of VEGFR2 phosphorylation in mice. ASCO Meeting Abstracts. 2005 Jun 1;23(16_suppl):9537.

146. Batchelor TT, Sorensen AG, di Tomaso E, Zhang W-T, Duda DG, Cohen KS, et al. AZD2171, a pan-VEGF receptor tyrosine kinase inhibitor, normalizes tumor vasculature and alleviates edema in glioblastoma patients. Cancer Cell. 2007 Jan;11(1):83–95.

147. Taguchi E, Nakamura K, Miura T, Shibuya M, Isoe T. Cancer Science. 2008 Mar;99(3):623–30.

148. Zhou Q, Gallo JM. Differential effect of sunitinib on the distribution of temozolomide in an orthotopic glioma model. Neuro-Oncology. Oxford University Press; 2009 Jun 8;11(3):301–10.

149. Bergers G, Hanahan D. Modes of resistance to anti-angiogenic therapy. Nat Rev Cancer. 2008 Aug;8(8):592–603.

150. Ebos JML, Lee CR, Cruz-Munoz W, Bjarnason GA, Christensen JG, Kerbel RS. Accelerated Metastasis after Short-Term Treatment with a Potent Inhibitor of Tumor Angiogenesis. Cancer Cell. 2009 Mar;15(3):232–9.

151. Pàez-Ribes M, Allen E, Hudock J, Takeda T, Okuyama H, Viñals F, et al. Cancer Cell. 2009 Mar;15(3):220–31.

152. Miller KD, Burstein HJ, Elias AD, Rugo HS, Cobleigh MA, Pegram MD, et al. Phase II study of SU11248, a multitargeted receptor tyrosine kinase inhibitor (TKI), in patients (pts) with previously treated metastatic breast cancer (MBC). ASCO Meeting Abstracts. 2005 Jun 1;23(16_suppl):563.

153. Saltz LB, Lenz H-J, Kindler HL, Hochster HS, Wadler S, Hoff PM, et al. Randomized phase II trial of cetuximab, bevacizumab, and irinotecan compared with cetuximab and bevacizumab alone in irinotecan-refractory colorectal cancer: the BOND-2 study. J Clin Oncol. 2007 Oct 10;25(29):4557–61.

154. Kindler HL, Karrison TG, Gandara DR, Lu C, Krug LM, Stevenson JP, et al. Multicenter, double-blind, placebo-controlled, randomized phase II trial of gemcitabine/cisplatin plus bevacizumab or placebo in patients with malignant mesothelioma. JCO. 2012 Jul 10;30(20):2509–15.

155. Kerbel RS, Yu J, Tran J, Man S, Viloria-Petit A, Klement G, et al. Possible mechanisms of acquired resistance to anti-angiogenic drugs: implications for the use of combination therapy approaches. Cancer Metastasis Rev. 2001;20(1-2):79–86.

156. Casanovas O, Hicklin DJ, Bergers G, Hanahan D. Drug resistance by evasion of antiangiogenic targeting of VEGF signaling in late-stage pancreatic islet tumors. Cancer Cell. 2005 Oct;8(4):299–309.

157. Allen E, Walters IB, Hanahan D. Brivanib, a dual FGF/VEGF inhibitor, is active both first and second line against mouse pancreatic neuroendocrine tumors developing adaptive/evasive resistance to VEGF inhibition. Clin Cancer Res. 2011 Aug 15;17(16):5299–310.

158. Llovet JM, Decaens T, Raoul JL, Boucher E, Kudo M, Chang C, et al. Brivanib in patients with advanced hepatocellular carcinoma who were intolerant to sorafenib or for whom sorafenib failed: results from the randomized phase III BRISK-PS study. JCO. American Society of Clinical Oncology; 2013 Oct 1;31(28):3509–16.

159. Mizukami Y, Jo W-S, Duerr E-M, Gala M, Li J, Zhang X, et al. Induction of interleukin-8 preserves the angiogenic response in HIF-1alpha-deficient colon cancer cells. Nat Med. 2005 Sep;11(9):992–7.

160. Fernando NT, Koch M, Rothrock C, Gollogly LK, D'Amore PA, Ryeom S, et al. Tumor escape from endogenous, extracellular matrix-associated angiogenesis inhibitors by up-regulation of multiple proangiogenic factors. Clin Cancer Res. 2008 Mar 1;14(5):1529–39.

161. Hattori K, Heissig B, Wu Y, Dias S, Tejada R, Ferris B, et al. Placental growth factor reconstitutes hematopoiesis by recruiting VEGFR1(+) stem cells from bone-marrow microenvironment. Nat Med. 2002 Aug;8(8):841–9.

162. Kaplan RN, Riba RD, Zacharoulis S, Bramley AH, Vincent L, Costa C, et al. Nature. 2005 Dec 8;438(7069):820–7.

163. Bergers G, Song S, Meyer-Morse N, Bergsland E, Hanahan D. J Clin Invest. 2003 May 1;111(9):1287–95.

164. Jain RK, Booth MF. What brings pericytes to tumor vessels? - PubMed - NCBI. J Clin Invest. 2003 Oct 15;112(8):1134–6.

165. Benjamin LE, Hemo I, Keshet E. A plasticity window for blood vessel remodelling is defined by pericyte coverage of the preformed endothelial network and is regulated by PDGF-B and VEGF. Development. 1998 May;125(9):1591–8.

166. Rubenstein JL, Kim J, Ozawa T, Zhang M, Westphal M, Deen DF, et al. Anti-VEGF antibody treatment of glioblastoma prolongs survival but results in increased vascular cooption. Neoplasia. 2000 Jul;2(4):306–14.

167. Blouw B, Song H, Tihan T, Bosze J, Ferrara N, Gerber HP, et al. The hypoxic response of tumors is dependent on their microenvironment. Cancer Cell. 2003 Aug;4(2):133–46.

168. Du R, Lu KV, Petritsch C, Liu P, Ganss R, Passegué E, et al. HIF1α Induces the Recruitment of Bone Marrow-Derived Vascular Modulatory Cells to Regulate Tumor Angiogenesis and Invasion. Cancer Cell. 2008 Mar;13(3):206–20.

169. Norden AD, Young GS, Setayesh K, Muzikansky A, Klufas R, Ross GL, et al. Bevacizumab for recurrent malignant gliomas: efficacy, toxicity, and patterns of recurrence. - PubMed - NCBI. Neurology. 2008 Mar 3;70(10):779–87.

170. Narayana A, Kelly P, Golfinos J, Parker E, Johnson G, Knopp E, et al. Antiangiogenic therapy using bevacizumab in recurrent high-grade glioma: impact on local control and patient survival. J Neurosurg. 2009 Jan;110(1):173–80.

171. Leenders WPJ, Küsters B, de Waal RMW. Vessel co-option: how tumors obtain blood supply in the absence of sprouting angiogenesis. Endothelium. 2002;9(2):83–7.

172. Donnem T, Hu J, Ferguson M, Adighibe O, Snell C, Harris AL, et al. Vessel co-option in primary human tumors and metastases: an obstacle to effective anti-angiogenic treatment? Cancer Medicine. 2013 Jul 8;2(4):427–36.

173. Frentzas S, Thompson VL, Vermeulen PB, Foo S, Brown G, Cunningham D, et al. Abstract 2997: Vessel co-option in colorectal cancer liver metastases mediates resistance to VEGF-targeted therapy. Cancer Res. American Association for Cancer Research; 2014 Oct 1;74(19 Supplement):2997–7.

174. Welti JC, Powles T, Foo S, Gourlaouen M, Preece N, Foster J, et al. Contrasting effects of sunitinib within in vivo models of metastasis. Angiogenesis. 2012 Jul 28;15(4):623–41.

175. Singh M, Couto SS, Forrest WF, Lima A, Cheng JH, Molina R, et al. Anti-VEGF antibody therapy does not promote metastasis in genetically engineered mouse tumour models. J Pathol. 2012 Jun 28;227(4):417–30.

176. Chung AS, Kowanetz M, Wu X, Zhuang G, Ngu H, Finkle D, et al. Differential drug class-specific metastatic effects following treatment with a panel of angiogenesis inhibitors. J Pathol. John Wiley & Sons, Ltd; 2012 Jul 3;227(4):404–16.

177. Blagoev KB, Wilkerson J, Stein WD, Motzer RJ, Bates SE, Fojo AT. Sunitinib does not accelerate tumor growth in patients with metastatic renal cell carcinoma. Cell Rep. Elsevier; 2013 Feb 21;3(2):277–81.

178. Xiong Y-Q, Sun H-C, Zhang W, Zhu X-D, Zhuang P-Y, Zhang J-B, et al. Human hepatocellular carcinoma tumor-derived endothelial cells manifest increased angiogenesis capability and drug resistance compared with normal endothelial cells. Clin Cancer Res. American Association for Cancer Research; 2009 Aug 1;15(15):4838–46.

179. McIntyre A, Harris AL. Metabolic and hypoxic adaptation to anti-angiogenic therapy: a target for induced essentiality. EMBO Mol Med. 2015 Apr;7(4):368–79.

180. Rouschop KM, Dubois LJ, Keulers TG, van den Beucken T, Lambin P, Bussink J, et al. PERK/eIF2α signaling protects therapy resistant hypoxic cells through induction of glutathione synthesis and protection against ROS. PNAS. 2013 Mar 19;110(12):4622–7.

181. Pike LRG, Phadwal K, Simon AK, Harris AL. ATF4 orchestrates a program of BH3-only protein expression in severe hypoxia. Mol Biol Rep. 2012 Oct 23;39(12):10811–22.

182. Kumar K, Wigfield S, Gee HE, Devlin CM, Singleton D, Li J-L, et al. Dichloroacetate reverses the hypoxic adaptation to bevacizumab and enhances its antitumor effects in mouse xenografts. J Mol Med. 2013 Jan 30;91(6):749–58.

183. Hu YL, Jahangiri A, DeLay M, Aghi MK. Tumor cell autophagy as an adaptive response mediating resistance to treatments such as antiangiogenic therapy. Cancer Res. American Association for Cancer Research; 2012 Aug 30;72(17):4294–9.

184. Sounni NE, Cimino J, Blacher S, Primac I, Truong A, Mazzucchelli G, et al. Blocking lipid synthesis overcomes tumor regrowth and metastasis after antiangiogenic therapy withdrawal. Cell Metabolism. 2014 Aug;20(2):280–94.

185. Jain RK, Duda DG, Willett CG, Sahani DV, Zhu AX, Loeffler JS, et al. Biomarkers of response and resistance to antiangiogenic therapy. Nat Rev Clin Oncol. 2009 Jun;6(6):327–38.

186. Pulaski BA, Ostrand-Rosenberg S. Mouse 4T1 breast tumor model. Curr Protoc Immunol. 2001 May;Chapter 20:Unit20.2.

187. Barrios CH, Liu M-C, Lee SC, Vanlemmens L, Ferrero J-M, Tabei T, et al. Phase III

randomized trial of sunitinib versus capecitabine in patients with previously treated HER2-negative advanced breast cancer. Breast Cancer Res Treat. 2010 May;121(1):121–31.

188. Crown JP, Dieras V, Staroslawska E, Yardley DA, Bachelot T, Davidson N, et al. Phase III trial of sunitinib in combination with capecitabine versus capecitabine monotherapy for the treatment of patients with pretreated metastatic breast cancer. JCO. American Society of Clinical Oncology; 2013 Aug 10;31(23):2870–8.

189. Bergh J, Bondarenko IM, Lichinitser MR, Liljegren A, Greil R, Voytko NL, et al. First-line treatment of advanced breast cancer with sunitinib in combination with docetaxel versus docetaxel alone: results of a prospective, randomized phase III study. JCO. American Society of Clinical Oncology; 2012 Mar 20;30(9):921–9.

190. Robert NJ, Saleh MN, Paul D, Generali D, Gressot L, Copur MS, et al. Sunitinib plus paclitaxel versus bevacizumab plus paclitaxel for first-line treatment of patients with advanced breast cancer: a phase III, randomized, open-label trial. Clinical Breast Cancer. Elsevier; 2011 Apr;11(2):82–92.

191. Maciag T, Cerundolo J, Ilsley S, Kelley PR, Forand R. An endothelial cell growth factor from bovine hypothalamus: identification and partial characterization. Proceedings of the National Academy of Sciences of the United States of America. 1979 Nov;76(11):5674–8.

192. Fang L, Lee VC, Cha E, Zhang H, Hwang ST. CCR7 regulates B16 murine melanoma cell tumorigenesis in skin. Journal of Leukocyte Biology. 2008 Jun 17;84(4):965–72.

193. Swift S, Lorens J, Achacoso P, Nolan GP. Rapid production of retroviruses for efficient gene delivery to mammalian cells using 293T cell-based systems. Hoboken, NJ, USA: John Wiley & Sons, Inc; 2001 May.

194. Crampton SP, Davis J, Hughes CCW. Isolation of human umbilical vein endothelial cells (HUVEC). J Vis Exp. 2007;(3):183–3.

195. Paquet Y, Dudoit S. marray: Exploratory analysis for two-color spotted microarray [Internet]. R package version .. 2009 [cited 2015 Sep 14]. Available from: http://www.maths.usyd.edu.au/u/jeany/.

196. Smyth GK. Linear models and empirical bayes methods for assessing differential expression in microarray experiments. Stat Appl Genet Mol Biol. 2004;3:Article3.

197. Holthöfer H, Virtanen I, Kariniemi AL, Hormia M, Linder E, Miettinen A. Ulex europaeus I lectin as a marker for vascular endothelium in human tissues. Lab Invest. 1982 Jul;47(1):60–6.

198. Fleige S, Pfaffl MW. RNA integrity and the effect on the real-time qRT-PCR

performance. Mol Aspects Med. 2006 Apr;27(2-3):126–39.

199. Romero IG, Pai AA, Tung J, Gilad Y. RNA-seq: impact of RNA degradation on transcript quantification. BMC Biology. BioMed Central Ltd; 2014 May 30;12(1):42.

200. Muller WA, Weigl SA, Deng X, Phillips DM. PECAM-1 is required for transendothelial migration of leukocytes. J Exp Med. 1993 Aug 1;178(2):449–60.

201. Wragg JW, Bicknell R. Next-generation transcriptomic analysis in cancer vascular research. European Pharmaceutical Review. 2015 Sep 3;4:10–3.

202. Stewart BW, Wild CP. World Cancer Report. World Health Organisation. 2014.

203. Jemal A, Siegel R, Ward E, Murray T, Xu J, Smigal C, et al. Cancer statistics, 2006. CA Cancer J Clin. 2006 Mar;56(2):106–30.

204. Dukes CE, Bussey HJ. The spread of rectal cancer and its effect on prognosis. British Journal of Cancer. 1958 Sep;12(3):309–20.

205. Quirke P, Durdey P, Dixon MF, Williams NS. Local recurrence of rectal adenocarcinoma due to inadequate surgical resection. Histopathological study of lateral tumour spread and surgical excision. Lancet. 1986 Nov 1;2(8514):996–9.

206. Tebbutt NC, Cattell E, Midgley R, Cunningham D, Kerr D. Systemic treatment of colorectal cancer. Eur J Cancer. 2002 May;38(7):1000–15.

207. Mulcahy MF. Bevacizumab in the therapy for refractory metastatic colorectal cancer. Biologics : Targets & Therapy. Dove Press; 2008 Mar 1;2(1):53.

208. Van Cutsem E, Lambrechts D, Prenen H, Jain RK, Carmeliet P. Lessons From the Adjuvant Bevacizumab Trial on Colon Cancer: What Next? JCO. American Society of Clinical Oncology; 2011 Jan 1;29(1):1–4.

209. Hughes CS, Postovit LM, Lajoie GA. Matrigel: a complex protein mixture required for optimal growth of cell culture. Proteomics. 2010 Feb 16;10(9):1886–90.

210. Arnaoutova I, George J, Kleinman HK, Benton G. The endothelial cell tube formation assay on basement membrane turns 20: state of the science and the art. Angiogenesis. 2009 Apr 28;12(3):267–74.

211. Hollmann M. Structure of Ionotropic Glutamate Receptors. Berlin, Heidelberg: Springer Berlin Heidelberg; 1999;141(Chapter 1):3–98.

212. Ikeda K, Araki K, Takayama C, Inoue Y, Yagi T, Aizawa S, et al. Reduced spontaneous activity of mice defective in the epsilon 4 subunit of the NMDA

receptor channel. Brain Res Mol Brain Res. 1995 Oct;33(1):61–71.

213. Miyamoto Y, Yamada K, Noda Y, Mori H, Mishina M, Nabeshima T. Lower sensitivity to stress and altered monoaminergic neuronal function in mice lacking the NMDA receptor epsilon 4 subunit. J Neurosci. 2002 Mar 15;22(6):2335–42.

214. Moghaddam B, Javitt D. From revolution to evolution: the glutamate hypothesis of schizophrenia and its implication for treatment. Neuropsychopharmacology. 2012 Jan;37(1):4–15.

215. Gualandris A, Noghero A, Geuna M, Arese M, Valdembri D, Serini G, et al. Microenvironment drives the endothelial or neural fate of differentiating embryonic stem cells coexpressing neuropilin-1 and Flk-1. FASEB J. Federation of American Societies for Experimental Biology; 2008 Dec 31;23(1):68–78.

216. Hamdollah Zadeh MA, Glass CA, Magnussen A, Hancox JC, Bates DO. VEGF-mediated elevated intracellular calcium and angiogenesis in human microvascular endothelial cells in vitro are inhibited by dominant negative TRPC6. Microcirculation. 2008 Oct;15(7):605–14.

217. Fiorio Pla A, Grange C, Antoniotti S, Tomatis C, Merlino A, Bussolati B, et al. Arachidonic acid-induced Ca2+ entry is involved in early steps of tumor angiogenesis. Mol Cancer Res. 2008 Apr;6(4):535–45.

218. Munaron L, Scianna M. Multilevel complexity of calcium signaling: Modeling angiogenesis. World J Biol Chem. 2012 Jun 26;3(6):121–6.

219. Wyllie DJ, Béhé P, Colquhoun D. Single-channel activations and concentration jumps: comparison of recombinant NR1a/NR2A and NR1a/NR2D NMDA receptors. J Physiol (Lond). 1998 Jul 1;510 (Pt 1):1–18.

220. Cull-Candy S, Brickley S, Farrant M. NMDA receptor subunits: diversity, development and disease. Curr Opin Neurobiol. 2001 Jun;11(3):327–35.

221. Munaron L, Tomatis C, Fiorio Pla A. The secret marriage between calcium and tumor angiogenesis. Technol Cancer Res Treat. 2008 Aug;7(4):335–9.

222. Stepulak A, Luksch H, Gebhardt C, Uckermann O, Marzahn J, Sifringer M, et al. Expression of glutamate receptor subunits in human cancers. Histochem Cell Biol. 2009 Oct;132(4):435–45.

223. Herner A, Sauliunaite D, Michalski CW, Erkan M, De Oliveira T, Abiatari I, et al. Glutamate increases pancreatic cancer cell invasion and migration via AMPA receptor activation and Kras-MAPK signaling. Int J Cancer. 2011 Nov 15;129(10):2349–59.

224. Koochekpour S. Glutamate, a metabolic biomarker of aggressiveness and a potential therapeutic target for prostate cancer. Asian J Androl. 2013

Mar;15(2):212–3.

225. Stepulak A, Rola R, Polberg K, Ikonomidou C. Glutamate and its receptors in cancer. J Neural Transm. 2014 Aug;121(8):933–44.

226. Markman B, Ramos FJ, Capdevila J, Tabernero J. EGFR and KRAS in colorectal cancer. Adv Clin Chem. 2010;51:71–119.

227. Zhou Q, Nicholas Verne G. NMDA Receptors and Colitis: Basic Science and Clinical Implications. Rev Analg. 2008 Nov 1;10(1):33–43.

228. Lampson LA. Monoclonal antibodies in neuro-oncology: Getting past the blood-brain barrier. MAbs. 2011 Mar;3(2):153–60.

229. Mege D, Ouaissi M, Fuks D, Metellus P, Peltier J, Dufour H, et al. Patients with brain metastases from colorectal cancer are not condemned. Anticancer Res. 2013 Dec;33(12):5645–8.

230. Pircher A, Fiegl M, Untergasser G, Heidegger I, Medinger M, Kern J, et al. Favorable prognosis of operable non-small cell lung cancer (NSCLC) patients harboring an increased expression of tumor endothelial markers (TEMs). Lung Cancer. 2013 Aug;81(2):252–8.

231. Jones CA, Nishiya N, London NR, Zhu W, Sorensen LK, Chan AC, et al. Slit2-Robo4 signalling promotes vascular stability by blocking Arf6 activity. Nature. 2009 Oct 18;11(11):1325–31.

232. Jemal A, Bray F, Center MM, Ferlay J, Ward E, Forman D. Global cancer statistics. CA Cancer J Clin. 2011 Mar;61(2):69–90.

233. Rini BI, Rathmell WK, Godley P. Renal cell carcinoma. Curr Opin Oncol. 2008 May;20(3):300–6.

234. Patil S, Manola J, Elson P, Negrier S, Escudier B, Eisen T, et al. Improvement in overall survival of patients with advanced renal cell carcinoma: prognostic factor trend analysis from an international data set of clinical trials. J Urol. 2012 Dec;188(6):2095–100.

235. Cohen HT, McGovern FJ. Renal-cell carcinoma. N Engl J Med. 2005 Dec 8;353(23):2477–90.

236. Singer EA, Gupta GN, Marchalik D, Srinivasan R. Evolving therapeutic targets in renal cell carcinoma. Curr Opin Oncol. 2013 May;25(3):273–80.

237. Cowey CL, Rathmell WK. VHL gene mutations in renal cell carcinoma: role as a biomarker of disease outcome and drug efficacy. Curr Oncol Rep. 2009 Mar;11(2):94–101.

238. Flanagan K, Fitzgerald K, Baker J, Regnstrom K, Gardai S, Bard F, et al. Laminin-

411 is a vascular ligand for MCAM and facilitates TH17 cell entry into the CNS. Meuth SG, editor. PLoS ONE. 2012;7(7):e40443.

239. Baker A-M, Bird D, Welti JC, Gourlaouen M, Lang G, Murray GI, et al. Lysyl oxidase plays a critical role in endothelial cell stimulation to drive tumor angiogenesis. Cancer Res. 2013 Jan 15;73(2):583–94.

240. Yan X, Lin Y, Yang D, Shen Y, Yuan M, Zhang Z, et al. A novel anti-CD146 monoclonal antibody, AA98, inhibits angiogenesis and tumor growth. Blood. 2003 Jul 1;102(1):184–91.

241. Gonzalez AM, Gonzales M, Herron GS, Nagavarapu U, Hopkinson SB, Tsuruta D, et al. Complex interactions between the laminin alpha 4 subunit and integrins regulate endothelial cell behavior in vitro and angiogenesis in vivo. Proceedings of the National Academy of Sciences of the United States of America. 2002 Dec 10;99(25):16075–80.

242. Soker S, Takashima S, Miao HQ, Neufeld G, Klagsbrun M. Neuropilin-1 is expressed by endothelial and tumor cells as an isoform-specific receptor for vascular endothelial growth factor. Cell. 1998 Mar 20;92(6):735–45.

243. Fisher C, Gilbertson-Beadling S, Powers EA, Petzold G, Poorman R, Mitchell MA. Interstitial collagenase is required for angiogenesis in vitro. Dev Biol. 1994 Apr;162(2):499–510.

244. Kasai A, Shintani N, Oda M, Kakuda M, Hashimoto H, Matsuda T, et al. Apelin is a novel angiogenic factor in retinal endothelial cells. Biochemical and Biophysical Research Communications. 2004 Dec 10;325(2):395–400.

245. Jendraschak E, Sage EH. Regulation of angiogenesis by SPARC and angiostatin: implications for tumor cell biology. Semin Cancer Biol. 1996 Jun;7(3):139–46.

246. Colognato H, Yurchenco PD. Form and function: the laminin family of heterotrimers. Dev Dyn. 2000 Jun;218(2):213–34.

247. Miner JH, Yurchenco PD. Laminin functions in tissue morphogenesis. Annu Rev Cell Dev Biol. 2004;20(1):255–84.

248. Huang X, Ji G, Wu Y, Wan B, Yu L. LAMA4, highly expressed in human hepatocellular carcinoma from Chinese patients, is a novel marker of tumor invasion and metastasis. J Cancer Res Clin Oncol. 2008 Jun;134(6):705–14.

249. Ross JB, Huh D, Noble LB, Tavazoie SF. Identification of molecular determinants of primary and metastatic tumour re-initiation in breast cancer. Nature. 2015 May;17(5):651–64.

250. Vainionpää N, Lehto V-P, Tryggvason K, Virtanen I. Alpha4 chain laminins are widely expressed in renal cell carcinomas and have a de-adhesive function. Lab Invest. 2007 Aug;87(8):780–91.

251. Jiang T, Zhuang J, Duan H, Luo Y, Zeng Q, Fan K, et al. CD146 is a coreceptor for VEGFR-2 in tumor angiogenesis. Blood. 2012 Sep 13;120(11):2330–9.

252. Bardin N, Anfosso F, Massé JM, Cramer E, Sabatier F, Le Bivic A, et al. Identification of CD146 as a component of the endothelial junction involved in the control of cell-cell cohesion. Blood. 2001 Dec 15;98(13):3677–84.

253. Ouhtit A, Gaur RL, Abd Elmageed ZY, Fernando A, Thouta R, Trappey AK, et al. Towards understanding the mode of action of the multifaceted cell adhesion receptor CD146. Biochim Biophys Acta. 2009 Apr;1795(2):130–6.

254. Lehmann JM, Riethmüller G, Johnson JP. MUC18, a marker of tumor progression in human melanoma, shows sequence similarity to the neural cell adhesion molecules of the immunoglobulin superfamily. Proceedings of the National Academy of Sciences of the United States of America. 1989 Dec;86(24):9891–5.

255. Wu G-J, Peng Q, Fu P, Wang S-W, Chiang C-F, Dillehay DL, et al. Ectopical expression of human MUC18 increases metastasis of human prostate cancer cells. Gene. 2004 Mar 3;327(2):201–13.

256. Zabouo G, Imbert A-M, Jacquemier J, Finetti P, Moreau T, Esterni B, et al. CD146 expression is associated with a poor prognosis in human breast tumors and with enhanced motility in breast cancer cell lines. Breast Cancer Res. 2009;11(1):R1.

257. Wu Z, Wu Z, Li J, Yang X, Wang Y, Yu Y, et al. MCAM is a novel metastasis marker and regulates spreading, apoptosis and invasion of ovarian cancer cells. Tumour Biol. 2012 Oct;33(5):1619–28.

258. Feng G, Fang F, Liu C, Zhang F, Huang H, Pu C. CD146 gene expression in clear cell renal cell carcinoma: a potential marker for prediction of early recurrence after nephrectomy. Int Urol Nephrol. 2012 Dec;44(6):1663–9.

259. Zhang X, Wang Z, Kang Y, Li X, Ma X, Ma L. MCAM expression is associated with poor prognosis in non-small cell lung cancer. Clin Transl Oncol. 2014 Feb;16(2):178–83.

260. Ishikawa T, Wondimu Z, Oikawa Y, Gentilcore G, Kiessling R, Egyhazi Brage S, et al. Laminins 411 and 421 differentially promote tumor cell migration via α6β1 integrin and MCAM (CD146). Matrix Biol. 2014 Sep;38:69–83.

261. Yoshioka S, Fujiwara H, Higuchi T, Yamada S, Maeda M, Fujii S. Melanoma cell adhesion molecule (MCAM/CD146) is expressed on human luteinizing granulosa cells: enhancement of its expression by hCG, interleukin-1 and tumour necrosis factor-alpha. Mol Hum Reprod. 2003 Jun;9(6):311–9.

262. Bardin N, Blot-Chabaud M, Despoix N, Kebir A, Harhouri K, Arsanto J-P, et al. CD146 and its soluble form regulate monocyte transendothelial migration. Arteriosclerosis, Thrombosis, and Vascular Biology. 2009 May;29(5):746–53.

263. Ueno K, Hirata H, Majid S, Tabatabai ZL, Hinoda Y, Dahiya R. IGFBP-4 activates the Wnt/beta-catenin signaling pathway and induces M-CAM expression in human renal cell carcinoma. Int J Cancer. 2011 Nov 15;129(10):2360–9.

264. Younes A, Forero-Torres A, Bartlett NL, Leonard JP, Rege B, Kennedy DA, et al. Objective responses in a phase I dose-escalation study of SGN-35, a novel antibody-drug conjugate (ADC) targeting CD30, in patients with relapsed or refractory Hodgkin lymphoma. ASCO Meeting Abstracts. 2008 May 20;26(15_suppl):8526.

265. Verma S, Miles D, Gianni L, Krop IE, Welslau M, Baselga J, et al. Trastuzumab emtansine for HER2-positive advanced breast cancer. N Engl J Med. 2012 Nov 8;367(19):1783–91.

266. Siemann DW, Shi W. Efficacy of combined antiangiogenic and vascular disrupting agents in treatment of solid tumors. Int J Radiat Oncol Biol Phys. 2004 Nov 15;60(4):1233–40.

267. Ma J, Jemal A. Breast Cancer Statistics. Breast Cancer Metastasis and Drug Resistance. Springer New York; 2012;:1–18.

268. Bao T, Rudek MA. The Clinical Pharmacology of Anastrozole. European Oncology Haematology. 2011;7(2):106–8.

269. Burstein HJ, Temin S, Anderson H, Buchholz TA, Davidson NE, Gelmon KE, et al. Adjuvant endocrine therapy for women with hormone receptor-positive breast cancer: american society of clinical oncology clinical practice guideline focused update. JCO. 2014. pp. 2255–69.

270. Jahanzeb M. Adjuvant trastuzumab therapy for HER2-positive breast cancer. Clinical Breast Cancer. 2008 Aug;8(4):324–33.

271. Foulkes WD, Smith IE, Reis-Filho JS. Triple-negative breast cancer. N Engl J Med. 2010 Nov 11;363(20):1938–48.

272. Roskoski R. Sunitinib: a VEGF and PDGF receptor protein kinase and angiogenesis inhibitor. Biochemical and Biophysical Research Communications. 2007 May 4;356(2):323–8.

273. Burstein HJ, Elias AD, Rugo HS, Cobleigh MA, Wolff AC, Eisenberg PD, et al. Phase II study of sunitinib malate, an oral multitargeted tyrosine kinase inhibitor, in patients with metastatic breast cancer previously treated with an anthracycline and a taxane. JCO. 2008 Apr 10;26(11):1810–6.

274. Curigliano G, Pivot X, Cortés J, Elias A, Cesari R, Khosravan R, et al. Randomized phase II study of sunitinib versus standard of care for patients with previously treated advanced triple-negative breast cancer. The Breast. 2013 Oct;22(5):650–6.

275. Crown J, Dieras V, Staroslawska E, Yardley DA, Davidson N, Bachelot TD, et al. Phase III trial of sunitinib (SU) in combination with capecitabine (C) versus C in previously treated advanced breast cancer (ABC). ASCO Meeting Abstracts. 2010 Jun 20;28(18_suppl):LBA1011.

276. Bergh J, Bondarenko IM, Lichinitser MR, Liljegren A, Greil R, Voytko NL, et al. First-line treatment of advanced breast cancer with sunitinib in combination with docetaxel versus docetaxel alone: results of a prospective, randomized phase III study. JCO. 2012 Mar 20;30(9):921–9.

277. Kaur P, Nagaraja GM, Zheng H, Gizachew D, Galukande M, Krishnan S, et al. A mouse model for triple-negative breast cancer tumor-initiating cells (TNBC-TICs) exhibits similar aggressive phenotype to the human disease. BMC Cancer. BioMed Central Ltd; 2012 Mar 27;12(1):120.

278. Barrios CH, Liu M-C, Lee SC, Vanlemmens L, Ferrero J-M, Tabei T, et al. Phase III randomized trial of sunitinib versus capecitabine in patients with previously treated HER2-negative advanced breast cancer. Breast Cancer Res Treat. 2010 May;121(1):121–31.

279. Engelman JA, Settleman J. Acquired resistance to tyrosine kinase inhibitors during cancer therapy. Curr Opin Genet Dev. 2008 Feb;18(1):73–9.

280. Yin T, He S, Ye T, Shen G, Wan Y, Wang Y. Antiangiogenic therapy using sunitinib combined with rapamycin retards tumor growth but promotes metastasis. Translational Oncology. 2014 Apr;7(2):221–9.

281. Ebos JML, Lee CR, Christensen JG, Mutsaers AJ, Kerbel RS. Multiple circulating proangiogenic factors induced by sunitinib malate are tumor-independent and correlate with antitumor efficacy. Proceedings of the National Academy of Sciences of the United States of America. 2007 Oct 23;104(43):17069–74.

282. Okazaki T, Ebihara S, Asada M, Kanda A, Sasaki H, Yamaya M. Granulocyte colony-stimulating factor promotes tumor angiogenesis via increasing circulating endothelial progenitor cells and Gr1+CD11b+ cells in cancer animal models. Int Immunol. 2006 Jan;18(1):1–9.

283. Karaman MW, Herrgard S, Treiber DK, Gallant P, Atteridge CE, Campbell BT, et al. A quantitative analysis of kinase inhibitor selectivity. Nat Biotechnol. 2008 Jan 8;26(1):127–32.

284. Van Putten LM, Kram LK, van Dierendonck HH, Smink T, Füzy M. Enhancement by drugs of metastatic lung nodule formation after intravenous tumour cell injection. Int J Cancer. 1975 Apr 15;15(4):588–95.

285. Vollmer TL, Conley FK. Effect of cyclophosphamide on survival of mice and incidence of metastatic tumor following intravenous and intracardial inoculation of tumor cells. Cancer Res. 1984 Sep;44(9):3902–6.

286. De Ruiter J, Cramer SJ, Lelieveld P, Van Putten LM. Comparison of metastatic disease after local tumour treatment with radiotherapy or surgery in various tumour models. Eur J Cancer Clin Oncol. 1982 Mar;18(3):281–9.

287. Keskin D, Kim J, Cooke VG, Wu C-C, Sugimoto H, Gu C, et al. Targeting vascular pericytes in hypoxic tumors increases lung metastasis via angiopoietin-2. Cell Rep. 2015 Feb 24;10(7):1066–81.

288. Walpole SC, Prieto-Merino D, Edwards P, Cleland J, Stevens G, Roberts I. The weight of nations: an estimation of adult human biomass. BMC Public Health. BioMed Central Ltd; 2012 Jun 18;12(1):439.

289. Bhatt RS, Wang X, Zhang L, Collins MP, Signoretti S, Alsop DC, et al. Renal cancer resistance to antiangiogenic therapy is delayed by restoration of angiostatic signaling. Mol Cancer Ther. 2010 Oct 10;9(10):2793–802.

290. Huang D, Ding Y, Zhou M, Rini BI, Petillo D, Qian CN, et al. Interleukin-8 mediates resistance to antiangiogenic agent sunitinib in renal cell carcinoma. Cancer Res. 2010 Jan 31;70(3):1063–71.

291. Weidner N, Semple JP, Welch WR, Folkman J. Tumor angiogenesis and metastasis--correlation in invasive breast carcinoma. N Engl J Med. 1991 Jan 3;324(1):1–8.

292. Ebos JML, Mastri M, Hudson JM, Lee CR, Tracz A, Attwood K, et al. Effect of the timing of sunitinib administration on the predictive value of biomarkers in renal cell cancer (mRCC). ASCO Meeting Abstracts. 2015 May 20;33(15_suppl):11096.

293. Dror Michaelson M, Regan MM, Oh WK, Kaufman DS, Olivier K, Michaelson SZ, et al. Phase II study of sunitinib in men with advanced prostate cancer. Annals of Oncology. 2009 May;20(5):913–20.

294. Lo H-M, Shieh J-M, Chen C-L, Tsou C-J, Wu W-B. Vascular Endothelial Growth Factor Induces CXCL1 Chemokine Release via JNK and PI-3K-Dependent Pathways in Human Lung Carcinoma Epithelial Cells. International Journal of Molecular Sciences 2013, Vol 14, Pages 10090-10106. Multidisciplinary Digital Publishing Institute; 2013 May 10;14(5):10090–106.

295. Mousseau Y, Mollard S, Faucher-Durand K, Richard L, Nizou A, Cook-Moreau J, et al. Fingolimod potentiates the effects of sunitinib malate in a rat breast cancer model. Breast Cancer Res Treat. 2011 Dec 9;134(1):31–40.

296. Lynn KD, Roland CL, Brekken RA. VEGF and pleiotrophin modulate the immune profile of breast cancer. Cancers (Basel). 2010;2(2):970–88.

297. Saito Y, Tanaka Y, Aita Y, Ishii KA, Ikeda T, Isobe K, et al. Sunitinib induces apoptosis in pheochromocytoma tumor cells by inhibiting VEGFR2/Akt/mTOR/S6K1 pathways through modulation of Bcl-2 and BAD.

AJP: Endocrinology and Metabolism. 2012 Mar 15;302(6):E615–25.

298. Radulovic S, Bjelogrlic SK. Sunitinib, sorafenib and mTOR inhibitors in renal cancer. J BUON. 2007 Sep;12 Suppl 1:S151–62.

299. Sakai I, Miyake H, Fujisawa M. Acquired resistance to sunitinib in human renal cell carcinoma cells is mediated by constitutive activation of signal transduction pathways associated with tumour cell proliferation. BJU Int. 2013 Jul;112(2):E211–20.

300. Guo T, Hajdu M, Agaram NP, Shinoda H, Veach D, Clarkson BD, et al. Mechanisms of sunitinib resistance in gastrointestinal stromal tumors harboring KITAY502-3ins mutation: an in vitro mutagenesis screen for drug resistance. Clin Cancer Res. 2009 Nov 15;15(22):6862–70.

301. Maunsbach AB, Marples D, Chin E, Ning G, Bondy C, Agre P, et al. Aquaporin-1 water channel expression in human kidney. J Am Soc Nephrol. 1997 Jan;8(1):1–14.

302. Galán-Cobo A, Ramírez-Lorca R, Toledo-Aral JJ, Echevarría M. Aquaporin-1 Plays Important Role in Proliferation by Affecting Cell Cycle Progression. J Cell Physiol. 2015 Jun 16.

303. Kumar M, Panka D, Bhatt R, Schor-Bardach R, Zhang L, Atkins M, et al. Mechanism of acquired resistance to sunitinib in RCC. Cancer Res. American Association for Cancer Research; 2008 May 1;68(9 Supplement):1127–7.

304. Huebert RC, Vasdev MM, Shergill U, Das A, Huang BQ, Charlton MR, et al. Aquaporin-1 facilitates angiogenic invasion in the pathological neovasculature that accompanies cirrhosis. Hepatology. 2010 Jul;52(1):238–48.

305. Fiedler U, Reiss Y, Scharpfenecker M, Grunow V, Koidl S, Thurston G, et al. Angiopoietin-2 sensitizes endothelial cells to TNF-alpha and has a crucial role in the induction of inflammation. Nat Med. 2006 Feb 5;12(2):235–9.

306. Lassalle P, Molet S, Janin A, Heyden JV, Tavernier J, Fiers W, et al. ESM-1 is a novel human endothelial cell-specific molecule expressed in lung and regulated by cytokines. J Biol Chem. 1996 Aug 23;271(34):20458–64.

307. Clutter SD, Wilson DC, Marinov AD, Hirsch R. Follistatin-like protein 1 promotes arthritis by up-regulating IFN-gamma. The Journal of Immunology. 2009 Jan 1;182(1):234–9.

308. Scapini P, Crepaldi L, Pinardi C, Calzetti F, Cassatella MA. CCL20/macrophage inflammatory protein-3alpha production in LPS-stimulated neutrophils is enhanced by the chemoattractant formyl-methionyl-leucyl-phenylalanine and IFN-gamma through independent mechanisms. Eur J Immunol. 2002 Dec;32(12):3515–24.

309. DiRaimondo TR, Klock C, Khosla C. Interferon-γ activates transglutaminase 2 via a phosphatidylinositol-3-kinase-dependent pathway: implications for celiac sprue therapy. Journal of Pharmacology and Experimental Therapeutics. 2012 Mar 14;341(1):104–14.

310. Chen W-B, Lenschow W, Tiede K, Fischer JW, Kalthoff H, Ungefroren H. Smad4/DPC4-dependent regulation of biglycan gene expression by transforming growth factor-beta in pancreatic tumor cells. J Biol Chem. 2002 Sep 27;277(39):36118–28.

311. Fujita T, Shiba H, Sakata M, Uchida Y, Ogawa T, Kurihara H. Effects of transforming growth factor-beta 1 and fibronectin on SPARC expression in cultures of human periodontal ligament cells. Cell Biol Int. 2002;26(12):1065–72.

312. Krohn K, Laping NJ, Morgan TE, Finch CE. Expression of vimentin increases in the hippocampus and cerebral cortex after entorhinal cortex lesioning and in response to transforming growth factor beta 1. J Neuroimmunol. 1995 Jan;56(1):53–63.

313. Denko NC, Fontana LA, Hudson KM, Sutphin PD, Raychaudhuri S, Altman R, et al. Investigating hypoxic tumor physiology through gene expression patterns. Oncogene. 2003 Sep 1;22(37):5907–14.

314. Jin Y, An X, Ye Z, Cully B, Wu J, Li J. RGS5, a hypoxia-inducible apoptotic stimulator in endothelial cells. Journal of Biological Chemistry. 2009 Aug 21;284(35):23436–43.

315. Chen B, Siderovski DP, Neubig RR, Lawson MA, Trejo J. Regulation of Protease-activated Receptor 1 Signaling by the Adaptor Protein Complex 2 and R4 Subfamily of Regulator of G Protein Signaling Proteins. Journal of Biological Chemistry. American Society for Biochemistry and Molecular Biology; 2014 Jan 17;289(3):1580–91.

316. Noy PJ, Lodhia P, Khan K, Zhuang X, Ward DG, Verissimo AR, et al. Blocking CLEC14A-MMRN2 binding inhibits sprouting angiogenesis and tumour growth. Oncogene. 2015 Mar 9.

317. Benjamini Y, Hochberg Y. Controlling the False Discovery Rate: A Practical and Powerful Approach to Multiple Testing. JSTOR. 1995;57(1):289–300.